Universidad de Valladolid

FACULTAD DE CIENCIAS

FÍSICA DE LA MATERIA CONDENSADA, CRISTALOGRAFÍA Y MINERALOGÍA

TESIS DOCTORAL:

Fabricación y Caracterización de las Propiedades Físicas de Polímeros Nanocelulares: Transición de la Escala Micro a la Nano

Presentada por BELÉN NOTARIO COLLADO para optar al grado de doctor /ra por la Universidad de Valladolid

Dirigida por:
Miguel Ángel RODRÍGUEZ PÉREZ
Javier PINTO SANZ

"Considero más valiente al que conquista sus deseos

que al que conquista a sus enemigos,

ya que la victoria más dura es la victoria sobre uno mismo".

ARISTÓTELES

A mi familia

A Álvaro

Financiación

He de agradecer la financiación para llevar a cabo esta investigación que he recibido de diversas instituciones, comenzando por una beca de Introducción a la Investigación de 3 meses concedida por la UVa, unos meses de beca concedida también por la UVa, y finalmente una beca FPI concedida por el Ministerio de Educación (BES-2013-062852). Mientras que la realización de estancias han sido financiadas por la beca FPI y por la beca *International Summer Student Programme* concedida por el centro Helmholtz Zentrum Berlin (Berlin, Alemania). También he de agradecer la financiación recibida por el grupo CellMat para el estudio de materiales poliméricos nanocelulares proveniente de los siguientes proyectos:

1. PROYECTO "NANCORE: MICROCELLULAR NANOCOMPOSITE FOR SUBSTITUTION OF BALSA WOOD AND PVC CORE MATERIAL". VII PROGRAMA MARCO. Número de Proyecto 214148. 2008-2012
2. PROYECTO "SENSOTUBO: SISTEMA DE OPTIMIZACIÓN DE LAS REDES DESTINADAS AL TRANSPORTE DE AGUA". FINANCIADO POR EL MCINN. PROGRAMA INNPACTO. IPT-2011-0725-310000. 2011-2014

Funding

Financial assistance during the course of this thesis from UVa, and FPI grant (BES-2013-062852) is gratefully acknowledged.

Financial assistance provided by the following research projects is also acknowledged:

1. PROJECT "NANCORE: MICROCELLULAR NANOCOMPOSITE FOR SUBSTITUTION OF BALSA WOOD AND PVC CORE MATERIAL". VII PROGRAMA MARCO. EC PROJECT NUMBER 214148. 2008-2012
2. PROJECT "SENSOTUBO: SISTEMA DE OPTIMIZACIÓN DE LAS REDES DESTINADAS AL TRANSPORTE DE AGUA". FUNDED BY THE MCINN. PROGRAMA INNPACTO. IPT-2011-0725-310000. 2011-2014

Contents

RESUMEN EN ESPAÑOL

Resumen en Español

S1. Introducción

La Ciencia de Materiales, definida como la rama de la ciencia encargada de investigar la relación entre la estructura y las propiedades de los materiales, permite por un lado desarrollar materiales con propiedades exclusivas, o bien mejorar las propiedades o rutas de producción de materiales de uso común. De esta manera se consigue ampliar el rango de aplicación o incluso se da lugar a aplicaciones completamente nuevas para dichos materiales. Conviene matizar que es la ingeniería de materiales, quien basándose en la relación estructura-propiedades-producción-aplicaciones, diseña o proyecta la estructura de un material para conseguir un conjunto predeterminado de propiedades. A veces es difícil definir una frontera entre ambos conceptos pues existe una zona de uso común. Lo que sí es evidente es que ambos deben caminar unidos de forma obligada.

Los avances obtenidos en otras ramas de la ciencia y la tecnología requieren de nuevos o mejorados materiales para poder llevar a cabo dichos avances. Por estos motivos la Ciencia de Materiales es una de las principales áreas de interés tanto de organismos públicos de investigación como de centros de investigación privados.

De hecho, la Unión Europea (UE) estableció en diciembre de 2013 los objetivos de investigación del programa "Horizonte 2020" (Horizonte 2020, el programa de Investigación e Innovación de la UE para el periodo 2014-2020) [1], entre los que se encuentran múltiples objetivos centrados en la Ciencia de Materiales. Horizonte 2020 tiene un fuerte enfoque en el desarrollo de las capacidades industriales europeas en lo que se conoce como Key Enabling Technologies (KETs). Esta parte del programa cubre diferentes áreas de investigación como la nanotecnología, los materiales avanzados, la fabricación y el procesamiento avanzado, y la biotecnología. En particular, dentro de esos objetivos una de las prioridades de la UE es la "*Producción y control de materiales nanoporosos*".

La presente tesis titulada ***"Fabricación y caracterización de las propiedades físicas de polímeros nanocelulares: transición de la escala micro a la escala nanométrica"*** se encuadra por tanto dentro de este campo de investigación prioritario, en la actualidad y el futuro, para la UE.

De manera general los materiales celulares poliméricos se pueden definir como una estructura de dos fases en la cual la fase gaseosa procedente de un agente espumante, ya sea físico o químico, se ha dispersado a lo largo de una matriz polimérica sólida [2].

Aunque en algunas ocasiones se hace referencia a los materiales celulares como espumas, es necesario aclarar que una espuma es un tipo específico de material celular que se ha generado por expansión de un material en estado líquido. A lo largo de la tesis se utilizarán indistintamente el término de material celular y el de espuma, pero hay que tener claro que cuando se habla de espuma nos estamos refiriendo a material celular.

Los materiales celulares pueden ser clasificados atendiendo a distintos criterios. El primero de ellos hace referencia al tipo de estructura celular y a la conectividad de las celdas. Así, es

posible encontrar materiales celulares de *Celda Abierta* (Figura 0.1 izquierda) donde el gas puede circular libremente entre las celdillas ya que éstas están interconectadas, o materiales de *Celda Cerrada* (Figura 0.1 derecha), en los cuales el gas está ocluido en el interior de las mismas. Habitualmente es fácil encontrar materiales con una estructura intermedia: una fracción de la estructura celular está formado por una estructura de celda abierta mientras que otra fracción de la estructura celular está formado por una estructura de celda cerrada [2].

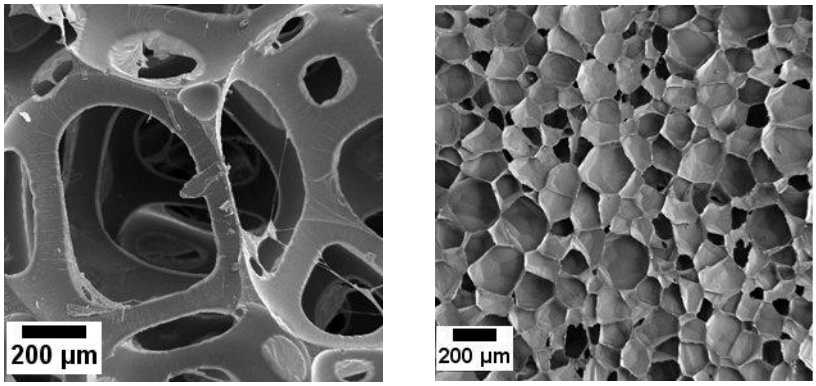

Figura 0.1. Izquierda) material celular de celda abierta, Derecha) material celular de celda cerrada

Otra clasificación de los materiales celulares se puede realizar atendiendo a su densidad. Este parámetro determina fuertemente las propiedades finales del material, y en consecuencia sus aplicaciones [2, 3].

Cuando se habla de la densidad de un material celular es común hacerlo refiriéndose a su *Densidad Relativa* ($\rho_{relativa}$), que es la relación entre la densidad del material celular ($\rho_{material\ celular}$) y la del correspondiente material sólido ($\rho_{sólido}$) [2, 3]:

$$\rho_{relativa} = \frac{\rho_{material\ celular}}{\rho_{sólido}} \tag{0-1}$$

De acuerdo a su densidad relativa, los materiales celulares se pueden clasificar en tres grupos:

- Materiales celulares de baja densidad: densidades relativas por debajo de 0.3.
- Materiales celulares de media densidad: densidades relativas entre 0.3 y 0.6.
- Materiales celulares de alta densidad: densidades relativas mayores de 0.6.

La producción de material celulares tiene como finalidad mejorar las propiedades de materiales conocidos, o bien incrementar el rango de sus potenciales aplicaciones [2]. Además de ofrecer una reducción de la densidad del material de partida (obteniendo así piezas más ligeras para unas mismas dimensiones/aplicación), los materiales celulares pueden presentar mejores propiedades que los materiales sólidos en diferentes áreas/aplicaciones, como por ejemplo mejor capacidad como aislantes térmicos, mejor absorción de impacto, absorción acústica, etc.

Sin embargo los materiales celulares no son una invención del ser humano, sino que la naturaleza ha utilizado ampliamente esta aproximación durante la evolución de la vida en la

Tierra. La madera, el corcho, los corales, las esponjas marinas o los huesos de distintas especies de vertebrados (Figura 0.2, izquierda) son algunos de los ejemplos más representativos [4].

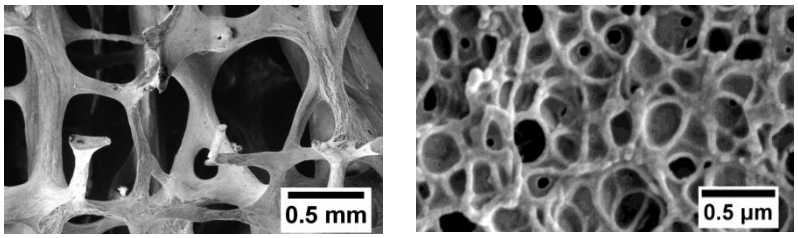

Figura 0.2. Estructura porosa de un hueso humano (izquierda) y estructura porosa de un polímero nanocelular (derecha)

Pero reproducir estas estructuras vivas por medios artificiales dista mucho de ser simple. Actualmente es posible fabricar materiales celulares a partir de múltiples materiales de partida. Estos materiales artificiales abarcan desde la simple repetición de una celda unidad en el caso de los paneles tipo abeja (usados como núcleos en paneles sándwich para aplicaciones estructurales) hasta materiales celulares tridimensionales estructuradas estocásticamente a partir de líquidos, polímeros, metales, cerámicas, etc. [3, 5-8]. Estos materiales pueden presentar propiedades mejoradas y densidades relativas bajas que les permiten encontrar aplicación en embalajes, industria aeronáutica, industria del automóvil [9], aislamiento térmico [10] y acústico [11], así como en procesos de catálisis debido a su elevada área superficial [12].

La producción de materiales celulares ha experimentado una progresión significativa con el desarrollo de la Nanotecnología. Este concepto fue introducido por primera vez por el premio Nobel de Física Richard P. Feynman en 1959, así como por otros investigadores como Norio Taguchi quien propuso el término "*nano-tecnología*". Gracias a la manipulación de la materia a escala atómica, molecular, o supramolecular empezó una nueva era en el campo de la Ciencia de Materiales.

De hecho, algunas de las actuales vías de investigación de mayor relevancia en espumas poliméricas son la adición de nanopartículas a la matriz polimérica (con el fin de modificar el proceso de espumado o para mejorar/modificar la estructura y propiedades del material celular) y la fabricación de materiales celulares poliméricas cuyo tamaño de poro se encuentre en el rango nanométrico (en torno a 200 nm, siendo 1 nm = 10^{-9} m) (polímeros nanocelulares). Debido al creciente interés en este campo, este trabajo de investigación se ha centrado en la producción y caracterización de polímeros nanocelulares. La Figura 0.2 (derecha) muestra la estructura típica de uno de los polímeros nanocelulares producidos en esta investigación en el que se puede observar que el tamaño de celda está por debajo de la micra.

Desde el punto de vista de sus potenciales propiedades estos materiales nanocelulares son muy prometedores ya que además de las esperadas mejoras en las propiedades mecánicas frente a los materiales celulares convencionales y microcelulares, habría que sumar la reducción de la conductividad térmica debido a la baja contribución del término de conducción a través de la fase gaseosa (efecto Knudsen) [13], y la transparencia de estos productos cuando

se fabrican a partir de materiales amorfos y cuando los tamaños de celda están por debajo de los 50 nm [14]. Además, las dimensiones del tamaño de poro y del espesor de pared en el rango nanométrico pueden dar lugar en estos materiales a la aparición de nuevos efectos o comportamientos no esperados. Sin embargo, a día de hoy existen pocos trabajos que demuestren estos aspectos. La principal limitación para la caracterización de las distintas propiedades físicas de los polímeros nanocelulares es la producción de muestras suficientemente grandes o con geometrías apropiadas para ser sometidas a protocolos estándar de análisis.

La fabricación de polímeros nanoporosos a partir de films poliméricos es bien conocida, ya sea mediante el empleo de nanoestructuras (técnicas de transferencia de patrones [15-18]) o mediante la degradación o disolución selectiva de bloques [15, 17-24]. Por otra parte, la bibliografía muestra que hasta el momento no ha sido posible obtener materiales nanocelulares mediante el empleo de técnicas de espumado empleando un agente de espumado químico.

Por otro lado, el proceso de espumado por disolución de gas a altas presiones (típicamente N_2 o CO_2) es quizás menos conocido [18, 25-27], pero es una técnica versátil, eficaz, barata y medioambientalmente sostenible, especialmente si se utiliza CO_2 (el cual presenta una excelente capacidad de difusión en el estado supercrítico (por encima de 31° C y 7.3 MPa)) y con el potencial de producir polímeros nanocelulares con dimensiones macroscópicas.

El proceso de espumado mediante disolución de gas consta de tres etapas (Figura 0.3):

- Etapa I: saturación del polímero bajo presión.
- Etapa II: desorción del gas tras liberar la presión.
- Etapa III: espumado a una temperatura superior o cercana a la temperatura de transición vítrea efectiva del polímero plastificado ($T_{g,ef}$) con el agente espumante.

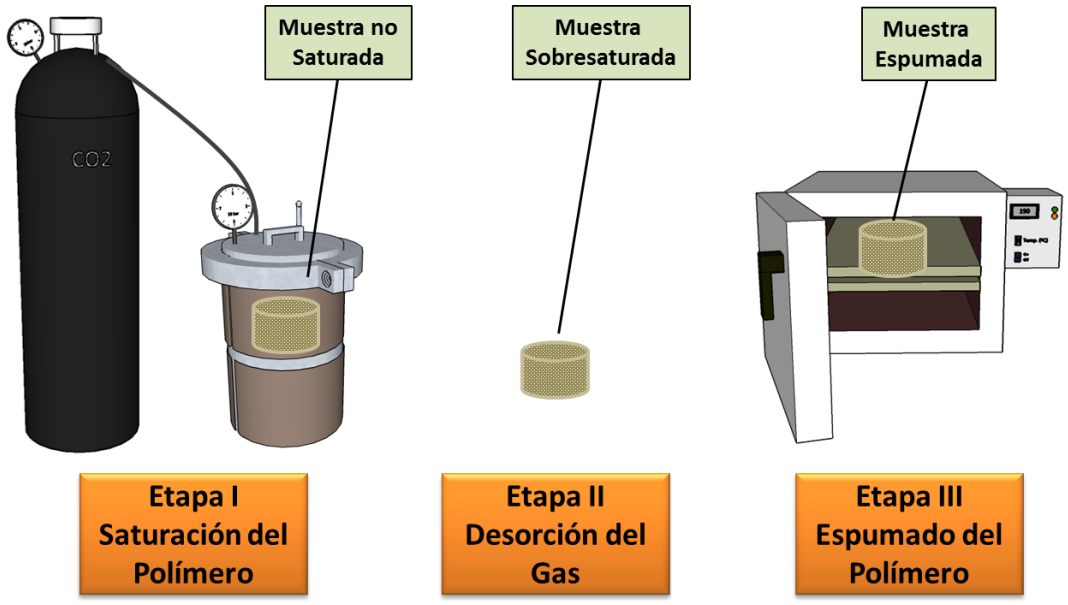

Figura 0.3. Esquema del proceso de disolución de gas para el caso específico del *solid state foaming*

Si la nucleación y crecimiento de las celdas se produce durante la liberación de la presión el proceso es calificado como un proceso de espumado en una etapa [26, 28] (también llamado *batch foaming*), para lo cual la temperatura del polímero durante el proceso de liberación de la presión deberá ser próxima o superior a su $T_{g,ef}$. En este caso, las etapas II y III son indistinguibles pues suceden simultáneamente.

Por el contrario, si durante la liberación de la presión el polímero se encuentra en estado vítreo será necesario llevar a cabo el proceso de espumado, en el que se produce el crecimiento celular calentando la muestra polimérica saturada de gas a un temperatura cercana o superior a su $T_{g,ef}$. En este caso el proceso de espumado se llevará a cabo en dos etapas (Etapa II y Etapa III) [29]. El proceso completo constituido por estas tres etapas es conocido como *solid state foaming*. La descripción que se utiliza en esta sección es válida para polímeros amorfos.

La obtención de polímeros nanocelulares mediante el proceso de espumado por disolución de gas requiere alcanzar una densidad de nucleación de celdas muy elevada (N_0, número de núcleos por cm^3 de la muestra sin espumar), típicamente con valores del orden de 10^{14}-10^{15} núcleos/cm^3. Para ello, existen diversas aproximaciones que permiten incrementar la densidad de nucleación como se muestra en la Figura 0.4.

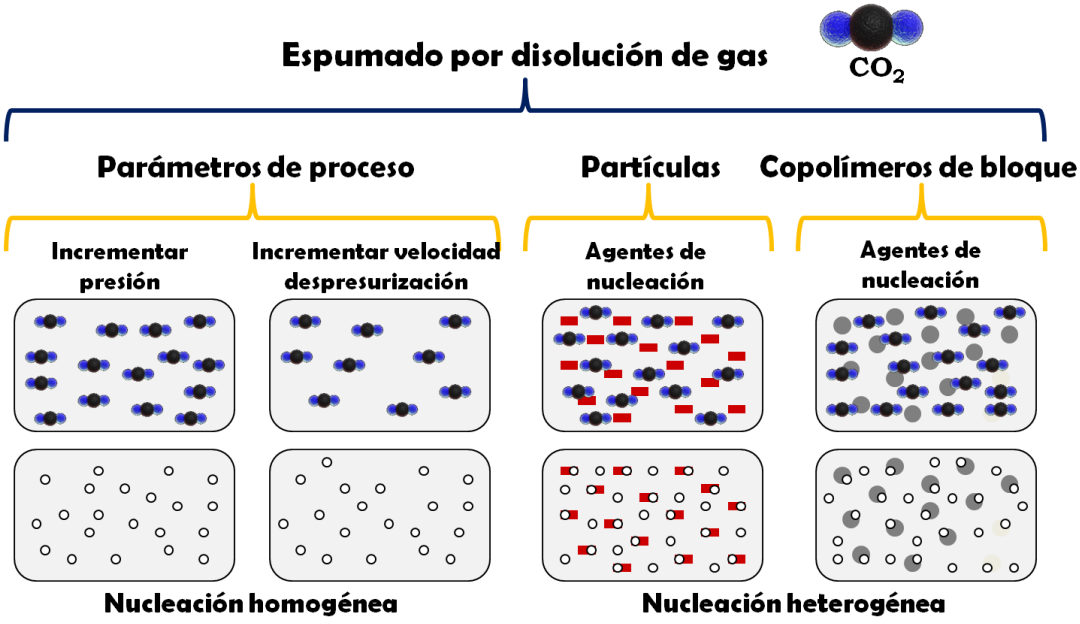

Figura 0.4. Métodos para incrementar la densidad de nucleación en los procesos de espumado por disolución de gas

En materiales que presentan un mecanismo de **nucleación homogénea** la densidad de nucleación está controlada por los parámetros de proceso de espumado, principalmente la presión de saturación y la velocidad de liberación de la presión [26, 30, 31].

Mientras que en los materiales que presentan un mecanismo de **nucleación heterogénea** es posible incrementar la tasa de nucleación mediante: a) la adición de partículas (talco, óxido de titanio, caolín, nanosílicas, etc.) siempre y cuando dichas partículas estén bien dispersadas en la matriz polimérica y tengan un tamaño apropiado (del mismo orden o superior al radio crítico de nucleación del sistema polímero/gas) [32]; b) mediante el uso de copolímeros de bloque (de tipo A-B o A-B-A, siendo A y B diferentes cadenas poliméricas) [33]. Estos copolímeros permiten la formación de nanoestructuras en la matriz polimérica, pudiendo actuar como puntos de nucleación para las celdas. Además, si alguno de los bloques del copolímero presenta una mayor afinidad por el CO_2 que el otro, las nanoestructuras conformadas por ese bloque podrán almacenar más gas para inducir la nucleación y el crecimiento de las celdas [32].

En este campo de investigación los mejores resultados obtenidos mediante el empleo de la variación de presión fueron logrados por J. Pinto et al. [34] a partir de muestras de PMMA (poli(metil metacrilato)). En este trabajo se lograron tasas de nucleación cercanas a 10^{15} núcleos/cm^3 y tamaños de celda en torno a 90 nm para una presión de saturación de 30 MPa. De forma similar S. Costeux et al. [35] lograron tasas de nucleación cercanas a $5{\cdot}10^{15}$ núcleos/cm^3 para una presión de saturación de 33 MPa y utilizando como polímero el PMMA-co-EA (poli(metil metacrilato)-co-etil acrilato). Los tamaños de celda obtenidos en este caso estaban por debajo de los 100 nm y las porosidades logradas rondaban el 60 %. En el caso del uso de copolímeros de bloque, los mejores resultados obtenidos fueron logrados por Yokoyama et al. [36] y Yokoyama y Sugiyama [37], que obtuvieron densidades de nucleación cercanas a los 10^{16} núcleos/cm^3 y tamaños de celda en torno a 15-30 nm en films de PS-*b*-PFMA (poliestireno-b-poli(perfluorooctyl etilmetacrilato)) y PS-*b*-PFS (poliestireno-b-poly(perfluorooctyl propiloxi estireno)). En ambos casos los bloques fluorados presentaban una mayor afinidad por el CO_2 que la matriz de poliestireno

S2. Marco de la Tesis

Este trabajo forma parte de las investigaciones en materiales celulares dirigidas por el profesor Miguel Ángel Rodríguez-Pérez en el Laboratorio CellMat del Departamento de Física de la Materia Condensada de la Universidad de Valladolid.

El Laboratorio CellMat se creó en 1999 en la Universidad de Valladolid tras la defensa de la primera tesis doctoral dentro de una línea de trabajo sobre propiedades térmicas y mecánicas de espumas de poliolefinas llevada a cabo por Miguel Ángel Rodríguez Pérez y dirigida por el profesor José Antonio de Saja Sáez [38]. A partir de entonces, bajo la dirección del profesor Miguel Ángel Rodríguez Pérez y del profesor José Antonio de Saja Sáez, se han desarrollado veintidós tesis doctorales [39-55] y se han publicado más de 150 artículos en revistas internacionales en el ámbito de los materiales celulares. En la actualidad CellMat mantiene cinco líneas de investigación principales: polímeros microcelulares y nanocelulares [56-59], nanocomposites celulares [60-63], polímeros celulares a partir de bioplásticos [64-66], espumas metálicas [67-70], y desarrollo de nuevas técnicas experimentales y dispositivos para el estudio de los mecanismos de espumado [71-74].

Dentro del campo de los polímeros microcelulares y nanocelulares, en el año 2014 se presentó en el laboratorio CellMat la primera tesis doctoral centrada en el campo de los materiales nanocelulares [51]. Esta tesis se enfocó fundamentalmente en la producción y en los mecanismos de espumado de polímeros nanocelulares obtenidos a partir de mezclas de poli(metil metacrilato) (PMMA) y MAM (copolímero de bloque compuesto por un bloque de PMMA, un bloque de PBA (poli(butil acrilato)) y otro bloque de PMMA). Además se empezaron a estudiar algunas de las propiedades físicas de estos sistemas: conductividad térmica, temperatura de transición vítrea y módulo de Young, encontrándose ciertas diferencias con las propiedades de los materiales microcelulares (materiales con tamaños de celda mayores de 10 µm y densidades de celda en torno a 10^9 celdas/cm^3).

Así pues, una vez establecidos y conocidos los mecanismos dominantes en la producción y espumado de estos materiales, la presente investigación se centra en el análisis detallado de las distintas propiedades físicas de los polímeros nanocelulares y su comparación con las polímeros celulares convencionales y los microcelulares. De esta forma se presenta un estudio exhaustivo que va a arrojar luz sobre la validez de las hipótesis ampliamente extendidas sobre las diversas propiedades y ventajas esperadas de los nuevos materiales nanocelulares frente a los existentes actualmente.

S3. Objetivos

Tradicionalmente existen cuatro áreas principales de interés en el estudio de un nuevo material celular: su ruta de producción, su estructura celular, sus propiedades y sus potenciales aplicaciones. Estos aspectos están fuertemente interrelacionados, tal y como muestra el tetraedro de la Figura 0.5.

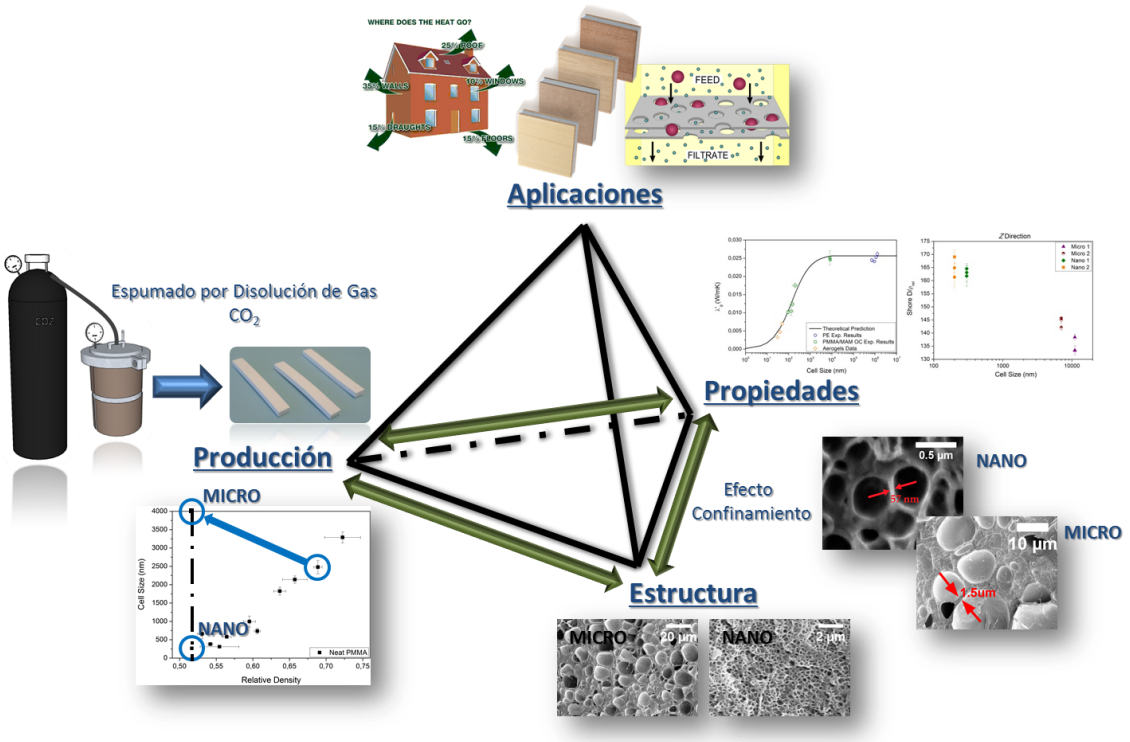

Figura 0.5. Tetraedro de la ciencia de los materiales y sus inter-relaciones para los materiales celulares

Basándonos en este concepto, el objetivo de este trabajo ha sido estudiar de forma sistemática los cambios en las propiedades físicas entre los polímeros micro y nanocelulares. Con este propósito el proceso de producción tuvo que ser optimizado para obtener polímeros micro y nanocelulares con densidades relativas similares así como con dimensiones y geometrías apropiadas para su posterior caracterización. El sistema empleado para ello fueron polímeros celulares basados en PMMA (poli(metil metacrilato)) y mezclas de PMMA/MAM. Como ya se ha mencionado, este sistema fue estudiado con anterioridad en lo referente a mecanismos de producción y espumado, de manera que este estudio se ha centrado en la realización de un estudio sistemático de las propiedades físicas de los polímeros nanocelulares en comparación con los polímeros microcelulares y en la comprensión de las diferencias claves teniendo en cuenta las diferencias estructurales entre los materiales.

Así, los tres principales objetivos técnicos de este trabajo pueden resumirse como sigue:

1. Solventar las limitaciones existentes para producir polímeros micro y nanocelulares con dimensiones y geometrías apropiadas así como densidades relativas similares para realizar una caracterización de las propiedades físicas usando métodos estándar (“Producción”).

2. Proporcionar una mejor compresión de los mecanismos involucrados en la aparición de las distintas propiedades físicas de los sistemas nanocelulares (“Estructura ↔ Propiedades”).

3. Estudiar si existe una transición en las propiedades de estos materiales cuando el tamaño de celda pasa del rango microcelular al rango nanocelular y determinar la validez de las hipótesis efectuadas al respecto en los últimos años..

Asimismo se han definido objetivos parciales dentro de los objetivos principales de cara a definir precisamente el enfoque y la extensión de cada uno de ellos.

Desde el punto de vista de la técnica de producción queremos obtener polímeros nanocelulares con los siguientes requisitos:

- Los materiales de partida deben ser fácilmente accesibles y preferiblemente ser polímeros comerciales.

- Las mezclas sólidas polímero/copolímero deben presentar nanoestructuración mediante auto organización.

- Deben obtenerse muestras con un tamaño suficientemente grande y geometrías apropiadas que permitan su posterior caracterización mediante protocolos estándar.

- Deben obtenerse muestras con densidades relativas similares y que presenten una reducción significativa de la densidad (en torno al 50 % en comparación con el material sólido), no afectando el grado de reducción de densidad a la presencia de estructuras celulares micro o nanométricas.

- La ruta de producción debe ser escalable industrialmente, evitando requerimientos como velocidades de despresurización extremadamente altas, elevadas presiones de saturación, bajas temperaturas de saturación (por debajo de temperatura ambiente), etc.

Desde el punto de vista científico, hemos centrado parte de nuestra investigación en los mecanismos subyacentes que dan lugar a la aparición de fenómenos o mecanismos no esperados. En particular nos hemos preguntado:

- ¿La reducción del tamaño de celda al rango nanométrico produce un confinamiento de las macromoléculas poliméricas?

- ¿Qué influencia tiene el confinamiento de la fase gaseosa en las propiedades físicas?

- ¿Cómo influye la tortuosidad en las propiedades físicas cuando cambiamos de la escala de tamaños celulares micrométricos a la escala de tamaños celulares nanométricos?

Y finalmente, desde el punto de vista del análisis de la esperada mejora de las propiedades físicas de los polímeros nanocelulares respecto a las microcelulares, nos hemos centrado en:

- Conductividad térmica: se espera que la conductividad térmica de la fase gaseosa de los polímeros nanocelulares sea menor que la de los polímeros microcelulares debido al efecto Knudsen [75].

- Propiedades mecánicas: en los polímeros microcelulares se ha descrito tradicionalmente una mejora de sus propiedades mecánicas con la reducción del tamaño de celda en comparación con los polímeros celulares convencionales [76]. Se espera por tanto que los polímeros nanocelulares presenten mejores propiedades mecánicas que los polímeros microcelulares.

- Propiedades dieléctricas: se espera que el comportamiento dieléctrico de los polímeros nanocelulares sea diferente al de las microcelulares debido al confinamiento de la fase sólida y gaseosa.

- Propiedades acústicas: se espera que el comportamiento acústico de los polímeros nanocelulares difiera del de las microcelulares debido al cambio estructural de las unas con respecto a las otras.

S4. Estructura de la Tesis

El trabajo de investigación presentado en esta tesis se presenta para optar al grado de *Doctor* con mención *Internacional*. Por este motivo el cuerpo principal de la tesis está redactado en inglés.

Además esta tesis está escrita como compendio de publicaciones. Incluyendo seis artículos enviados a revistas internacionales (cuatro ya publicados y dos de ellos pendientes de ser aceptados). Así mismo se han incluido algunos resultados no publicados para proporcionar una mejor comprensión del trabajo y para alcanzar los objetivos previamente definidos. La Tabla 0-1 muestra los artículos incluidos en la tesis, indicando en qué capítulo se encuentran.

Otras publicaciones en revistas con proceso de revisión por pares, contribuciones a congresos internacionales (relativas a la tesis u otros campos de investigación), estancias de investigación en otras instituciones, y la participación en proyectos de investigación durante los últimos cuatro años se muestran en las tablas 0-2, 0-3, 0-4, 0-5 y 0-6, respectivamente.

La tesis está dividida en siete capítulos, incluyendo la siguiente información:

La introducción describe el estado del arte referente a las distintas propiedades físicas de los polímeros nanocelulares poliméricas, comparándolo a su vez con otros materiales nanocelulares no poliméricos. En dicha introducción también se describen brevemente los distintos métodos de fabricación de los polímeros nanocelulares, los parámetros que pueden verse afectados por el cambio de escala, y las potenciales aplicaciones que estos polímeros celulares pueden tener en un futuro cercano.

El capítulo 1 describe los materiales de partida usados en esta investigación, PMMA y MAM, y las rutas de producción de las mezclas de PMMA/MAM y de los polímeros microcelulares y nanocelulares. Se describen las técnicas de caracterización y las estructuras celulares obtenidas.

El capítulo 2 pone de manifiesto un interesante efecto que puede aparecer como consecuencia de la reducción del tamaño de poro al rango nanométrico y del aumento de la densidad celular. En este capítulo se demuestra cómo la reducción del espesor de la pared de las celdas confina las cadenas poliméricas dentro de las paredes celulares conduciendo a una reducción de la movilidad de las macromoléculas poliméricas (efecto de confinamiento) dando lugar a efectos macroscópicos cuantificables.

El capítulo 3 estudia la conductividad térmica de los polímeros nanocelulares en comparación con la de los polímeros microcelulares. En este caso se demuestra cómo el confinamiento de las fases constituyentes de la espuma (gas y sólido) permite reducir notablemente la conductividad térmica del sistema.

El capítulo 4 realiza un estudio comparativo de las propiedades mecánicas entre polímeros microcelulares y nanocelulares de PMMA de densidades relativas similares. En este apartado se demuestra que los polímeros nanocelulares presentan un módulo de Young, una resistencia al impacto y una dureza shore superior a la de los polímeros microcelulares.

En el capítulo 5 se estudian las propiedades dieléctricas de polímeros micro y nanocelulares de PMMA, encontrando una clara transición en dichas propiedades. Se muestra una evolución desde un comportamiento capacitivo a una combinación de un comportamiento capacitivo y resistivo cuando el tamaño de celda pasa del rango micro al nanométrico.

El capítulo 6 analiza las propiedades acústicas de polímeros de PMMA nanocelulares comparadas con las propiedades acústicas de polímeros microcelulares de PMMA de densidades relativas similares. Además se realiza un estudio comparativo de los distintos modelos teóricos que podrían utilizarse para modelizar los resultados obtenidos.

El último capítulo recoge las principales conclusiones de este trabajo, e incluye sugerencias para la continuación de esta línea de investigación en el futuro. Asimismo, se incluye una discusión general sobre el efecto que cada uno de los parámetros (confinamiento de las fases sólida y gaseosa, tortuosidad, etc.) tiene sobre las propiedades de los polímeros nanocelulares.

Con el ánimo de proporcionar una mejor compresión de la estructura de la tesis y las relaciones entre los distintos capítulos se ha incluido el esquema de la Figura 0.6.

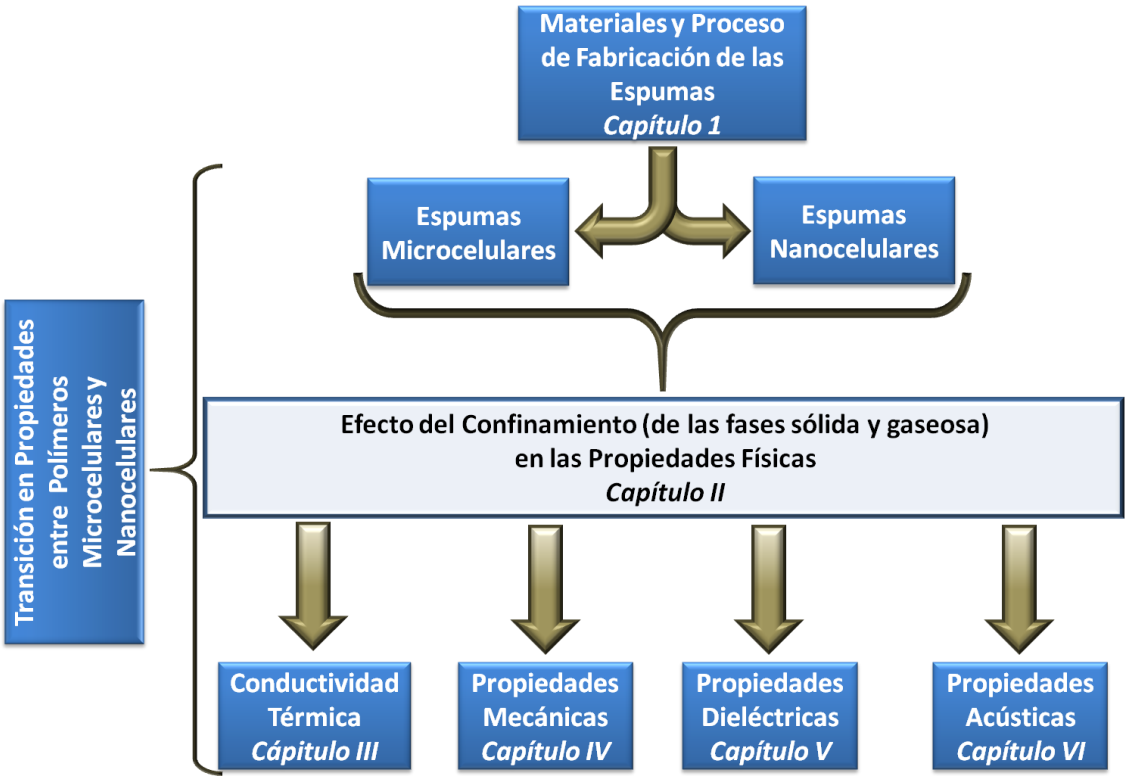

Figura 0.6. Esquema de la estructura de la tesis

Tabla 0-1. Publicaciones en revistas internacionales incluidas en la tesis

Publicaciones enviadas a revistas internacionales	Capítulo
B. Notario, J. Pinto, E. Solórzano, J. A. de Saja, M. Dumon, M. A. Rodríguez-Pérez **Experimental Validation of the Knudsen Effect in Nanocellular Polymeric Foams** *Polymer 56, 57-67 (2015)* ***Invited Article***	III
B. Notario, J. Pinto, M. A. Rodríguez-Pérez **Towards a New Generation of Polymeric Foams: PMMA Nanocellular Foams with Enhanced Physical Properties** *Polymer 63, 116-126 (2015)*	IV
J. Pinto, B. Notario, R. Verdejo, M. Dumon, S. Costeux, M. A. Rodríguez-Pérez **Molecular Confinement of Solid and Gaseous Phases of Self-Standing Nanoporous Polymers Inducing Enhanced and Unexpected Physical Properties** *The Journal of Physical Chemistry Letters (2016) Enviado*	II
B. Notario, J. Pinto, M. A. Rodríguez-Pérez **Nanoporous Polymeric Materials: a New Class of Materials with Enhanced Properties** *Progress in Materials Science 78-79, 93-139 (2016)*	0
B. Notario, J. Pinto, R. Verdejo, M. A. Rodríguez-Pérez **Dielectric Behavior of Porous PMMA: from the Micrometer to the Nanometer Scale** *Polymer (2015) Enviado*	V
B. Notario, A. Ballesteros, J. Pinto, M. A. Rodríguez-Pérez **Nanoporous PMMA: a Novel System with Different Acoustic Properties** *Materials Letters 168, 76-79 (2016)*	VI

Tabla 0-2. Otras publicaciones en revistas internacionales

Otras publicaciones enviadas a revistas internacionales
B. Notario, J. Pinto, E. Solórzano, J. Escudero, J. Martín-de León, D. Velasco, M. A. Rodríguez-Pérez **In-Situ Optical Analysis of Structural Changes in Polylactic Acid (PLA) during the Gas Dissolution Process** *Defect and Diffusion Forum 353, 131-136 (2014)*
J. Escudero, B. Notario, C. Jiménez, M. A. Rodríguez-Pérez **Characterization of Nanoclays Intercalation during Foaming by Using in Situ Energy-Dispersive X-Ray Diffraction** *Journal of Applied Polymer Science 133, 43432-43440 (2016)*

Tabla 0-3. Contribuciones en congresos internacionales relativas a la tesis

Contribuciones en congresos internacionales relativas a la tesis
B. Notario, J. Pinto, E. Solórzano, J. Escudero, J. Martín-de León, D. Velasco, M. A. Rodríguez-Pérez **Analysis of Structural Changes in Amorphous Polymers during the Gas Dissolution Process** **Oral**. *DSL 2013, Madrid (España) (2013)*
B. Notario, J. Pinto, E. Solórzano, A. Martín-Cid, M. A. Rodríguez-Pérez, M. Dumon **Physical Properties of Nanocellular Foams: the Transition from the Micro to the Nano Scale** **Oral**. *International Conference on Foams and Foams Technology, FOAMS 2014, Nueva Jersey (EEUU) (2014)*
S. Perez-Tamarit, B. Notario, E. Solorzano, M. A. Rodríguez-Pérez **Cell Size Determination by means of Light Scattering Methodologies in Micro and Nanoporous Foams** **Oral**. *7th European School on Molecular Nanoscience (ESMolNa), Gandía (España) (2014)*
M. A. Rodríguez-Pérez, B. Notario, J. Pinto **Physical Properties of Nanocellular Foams: the Transition from the Micro to the Nano Scale** **Oral. Invitada**. *IMP Workshops, Processing and Applications of Polymer Foams, Lyon-Villeurbanne (Francia) (2015)*
B. Notario, J. Pinto, M. A. Rodríguez-Pérez **The Influence of Reducing the Cell Size to the Nanoscale on the Physical Properties of Polymeric Nanocellular Foams** **Oral**. *International Conference on Composite Materials, Copenhage (Dinamarca) (2015)*
B. Notario, J. Pinto, M. A. Rodríguez-Pérez **Improving the Properties of Polymer Foams by Reducing the Cell Size to the Nanoscale** **Keynote**. *Polymer Foams Conference, Colonia (Alemania) (2015)*

Tabla 0-4. Otras comunicaciones en congresos internacionales

Otras comunicaciones en congresos internacionales
B. Notario, C. Jiménez, J. Escudero, M. A. Rodríguez-Pérez, M. Klaus **Seguimiento In-Situ de la Exfoliación de Nanoarcillas mediante ED-XRD durante el Espumado de Materiales Termoplásticos** **Oral**. *XIII Escuela Nacional de Materiales Moleculares, El Escorial, Madrid (España) (2012)*
A. Esteban-Cubillo, J. Santaren, A. Alvarez, B. Notario, D. Velasco, M. A. Rodríguez-Pérez **Improving the Cellular Structure and Thermal Conductivity of Polystyrene Foams by Using Sepiolite** **Oral**. *International Conference on Foams and Foams Technology, FOAMS 2012, Barcelona (España) (2012)*
B. Notario, J. Escudero, M. A. Rodríguez-Pérez **In-Situ Study of the Foaming Process of Polyethylene Reinforced with Nanoclays** **Poster**. *International Conference on Foams and Foams Technology, FOAMS 2012, Barcelona (España) (2012)*
B. Notario, J. Escudero, A. López, M. A. Rodríguez-Pérez **Foaming Induces Exfoliation in Polyolefins containing Clay Nanoparticles: In-Situ Evolution of the Process by using XRD of Synchrotron Light and Applicability to the Production of Foams with Improved Properties** **Oral**. *International Conference on Foams and Foams Technology, FOAMS 2013, Seattle (EEUU) (2013)*
B. Notario, J. Escudero, M. A. Rodríguez-Pérez, C. Jiménez, M. Klaus **Characterization by Synchrotron Radiation of the Foaming Process of Polyethylene Reinforced with Nanoclays: Analysis of the Exfoliation induced by Foaming Phenomenon** **Poster**. *International Conference on Foams and Foams Technology, FOAMS 2014, Nueva Jersey (USA) (2014)* ***Best Poster Award***
B. Notario, J. Escudero, M. A. Rodríguez-Pérez, C. Jiménez, M. Klaus **Characterization by Synchrotron Radiation of the Foaming Process of Polyethylene Reinforced with Nanoclays: Analysis of the Exfoliation induced by Foaming Phenomenon** **Poster**. *HZB User Meeting, Berlin (Alemania) (2014)*
C. Jimenez, M. Paeplow, Ch. Fella, A. Balles, W. Wiest, B. Notario, S. Zabler, F. García-Moreno **Possibilities for In-Situ Imaging of Metallic and Polymeric Foams using Laboratory Liquid Metal Jet and Microfocus X-Ray Sources** **Poster**. *Metfoam 2015, Barcelona (España) (2015)*
B. Notario, E. Laguna-Gutiérrez, J. Pinto, M. A. Rodríguez-Pérez **Final Year Project in Physics´s Degree: a New Challenge for the Scientific and Technical Training of Students in their Last Year of the Physics' Degree** **Virtual**. *7th International Conference on Education and New Learning Technologies (EDULEARN15), Barcelona (España) (2015)*
E. Laguna-Gutiérrez, B. Notario, J. Pinto, M. A. Rodríguez-Pérez **Preparing Students of Scientific and Technical Degrees for their Future Professional Careers** **Virtual**. *7th International Conference on Education and New Learning Technologies (EDULEARN15), Barcelona (España) (2015)*

Tabla 0-5. Estancias en otros centros de investigación

Estancias en otros centros de investigación
Dos meses en el Helmholtz-Zentrum Berlin (HZB) de Berlín (Alemania) en 2011 **Objetivo: Estudio comparativo del espumado de metales y polímeros mediante técnicas in-situ**
Tres meses en el Microcellular Plastics Laboratory (Mechanical Engineering Department) de la Universidad de Washington (EEUU) en 2015 **Objetivo: Fabricación de polímeros nanocelulares basados en PMMA mediante el método de disolución de gas a bajas temperaturas de saturación. Estudio de la conductividad térmica de espumas microcelulares de PEI, PC y ABS.**

Tabla 0-6. Participación en otros proyectos de investigación financiados en los últimos 4 años

Research funded projects
Ministerio de Ciencia e Innovación (Plan Nacional de Materiales). **MAT2012-34901**
Junta de Castilla y León. **VA035U13**
Ministerio de Ciencia e Innovación (Programa Impacto). **IPT-2011-0725-310000**
Junta de Castilla y León. **VA174A12-2**
Ministerio de Ciencia e Innovación (Plan Nacional de Materiales). **MAT209-14001-C02-01**
FP7 Comisión Europea. **NANCORE 214148**
Agencia Espacial Europea. **UGFOAM 14308/00/NL/SH**
ABN PIPE SYSTEMS SLU. **FINANCIACIÓN PRIVADA**
Dow Chemical. **FINANCIACIÓN PRIVADA**
Tolsa S.A. **FINANCIACIÓN PRIVADA**
FERRO SPAIN. **FINANCIACIÓN PRIVADA**

S5. Principales Resultados

A continuación se van a introducir las principales conclusiones obtenidas en este trabajo de investigación:

- El PMMA y las mezclas de PMMA/MAM han mostrado ser excelentes materiales para la producción de materiales poliméricos nanocelulares de densidades medias, siendo estos materiales de partida comerciales de fácil acceso.

- Se han obtenido polímeros nanocelulares a partir de muestras sólidas de varios milímetros de espesor, por medio del proceso de espumado por disolución de CO_2 y usando condiciones de proceso accesibles. Por ejemplo no se han utilizado presiones superiores a 30 MPa ni temperaturas de saturación superiores a 23 ºC.

- Se han obtenido de manera controlada polímeros microcelulares y nanocelulares con densidades relativas similares (en torno a 0.5) y dimensiones macroscópicas y geometrías apropiadas para poder realizar una caracterización de las propiedades físicas usando técnicas estándar. El tipo de polímero celular final (micro o nanocellular)

puede elegirse ajustando la presión de saturación y las condiciones de espumado (tiempo y temperatura).

- Se han encontrado nuevos efectos o comportamientos no esperados debidos al confinamiento de los elementos constituyentes de la espuma en el rango nanométrico, entre los que cabe destacar: un aumento de la temperatura de transición vítrea, una disminución de la conductividad térmica de la fase sólida y un aumento de la rigidez de la matriz polimérica.

- Se ha encontrado una reducción clara de la conductividad térmica de la fase gaseosa en polímeros celulares basadas en PMMA para tamaños de celda por debajo de la micra, validándose experimentalmente por primera vez la aparición del efecto Knudsen en materiales celulares poliméricos.

- Se ha encontrado una clara transición entre los polímeros microcelulares y nanocelulares de PMMA en cuanto a las propiedades mecánicas a altas deformaciones (impacto Charpy). A bajas deformaciones, existe una clara mejora de la dureza shore y del módulo de Young de los polímeros nanocelulares frente a los microcelulares. Sin embargo, la deformación a rotura y el esfuerzo de fluencia de los polímeros nanocelulares es inferior a los microcelulares.

- Se ha encontrado una clara transición en el comportamiento dieléctrico entre polímeros microcelulares y nanocelulares de PMMA, pasando de un comportamiento capacitivo (en el caso de los polímeros microcelulares) a una combinación de comportamiento capacitivo y resistivo (en el caso de los polímeros nanocelulares). Así mismo, se muestra una importante reducción de la constante dieléctrica de los polímeros nanocelulares con respecto al sólido, y la existencia de un efecto de confinamiento de las cadenas poliméricas en el dominio de la temperatura (desde -20 hasta 110 ºC) cuando nos movemos al rango nanométrico.

- Se ha encontrado un comportamiento acústico diferente, tanto en absorción como en transmisión, entre los polímeros microcelulares y nanocelulares. El diferente mecanismo de propagación de la onda en la escala micro y nanométrica (el cual está determinado por el confinamiento tanto de la fase sólida como de la gaseosa) podría ser la razón de estas diferencias.

S6. Referencias

1. EU EU. Horizon 2020. Work Programme 2014-2015. 2013.
2. Gibson LJ and Ashby MF. Cellular Solids: Structure and Properties, 2nd ed. Cambridge: Cambridge University Press, 1997.
3. Klempner D, Sendijarevi'c V, and Aseeva RM. Handbook of Polymeric Foams and Foam Technology. Munich: Hanser Publishers, 2004.
4. Gibson LJ, Ashby MF, and Harley BA. Cellular Materials in Nature and Medicine. Cambridge, U.K.: Cambridge University Press, 2010.
5. Weaire D and Hutzler S. The Physics of Foams. Oxford, U.K.: Oxford University Press, 1999.
6. Davies GJ and Zhen S. Journal of Materials Science 1983;18(7):1899-1911.
7. Eaves D. Handbook of Polymer Foams: Rapra Technology, 2004.
8. Bhaduri SB. Advanced Performance Materials 1994;1(3):205-220.
9. Solórzano E and Rodriguez-Perez MA. Polymer Foams. In: Busse M, Herrmann AS, Kayvantash K, and Lehmhus D, editors. Structural Materials and Processes in Transportation. Weinheim (Germany): Wiley-VCH, 2013.
10. Papadopoulos AM. Energy and Buildings 2005;37(1):77-86.
11. Díez-Gutiérrez S, Rodriguez-Perez MA, Machimbarranea M, González J, and De Saja JA. Journal of Building and Acoustics 2003;10(3):261-271.
12. Twigg MV and Richardson JT. Chemical Engineering Research and Design 2002;80(2):183-189.
13. Schmidt D, Raman VI, Egger C, du Fresne C, and Schädler V. Materials Science and Engineering: C 2007;27(5–8):1487-1490.
14. Pajonk GM. Journal of non-crystalline solids 1998;225:307-314.
15. Hentze HP and Antonietti M. Reviews in molecular biotechnology 2002;90(1):27-53.
16. Madou MJ. Fundamentals of Microfabrication: The Science of Miniaturization, Second Edition. Boca Raton: CRC, 2002.
17. Hillmyer MA. Nanoporous materials from block copolymer precursors. Block Copolymers II: Springer, 2005. pp. 137-181.
18. Olson DA, Chen L, and Hillmyer MA. Chemistry of materials 2007;20(3):869-890.
19. Hedrick JL, Miller RD, Hawker CJ, Carter KR, Volksen W, Yoon DY, and Trolls\aas M. Advanced Materials 1998;10(13):1049-1053.
20. Hentze HP and Antonietti M. Current Opinion in Solid State and Materials Science 2001;5(4):343-353.
21. Jackson EA and Hillmyer MA. ACS nano 2010;4(7):3548-3553.
22. Hedrick JL, Carter KR, Labadie JW, Miller RD, Volksen W, Hawker CJ, Yoon DY, Russell TP, McGrath JE, and Briber RM. Nanoporous polyimides. Progress in Polyimide Chemistry II: Springer, 1999. pp. 1-43.
23. Lazzari M and López-Quintela MA. Advanced Materials 2003;15(19):1583-1594.
24. Park C, Yoon J, and Thomas EL. Polymer 2003;44(22):6725-6760.
25. Kazarian SG. Polymer Science, Series C 2000;42(1):78-101.
26. Tsivintzelis I, Angelopoulou AG, and Panayiotou C. Polymer 2007;48(20):5928-5939.
27. Reverchon E and Cardea J. Journal of Supercritical Fluids 2007;40:144-152.
28. Reglero Ruiz JA, Viot P, and Dumon M. Journal of Applied Polymer Science 2010;118(1):320-331.
29. Kumar V and Suh NP. Polymer Engineering & Science 1990;30(20):1323-1329.
30. Goel SK and Beckman EJ. Polymer Engineering & Science 1994;34(14):1148-1156.
31. Guo Q, Wang J, and Park CB. Industrial & Engineering Chemistry Research 2006;45(18):6153-6161.
32. Spitael P, Macosko CW, and McClurg RB. Macromolecules 2004;37(18):6874-6882.

33. Ruckdäschel H, Gutmann P, Altstädt V, Schmalz H, and Müller AHE. Foaming of microstructured and nanostructured polymer blends. Complex Macromolecular Systems I: Springer, 2010. pp. 199-252.
34. Pinto J, Dumon M, Pedros M, Reglero JA, and Rodriguez-Perez MA. Chemical Engineering Journal 2014;243C:428-435.
35. Costeux S, Bunker SP, and Jeon HK. Journal of Materials Research 2013;28(17):2351-2365.
36. Yokoyama BH, Li L, Nemoto T, and Sugiyama K. Advanced Materials 2004;16(17):1542-1546.
37. Yokoyama H and Sugiyama K. Macromolecules 2005;38(25):10516-10522.
38. Rodriguez-Perez MA. Propiedades Térmicas y Mecánicas de Espumas de Poliolefinas. Universidad de Valladolid, 1998.
39. Almanza O. Caracterización y Modelización de las Propiedades Térmicas y Mecánicas en Espumas de Poliolefinas. Universidad de Valladolid, 2000.
40. Arcos y Rábado LO. Propiedades Térmicas y Mecánicas de Espumas de Poliolefinas Fabricadas en un Proceso de Moldeo por Compresión. Universidad de Valladolid, 2002.
41. Ruiz-Herrero JL. Impacto y Fluencia de Espumas con Base Polietileno. Universidad de Valladolid, 2004.
42. González-Peña JI. Efecto de los Tratamientos Térmicos en Bloques de Espuma de Polietileno de Baja Densidad Producidos Mediante Moldeo por Compresión. Universidad de Valladolid, 2006.
43. Álvarez-Laínez M. Propiedades Térmicas, Mecánicas y Acústicas de Espumas de Poliolefina de Celda Abierta. Universidad de Valladolid, 2007.
44. Reglero Ruiz JA. Manufacture and characterization of aluminium foams: Applications in the aeronautical sector. Universidad de Valladolid, 2007.
45. Solórzano E. Aluminium foams: Foaming process, cellular structure & properties. Universidad de Valladolid, 2008.
46. Hidalgo-González F. Diseño Optimizado de los Parámetros de Proceso de Fabricación de Espuma de Poliolefina Reticulada mediante Moldeo por Compresión. Universidad de Valladolid, 2008.
47. Román-Lorza S. Fabrication and characterization of flame retardant halogen free polyolefin based cellular materials. Universidad de Valladolid, 2010.
48. Campo-Arnáiz R. Aplicación de Técnicas Espectroscópicas al Estudio de la Morfología Polimérica, Propiedades Térmicas y de Emisión de Espumas de Baja Densidad con Base Poliolefina. Universidad de Valladolid, 2011.
49. Saiz-Arroyo C. Fabricación de materiales celulares mejorados basados en poliolefinas. Relación procesado-composición-estructura-propiedades. Universidad de Valladolid, 2012.
50. Lobos Martín J. Improving the stiffness and strength of porous materials by enhancement of the matrix microstructure and cellular morphology. Universidad de Valladolid, 2013.
51. Pinto J. Fabrication and characeterization of nanocellular polymeric materials from nanostructured polymers. University of Valladolid & University of Bordeaux, 2014.
52. Pardo-Alonso S. X-Ray Imaging Applied to the Characterization of Polymer Foams' Cellular Structure and Its Evolution. University of Valladolid, 2014.
53. Estravis S. CELLULAR NANOCOMPOSITES BASED ON RIGID POLYURETHANE AND NANOCLAYS: FABRICATION, CHARACTERIZATION AND MODELING OF THE MECHANICAL AND THERMAL PROPERTIES. University of Valladolid, 2014.
54. Oliveira-Salmazo L. CINÉTICAS DE ESPUMACIÓN Y CONTROL DE LA ESTRUCTURA CELULAR EN MATERIALES BASADOS EN CAUCHO NATURAL Y POLIOLEFINAS University of Valladolid & Universidad Estadual Paulista "Julio de Mesquita Filho", 2015.

55. Lázaro J. Optimización de la Estructura Celular en Espumas de Aluminio. University of Valladolid, 2014.
56. Rodriguez-Perez MA, Lobos J, Perez-Muñoz CA, and Saja JAd. Journal of Cellular Plastics 2009;45(5):389-403.
57. Reglero Ruiz JA, Saiz-Arroyo C, Dumon M, Rodríguez-Perez MA, and Gonzalez L. Polymer international 2011;60(1):146-152.
58. Pinto J, Reglero-Ruiz JA, Dumon M, and Rodriguez-Perez MA. The Journal of Supercritical Fluids 2014;94:198-205.
59. Pinto J, Dumon M, Rodriguez-Perez MA, Garcia R, and Dietz C. The Journal of Physical Chemistry C 2014;118(9):4656-4663.
60. Verdejo R, Saiz-Arroyo C, Carretero-Gonzalez J, Barroso-Bujans F, Rodriguez-Perez MA, and Lopez-Manchado MA. European Polymer Journal 2008;44(9):2790-2797.
61. Velasco JI, Antunes M, Ayyad O, Saiz-Arroyo C, Rodríguez-Pérez MA, Hidalgo F, and de Saja JA. Journal of Applied Polymer Science 2007;105(3):1658-1667.
62. Román-Lorza S, Rodriguez-Perez MA, Sáez JADS, and Zurro J. Journal of Cellular Plastics 2010;46(3):259-279.
63. Ma Y, Pyrz R, Rodriguez-Perez MA, Escudero J, Rauhe JC, and Su X. Cellular polymers 2011;30(3):95-109.
64. Wang Y, Rodriguez-Perez MA, Reis RL, and Mano JF. Macromolecular Materials and Engineering 2005;290(8):792-801.
65. Simoes RD, Rodriguez-Perez MA, De Saja JA, and Constantino CJL. Polymer Engineering & Science 2009;49(11):2150-2157.
66. Rodriguez-Perez MA, Simoes RD, Roman-Lorza S, Alvarez-Lainez M, Montoya-Mesa C, Constantino CJL, and de Saja JA. Polymer Engineering & Science 2012;52(1):62-70.
67. Solórzano E, Rodríguez-Perez MA, Reglero JA, and de Saja JA. Advanced Engineering Materials 2007;9(11):955-958.
68. Solórzano E, Rodriguez-Perez MA, and de Saja JA. Advanced Engineering Materials 2008;10(4):371-377.
69. Lázaro J, Solórzano E, Saja JAd, and Rodríguez-Pérez MA. Journal of materials science 2013;48(14):5036-5046.
70. Garcia-Moreno F, Solórzano E, and Banhart J. Soft Matter 2011;7(19):9216-9223.
71. Solórzano E, Pinto J, Pardo S, Garcia-Moreno F, and Rodriguez-Perez MA. Polymer Testing 2013;32(2):321-329.
72. Solórzano E, Pardo-Alonso S, Saja JAd, and Rodriguez-Perez MA. Colloids and Surfaces A: Physicochemical and Engineering Aspects 2013;438:167-173.
73. Solórzano E, Antunes M, Saiz-Arroyo C, Rodríguez-Pérez MA, Velasco JI, and de Saja JA. Journal of Applied Polymer Science 2012;125(2):1059-1067.
74. Pardo-Alonso S, Solórzano E, Brabant L, Vanderniepen P, Dierick M, Van Hoorebeke L, and Rodríguez-Pérez MA. European Polymer Journal 2013;49(5):999-1006.
75. Lu X, Caps R, Fricke J, Alviso CT, and Pekala RW. Journal of non-crystalline solids 1995;188(3):226-234.
76. Weller E and Kumar V. Handbook of Polymeric Foams. UK: Rapra Technology, 2004.

INTRODUCTION

0. Introduction

0.1 Introduction

Materials Science is an interdisciplinary field which deals with the investigation of the relationship between the structure and properties of the materials. This field allows, on the one hand, developing materials with unique properties, or improving the properties or production routes of known materials. This fact expands the range of application of these materials or even leads to completely new applications. It should be clarified that it is the materials engineering, who based on the structure-property-production-applications relationship, designs or projects the structure of a material to achieve a predetermined set of properties. Sometimes it is difficult to define a border between the two concepts because both present a common area. What is clear is that both must walk together to achieve the goal.

Advances on other scientific fields and development of new technological devices usually require new or tailored materials with specific properties. Owing to this duality, Materials Science is one of the main fields of interest of both public and private research organizations.

Indeed, the European Union (EU) established in December 2013 the research objectives of the program "*Horizon 2020*" (Horizon 2020, the EU Research and Innovation program for the period 2014-2020 [1]), in which multiple objectives are focused on Materials Science. Horizon 2020 has a strong focus on developing European industrial capabilities in Key Enabling Technologies (KETs). This part of the program covers different research areas such as nanotechnologies, advanced materials, advanced manufacturing and processing, and biotechnology. In particular, within these goals, a priority of the EU is the "*Manufacturing and control of nanoporous materials*".

The present thesis entitled "***Fabrication and characterization of the physical properties of nanocellular polymers: the transition from the micro to the nanoscale***" is part of this priority research field for the EU present and next period.

Generally speaking, polymeric cellular materials can be defined as a two-phase system in which a gas phase from a blowing agent, either physical or chemical, is dispersed throughout a solid polymeric matrix.

Although sometimes cellular materials are referred as foams it is necessary to clarify that a foam is a specific type of cellular material that has been produced by the expansion of a material in liquid state. Throughout the thesis the term of cellular material and foam will be used independently, but it must be clear that when we talk about foams we are referring to cellular materials.

Cellular materials can be classified attending to different criteria. A first classification can be made referring to the cellular structure and the connectivity of the cells: the structure can be open or closed, i.e. the gas volume forms a continuous phase (*Open Cell* structure, Figure 0.1 left) or a discontinuous phase (*Closed Cell* structure, Figure 0.1 right). Normally, it is easy to find materials with an intermediate structure: a fraction of the cellular structure is formed by open cells while other fraction of the cellular structure is formed by closed cells [2].

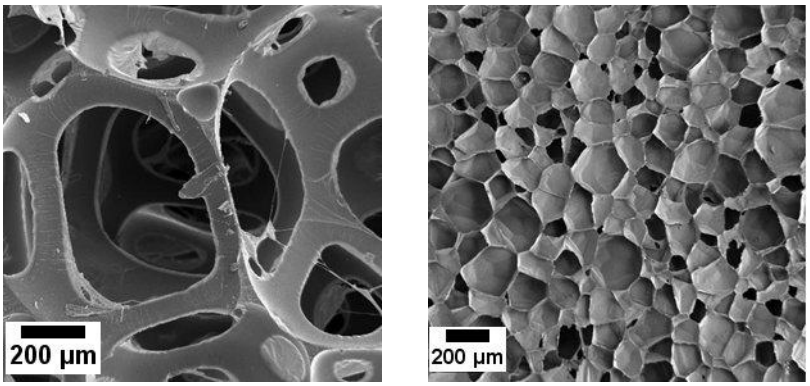

Figure 0.1. Left) open cell cellular polymer, Right) closed cell cellular polymer

Other classification of cellular materials can be made attending to their density, which highly determines the final properties, and consequently the final applications [2, 3]. In foamed materials it is usual to employ the parameter *Relative Density* ($\rho_{relative}$), which is the relationship between the cellular polymer density ($\rho_{cellular\ polymer}$) and the solid material density (ρ_{solid}) [2, 3]:

$$\rho_{relative} = \frac{\rho_{cellular\ polymer}}{\rho_{solid}} \tag{0-1}$$

According to their relative density, cellular materials can be classified in three different groups:

- Low density cellular materials: relative densities lower than 0.3.
- Medium density cellular materials: relative densities between 0.3 and 0.6.
- High density cellular materials: relative densities higher than 0.6.

Cellular polymer production aims to improve the properties of known materials, or to increase the range of their potential applications [2]. Besides offering a reduced density of the starting material (and then obtaining lighter pieces for the same size/application), cellular materials may present better properties than solid materials in different areas/applications, such as better insulating capacity, better impact resistance, sound absorption, etc.

However cellular materials are not a man invention, nature has widely used this approach in the evolution of life on the Earth. Wood, cork, corals, marine sponges, or bones of different species of vertebrates (Figure 0.2, left) are some of the best examples [4].

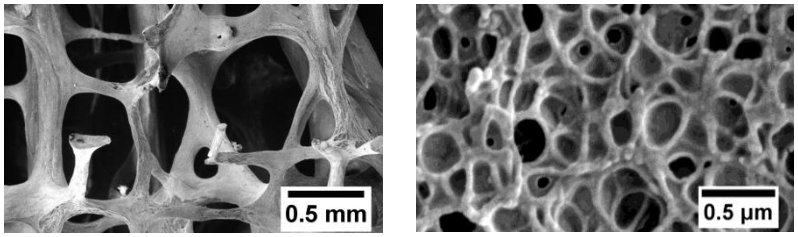

Figure 0.2. Porous structure of a human bone (left) and porous structure of a nanocellular polymer (right)

However, reproducing living structures by artificial means is never simple. Nowadays, cellular materials can be manufactured from multiple starting materials. These man-made materials cover from a simple unit cell repetition in the case of honeycombs (used as core in sandwich panels for structural applications) to three-dimensional stochastically structured cellular polymers made from liquids, polymers, metals, ceramics, etc. [3, 5-8]. These materials have applications in packaging, aeronautic industry, automotive industry [9], thermal [10] and acoustic insulation [11], as well as in filtration and catalysis processes due to their structure and high specific surface area [12, 13].

The production of cellular polymers has experienced a significant progression with the development of Nanotechnology. This concept was firstly introduced by the Nobel Prize in Physics Richard P. Feynman in 1959 and by other scientists like Norio Taniguchi, who introduced the term *"nano-technology"*. With the manipulation of matter at an atomic, molecular, or supramolecular scale began a new era for Materials Science.

Indeed, some of the current frontiers in cellular polymers research are the addition of nanoparticles (to modify the foaming process or to enhance/modify the structure and properties of the cellular polymer) and the production of cellular polymers with cell sizes in the nanometric range (around 200 nm, being 1 nm = 10^{-9} m) (nanocellular polymers). As in the 80s it was proposed to move from cell sizes on the order of 300 microns to cell sizes below 50 microns (microcellular polymers, i.e., materials with cell sizes higher than 10 µm and cell densities around 10^9 cells/cm^3), nowadays, the next step is to reduce cell sizes below the micron (Figure 0.3), obtaining cell densities of the order of 10^{13}-10^{14} cells / cm^3. Due to the enormous interest of the field of nanocellular materials, this research work has been focused on the production and characterization of nanocellular polymers. Figure 0.2 (right) shows the typical structure of one of the nanocellular polymers produced in this investigation. This material has cell sizes below 1 µm.

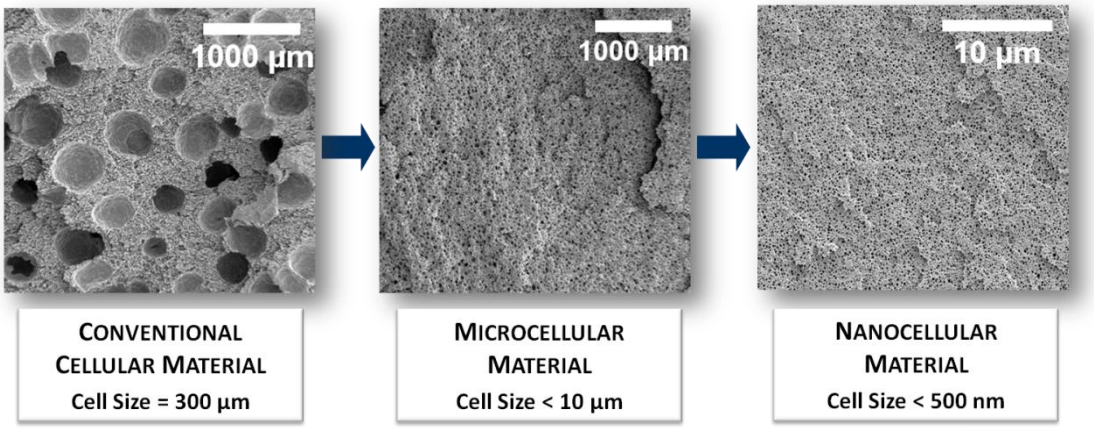

Figure 0.3. Successive reductions in the cell size from conventional to nanocellular materials. The three materials, manufactured in our laboratory, have the same relative density (around 0.5). The scale used in the image of the nanocellular polymer is different due to the very small cell size of this material.

Along this thesis the terminology nanoporous materials or nanocellular materials will be used independently to refer to the same concept (nanocellular foams). Some of the articles

published covering issues not only concerning cellular polymers (such as the physical properties of nanoporous materials or the molecular confinement in self-standing nanoporous materials) the nanoporous terminology will be used due to its more general character. However, in general, the term nanocellular will be employed with more frequency.

From the point of view of their potential properties, nanocellular materials are very promising since it is expected that these materials will have better mechanical properties than those of conventional cellular or microcellular materials. In addition, the cell size reduction will permit significant reduction of the thermal conductivity due to the decrease of the heat conduction transfer (Knudsen effect) [14]. Furthermore, it is expected that nanocellular polymers produced from amorphous polymers with a well-defined cellular structure with cell sizes under the wavelength of the visible radiation could keep, up to some extent, the transparent character of the former solid [15]. Finally, with these new materials it could be possible to achieve non-expected modifications in other properties or some new effects could appear due to the dimension of the cell size and cell walls in the nanometer range. Nevertheless, although it is commonly accepted that nanocellular polymers will exhibit an enhancement of the aforementioned properties with respect to microcellular and conventional cellular polymers, there is little evidence about this. The main limitation to characterize the different physical properties of nanocellular polymers is the production of samples with appropriate dimensions and geometries to be subjected to standard protocols.

The production of nanoporous polymers from polymer films is well known, either by using nanostructures (pattern transfer techniques [16-19]) or by selective dissolution or degradation of blocks [16, 18-25]. On the other hand, literature shows that it has not been possible to achieve nanocellular materials by means of foaming techniques using chemical blowing agents.

On the other side, gas dissolution foaming at high pressures (typically N_2 or CO_2) is perhaps less known, but it is a versatile, efficient, inexpensive, and environmentally sustainable technique, especially if CO_2 is used (which exhibits excellent diffusion in the supercritical state (above 31° C and 7.3 MPa)).

Gas dissolution foaming process consists of the following steps (Figure 0.4):

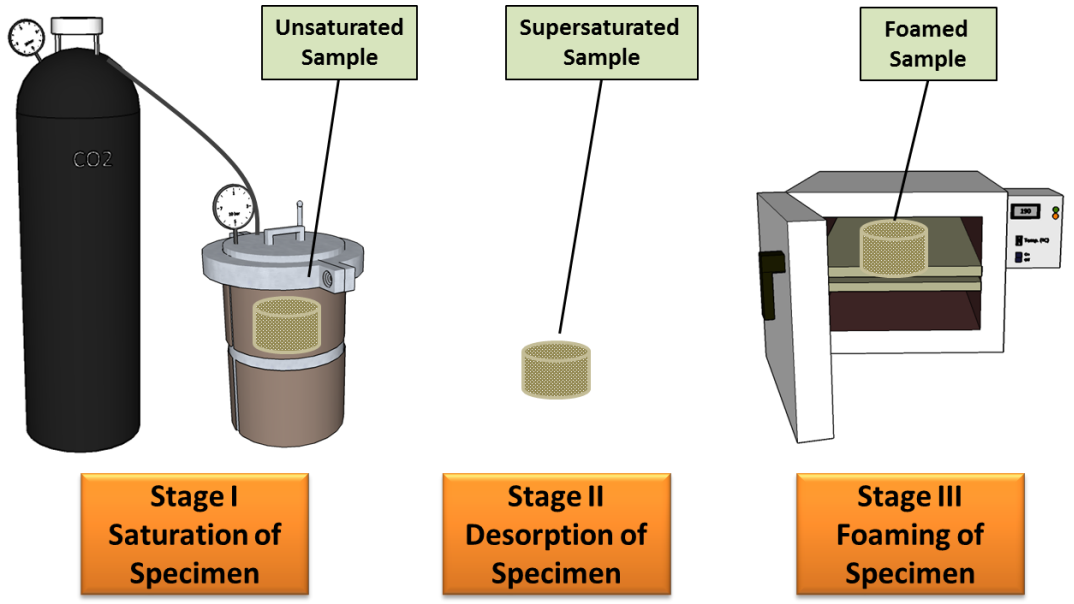

Figure 0.4. Gas dissolution foaming process scheme for the specific case of *solid state foaming*

- Stage I. Saturation Stage: a polymer is introduced into a pressure vessel under a controlled gas pressure and temperature. During this stage the gas diffuses into the polymer, occupying the gas molecules the free space between the polymer chains [26, 27]. This stage usually ends when the polymer sample is completely saturated (i.e. it reaches the maximum amount of gas that can absorb at the pressure and temperature used).

- Stage II. Desorption Stage: gas pressure is released, and the sample enters into a supersaturated sate. The polymer starts to release the excess of gas, either by diffusion to the outside or by the formation of discontinuities/voids inside the matrix. These voids will act as nuclei for the cells formation [28, 29].

- Stage III. Foaming Stage: when the saturated sample reaches a temperature over or close to its glass transition temperature (T_g) the nuclei previously formed can grow into cells (this description is valid for amorphous polymers). Cell growing is promoted by the pressure difference between the gas inside the sample and the external pressure. As a consequence of the increment of the cell size the sample presents a macroscopic expansion and, consequently, a density reduction. Final cell size is controlled by the magnitude of the pressure inside the sample, and the viscoelastic properties of the polymeric matrix at the foaming temperature (depending on these properties the polymer will show more or less opposition to the cell grown). Other factor that can influence the final cell size is the phenomena of coalescence, whereby several cells can collapse into one single cell [30].
  Furthermore the plasticization effect of the CO_2 on amorphous polymers decreases the effective value of the glass transition temperature ($T_{g,ef}$) [31-33] and this effect also plays an important role on the sample density. The relationships between this

effective glass transition temperature and the temperature of the saturation stage allows differentiating two main gas types of processes.

On one hand, when the saturation temperature is higher than the effective glass transition temperature of the polymer (i.e. the polymer is in the rubbery state at the end of the saturation stage) the foaming occurs during the pressure release, being the foaming triggered by the pressure difference. This process is called *one-step* or *batch foaming* [34, 35]. In this foaming process the desorption stage disappears, then, after the pressure release the cell nucleation and growth processes take place immediately one after another.

On the other hand, at saturation temperatures lower than the effective glass transition temperature of the polymer (i.e. the polymer is in the glassy state at the end of the saturation stage) the foaming process is triggered in a second stage by heating the sample over its $T_{g,ef}$. This process is usually called *two-step* or *solid state foaming* [36].

Development of nanocellular polymers by gas dissolution foaming requires reaching very high cell nucleation densities (N_0, number of nuclei/cells per cubic centimeter of the unfoamed material) and nearly negligible coalescence.

Coalescence can be avoided, or reduced to a low level, by an appropriate selection of the polymer matrix and of the foaming temperature in comparison with the effective glass transition temperature.

Regarding to high cell nucleation densities, there are several approaches to promote the cells nucleation up to the desired levels (typically higher than 10^{14}-10^{15} nuclei/cm^3) depending on the nucleation mechanisms involved (Figure 0.5).

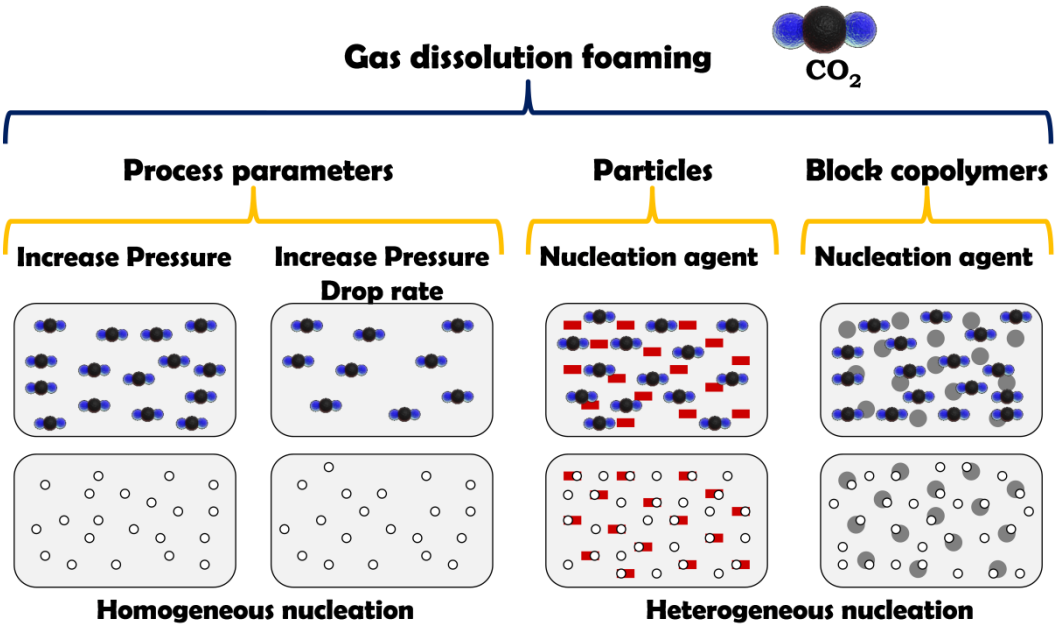

Figure 0.5. Methods to enhance the cell nucleation in gas dissolution foaming processes

In **homogeneous materials** (i.e. systems with a homogeneous nucleation) there are two approaches to promote the nucleation by varying two key processing parameters, mainly the

saturation pressure and the pressure drop rate [28, 35, 37]. Saturation pressure controls the amount of gas molecules dissolved into the polymer sample, being directly related to the CO_2 uptake. Increasing the amount of gas molecules into the polymer will enhance the probability of aggregation between molecules to produce a nucleus/bubble, and consequently, the nucleation density. Therefore, a higher nucleation density can be promoted by increasing the saturation pressure.

In the case of the pressure drop rate, higher pressure drop rates during the pressure release produces higher thermodynamic instability (reducing the activation energy needed to nucleate a bubble), and therefore a higher probability of nuclei formation [29].

Heterogeneous materials (i.e. systems in which a heterogeneous nucleation takes place) offer other two main approaches to increase the nucleation independently of the processing parameters.

On the one side, addition of particles to the polymer (such as talc, tituanium oxide, kaolin, nanosilica, and other nanoparticles) can increase the nucleation ratio. Particles should be well dispersed to increase the potential nucleation sites (the number of particles per unit volume should be of the same order, or higher, than the desired nucleation density). Also, size of the individual particles is a main issue; they should present a size of the same order of magnitude, or higher, than the critical nucleation radius of the polymer-CO_2 system (nucleation radius around tens of nanometers, depending on the system) [38].

On the other side, additional nucleation sites or interfaces to promote nucleation can be generated by using heterogeneous polymer/polymer or polymer/block copolymer blends (either A-B diblock or A-B-A tricblock copolymers) [39]. Well-chosen block or random copolymers are readily miscible with their corresponding homopolymer, and can lead to the formation of nanostructures. Low contents of copolymer (< 15wt.%) can self-assemble into a large number of spherical micelles (up to 10^{13}-10^{16} micelles/cm^3) that can act as nucleation sites. In addition, the use of CO_2-philic blocks can increase the effectiveness of these nanostructures as nucleating agents, becoming CO_2 reservoirs.

The main difficulty of foaming processes to produce nanocellular structures resides in the thermodynamics of the polymer-gas systems. Formation of nanometric cells leads to a huge increment of the interfacial (surface) area and the interfacial (surface) free energy. In addition, the nucleation mechanisms of the cells are governed by thermodynamics. In gas dissolution foaming processes the abrupt modification of the process parameters (pressure or temperature) reduces the gas solubility into the polymer, inducing gas phase segregation and a new disposal of the gas into cells that will tend to reduce the free energy of the foaming systems [29]. After the nucleation process, each nucleus should overcome an energy barrier to become into a cell (Gibbs free energy barrier). This energy barrier on homogeneous polymers depends on the surface tension of the polymer matrix in the presence of CO_2 and the pressure difference between the bubble and the bulk (related to the CO_2 concentration); whereas in heterogeneous polymers the dispersed particles or phases can provide potential nucleation sites with lower energy barrier than the surrounding polymeric matrix [40].

In this field of research, some of the best results obtained using the variation of the saturation pressure (homogeneous nucleation) were accomplished by J. Pinto et al. [41] from PMMA (poly(methyl methacrylate) samples. In this work nucleation rates close to 10^{15} nuclei/cm^3 and cell sizes around 90 nm were achieved for a saturation pressure of 30 MPa. Similarly, S. Costeux et al. [42] managed nucleation rates close to $5{\cdot}10^{15}$ nuclei/cm^3 for a saturation pressure of 33 MPa, using PMMA-co-EA (poly(methyl methacrylate-co-ethyl acrylate)) as polymeric precursor. In this case cell sizes were below 100 nm and the porosities achieved were around 60 %. Regarding to the use of block copolymers (heterogeneous nucleation), the best results obtained were achieved by Yokoyama et al. [43] and Yokoyama and Sugiyama [44]. They obtained nucleation rates close to 10^{16} nuclei/cm^3 and cell sizes about 15 – 30 nm in films of PS-*b*-PFMA (polystyrene-*block*-poly(perfluorooctylethyl methacrylate)) and PS-*b*-PFS (polystyrene-block-poly(perfluorooctylpropyloxy)styrene). In both cases the fluorinated blocks had a greater affinity for CO_2 than the polystyrene matrix.

This introducing chapter (*Chapter 0*) is divided into five sections. First is a description of the scientific framework where this work was carried out. Secondly, an overall view of the state of the art on nanocellular polymers is provided. Then, the scope and objectives are described. Also, an explanation about the body of the manuscript, its organization and a global schematic view of the investigation are included. Finally, the main novelties and contributions of this work to the field of nanocellular polymers field are enumerated.

0.2 Framework of this Thesis

This investigation is part of the research focused on cellular materials leaded by Prof. Dr. Miguel Ángel Rodríguez Pérez at CellMat Laboratory in the Condensed Matter Physics Department of the University of Valladolid.

CellMat laboratory was founded in 1999 at University of Valladolid after a PhD thesis focused on thermal and mechanical properties of polyolefin foams defended by Miguel Ángel Rodríguez-Pérez and supervised by Prof. Dr. José Antonio de Saja Sáez [45]. Thenceforth, under the direction of Prof. Dr. Miguel Ángel Rodríguez Pérez and Prof. Dr. José Antonio de Saja twenty two PhD thesis [46-62] and about 150 journal papers have been published on cellular materials. Research activity of CellMat began with the study of the structure-property relationships of cellular polymers based on polyolefins [63-77]. After a few years the research topics were extended to the production of cellular polymers both by chemical and physical blowing agents. In 2002 a new research line in metal foams was introduced [51, 52]. Finally, in the last years significant efforts have been done in the development of non-conventional characterization techniques and experimental devices, with the aim to provide a better understanding of the mechanisms taking place during the foaming process.

Nowadays CellMat sustain five main research lines: microcellular and nanocellular polymers [78-81], cellular nanocomposites [82-85], bioplastic foams [86-88], metallic foams [89-92], and development of new experimental techniques and devices [93-96].

Within the field of microcellular and nanocellular polymers, in 2014 it was defended the first PhD thesis in CellMat laboratory. This thesis, focused on the field of nanocellular materials [58], mainly studied the production and identification of the foaming mechanisms of nanocellular polymers obtained from blends of poly(methyl methacrylate) (PMMA) and poly(methyl methacrylate)-*b*-poly(butyl acrylate)-*b*-poly(methyl methacrylate) (MAM). Furthermore, this work mentioned some preliminary evidence about potential differences on some physical properties of these systems, such as thermal conductivity, glass transition temperature, and Young´s modulus in comparison with microcellular polymers.

Then, once the dominant mechanisms in the production and foaming of these materials were established and well-known, the present research was focused on a detailed analysis of the different physical properties of nanocellular polymers and their comparison with those of conventional and microcellular polymers. Thus, this thesis presents a detailed study that will shed light on the validity of the widespread assumptions about the improved properties and expected benefits of nanocellular polymers against the existing porous materials.

Therefore, due to the great interest that this kind of materials have generated, it is not surprising that multinational companies like Dow Chemical, BASF, and Sabic, or leading laboratories such as Osaka University (Prof. Ohshima), the University of Washington (Prof.Kumar) or our laboratory at the University of Valladolid (CellMat) have begun to work seriously in this field.

0.3 Summary of the State of the Art

In the present section prior knowledge of the key physical properties of nanocellular polymers is presented and compared with the results found in other nanocellular materials. Moreover, the main production methods leading to these nanoporous materials are described briefly, and some specific characteristics of these materials like the consequences of the confinement of the constituent phases of the cellular polymer are also analyzed. Finally, the potential applications they could cover in the future are illustrated as well.

The explanations of these topics are covered in the first journal article enclosed in this thesis. This comprehensive review was published in **Progress in Materials Science 78-79 (2016)** with the title **“Nanoporous Polymeric Materials: a New Class of Materials with Enhanced Properties”**.

Progress in Materials Science 78-79 (2016) 93–139

Contents lists available at ScienceDirect

Progress in Materials Science

journal homepage: www.elsevier.com/locate/pmatsci

Nanoporous polymeric materials: A new class of materials with enhanced properties

B. Notario [a], J. Pinto [b], M.A. Rodriguez-Perez [a,*]

[a] Cellular Materials Laboratory (CellMat), Condensed Matter Physics Department, University of Valladolid, 47011 Valladolid, Spain
[b] Nanophysics – Smart Materials Group, Istituto Italiano di Tecnologia (IIT), Via Morego 30, 16163 Genova, Italy

ARTICLE INFO

Article history:
Received 15 August 2015
Received in revised form 5 February 2016
Accepted 8 February 2016
Available online 19 February 2016

Keywords:
Nanoporous polymeric materials
Properties
Nanocellular foams
Cellular polymers
Mechanical properties
Thermal properties
Dielectric properties
Optical properties

ABSTRACT

Nanoporous polymeric materials are porous materials with pore sizes in the nanometer range (i.e., below 200 nm), processed as bulk or film materials, and from a wide set of polymers. Over the last several years, research and development on these novel materials have progressed significantly, because it is believed that the reduction of the pore size to the nanometer range could strongly influence some of the properties of porous polymers, providing unexpected and improved properties compared to conventional porous and microporous polymers and non-porous solids.

In this review, the key properties of these nanoporous polymeric materials (mechanical, thermal, dielectric, optical, filtration, sensing, etc.) are analyzed. The experimental and theoretical results obtained up to date related to the structure–property relations are presented. In several sections, in order to present a more compressive approach, the trends obtained for nanoporous polymers are compared to those for metallic and ceramic nanoporous systems. Moreover, some specific characteristics of these materials, such as the consequences of the confinement of both gas and solid phases, are described. Likewise, the main production methods are briefly described. Finally, some of the potential applications of these materials are also discussed in this paper.

* Corresponding author.
E-mail address: marrod@fmc.uva.es (M.A. Rodriguez-Perez).

http://dx.doi.org/10.1016/j.pmatsci.2016.02.002
0079-6425/

Contents

1. Introduction

1.1. General concepts

Porous polymers, defined as two-phase systems composed of a continuous solid polymeric phase and an either continuous or discontinuous gaseous phase [1–4], are widely used and have a very promising future in important technological sectors such as the automotive and aeronautical industries, renewable energies, construction, cushioning and packaging, and biotechnology. The global market of porous polymeric materials is significant; in fact, around 10% of annual consumption of plastics is intended for the manufacture of different types of polymeric foams (mainly polyurethane, polyolefin, polystyrene, and polyvinyl chloride (PVC)) [5]. In the year 2013, 19.1 million tons were produced with an economic impact of $86.9 billion. In the period of 2013–2019, an annual growth rate of 4.8% is expected, and therefore the estimated production for the year 2019 is 23.5 million tons.

The increasing interest in these materials relies on reductions in weight, production costs, and raw material needed, as well as on the excellent properties (tailor-made) that can be achieved with them. Moreover, these materials can find application in different fields depending on their structural morphology. For instance, porous materials with highly interconnected open-cell or open-pore morphologies (i.e., the gas and solid phases show continuity) are suitable for filtration, catalysis, cushioning, acoustic absorption, etc., while morphologies with isolated pores in which the gas is enclosed (closed-cell or closed-pore morphologies) have better characteristics for structural applications and for thermal insulation.

Materials with a porous structure are widespread in nature in plant and animal tissues: examples include wood, cork, trabecular bone, or plant parenchyma. After their discovery, human civilization advanced one step further with the development of synthetic porous materials. However, the first polymeric porous materials (typically called "polymeric foams", where foams have pore sizes larger than 200 μm) presented a major drawback: the mechanical properties of the foam were much inferior to those of the former solid even for small density reductions. Microporous polymers, characterized by pore sizes on the order of 1 μm, were developed at the Massachusetts Institute of Technology (MIT) in the early 1980s [6–8] in order to address this disadvantage. Since their discovery, microporous polymers with high relative densities (low porosities) and their corresponding technologies have been under continuous development. These materials show significant improvements: for instance, they exhibit higher Charpy impact strength, toughness, fatigue life, and thermal stability and lower thermal conductivity than unfoamed plastics and much better mechanical properties than conventional foams [9–12]. These excellent properties allow these materials to cover a significant number of applications, because it is possible to reduce the density of a given polymer with little decrease in their mechanical properties while simultaneously improving other features.

Similar or even greater improvements than those obtained when MIT invented microporous foams are expected to be achieved for the next generation of nanoporous polymers.

In particular, these novel materials with pore sizes below 200 nm could have better mechanical properties than microporous foams [13] and thermal conductivities well below those of the best thermal insulators currently on the market [14]. Furthermore, it is expected that the confinement of the constituent phases of these materials (polymer and gas phases) at the nanoscale will enhance several properties involved in transport phenomena, such as radiation–matter interaction, gas storage, sensing properties, and more. This opens the door to a significant number of applications such as super thermal insulation, structural applications, dielectric and optical applications, filtering, sensing, and catalysis.

However, it has not been until recent years when technological development has allowed materials with these features to be manufactured in adequate quantities or with appropriate dimensions to thoroughly study their properties or to become actual candidates for industrial applications. Thus, only recently has it been possible to start verifying the expected properties of these materials experimentally.

In this review, the first reliable experimental results obtained in nanoporous polymeric materials are collected and compared either with the developed theoretical models or with the properties of other nanoporous materials (metallic and ceramic) that share some features with them, mainly the dimensions of their elements in the nanoscale. In this way, the validity of the predictions and the expected properties, such as the mechanical, thermal, dielectric, optical, filtration, and sensing properties, are discussed in detail. Furthermore, non-predicted behaviors or new effects that have been found experimentally with these materials because of the confinement of the constituent phases are also analyzed. Likewise, the key methods leading to these nanoporous polymers (based on the use of solvents, thermal degradation, the gas dissolution foaming technique, etc.) are described briefly in order to provide a more comprehensive understanding of these materials. In addition, the potential applications they could cover in the future because of these enhanced properties are briefly mentioned.

1.2. Fabrication process

The fabrication of nanoporous polymeric materials requires the use of specific procedures that overcome the difficulties associated with the production of separated phases at the nanoscale. Several approaches have been developed over the past years in order to achieve polymeric structures with pores on the nanoscale [15]: molecular imprinting, microemulsion templating, phase separation techniques, selective removal of one of the blocks in nanostructured block neat copolymers, foaming, etc. A scheme of the different fabrication processes that exist nowadays is shown in Fig. 1, together with some transmission electron microscopy (TEM) and scanning electron microscopy (SEM) images of nanoporous polymeric materials obtained with some of these techniques.

Regarding phase separation techniques, phase separation can be produced during polymerization and cross-linking in different ways: (1) by the addition of a non-solvent to a polymer/solvent mixture (immersion techniques) [22,23], (2) by chemical induction (i.e., the polymerization is performed in a monomer/non-solvent mixture, the polymerization itself depletes the monomer, and insolubility is induced) [24], and (3) by thermal induction phase separation (TIPS) [25,26]. For the latter, three different mechanisms can be distinguished: spinodal decomposition (liquid–liquid phase separation), physical gelation, crystallization (solid–liquid phase separation), or combinations of these.

For instance, thin films (with a thickness around 500 nm) of polystyrene and poly(2-vinylpyridine) with co-continuous morphologies were manufactured by Li et al. [16] based on phase separation immersion techniques. These films presented pore sizes of tens of nanometers and served as templates for thin nanoporous membranes. Another example of the immersion technique can be found in the work of Walheim et al. [27]. They produced nanoporous PMMA films with a thickness lower than 150 nm by exposing the initial film of PS and PMMA to a selective solvent (cyclohexane) that dissolved the PS. The obtained films presented pore sizes lower than 100 nm and a surface with high optical transmission.

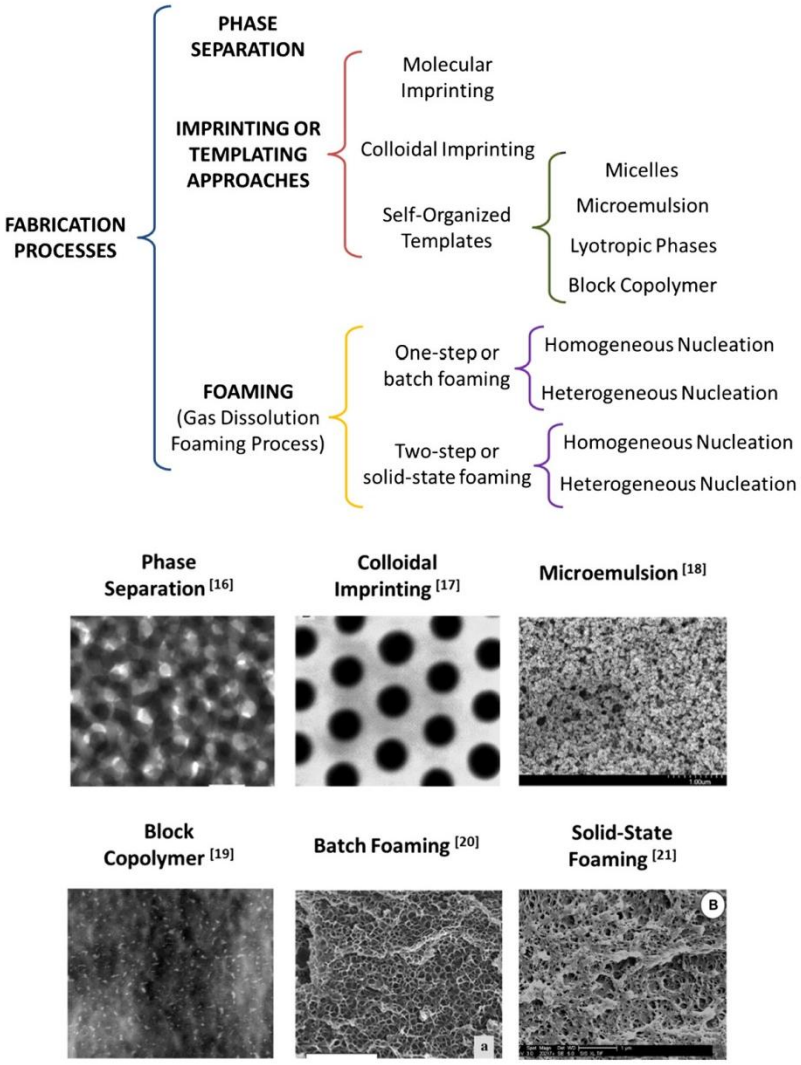

Fig. 1. Different fabrication processes for the production of nanoporous polymeric materials along with some TEM and SEM images of the nanoporous polymers obtained with the different techniques. TEM and SEM images have been included with permission from Refs. [16–21].

In the case of imprinting or templating approaches [28,29], the templates induce a special structure by specific interactions with the growing polymer matrix (i.e., electrostatic interactions, hydrogen bonding, or pattern recognition). The highest target of a template system is the direct replication of a self-organized structure into a permanent (polymeric) material. Nevertheless, this process is complicated because of changes of the mixing thermodynamics throughout polymerization.

One type of templating approach is so-called molecular imprinting. This technique is used to create polymer matrices with pores structured on a molecular scale and is based on the system used by enzymes for substrate recognition. The synthesis is carried out by copolymerization of functional and cross-linking monomers in the presence of a molecular template (imprint molecule) and additional solvents. After polymerization, the template molecules are eliminated from the matrix under certain conditions, leaving behind a cavity complementary in size and shape to the imprinting molecules.

Another templating technique is colloidal imprinting. In this case, a colloidal crystal is used as a template together with precursors, which enables replication of the crystal morphology followed by swelling and polymerization of the precursors. After polymerization, the template is removed by extraction, dissolution, or calcination, resulting in a porous, ordered polymer.

Examples of both molecular and colloidal imprinting can be found in the literature [17,30–33]. For instance, molecular imprinting was used by Cheong et al. [32] to create a method for the synthesis of a testosterone-specific polymer. The porous polymer obtained was found to interact specifically with testosterone with functional and stereochemical memory similar to artificial antibodies or enzymes.

The colloidal imprinting method was used by Park and coworkers [17] to produce porous polyurethane (PU) membranes (with a thickness of about 10 μm) by using polystyrene (PS) beads as templates. The films obtained presented pore sizes from 0.2 to 3 μm and a porosity around 74%.

Perhaps two of the most common self-organized templating techniques are the microemulsion and block copolymer techniques.

Microemulsions are macroscopically homogeneous, optically isotropic, two-phase mixtures of immiscible liquids, which use surfactants to provide a thermodynamically stable microstructure. The exact nature of this microstructure depends on the organization of the surfactant film separating the water and oil domains, which typically have dimensions of 10–500 nm. du Fresne von Hohenesche et al. studied the polycondensation behavior of melamine formaldehyde (MF) resins under acidic polymerization conditions within a bicontinuous microemulsion composed of an oil phase, a water phase, and an *iso*-C13-(EO)7 type nonionic surfactant [18]. They were able to achieve gels with porosities between 80 and 85 vol% and pore sizes between 65 and 400 nm.

However, the block copolymers used for this purpose comprise a stable block and a sacrificial block, such that the morphology provides a matrix of the stable material with the labile material as the dispersed phase. Upon a thermal treatment or chemical attack with solvents the unstable block is removed, leaving pores where the size and shape are dictated by the initial copolymer morphology [19,24,35].

Multiblock and triblock copolymers, composed of rigid, semi-rigid, and flexible polyimide matrices with either poly(propylene oxide) or poly(methyl methacrylate) as the thermally labile coblocks, were prepared by Hedrick and coworkers [36]. They produced nanoporous polymeric films of 10 μm thickness based on flexible polyimide with pore sizes on the order of tens of nanometers.

The aforementioned techniques are generally restricted to the fabrication of thin films and require the use of organic solvents that have to be subsequently removed.

One promising technique used to overcome these drawbacks is the gas dissolution foaming process and in particular high-pressure or supercritical CO_2 gas dissolution foaming, where CO_2 is used as a physical blowing agent [34,37–39]. This gas is one of the best options for this type of process because of its excellent diffusion characteristics in the supercritical state and the relatively mild conditions to reach this state (31 °C and 7.3 MPa). Furthermore, carbon dioxide is a *green* solvent that can be removed without residue or the production of any pollutant compound [40,41].

In its most general form, the equipment used in the gas dissolution foaming technique consists of a high pressure vessel equipped with an accurate pressure pump controller, which is controlled automatically to maintain the temperature and pressure at the desired values. The usual gas dissolution foaming process (called the *two-step* or *solid-state foaming process* [8]) has three stages [42]: gas saturation of the polymer sample (under fixed gas pressure and temperature), gas desorption during and after the pressure release (to room pressure and temperature), and foaming of the sample (at a temperature over or around the glass transition temperature (T_g) of the plasticized amorphous polymer or around the melt temperature (T_m) if the polymer is semi crystalline). Nevertheless, if the polymer specimen is in the rubbery state upon saturation with CO_2, foam expansion will occur during the pressure release, and the desorption stage will disappear. In this case, the procedure is called *one-step* or *batch foaming* [38,43].

Development of nanoporous polymers by gas dissolution foaming requires very high pore nucleation densities (N_0, number of nuclei/cells per cubic centimeter of the unfoamed material) and reduced coalescence of the growing pores.

Coalescence can be avoided, or maintained without significant influence, by the appropriate selection of a polymer matrix and a foaming temperature near the effective glass transition temperature of amorphous polymers or the melt temperature of semi crystalline polymers.

In order to increase cell nucleation to the desired levels (typically higher than 10^{14}–10^{15} nuclei/cm^3), several approaches have been developed depending on the nucleation mechanisms involved. With homogeneous materials (i.e., systems with a homogeneous nucleation), there are two approaches to promote nucleation: increasing the saturation pressure or increasing the pressure drop rate [21,38,44–48]. For instance, Pinto et al. [47] were able to produce nanoporous poly(methyl methacrylate) (PMMA) materials with relative densities of around 0.5 and pore sizes between 90 and 700 nm by increasing the saturation pressure. The same approach was used by Miller et al. [21] who produced nanoporous polyetherimide (PEI) foams with pore sizes between 30 and 120 nm and relative densities from 0.7 to 0.48. However, Janani and Famili [48] designed a specific high-pressure system capable of producing an instantaneous pressure release (around 300 MPa/s) and quenched the sample just after the pressure release in order to preserve the pore structure induced by the pressure release. Using this system, they manufactured nanoporous PS with pore sizes between 500 nm and 1 μm and relative densities of about 0.5.

Heterogeneous materials (i.e., systems in which heterogeneous nucleation occurs) offer another two main approaches to increase the nucleation rate: the addition of particles (mainly nanoparticles) to the polymer matrix [20,49–52] or the use of block copolymers [47,53–56]. Urbanczyk and coworkers [52] added nanoclays (montmorillonite (MMT)) to poly(styrene-co-acrylonitrile) (SAN) to obtain porous materials with pore sizes between the nanometric and micrometric scales at saturation pressures up to 30 MPa. They found that the addition of MMT allowed a decrease in the average pore size from values near 1 μm to below 500 nm, but at the same time the relative density of the porous system increased from 0.23 to 0.65. Costeux and coworkers [20] added either silica nanoparticles or POSS to acrylic and styrenic polymers, obtaining nanoporous polymers with an average pore size of 100 nm, a relative density of 0.15, and pore densities exceeding 10^{16} pores/cm^3. However, the block copolymer approach was employed by Pinto et al. [47] to produce nanoporous polymers with pores in the range of 90–200 nm and relative densities between 0.4 and 0.6 using blends of PMMA and a triblock copolymer (poly(methyl methacrylate)-block poly(butyl acrylate)-block poly(methyl methacrylate), MAM). Similarly, Yokoyama et al. [54] produced nanoporous foams with very high pore densities (i.e., 10^{16} pores/cm^3), pore sizes between 10 and 30 nm, and a relative density of 0.5 from monoliths of polystyrene-block-poly(perfluorooctylethyl methacrylate) (PS-b-PFMA).

1.3. Expected cellular structure

A detailed discussion about the expected characteristics of the porous structure of nanoporous polymers is presented in this section in order to provide a better understanding of the influence of nanoporous morphologies on several properties that will be discussed later. Thus, the evolution of the pore size, pore density (N_p, pores/cm^3 of porous material), pore wall thickness, and tortuosity of nanoporous polymers is studied. Likewise, the emerging side effects due to the reduction of the pore size to the nanometer scale are also analyzed.

The two fundamental characteristics of nanoporous materials are the average pore size and the relative density. These two parameters are correlated by the pore density; it is possible to represent the three magnitudes on a relative density-pore size map (Fig. 2). In this plot, data obtained from some of the most representative works obtained up to date have been included, and lines of constant pore density have been represented according to Eq. (1) [8]:

$$N_p = \frac{6(1-\rho_{rel})}{\pi \Phi_{3D}^3} \tag{1}$$

where Φ_{3D} is the average pore size in 3D, and ρ_{rel} ($\rho_{rel} = \rho_f/\rho_s$) represents the relative density, where ρ_f is the density of the nanoporous material and ρ_s is the density of the solid phase.

Fig. 2 illustrates the wide range of densities and pore sizes covered by different nanoporous polymeric systems. Nowadays, the main limitation is the difficulty of reaching porous materials with

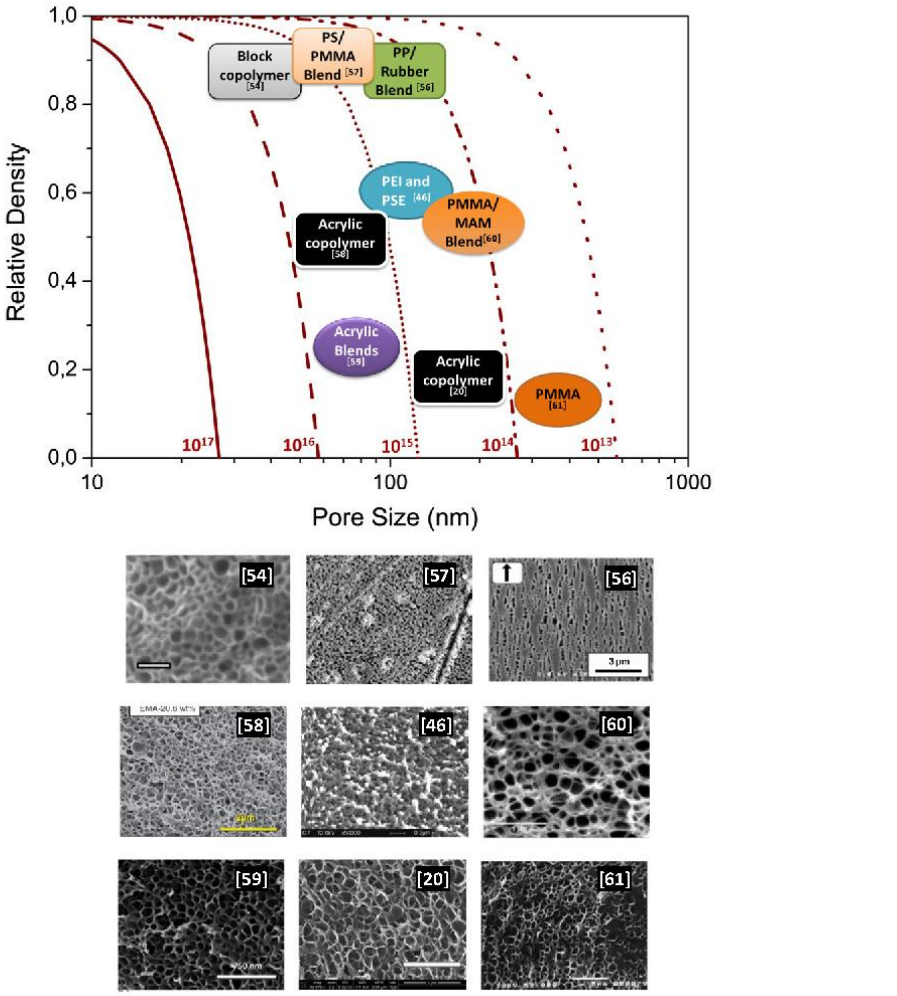

Fig. 2. Main characteristics (relative density, average pore size, and pore nucleation density) of nanoporous polymers achieved with various polymer systems. SEM images have been included with permission from Yokoyama et al. [54], Otsuka et al. [57], Nemoto et al. [56], Costeux et al. [20,58,59], Krause et al. [46], Pinto et al. [60], and Handa and Zhang [61].

medium to low densities and pore sizes below 50 nm. To achieve these requirements, higher pore densities (around 10^{17} pores/cm^3) are needed. Depending on the fabrication process, these pore densities can be achieved in different ways. For instance, in the case of imprinting or templating approaches, the pore density is determined by the pattern density of the porous structure, whereas, in the case of foaming, these pore densities can be achieved with sufficiently high pore nucleation densities (N_0, number of pore nuclei per cubic centimeter of the solid precursor), which can be calculated using equation [8]:

$$N_0 = \frac{N_p}{\rho_{rel}} \tag{2}$$

In addition, depending on the requirements of the final application, the choice of the production route is important, because no individual technique is capable of covering the entire spectrum of pore sizes and densities [62].

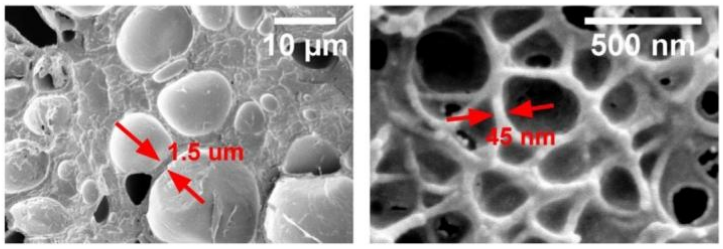

Fig. 3. Pore wall thickness of a microporous PMMA (ρ_{rel} = 0.5; pore size = 11 µm) (left) and a nanoporous PMMA (ρ_{rel} = 0.5; pore size = 300 nm) (right).

The reduction of the pore size to the nanometer range involves the confinement of the gaseous phase into nanometric voids. As a consequence, a reduction of the thermal conductivity of the gaseous phase is expected, because it is assumed that these nanoporous materials will present the well-known Knudsen effect [63,64]. This effect implies that, when pore size is comparable or smaller than the mean free path of the gas, the molecules of the latter collide more often with the molecules forming the surrounding solid part than among them. Thus, the energy transfer through the gas molecules is reduced.

Furthermore, other phenomena may appear because of the confinement of the gaseous phase to the nanoscale, as suggested by Pinto et al. [65]. They showed that nanopores can act as capacitors that can contribute to electrical conduction by dielectric breakdown or by other processes related to the Knudsen diffusion regime yet unidentified.

The reduction of the pore size from the micrometer to the nanometer range and the increase in pore density also lead to a reduction in the thickness of the pore walls. An example of this reduction is shown graphically in Fig. 3, in which the pore wall thickness of a porous PMMA is reduced from 1.5 µm to 45 nm when the pore size switches from the microscale (Fig. 3 left) to the nanoscale (Fig. 3 right).

An estimation of the expected pore wall thickness of both open- and closed-pore porous materials can be performed by considering the Gibson and Ashby equations [1]. A tetrakaidecahedral pore is assumed because of its similarity to a spherical one. Given this assumption, the expression of the pore wall thickness for an open-pore system is given by the relation:

$$t^2 = \frac{l^2 \rho_{rel}}{1.06} \tag{3}$$

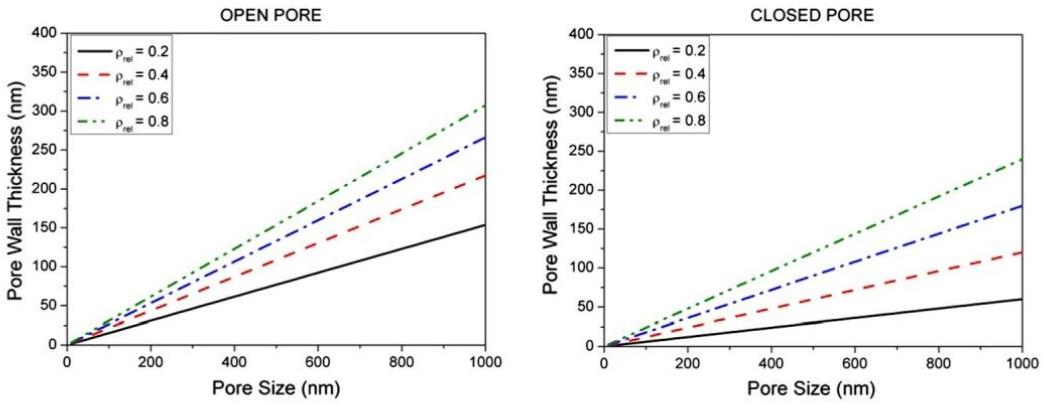

Fig. 4. Pore wall thickness as a function of the average pore size for both an open-pore polymeric system and a closed-pore polymeric material.

where t represents the pore wall thickness and l the edge length. For the case of a closed-pore system, the relation is given by:

$$t = \frac{l\rho_{rel}}{1.18} \tag{4}$$

It is well known that the edge length can be related to the average pore size through the following equation [1]:

$$\Phi = Bl \tag{5}$$

where B is a constant that relates the average pore size Φ of the polyhedron given its edge length l. In the case of a tetrakaidecahedral pore, B takes a value of 2.828.

Pore wall thickness values obtained for both open- and closed-pore polymeric systems are represented in Fig. 4 as a function of the pore size for different relative densities. The pore wall thickness decreases linearly with pore size, reaching values in the case of open-pore materials of below 25 nm when the pore size is around 100 nm. This effect is even more pronounced for closed-cell materials.

This reduction in the pore wall thickness confines the polymer chains within the pore walls, leading to a reduction in the mobility of the polymeric macromolecules. This effect, known as the confinement effect, was first detected by Reglero Ruiz et al. [66] in PMMA-based nanoporous materials (average pore size around 200 nm) by means of differential scanning calorimetry (DSC). They observed an increase of 11 °C of the glass transition temperature of nanoporous PMMA-based foams with respect to the bulk polymer.

This result was also detected later in nanoporous PEI (average pore size between 30 and 120 nm) by Miller and coworkers [13]. They also studied the thermal behavior of porous PEI by DSC, obtaining an increase in the glass transition temperature in the nanoporous system of 5 °C compared to the solid material. In addition, Notario et al. [67] showed this effect in nanoporous PMMA (average pore size between 200 and 300 nm) both by DSC and by dynamic mechanical analysis (DMA). In this study, the nanoporous system presented a glass transition temperature 7 °C higher than that of both the microporous material and the solid matrix. This phenomenon was confirmed by Pinto and coworkers [65] in PMMA-based foams by means of Raman spectroscopy. They observed that the differences found between relative intensities are associated with the hindering of the vibrational modes, proving the existence of a confinement effect of the polymeric macromolecules.

As a consequence of the confinement of polymeric macromolecules in very thin pore walls, unexpected modifications of different properties or new effects could appear.

Finally, the reduction in the size of the constituent phases (both solid and gas phases) to the nanometer range could also modify the architecture of the porous system, leading to an increase in the tortuosity of the solid and gas phases (see Fig. 5). Tortuosity, defined as the ratio between the dis-

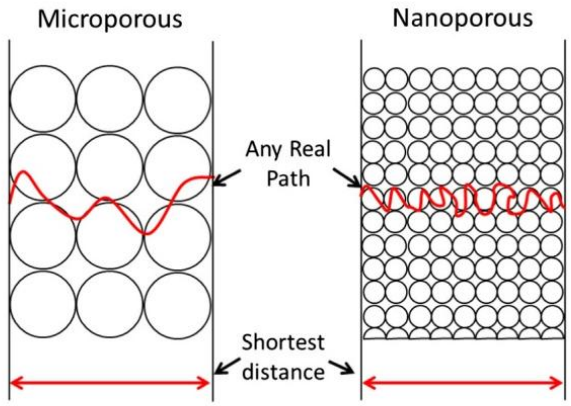

Fig. 5. Scheme of the tortuous path through the solid phase inside a microporous material (left) and a nanoporous one (right).

tance of any real path and the shortest distance between two points, is a parameter of extremely high importance for material transport properties through the solid phase (thermal and electrical conductivities) in open- and closed-pore morphologies as well as for the flow or transport of substances through the gaseous phase in open-pore morphologies (e.g., filtration processes).

Although there are no theoretical models that argue for this expected increase in tortuosity, it can be inferred from the theory of fractals. As already said by the mathematician Mandelbrot [68], the measured length of a stretch of coastline depends on the scale of the measurement. Empirical evidence suggests that the smaller the increment of the measurement, the longer the measured length becomes. This effect was experimentally observed by Ma et al. [69], who showed how the increase in tortuosity of the current path affected the induced eddy currents in microporous Cu and Fe.

Some evidence of this phenomenon has also been observed in nanoporous PMMA-based foams [14]. However, Notario et al. [14] suggested that the enhancement in the thermal insulation found with nanoporous PMMA could be attributed both to the confinement of the gaseous phase and to a reduction in the thermal conductivity of the polymer matrix, which is related to an increase in the tortuosity of the solid phase of the porous morphology. This behavior was confirmed by Pinto and coworkers [65] by measuring the DC electrical resistivity of nanoporous PMMA. Their results revealed clear evidence of the increased tortuosity in the transition from the microscale to the nanoscale.

Therefore, a reduction in the pore size to the nanometer scale leads to the confinement of both the solid phase and the gaseous phase as well as to modifications of the porous architecture. As a consequence, unexpected modifications of different properties or new phenomena could appear, which could explain some of the results found for different properties that will be discussed in the following sections. For each property analyzed, the main theoretical models developed to describe that property are explained first, and then the main experimental results published up to now are discussed.

2. Mechanical properties

The major drawback of conventional polymer foams is their low mechanical performance. Microporous materials, characterized by pore sizes of around one micron, were developed at MIT in the 1980s to address this problem. Since their discovery, much effort has been made to study the mechanical behavior of these systems. Results have shown that microporous materials exhibit improved tensile and impact properties over conventional foams in systems such as polycarbonate (PC) [70], polyethersulfone (PESF) and polyphenylsulfone (PPSF) [71], polyethylene terephthalate (PET) [9], and polyvinyl chloride (PVC) [72]. For instance, the tensile strength of microporous PET increases with a decrease in pore size [9]. Likewise, Young's modulus in compression and the elastic collapse strength of microcellular PESF and PPSF were higher than the theoretically predicted value at high relative densities [71]. These behaviors are better than expected, because the mechanical properties of polymeric foams usually depend on the square of the relative density. This dependence between density and the physical properties of a porous material is well established and is given by the Gibson and Ashby equation [1]:

$$P_f = C \cdot P_s \cdot \left(\frac{\rho_f}{\rho_s}\right)^n \tag{6}$$

According to this equation, the property of a porous material (P_f) is equal to the property of the same material that is 100% solid (P_s) multiplied by the relative density (ρ_f/ρ_s) to the power of n. C and n are two parameters that can be determined experimentally. C usually takes values around 1 for most physical properties and porous materials, whereas n normally takes values between 1 and 2 (in the case of mechanical properties, n usually takes a value around 2) and depends on the porous structure. By using this equation, it is possible to analyze the improvement in different physical properties of porous materials due to the reduction in pore size; in fact, for some of the microcellular systems previously mentioned and for some properties, the value of n was clearly lower than 2. In the following discussion, we will use this equation and the values of n that can be obtained when this equation is used to fit experimental data to compare the results obtained by different authors.

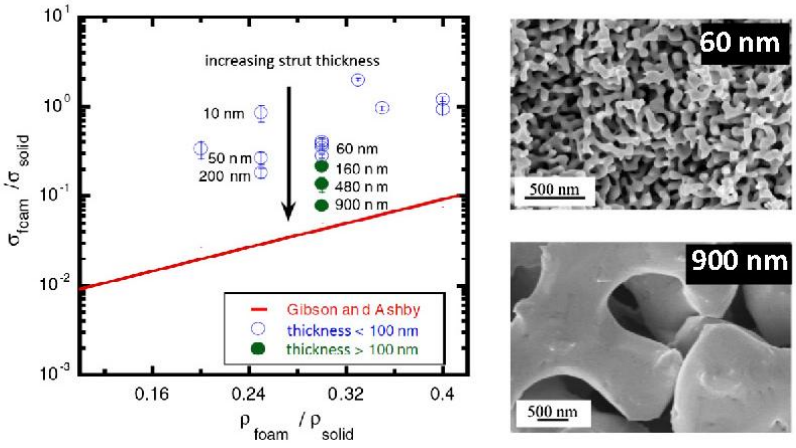

Fig. 6. Left: Yield strength values of nanoporous gold foams normalized by the yield strength of solid gold. The solid line represents the Gibson and Ashby prediction for nanoporous gold. Right: SEM micrographs of the nanoporous gold under study (top: strut thickness = 60 nm; bottom: strut thickness = 900 nm). All images have been adapted from Hodge et al. [73].

Since microporous polymers present better mechanical properties than conventional ones, it is expected that a further reduction in the pore size (nanoporous polymeric materials) will enhance the mechanical properties of porous polymers.

Several theoretical studies have modeled some of the expected improvements in these nanoporous materials [73–77], most of them focused on metallic and ceramic systems in which experimental data were available. These theoretical models led to either a scaling law to adjust the Gibson and Ashby equations to systems with pores in the nanometer regime or a new model that reproduces the behavior of these novel systems. All these models are focused on situations with low strain rates.

For instance, Hodge et al. [73] developed a scaling equation that predicts the yield strength of low-density ($\rho_{rel} < 0.3$), open-cell nanoporous gold (Eq. (7)):

$$\sigma_f = C\left(\sigma_s + k \cdot L^{-1/2}\right) \cdot \left(\frac{\rho_f}{\rho_s}\right)^n \tag{7}$$

where C is a fitting coefficient, σ_s is the bulk material yield strength, k is the Hall–Petch-type coefficient [78] for the theoretical yield strength of the porous metal in the regime of 10 nm to 1 μm, and L is the average thickness of the struts.

According to this equation, the lower the average thickness of the struts is, the greater the yield strength (see Fig. 6). Thus, at the nanoscale, the yield strength is governed by the strut thickness in addition to the relative density. A good agreement between the theoretical model and the experimental data for the nanoporous gold system were obtained when n had a value of 1.5.

The same result was observed by Fan and Fang [74], who obtained the same scaling law as Eq. (7) and suggested another one for nanoporous gold foams with relative densities greater than 0.3. In this case, the proposed equation was

$$\sigma_f = C\left(\sigma_s + k \cdot L^{-1/2}\right) \cdot \left(\frac{\rho_f}{\rho_s}\right)^n \cdot \left(1 + \left(\frac{\rho_f}{\rho_s}\right)^{1/2}\right) \tag{8}$$

They took experimental data on gold from the literature and showed that the experimental results were consistent with the developed model when n had a value of 1.5.

The effect of the strut thickness on the yield strength of nanoporous foams seems to be evident; nevertheless, the underlying mechanisms are still not well understood. Currently, there are several explanations for this effect in nanoporous metals [73,74]: (a) the dislocations are depleted from the small sample volumes, and deformation is limited by dislocation source activation; (b) the dislocations interact and pile up, and high dislocation densities are required to explain the high stresses;

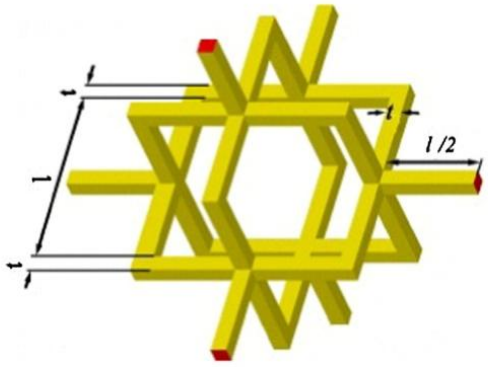

Fig. 7. Unit-cell model for open-cell nanoporous materials.

(c) there is an important reduction in the number of defects; and (d) surface stresses in nano struts can significantly affect their elastic properties. This last aspect has been studied in more detail in several studies. However, more studies are needed in order to understand these effects and to extrapolate them to polymeric systems.

The influence of surface effects on the elastic modulus and on the yield strength of open-pore nanoporous materials was analyzed by Xia and coworkers [75] by using the theory of surface elasticity. They assumed a small aspect ratio between the length (l) and thickness of the struts (t) (see Fig. 7).

With this consideration, they observed that, when the average thickness (t) of the struts in a porous material was reduced to values below 2 nm, surface stresses and surface elasticity influenced both the elastic modulus and the yield strength of nanoporous materials, slightly increasing their values. This result was confirmed in the particular case of nanoporous gold (see Fig. 8). For this reason, they proposed that these two parameters be considered to understand the mechanical behavior of nanoporous systems.

Similarly, Zhang et al. studied the effect of surface energy on the yield strength of nanoporous materials as a function of pore size [76]. They found that the surface energy has an important effect on the overall yield strength of nanoporous materials because of the increased surface area to bulk volume ratio. They observed that the effect of the surface energy on the yield strength is significant for pore sizes lower than 10 nm, but this influence is not so clear when the pore size is greater than this value. This result was confirmed in the particular case of nanoporous aluminum.

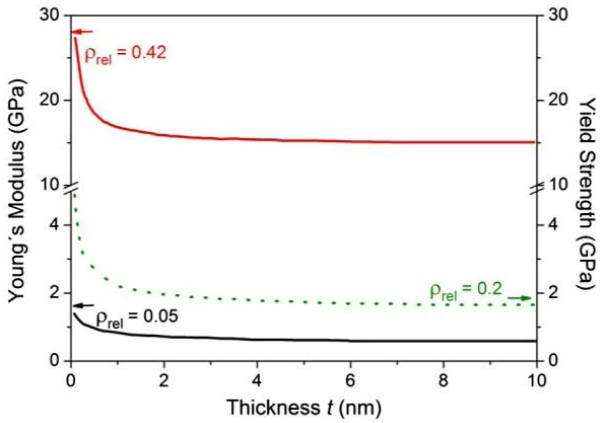

Fig. 8. Young's modulus and yield strength of nanoporous gold (considering surface effects) predicted by Xia et al. [75] according to the Timoshenko model.

Finally, Duan et al. [77] developed a theoretical model to demonstrate that nanochannel-array materials with cylindrical nanopores can be made stiffer than their non-porous parent materials by manipulating the pore surface elasticity. They showed that these materials will have high bending stiffness and strength and suggested two possible ways (valid for both open- and closed-pore materials) to achieve this: (1) by chemical modification of the pore surface and (2) by choosing a parent material with a smaller Poisson ratio. These results were verified for the case of an aluminum matrix.

To date, theoretical modeling seems to agree on the improvement of certain properties (such as the yield strength or the bending stiffness) with the reduction in the pore size to the nanometer range; nevertheless, there is a lack of theoretical studies specifically developed for nanoporous polymers. Although the mechanical characterization of nanoporous polymeric materials is a recent issue, many other experimental studies have been performed in different nanoporous systems, mainly nanoporous metals and ceramics, which will be discussed below briefly for the purpose of comparison.

It has been shown that nanoporous gold becomes as resistant as solid gold, exhibiting yield strength values similar to that of the bulk ($n \approx 1$) despite being a highly porous materials (porosities higher than 70%) [79–81]. Furthermore, Weissmuller et al. [81] demonstrated that the yield strength is higher when the strut thickness is smaller. These results are consistent with those expected theoretically [73,74]. However, the elastic modulus of nanoporous gold and that of nanoporous alumina (PAA) presents a similar value ($n \approx 1.2$, $\underline{\rho_{rel}} = 0.3$) [82] or a lower value ($n > 2.5$, $\underline{\rho_{rel}} = 0.7$) [83,84] than that of the former solid, respectively.

Nanoporous gold seems to have a fracture behavior dictated by the strut thickness [80], although Xia et al. [82] found that the ultimate tensile stress of nanoporous gold films is very sensitive to the presence of defects in the sample. In the case of low-density nanoporous alumina, the fracture toughness was comparable to that of the solid [84].

Finally, the hardness of low-density nanoporous alumina was studied by Xia et al. [84], who showed that nanoporous alumina exhibited a hardness three times lower than that observed in bulk alumina.

In general, improvements in nanoporous systems (at least in some metals and ceramics) are well established both theoretically and experimentally. The behavior of nanoporous polymers cannot be inferred from the behavior of metals or other materials, and therefore several attempts have been made to verify the expected improvements in the mechanical properties of nanoporous polymeric materials.

Nevertheless, one of the limitations of the mechanical testing of nanoporous polymeric materials is the production of sufficiently large samples that can be subjected to standard test protocols. For this reason, it has not been until recently that technological development has allowed the manufacture of samples in adequate quantities or with appropriate dimensions to thoroughly study these properties.

In order to better compare and understand the results obtained to date, the mechanical properties will be divided into those studied at low strain rates and those obtained at high strain rates.

For low strain rates, Miller and Kumar [13] observed an increase of the strain and stress at break (in tension) of polyetherimide (PEI) nanoporous foams (average pore size between 30 and 120 nm) with respect to those of microporous foams (average pore size between 2 and 4 μm) for several densities ($\rho_{rel} = 0.9$, 0.85 or 0.75). As a direct consequence of the increased strain at break, the toughness of nanoporous PEI was significantly improved compared to that of the microporous foam (by a factor of 2–3). In this case, they affirmed that the confinement effect cannot explain the increased toughness, or molecular mobility of the nanoporous tensile samples, because in fact the data suggest the opposite.

Sharudin and Ohshima [85] also found a slight increase in the stress at break and toughness in polypropylene/styrene-*b*-ethylene-butene-*b*-styrene (PP/SEBS) nanoporous polymers with densities (average pore size around 250 nm) similar to those of unfoamed materials; however, the strain at break was similar to that of the solid sample.

On the contrary, Notario et al. [67] produced microporous and nanoporous polymethylmethacrylate (PMMA) foams of similar densities ($\rho_{rel} = 0.5$) and found a reduction in the stress and strain at break (in tension) of nanoporous foams (pore size between 200 and 300 nm) in comparison with those of the microporous foams (pore size between 7 and 11 μm). As a direct result of the reduced strain at break, the toughness of the nanoporous foams was also significantly lower than that of microporous

PMMA. The confinement of the polymer chains within the pore walls together with the lower stress supported by the pore walls of the nanoporous foams could be the reason for the early breakdown of the nanoporous PMMA.

According to the tensile tests of Miller and Kumar [13], the pore size had no influence on the Young's modulus of nanoporous PEI compared to microporous PEI in the elastic regime; nevertheless, the yield strength was slightly reduced.

The opposite trend was found in nanoporous PMMA by Notario and coworkers [67], who showed an elastic modulus 11% better than that of microporous foams but a significant reduction of around 60% of the yield strength. This enhancement in the elastic modulus was confirmed by dynamic mechanical analysis (DMA). An improvement of approximately 37% of the elastic modulus (measured at room temperature) of nanoporous PMMA compared to that of microporous PMMA was again observed.

However, Sharudin and Ohshima [85] observed an increased yield stress and a similar Young's modulus in nanoporous PP/SEBS blends compared to the solid material.

The yield strength results of nanoporous PEI and PMMA are the opposite of those predicted theoretically by Fan and Fang [74] and by Hodge and coworkers [73]. The reason may lie in the fact that these models have been developed for nanoporous metals and therefore are not applicable to polymers, since the deformation mechanisms in this type of material are very different.

An analysis of the mechanical behavior at high strain rates of both the solid and the microporous and nanoporous polymeric foams was performed in two different systems: PEI and PMMA [13,67]. PEI nanoporous polymers were tested according to the falling dart procedure, while PMMA samples were analyzed according to the Charpy impact tests. Independently of the technique used and the system under study, the results show a significant increase in the impact resistance of nanoporous polymers in comparison to microporous ones (see Fig. 9). The improvement found between microporous and nanoporous PMMA was about 25% for a relative density of 0.5, while the solid material exhibited a behavior similar to that of the microporous foams. Nanoporous PEI foams always presented a higher value than microporous and solid PEI. For instance, for a given relative density of 0.90, nanoporous PEI presented a 600% increase over that of the microporous material and a 60% increase compared to solid PEI.

These significant increases in the impact resistance of nanoporous polymeric materials with respect to microporous ones have been attributed to the reduction in the pore size. It is well known that voids in a porous material act as stress concentrators, reducing the triaxial tension in front of the crack tip [86–88]. Recently, several research groups have studied the possible reduction of the stress

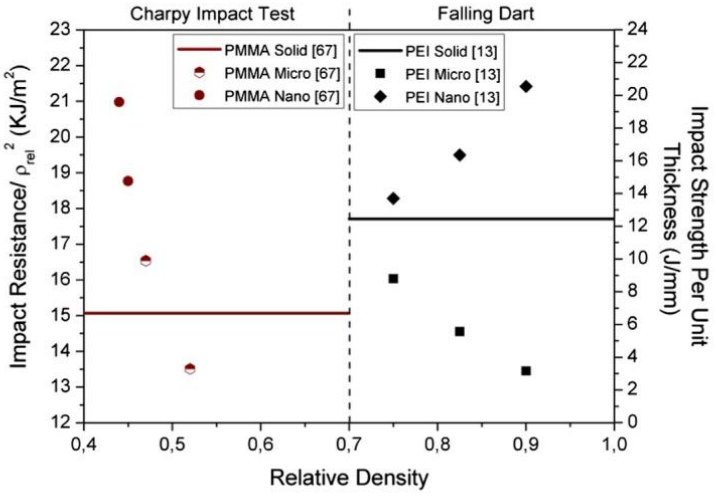

Fig. 9. Mechanical behavior at high strain rates for PMMA [67] and PEI [13] systems.

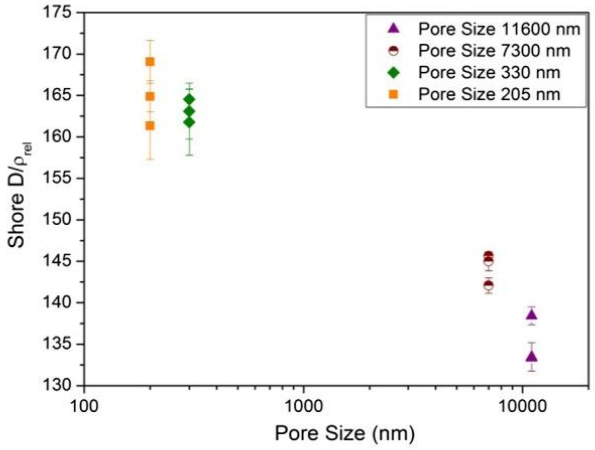

Fig. 10. Shore hardness normalized by the relative density for both microporous and nanoporous PMMA [67].

concentration when the pore size is reduced; however, no conclusive results in the relation between impact resistance and pore size were found, which is probably because of the small pore ranges analyzed [70,86–89]. Nevertheless, in the works of Miller and Kumar [13] and Notario et al. [67], the materials span the micrometer and nanometer range (a much larger range of pore sizes), demonstrating a significant effect.

Finally, the shore hardness of nanoporous and microporous PMMA foams was also studied by Notario et al. [67]. Again, a significant improvement of about 15% in the shore hardness of nanoporous foams compared to that of microporous foams was obtained (Fig. 10). This significant improvement was attributed to the presence of the nanoporous structure (with a more uniform porous structure and pore sizes in the nanometer range) and perhaps to the modification of the features of the polymer matrix owing to the observed confinement of the macromolecules on the nanometric scale.

In conclusion, it has been demonstrated that nanoporous polymers present several enhanced mechanical properties compared with microporous materials. It has been demonstrated that the mechanical behavior at high strain rates and the shore hardness of nanoporous polymers are significantly enhanced than those of both microporous and solid materials.

However, the results of the mechanical response at low strain rates (in tension) were inconclusive. Nanoporous PEI as well as nanoporous PP/SEBS blends presented an increased stress at break, strain at break, and toughness with respect to microporous materials, while nanoporous PMMA exhibited the opposite behavior. In general, the nanoporous systems had a yield strength similar to that of the microcellular systems, except in the case of PMMA, in which it was dramatically reduced. The modulus of elasticity also presented contradictory behavior: nanoporous PMMA exhibited a higher value than microporous systems, whereas nanoporous PEI showed the opposite behavior. However, all nanoporous polymers had a Young's modulus value lower than the solid.

A possible alteration of the fundamental properties of the base polymer due to the confinement of the polymer chains within the pore walls, or due to the stretching of the polymer chains induced during the manufacturing process [90], could be the cause of the different behaviors obtained. Nevertheless, more studies with different polymeric matrices are needed to understand, confirm or discard the contradictory tensile results that have been obtained up to now.

Thus, according to the works carried out to date, it can be concluded that nanoporous polymeric materials exhibit some mechanical properties superior to microporous materials at the same porosity, but it seems that the density, the nature of the confined material, and the morphology of the porous structure will also determine whether the mechanical properties of nanoporous systems will exceed those of the microporous material or the solid.

Moreover, the correlation between the experimental results on the yield strength of metals and polymers with the corresponding theoretical models is unclear, and it is necessary to develop more specific models for polymers.

3. Thermal conductivity

In recent years, there has been increasing interest in the development of efficient materials for thermal insulation applications. According to the project "*Energy Efficiency Trends in Buildings in the EU*", dwelling houses represent around 25% of the total energy consumption of western countries, where space heating represents more than 50% of this energy. If high efficiencies in household heating were reached, then it would be possible to achieve both economic savings and reductions in CO_2 emissions.

Porous polymeric materials with high porosities could lead to high-efficiency thermal insulators because of the good insulation capacity of the gaseous phase, which has a much lower conductivity than the polymer matrix. The evaluation of the thermal conductivity of porous materials from the conductivity data of the two component phases and the structure of the material is an interesting subject that has been approached by different authors [91–94]. In a porous material, it is assumed that there are four different contributions to the total thermal conductivity (λ_t) (Eq. (9)):

$$\lambda_t = \lambda_g + \lambda_s + \lambda_c + \lambda_r \tag{9}$$

where λ_g represents the conduction through the gas phase, λ_s is the conduction along the pore walls and struts of the solid material, λ_c represents the convection within the pores, and λ_r is the thermal radiation term.

In order to analyze the influence of the reduction in the pore size from the micrometer to the nanometer range on the thermal conductivity, it should be noted that convection plays a minor role in closed-pore materials with pore sizes below 4 mm in diameter [95] and in open-pore systems with pore sizes less than 2 mm [96] (and therefore will be negligible in closed and open micro- and nanoporous polymers). Likewise, the influence of the radiation term is well known in conventional and microporous materials, and this term is negligible for porous materials with relative densities over 0.2 [91]. However, the conventional models used to evaluate the radiation mechanism in porous polymers assumes that the wavelength of the infrared radiation is smaller than the pore size, but this presumption is incorrect in nanoporous polymers [97]. To overcome these difficulties, recent theoretical studies carried out in nanoporous materials have shown that the contribution of the radiation mechanism can be neglected even at low densities [98].

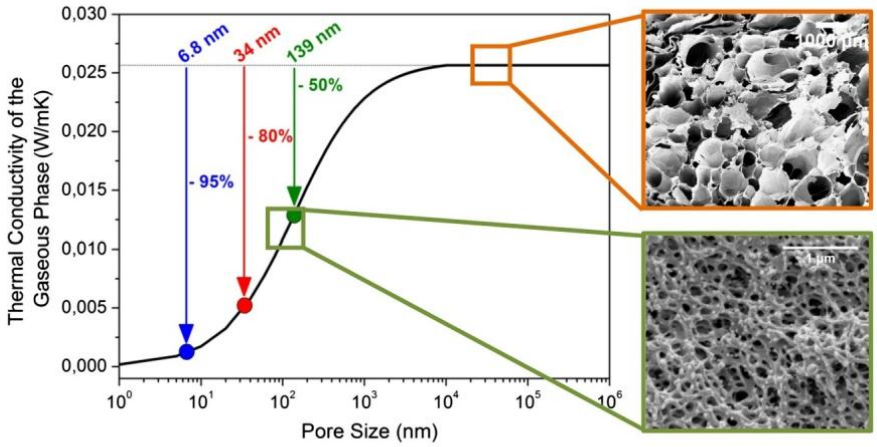

Fig. 11. Predicted relationship between the air thermal conductivity and the pore size due to the Knudsen effect, together with SEM micrographs (top: microporous PE; bottom: nanoporous PMMA/MAM) that have been included with permission from Notario et al. [14].

Therefore, it is expected that the change from the microscale to the nanoscale only affects the conduction through the gas and solid phases. Existing theoretical and experimental studies on this subject are discussed in the following paragraphs.

It is assumed that nanoporous polymeric materials will lead to a decrease in the thermal conductivity of the gaseous phase due to the so-called Knudsen effect [63,64]. This effect implies that the molecules of the gas collide more often with the molecules forming the surrounding solid part than with other gas molecules when pore size is comparable or smaller than the mean free path of the gas. Thus, the energy transfer through the gas molecules is decreased.

Then, the effective thermal conductivity of the gas in air-filled porous structures can be described by the Knudsen equation:

$$\lambda'_g = \frac{\lambda'_{g0}}{(1+\beta(l_g/\Phi))} \tag{10}$$

where λ'_{g0} is the thermal conductivity of free air (0.026 W/m K at room temperature), β is a parameter that takes into account the energy transfer between gas molecules and the limiting solid structure (about 2 for air), l_g is the mean free path of the gas molecules ($l_g \approx 70$ nm at room temperature), and Φ is the average pore diameter.

According to Eq. (10), a significant reduction in λ'_g is obtained when pore size decreases below a micron (see Fig. 11). Therefore, for porous materials with pore sizes in the nanometer regime, a reduction in the conduction through the gas phase should be expected. Furthermore, taking advantage of this benefit, it will be possible to reduce the thermal conductivity effectively over the long term.

The expected reduction in the thermal conductivity of the gas phase has been widely studies from a theoretical point of view [98–104]. For instance, Hrubesh and Pekala [99] studied the reduction of the thermal conductivity of open-pore nanoporous organic and inorganic aerogels (pore size between 10 and 90 nm) through the analysis of the three main components of thermal conductivity (conduction in the solid and gas phases and radiation). A significant reduction (around 90%) in the thermal conductivity of the gaseous phase was obtained when the pore size decreased from 90 nm to 10 nm; the Knudsen effect was identified as the main factor responsible for this reduction. The radiation term was analyzed using the classical diffusion approximation, but experimental values of the extinction coefficient were introduced. Using this model, they obtained a good agreement between experimental and theoretical thermal conductivity results, showing that the radiation term influences the overall thermal conductivity for relative densities lower than 0.1.

The diverse heat transfer mechanisms in a porous polystyrene with pore sizes both at the micrometer (pore size around 1 μm) and nanometer (two pore sizes used: 250 nm and 100 nm) scale were analyzed theoretically by Forest and coworkers [100]. They observed that, the lower the pore size, the lower the thermal conductivity because of the Knudsen effect.

A theoretical study (based on the Knudsen equations) of the coupled heat transfer by conduction and radiation in one-dimensional multi-phase media was developed by Ferkl et al. [98]. This model was used to understand the interplay of conduction and radiation on the micro- and nanoscales. A PS foam, with pore sizes ranging from 10 nm to 1 cm, open-pore morphology, and relative densities around 0.1, was used as an example. They observed that the lowest thermal conductivity was achieved by reducing the pore size to the nanometer range (because of the Knudsen effect) and that the contribution of the radiation term in low-density nanoporous materials can be neglected, which is contrary to the results of Hrubesh and Pekala [99].

Together with the Knudsen effect, which implies a confinement of the gaseous phase inside the pores, other mechanisms related to the conduction through the polymer matrix also arise and can justify the reduction in the thermal conductivity in the nanometer regime. In this case, the confinement of the matrix hinders the energy transfer through it because of a modified phonon scattering mechanism. In addition, the increase in the tortuosity described in Section 1.3 also contributes to the reduction in heat transfer because of the conduction to the solid phase (a longer distance to transmit the energy will also result in increased phonon scattering). Several works have studied this reduction in the solid-phase thermal conductivity from a theoretical point of view.

For instance, Sundarram and Li [101] used finite element analysis (FEA) and molecular dynamics (MD) to study the thermal behavior of open-pore polymers (in particular, PMMA and PEI). A reduction in the thermal conductivity when the pore size was decreased from 1 mm to 1 nm was predicted and was mainly attributed to the phonon scattering effect in the solid polymer matrix. Furthermore, two unusual results were also reported in this paper: first, they stated that the Knudsen effect has little relevance. Second, a decrease in the gaseous phase contribution when the pore size is reduced from 500 μm to 10 μm was also predicted for a constant density. These predictions do not match the well-known Knudsen equations and are also contrary to some experimental results found in porous polyethylene (PE) [14]. Therefore, it can be expected that the contribution of the phonon scattering mechanism is lower than the one assumed in this study.

The decrease in the phonon mean-free path, which arises from increased phonon scattering at the pore surfaces, was used by Lee et al. [102] to justify the reduction of two orders of magnitude in the thermal conductivity of open nanoporous Si (average pore size between 0.5 and 3 nm) with respect to the bulk. In this case, the Knudsen effect was not considered, because they only modeled the thermal conductivity along the solid phase. Furthermore, their MD approach (developed for an arrangement of nanometer-sized cylindrical pores) clearly showed that the thermal conductivity of nanoporous Si decreases as a function of pore size.

Using Monte Carlo simulations, Bera and coworkers [103] observed how the thermal conductivity of open nanoporous Si, nanoporous Ge, and nanoporous SiGe alloys decreases significantly when the pore size is lower than 100 nm. Again, this behavior was justified by the increased phonon scattering mechanisms without considering the Knudsen effect, because they only modeled the thermal conductivity of the solid matrix.

Finally, Tsui et al. [104] proposed a serial–parallel hybrid model to study the anisotropic behavior of the thermal conductivity of close-pore nanoporous silica films as a function of porosity (ranging from 21% to 64%) for a constant pore size (not specified in the article). Using this model, they were able to consider the inhomogeneities of the nanopore distribution (preferably oriented in the horizontal plane), and their thermal conductivity results were similar to those provided by the Gibson and Ashby model [105]. Furthermore, because of the high thermal conductivity of SiO_2 (1.4 W/m K) and the low-midrange porosity (20–60%), the contribution of the gas phase was very small regardless of the pore size. For this reason, it was impossible to assess whether considering the Knudsen effect will modify the results.

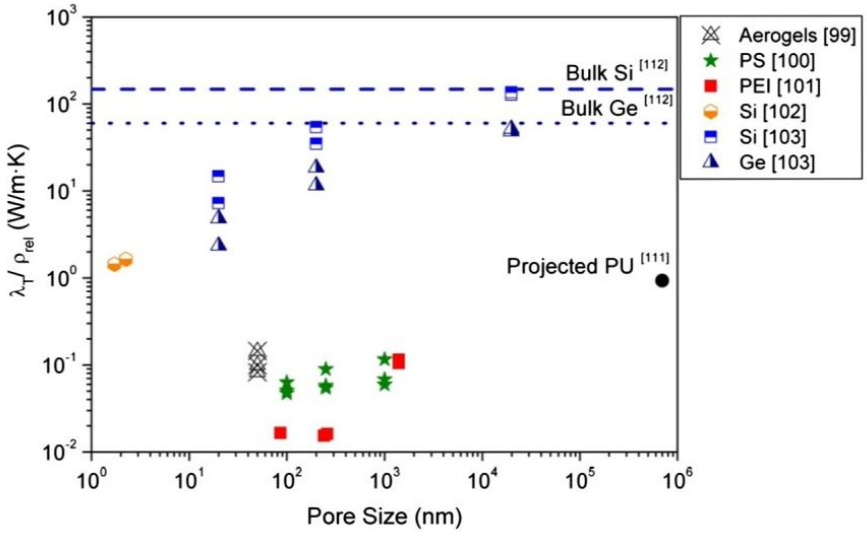

Fig. 12. Relationship between thermal conductivity divided by the relative density and the pore size for different nanoporous systems [99–103], together with the thermal conductivity of projected PU [111] and bulk Si and Ge [112].

Therefore, theoretical models developed for both nanoporous polymeric materials and other nanoporous systems agree that a reduction in the pore size implies a decrease in the thermal conductivity (see Fig. 12). In this figure, the thermal conductivity of nanoporous materials was divided by their relative density in order to analyze the influence of the pore size independently of the density. Furthermore, the thermal conductivity of a typical thermal insulator, rigid projected PU, and the thermal conductivity of typical semiconductors, bulk Si and Ge, were included for comparison purposes. Nanoporous thermal insulators are much better than conventional ones (projected PU), and the thermal conductivity of nanoporous semiconductors is lower than that of the solid. The confinement of the gas molecules within pores or a possible alteration of the phonon scattering mechanisms in the matrix are the mechanisms underlying this phenomenon. This expected reduction in the thermal conductivity has been previously experimentally demonstrated in aerogels [63,106–108], porous metals [109], and porous ceramics [110] (these works will be discussed below for comparison). However, the thermal conductivity of polymeric foams is a recent issue because of the technical difficulties found in the production of nanoporous polymers with adequate densities, pore sizes, and external dimensions to allow the characterization of their properties as thermal insulators. For this reason, experimental works on this topic are still scarce. These works are described in the following paragraphs.

A clear influenced of the pore size on the gaseous conductivity of aerogels with an average pore size between 10 and 90 nm (reductions of up to 39% of the gas phase [63]) due to the Knudsen effect was observed by Lu et al. [63] and by Lee and coworkers [106]. The thermal conductivity of these open-pore materials was measured from vacuum to ambient pressure by means of a transient hot-wire device, which led to extraordinarily low thermal conductivity values (0.015 W/m K for a relative density of 0.10).

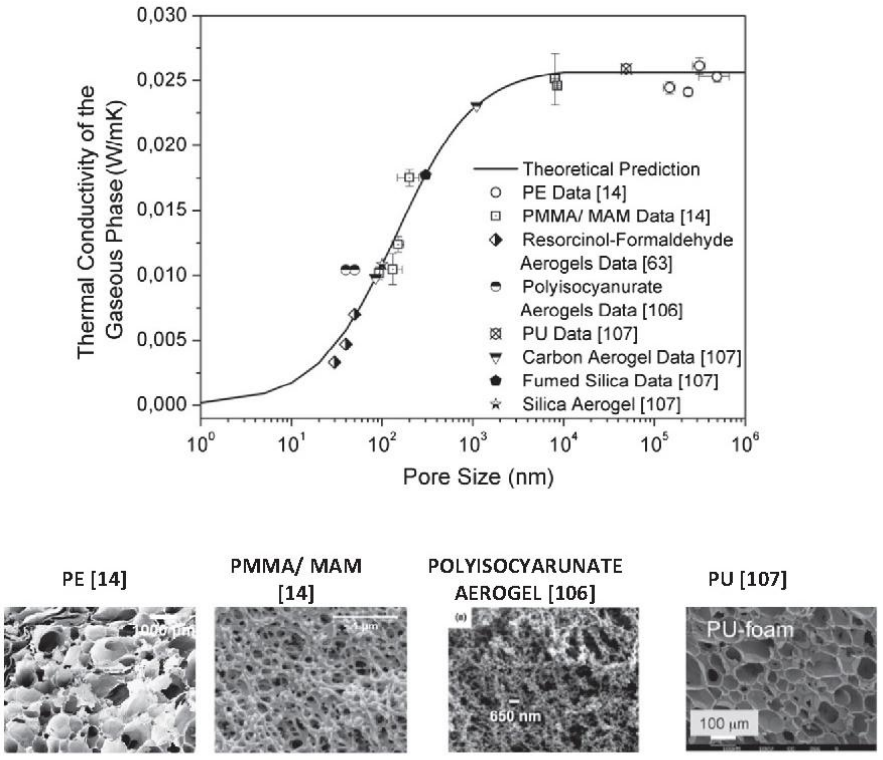

Fig. 13. Top: Effect of pore size on the gas thermal conductivity in open-pore polymeric materials [14], together with the theoretical prediction obtained from the Knudsen equation, and some of the previous results obtained in different nanoporous systems [63,106,107]. Bottom: SEM images of the samples analyzed that have been included with permission from [14,106,107].

Using the same procedure, Reichenauer et al. [107] measured the thermal conductivity of open-pore fumed silica, silica and carbon aerogels, solid glass spheres, and PU foams. Pore sizes of these samples ranged from about 100 nm to 1 mm. Again, a clear reduction of the thermal conductivity (around 88% when the pore size is reduced from 1100 to 85 nm) due to the Knudsen effect was detected. In this case, the nanoporous systems under study were not polymeric materials.

Thermal conductivity of open-pore nanoporous Bi films (pore sizes from 5 to 10 nm) was experimentally determined by Song et al. [109] by a differential 3-ω method. Nanoporous Bi exhibited an order of magnitude reduction in thermal conductivity compared to that of the solid, probably because of a reduction in the phonon mean free path. The Knudsen effect was not considered in this case, because the thermal conductivity of the gaseous phase was not taken into account.

Finally, the thermal conductivity of open-pore zirconia ceramics with pore sizes below 100 nm was also characterized by Nait-Ali et al. [110]. They pointed out that the pores should be as small as possible to reduce the thermal conductivity through the gas phase, as Knudsen effect predicts, and thus to achieve a thermally insulating material.

In general, thermal insulation improvements in nanoporous systems (at least in non-polymeric materials; see Fig. 13) are well established both theoretically and experimentally. Much effort have been made in recent years to demonstrate this expected improvement in nanoporous polymers as well. However, although there are patents [113,114] and articles [20,62,115] in which it is proposed to take advantage of this expected reduction in the thermal conductivity, to date there is only one experimental validation of this effect because of the technical difficulties associated with the production of nanoporous polymers.

Notario and coworkers [14] produced a wide set of PE- and PMMA-based polymeric foams with open-pore morphologies, pore sizes ranging from 90 nm to 100 μm, and relative densities from 0.12 to 0.6, and characterized their thermal conductivity (see Fig. 13). They demonstrated that it is possible to reduce the thermal conductivity of polymeric foams because of (a) a reduction of the gaseous conductivity due to the Knudsen effect, and there is good agreement between experimental data and theoretical predictions according to the Knudsen equation; and (b) a reduction of the thermal conductivity through the solid phase because of an increment of the tortuosity of the porous structure and/or a confinement effect in the polymeric matrix, which can be related to a different phonon scattering mechanism.

As a conclusion, theoretical models developed both for nanoporous polymers and for other nanoporous materials (aerogels and metals) predict a reduction of the thermal conductivity when the pore size is below a micron. The confinement of both the gaseous phase (Knudsen effect) and the solid phase (different phonon scattering mechanisms/increased tortuosity) are the phenomena underlying this effect.

Experimental results, both in polymers and other materials (aerogels, metals, and ceramics), verify this expected reduction in the thermal conductivity. The two theoretical arguments mentioned above are used to justify this decrease in the thermal conductivity.

The number of works in nanoporous polymers to date has been limited; however, the Knudsen effect depends only on the morphology of the porous structure and is independent of the solid matrix. Therefore, it can be stated that there is sufficient evidence to confirm its presence in a wide range of nanoporous materials, such as polymers, aerogels, metals, and ceramics. However, the analysis of the radiation term is still scarce, and there exist contradictory results on the weight of this contribution as a function of the density and cell size in nanoporous polymers.

4. Dielectric properties

The continuous miniaturization in the microelectronics industry (feature size below 100 nm) has led to the production of low-dielectric-constant (k) materials to mitigate interconnect resistance–capacitance (RC) delays, cross-talk noise, and power dissipation. According to the *National Technology Roadmap for Semiconductors (NTRS)* published in 1997 in California, USA [116], materials with dielectrics constants around 1.5–2.0 were required in the year 2006 (and are currently being pursued), and materials with $k \leqslant 1.5$ were demanded in the year 2012 to overcome these drawbacks. In addition,

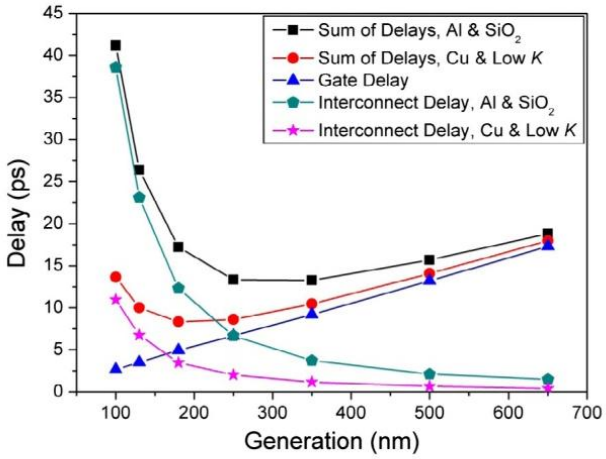

Fig. 14. Calculated gate and interconnect delay versus technology generation for conventional materials such as Al and SiO_2 and for new materials such as Cu or low-k materials. This figure has been adapted from [116].

these materials should have good thermal and chemical stability, low moisture uptake, high mechanical resistance, and high dielectric breakdown fields. These requirements have not been achieved yet in the microelectronics industry.

Implementation of low-k materials for 100-nm technology generation requires the development of new materials and technologies. Fig. 14 shows how the use of low-k materials will decrease the interconnect delays with respect to conventional materials used in microelectronics such as aluminum (Al) and silicon dioxide (SiO_2). However, this methodology will only cover the needs for the closest technological generations. Technology generations beyond 100 nm will demand either new systems or new approaches to interconnects.

This demand for low-k materials has stimulated great efforts to explore the applicability of porous materials, especially porous polymeric systems, to replace silicon dioxide (SiO_2, $k > 3.5$) as the interlevel dielectric. The low dielectric constant of the polymer ($k < 3$) [117] together with that of air ($k = 1$) make these porous polymeric systems promising candidates as low-k systems.

In this case, nanoporous materials are in demand because of the reduced dimensions of developing devices, where the pores must be smaller than the thickness of the film (preferably an order of magnitude lower [118]). However, it is not expected that these materials will show new effects due to the presence of porosity. Indeed, one of the objectives of this review is to analyze whether there is any real influence of pore size on the dielectric behavior of these nanoporous systems.

The equation that describes the dielectric constant k_t of a two-phase system is the so-called Lichterecker mixing rule [119]:

$$k_t^{\alpha} = k_s^{\alpha}(1 - V_g) + k_g^{\alpha} V_g \tag{11}$$

where k_s and k_g are the dielectric constants of the solid and gaseous phases, respectively, V_g is the volume fraction of voids (i.e., the porosity), and α is a parameter that determines the type of rule of mixtures. If $\alpha = -1$, then the serial mixing rule can be used (which represents a lower limit of the dielectric constant):

$$\frac{1}{k_t} = \frac{(1 - V_g)}{k_s} + \frac{V_g}{k_g} \tag{12}$$

When $\alpha = 1$, the parallel mixing rule (an upper limit of the dielectric constant) is given as:

$$k_t = k_s(1 - V_g) + k_g V_g \tag{13}$$

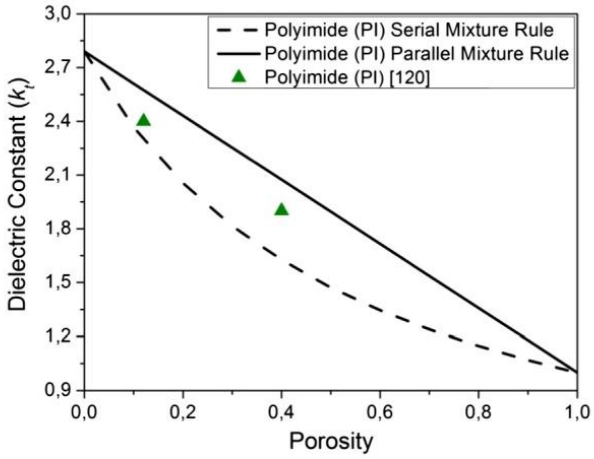

Fig. 15. Variation of the dielectric constant as a function of porosity according to Eqs. (12) and (13) for the particular case of a nanoporous polyimide ($k_s = 2.79$), together with some experimental results [120].

In the case where $\alpha \to 0$, an intermediate form between the serial and parallel forms (logarithmic mixture rule) is found:

$$\log k_t = (1 - V_g) \log k_s + V_g \log k_g \tag{14}$$

According to these expressions, increased porosity leads to a reduction in the dielectric constant (see Fig. 15, in which experimental results obtained by Krause et al. [120] in polyimide films are included. These experimental values show an intermediate behavior between the upper and lower limits). Nevertheless, this increased porosity also tends to reduce the mechanical resistance of the system. For this reason, control over pore size, shape, and distribution is important to obtain the appropriate mechanical properties to withstand the aforementioned requirements (close-pore morphologies are preferred in terms of their mechanical behavior).

This expected reduction in the dielectric constant of nanoporous systems has been experimentally demonstrated both in polymeric materials and in other systems, such as silica [121–123] or organosilicates [124–129]. The results concerning the latter will be described briefly below for comparison with the results obtained in polymeric materials.

Nanoporous silica films (also known as aerogels or xerogels) have been intensively developed in recent years. These materials exhibit high thermal stability, small pore sizes, and dielectric constants that can be tailored from 1 to 4 [121–123]; nevertheless, a surface treatment and film aging must be applied to minimize their moisture absorption. For instance, Baskaran et al. [122] synthesized closed-pore nanoporous silica films (thickness between 0.5 and 1.2 mm) with dielectric constants ranging from 1.8 to 2.5 and pore sizes less than 5 nm. In particular, they obtained a material with a dielectric constant of 2.2 (lower than that of the solid, $k_s \approx 4$) that had a stable dielectric response with time, a porosity around 55%, a good texture, and acceptable mechanical properties ($n = 2$ for the Young's modulus vs. density curve (Eq. (6))). Furthermore, an aging treatment was applied to reduce the moisture level.

Organosilicates are also promising materials for low-k dielectrics because of their intrinsic hydrophobic behavior and the high thermal stability of the solid matrix [124–129]. Yang and coworkers [124,125] produced poly(methyl silsesquioxane) (MSQ) nanoporous organosilicate films (thicknesses of 0.3–0.8 μm) with pore sizes between 2 and 6 nm, porosities from 30% to 50%, and k values from 2 to 1.5 (lower values than that of the solid, $k_s \approx 2.8$). This closed-pore organosilicate exhibited good thermal stability, acceptable mechanical strength ($n = 2$ for the Young's modulus, and $n = 3$ for the hardness of the system with a porosity of 0.3), and a high electrical breakdown field (>1.5 MV/cm). Similarly, closed pore nanoporous poly(methylsilsesquioxane) films with a final thickness around 1 μm were prepared by Nguyen et al. [126]. These organosilicate films presented

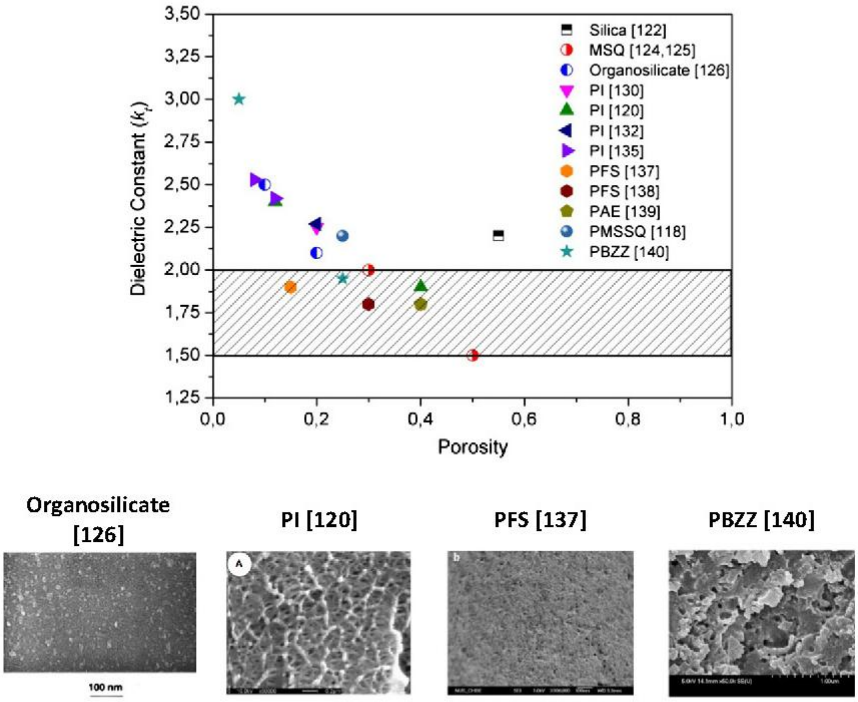

Fig. 16. Top: Dielectric constant values obtained for different nanoporous systems (both polymeric and non-polymeric) as a function of porosity. The shaded area represents the dielectric constant values required by NTRS. Bottom: SEM (PI, PFS, and PBZZ) and TEM (organosilicate) micrographs of some of the nanoporous materials under study included with permission from [120,126,137,140].

an average pore size of 20 nm, porosities ranging from 10% to 20%, dielectric constants from 2.5 to 2.1 (a reduction around 10% and 24%, respectively, with respect to the solid), a thermal stability around 250 °C, and a high dielectric breakdown (2–3 MV/cm).

Experimental results obtained in non-polymeric nanoporous materials clearly showed a reduced dielectric constant in comparison with the former solid, with values close to those required by the NTRS in the year 2006 (especially in the case of organosilicates with porosities higher than 0.2; see Fig. 16). However, further studies are needed to verify whether these materials are potential candidates to be used in microelectronics (see Table 1).

Nanoporous polymers have emerged in recent years as potential low k materials for use in the development of advanced integrated circuits. The low dielectric constant of the polymer matrix ($k < 3$) compared to the inorganic alternatives, together with the lower manufacturing costs and ease of processing, make these materials promising candidates. Nevertheless, their major drawback compared to inorganic materials is their low thermal stability. These materials must withstand the high temperatures associated with the processes used to deposit metal lines and anneal devices. Though a wide variety of polymers have been analyzed for use in microelectronics devices, only some of them meet the stringent requirements.

Polyimides (PI) are a favored material because of their high thermal stability, low stress coefficient of thermal expansion, low dielectric constant, high resistivity, and high dielectric breakdown [120,130–135]. For instance, Lee et al. [130] managed to develop a nanoporous PI films (thickness: 200 μm) with pore sizes from 10 to 40 nm, a porosity around 20%, and a dielectric constant of 2.25 (a reduction of 31% with respect to the solid). These closed-pore (with some interconnections) PI films exhibited a high thermal stability (>300 °C), and acceptable mechanical behavior ($n = 2$ for the Young modulus).

Table 1
Comparison between the requirements demanded by the NTRS in the year 2006 and the results obtained to date.

System	Porosity	Pore size (nm)	$1.5 < k < 2.0$	Thermal stability	Chemical stability	Low moisture uptake	High mechanical resistance	High dielectric breakdown
Silica [122]	0.55	<5	2.2	*Not Studied*	*Not Studied*	Acceptable	Acceptable Elastic Modulus: $n = 2$	*Not Studied*
Organosilicates [124,125]	0.3–0.5	2–6	2–1.5 ✓	*Not Studied*	*Not Studied*	Not studied, though by nature they are hydrophobic	Acceptable Elastic Modulus: $n = 2$ Acceptable-Bad Hardness: $n = 3$	>1.5 MV/cm
Organosilicates [126]	0.1–0.2	20	2.5–2.1	≈250 °C Acceptable	*Not Studied*	Not studied, though by nature they are hydrophobic	*Not Studied*	>2 MV/cm
Polyimides [130]	0.2	10–40	2.25	>300 °C	*Not Studied*	*Not Studied*	Acceptable Elastic Modulus: $n = 2$	*Not Studied*
Polyimides [120]	0.12–0.4	20–50	2.4–1.9 ✓	>250 °C	*Not Studied*	*Not Studied*	Good Elastic Modulus: $n = 1.4$	*Not Studied*
Polyimides [132]	0.2	10	2.27	>300 °C	*Not Studied*	Absorbs	Acceptable Elastic Modulus: $n > 2$	*Not Studied*
Polyimides [135]	0.08–0.12	35–70	2.53–2.42	≈250 °C	*Not Studied*	*Not Studied*	Very Good Yield Strength: $n \approx 1$	*Not Studied*
Polyimides/SiO_2 Nanocomposites [136]	0.1–0.45	20–50	3.5–2.6	*Not Studied*	*Not Studied*	*Not Studied*	*Not Studied*	*Not Studied*
Fluoropolymer [137]	0.15–0.4	30–50	1.9–1.8 ✓	≈300 °C	*Not Studied*	*Not Studied*	*Not Studied*	*Not Studied*
Fluoropolymer [138]	0.3	90–150	1.8 ✓	*Not Studied*	Good (THF & Chloroform)	*Not Studied*	*Not Studied*	*Not Studied*
Poly(aryl ether) [139]	0.4	3	1.8 ✓	>300 °C	*Not Studied*	Hydrophobic ✓	*Not Studied*	*Not Studied*
Poly (methylsilsesquioxane) [118]	0.09–0.25	<3	2.2	*Not Studied*	*Not Studied*	*Not Studied*	Bad Elastic Modulus and Hardness: $n \approx 4$	*Not Studied*
Polybenzoxazine [140]	0.05–0.25	50	3–1.95 ✓	≈340 °C	*Not Studied*	*Not Studied*	*Not Studied*	*Not Studied*

Five different nanoporous PI films (thickness around 100 μm) were produced by Krause and coworkers [120]. These nanoporous films exhibited porosities ranging from 12% to 40%, k values from 2.4 to 1.9, respectively (lower values than that of the solid, k_s = 2.79), and pores with a closed morphology and an average size from 20 to 50 nm. In this case, the thermal stability of nanoporous PI was higher than 250 °C, and the mechanical response was improved (n = 1.4 for the Young's modulus) with respect to the results obtained by Lee et al. [130].

Carter et al. [132] also produced closed-pore nanoporous PI films with an average thickness from 1 to 40 μm, an average pore size around 10 nm, a porosity around 20%, and a dielectric constant of 2.27 (a lower value than that of the bulk, k_s = 2.56). The mechanical behavior of these films was measured, and a value of $n > 2$ was obtained for the elastic modulus. These nanoporous PI films absorbed moisture, although less than the solid did, and exhibited a high thermal stability (>300 °C).

Similarly, Mehdipour-Ataei and Aram [135] developed nanoporous PI films (the thickness was not specified in the article) with pores exhibiting a closed morphology, pore sizes between 35 and 70 nm, porosities ranging from 8% to 12%, and dielectric constant values from 2.53 to 2.42 (the values were lower than that of the solid, k_s = 3.06). These films presented very good mechanical properties ($n \approx 1$ for the yield strength) but lower thermal stability values (≈250 °C) than the ones in previous works.

Li and coworkers [136] developed PI/silica nanocomposite nanoporous films with thicknesses between 100 and 200 μm. This closed-pore system exhibited pore sizes ranging from 20 to 50 nm, porosities from 0.1 to 0.45, and lower dielectric constants than that of the solid (from 3.5–2.6 for the porous film to 3.8 for the bulk system). In this case, the thermal and mechanical properties were not studied.

Other potential candidate for interlayer dielectric applications are fluoropolymers [137,138]. These materials are characterized by good chemical stability and by the lowest dielectric constants among the bulk polymers (around 2.4). However, their main drawback is their insufficient thermal stability for integration procedures, and furthermore there are concerns about fluoric acid evolution during processing and its reactions with the metals employed. Fu et al. [137] managed to overcome the problem of thermal stability and produce closed-pore nanoporous poly(pentafluorostyrene) (PFS) films with a thermal stability of around 300 °C. These nanoporous films exhibited a thickness of about 1–2 μm, an average size from 30 to 50 nm, porosities ranging from 15 to 40%, and k values from 1.9 to 1.8, respectively (a reduction of about 20% with respect to the bulk).

A good chemical resistance to common organic solvents such as tetrahydrofuran (THF) and chloroform was achieved by Fu and coworkers [138] by producing crosslinked nanoporous fluoropolymer films with a thickness of around 2–4 μm. This closed pore system had pores between 90 and 150 nm, a porosity around 30%, and a dielectric constant of 1.8 (a lower value than that of the bulk, k_s = 2.2). The dielectric constants obtained with fluoropolymers in this study and in the previous one were lower than those achieved in polyimide and are within the range demanded by the NTRS.

Another variety of nanoporous polymers that have been proposed as low k materials is polyaryl ether (PAE). This class of polymers presents attractive properties such as excellent chemical resistance, high thermal stability, and good mechanical properties. For instance, Xu and coworkers [139] obtained hydrophobic closed-pore nanoporous PAE films (thickness: 490 nm) with a porosity of 40%, pore sizes around 3 nm, a dielectric constant equal to 1.8 (a reduction of 32% with respect to the solid), and a thermal stability higher than 300 °C.

Another area of significant interest is polysilsesquioxanes (PSSQs) and, in particular, materials based on poly(methylsilsesquioxane) (PMSSQ). The synthesis of these materials can open the door to new materials with improved properties, especially materials with low dielectric constants. For instance, nanoporous PMSSQ films with a final thickness in the range of 600 nm to 1 μm were synthesized by Ro et al. [118]. These films presented a porosity from 9% to 25%, a pore size lower than 3 nm, and a dielectric constant of 2.2 for the material with a porosity of 25% (a lower value than that of the solid, k_s = 2.7). However, the mechanical properties of the nanoporous films must be improved, since the modulus of elasticity and the hardness decreased substantially with porosity ($n \approx 4$, for both the elastic modulus and the hardness).

Finally, polybenzoxazines (PBZZ) are also a novel material for use in microelectronics. This polymer is a newly developed high-performance thermoset that presents low moisture uptake and in some cases exhibits a glass transition temperature much higher than cure temperature. Su et al. [140] prepared closed-pore nanoporous PBZZ films (thickness between 0.125 and 0.75 mm) with a porosity ranging from 5 to 25%; k from 3 to 1.95, respectively (lower values than that of the solid, $k_s \approx 3.6$); pore sizes around 50 nm; and a thermal stability around 340 °C.

Therefore, as expected theoretically, nanoporous polymers reduce the dielectric constant of the former solid by the introduction of a gas phase into the polymer matrix. Some of them (fluoropolymers, polyaryl ethers, polyimides, and polybenzoxazines with porosities higher than 0.2) manage to achieve the dielectric constant values demanded by the NTRS to be implanted in integrated circuits (see Fig. 16). Likewise, as shown in Fig. 17, in principle, the pore size has no influence on the dielectric constant of nanoporous materials, and the porosity is primarily responsible for the reduction in this parameter (see Figs. 15 and 16). However, the existence, or future appearance, of side effects due to the reduction of pore size to the nanoscale cannot be completely neglected, since some evidence of a possible modification of the capacity and conduction mechanisms in nanoporous polymers has been found when the pore size moves from the micrometer to the nanometer range [65].

However, properties such as moisture uptake, chemical stability, and dielectric breakdown must be studied, and other properties such as the mechanical behavior and thermal resistance need to be improved, so that the development of these polymeric systems becomes a reality (see Table 1).

The key to achieving low dielectric constant values involves increasing the porosity, which, given the size of the system (and therefore the size of the pores to be formed), implies extraordinarily high cell densities. This fact, as it was mentioned at the beginning of this review (see the *Expected Cellular Structure* section), is currently one of the main goals for nanoporous materials.

Furthermore, it has been demonstrated that pore size does not seem to provide an additional advantage to nanoporous systems; this is only a requirement imposed by the dimensions of the devices to be developed. Further studies are needed with materials both at the micrometer and nanometer ranges (and thus with thicker systems) to confirm whether there may be a positive or negative influence of the pore size on the dielectric properties of the porous material.

Thus, new nanoporous low-k dielectric materials (both polymeric and non-polymeric) are actively being pursued. Low dielectric constants have been achieved, especially with materials with a porosity higher than 20%. However, because of the strict requirements demanded, they have not yet been implemented in the field of microelectronics, since the requirements demanded in the year 2006 have not been reached yet.

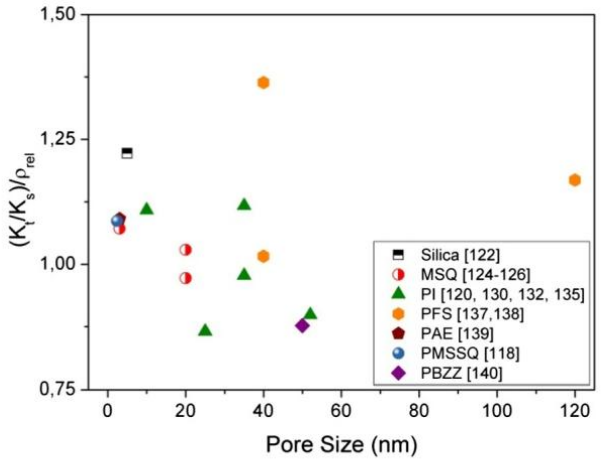

Fig. 17. Dielectric constant values of the foams normalized by the dielectric constant of the solid and divided by the relative density versus pore size for different nanoporous materials [118,120,122,124–126,130,132,135,137–140].

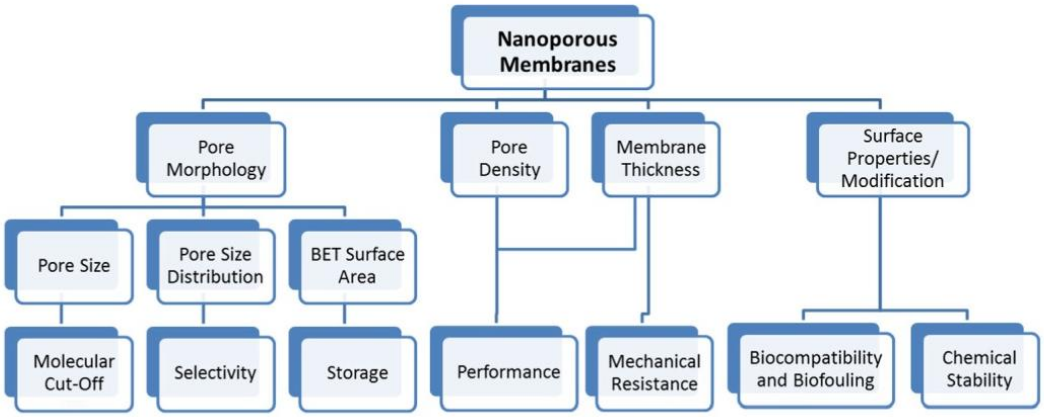

Fig. 18. Scheme of the main membrane features that influence performance.

5. Filtration and membranes

In recent years, the use of membranes developed using nanoporous materials and in particular nanoporous polymers has greatly increased in fields such as gas storage, tissue engineering, and water treatment, among others. The unique properties exhibited by nanoporous materials such as a large specific surface to volume ratio, a high inner surface area, or exclusive size sieving and shape selectivity, are some of the reasons that have led the industry and researchers to further develop these materials.

The successful design and application of a nanoporous membrane for a specific application depends on diverse critical membrane properties (see Fig. 18). First, the production of membranes with a specific pore size and a narrow pore size distribution will allow precise control over molecular sieving. Second, membranes with a high Brunauer–Emmett–Teller (BET) surface area will allow the storage of larger amounts of gas. Third, many applications required a low flow resistance to allow a high flux, which leads to high-porosity and low-thickness membranes. Fourth, an appropriate mechanical resistance, as well as good thermal and chemical stability in different environments, is crucial for long-term applications. Finally, for *in vivo* devices, good biocompatibility and good resistance against biofouling are essential to avoid immunological response and loss of functionality, respectively.

Several theoretical models for gas storage, gas permeation, or liquid flow across porous membranes have been developed over the years to study their behavior. There has been a resurgence in interest in hydrogen storage as a fuel owing to a decreased reliance on oil and to the potential need for a reduction in air pollution. However, before changing from petroleum to hydrogen, it is necessary to develop a suitable hydrogen storage mechanism that accomplishes the US Department of Energy (DOE) targets: gravimetric goals (net useful energy/max system mass) of 6 wt.% in the year 2010 and 9 wt.% in the year 2015 and volumetric goals (net useful energy/max system volume) of 1.5 kW h/l in 2010 and 2.7 kW h/l in 2015 [141]. Thus, several theoretical models have been developed in order to determine the main parameters that are going to govern the behavior of the system.

For instance, Cabria and coworkers [142] developed a quantum-mechanical and thermodynamical theoretical model to determine the optimal pore size for hydrogen storage in carbon nanoporous materials, in which the porosity and membrane thickness are not taken into account. This model, developed for the storage of hydrogen in slitpores, predicts that a material with a pore width equal to or larger than 5.6 Å can reach the DOE goals for the year 2010 for applications at low temperatures (77 K) and at any pressure. For applications at 300 K and at least 10 MPa, the width of the pore should be about 6 Å. This model was corroborated with experimental data presented in the literature for carbon-based materials, which showed a good agreement between the theoretical prediction and the experimental values.

Similarly, Bénard et al. [143] studied the physisorption of hydrogen on activated carbon (AC) nanoporous structures with slitpores (pore width varying from 0.9 to 2 nm) by means of the Ono–Kondo

adsorption isotherm model [144], in which the porosity and membrane thickness are neglected. Theoretical results showed that AC slitpores with a width higher than 1 nm show a maximum absorption around 7 wt.% at 77 K and 4 MPa (a value higher than that required by the DOE in 2010).

In the case of gas diffusion, the Knudsen number (i.e., the ratio between the mean free path and the pore diameter (l_g/Φ)) will determine the mechanism of gas permeation [145]. If the pores are in the range of 5–20 Å, the gases will be separated by molecular sieving (see Fig. 19, surface diffusion). This type of transport is complex and includes both diffusion in the gas phase and diffusion of adsorbed species on the surface of the pores.

If the mean free path of the gas is comparable with the pore diameter (Knudsen number around 1), transport is the result of collisions between the pore walls and the diffusing gas molecules (Knudsen diffusion [146,147], Fig. 19). The gas flow of a membrane in the Knudsen regime is given by

$$J = \frac{V_g \cdot (P_0 - P_l)}{\tau \cdot l \cdot RT} \cdot 0.33\Phi\sqrt{\frac{8RT}{\pi M_{gas}}} \tag{15}$$

where J is the gas flux through a membrane with a pore diameter Φ and a thickness l under a pressure difference $(P_0 - P_l)$, V_g is the porosity, R is the gas constant, T is the temperature, M_{gas} is the molecular weight of the gas, and τ is the tortuosity in the gas phase (as defined previously in Section 1.3).

However, when the mean free path of the molecules is much smaller than the pore size (a small Knudsen number), transport is the result of random collisions between them. In this situation, gases permeate the membrane by convective flow (see Fig. 19), as described by Poiseuille's law [147]:

$$J = \frac{V_g \Phi^2}{32\eta} \frac{(P_0 - P_l)(P_0 + P_l)}{l \cdot RT} \tag{16}$$

where η is the viscosity of the gas and $(P_0 + P_l)$ is a term that takes into account the expansion of the gas when it moves under a pressure gradient.

For instance, the low pressure transport of gases such as H_2, He, N_2, and Ar, among others, was modeled by Bhatia [148] in nanoporous membranes through an oscillator theory developed for cylindrical pores (pore diameters from 0.5 to 2.5 nm, corresponding to Knudsen diffusion transport). With

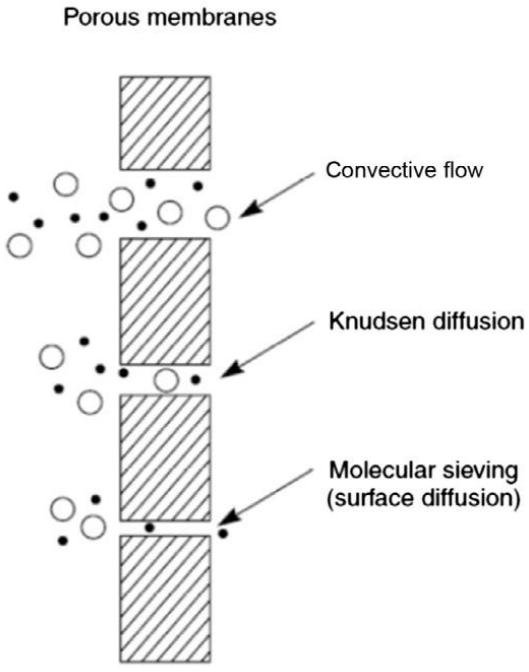

Fig. 19. Different mechanism for permeation of gases through porous membranes adapted from [145].

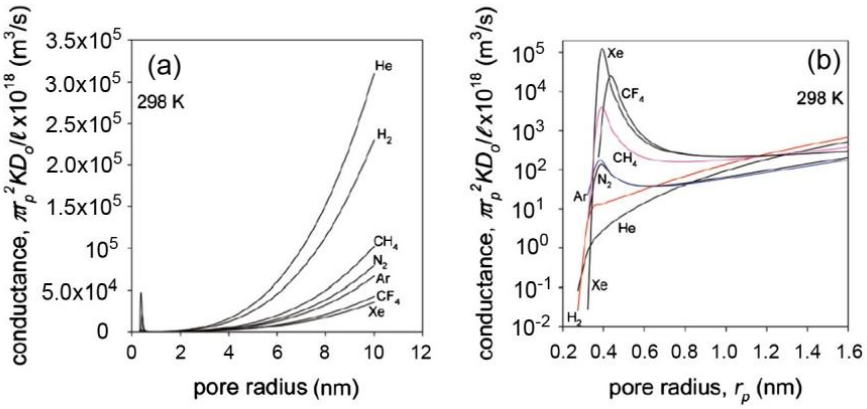

Fig. 20. Variation of pore conductance as a function of pore radius: (a) pore radius varying from 0 to 12 nm and (b) zoom view over the pore radius range of 0.2–1.6 nm. In the figure, r_p represents the pore radius, K is the Boltzmann constant, D_0 is the diffusion coefficient, and l is the pore length. The figure has been included with permission from Bhatia [148].

this model, it was demonstrated that the Knudsen approximation represents an upper bound in the diffusivity of gases. However, they showed that, as the pore size increases, the conductance (defined in terms of the diffusivity, as shown on the y axis of Fig. 20) of gases increases, since the gas molecules have more space to pass through the membrane (see Fig. 20), which reduces the molecular sieving. In Fig. 20(b), a sharp maximum around 0.4 nm is observed. This effect is known as the levitation effect and is discussed elsewhere [149,150]. Furthermore, a good correlation was obtained when the model was applied to permeability literature data from a zeolite membrane with a porosity of around 21% and a pore diameter lower than 1 nm. In addition, the model provides an expression for the tortuosity, showing that it can increase or decrease with the uniformity of the pore size distribution as well as with the temperature, because gases preferentially flow through more conducting pores. Thus, in this application, tortuosity does not depend exclusively on structural parameters.

However, a good correlation between the experimental diffusivities of gases (He, N_2, O_2, and Ar) and the Knudsen diffusion equation was obtained by Phillip et al. [151] in nanoporous PS membranes with a porosity of 26%, cylindrical nanopores with an average diameter of 17 nm, and a membrane thickness of 0.3 μm. They also showed that the diffusion coefficients calculated from classical kinetic theory overestimates the diffusivity values expected by 7%.

In the case of liquid flow through a nanoporous membrane, different theoretical models have been developed to analyze the liquid transport according to different pore geometries. In general, most of the models describe the membranes as a series of cylindrical capillary pores of diameter Φ. The liquid flow through a pore with this geometry is given by the Hagen–Poiseuille's equation [146] as follows:

$$J = \frac{V_g \Phi^2}{32\mu \cdot \tau \cdot l} \Delta P \tag{17}$$

where ΔP is the pressure difference through the pore, μ is the liquid viscosity, and l is the pore length.

Another important parameter that must be taken into account in liquid transport is the diffusivity. In general, in a porous membrane, the effective diffusion coefficient D_{eff} is related to the diffusion coefficient in free solution D_0 as follows [152]:

$$D_{eff} = \frac{D_0 V_g \delta}{\tau} \tag{18}$$

where δ is a constrictivity factor that accounts for the constricted transport paths caused by the small pores and takes values $\leqslant 1$, whereas τ is the tortuosity in the gas phase and takes values >1.

The diffusion permeability of different solutes (antibiotics, proteins, and several biomolecules) across gyroid nanoporous 1,2-polybutadiene (1,2-PB) membranes was studied by Li et al. [153] using Eq. (18). These membranes, which presented pore sizes around 10 nm, porosities around 40%, and membrane thicknesses of 20 μm, exhibited different diffusion rates depending on the solute (from

10^{-6} in the case of glucose to 10^{-9} in the case of cytochrome C). Furthermore, the constrictivity factor was calculated from the experimental results obtained for D_{eff} according to Eq. (18), showing that, apart from size exclusion, there are other factors that strongly affect the diffusion of molecules through nanoporous membranes such as solute–solute and solute–membrane interactions (electrostatic, hydrophobic, charge transfer, or hydrogen bonding interactions).

Adiga and coworkers [154] reviewed the basic mechanisms underlying liquid transport in nanoporous membranes with cylindrical nanopores for biomedical applications. In this case, two different expressions were proposed for the effective diffusion coefficient of rigid molecules:

$$\frac{D_{eff}}{D_0} = \frac{\left(1 - \frac{\Phi_s}{\Phi}\right)^2}{\left(1 + 2.4\frac{\Phi_s}{\Phi}\right)} \tag{19}$$

$$\frac{D_{eff}}{D_0} = \left(1 - \frac{\Phi_s}{\Phi}\right)^2 \left(1 - 2.104\frac{\Phi_s}{\Phi} + 2.09\frac{\Phi_s{}^3}{\Phi} - 0.95\frac{\Phi_s{}^5}{\Phi}\right) \tag{20}$$

where Φ_s represents the solute diameter. Eq. (19) [155] is normally used when the molecules have to pass through very tiny pores, while Eq. (20) [156] is more commonly used and gives accurate results when $D_{eff}/D_0 < 0.4$.

Finally, the water transport through nanoporous PS membranes was analyzed by Phillip et al. [151] by means of the Hagen–Poiseuille's law. These membranes possessed a porosity of 26%, nanopores with a cylindrical pore morphology and an average pore diameter of 17 nm, and a thickness of 0.3 μm. This system showed that the flow of water in the nanopores was consistent with the Hagen–Poiseuille's equation.

Therefore, theoretical models developed for both nanoporous polymeric materials and other nanoporous systems seem to describe the gas storage or fluid transport (both gas and liquid) of solutes through nanoporous membranes accurately. Furthermore, all of them seem to agree that a reduction in the pore size implies an increase either in the gas storage capacity or in molecular sieving. These expected improvements have been experimentally demonstrated both in polymeric materials and in other systems such as carbon, silicon, and alumina. The results concerning the latter will be described briefly below for comparison with the results obtained with polymeric materials.

Gas storage (in particular hydrogen storage) in porous materials such as zeolites, carbon materials, and metal–organic frameworks (MOFs) has been widely studied [157,158]. Morris and coworkers [157] compared the hydrogen adsorption capacity of different nanoporous systems such as zeolites, MOFs, and carbon materials using literature data (see Fig. 21), showing that the higher the BET surface area, the higher the amount of H_2 adsorbed. The same result was obtained by Thomas [158], who found that the porosity and the BET surface area have the most influence on the maximum hydrogen

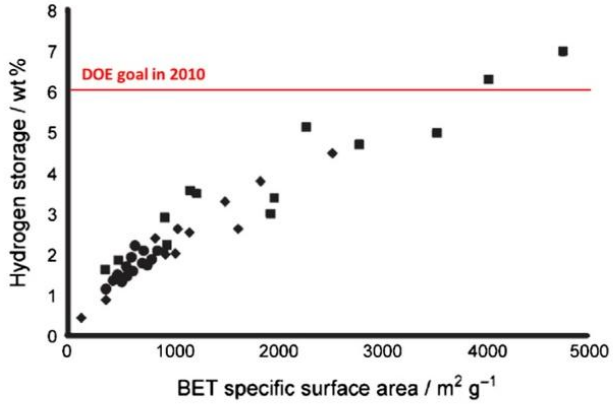

Fig. 21. Maximum H_2 adsorption capacity at different pressures and temperatures as a function of the BET surface area for porous materials: zeolites (●), MOFs (■), and carbon materials (◆). This figure has been adapted from Morris and Wheatley [157].

uptakes of all porous materials. Therefore, if one could obtain very high surface areas and high porosity simultaneously, a significantly increased adsorption would occur. Likewise, Fig. 21 illustrates that the only materials that are able to reach the requirements demanded by the DOE in 2010 are the MOFs.

Membrane-based gas separation currently involves innovative nanoporous membrane systems such as carbons [159–161], alloys [162], carbon/silica [163], zeolites [164,165], and crystalline aerogels [166]. For instance, Park and Lee [163] studied the permeability of several gases (H_2, He, CO_2, O_2, N_2, etc.) through a nanoporous carbon/silica membrane (thickness: 25–30 μm; porosity and pore size: not specified), showing improved O_2/N_2 and CO_2/CH_4 selectivity (around 2.3% and 5%, respectively) with respect to polymeric membranes and an improved C_2H_4/C_2H_6 selectivity around 0.7% for carbon membranes. In addition, the O_2/N_2 selectivity was also 3.3 times higher than that obtained by Shiflett and Foley [159] in a nanoporous C membrane (porosity: 20%; thickness: 8–23 μm; pore size: 0.3–0.7 nm). Differences in porosity, membrane thickness, and pore size could be the reasons underlying this phenomenon.

Nanoporous membranes for liquid transport or filtration have been also manufactured from a wide variety of materials [167]: alumina [168–171], silicon [172], SiC [173], silica [174], carbon [161], nanoporous crystalline aerogels [166], etc. Thormann et al. [171] observed that the flow rate of ethanol in nanoporous alumina membranes increased both with larger pore diameters and with thinner samples. However, the superior adsorptive behavior of bulky dyes (10 times higher in the best case) compared to commercial AC was found by Han and coworkers [161] in nanoporous carbon membranes. The high pore volumes and the high surface areas could be the reasons underlying this improvement.

Thus, gas storage and solute transport enhancement through non-polymeric nanoporous membranes are well established both theoretically and experimentally. Although the aforementioned porous materials present good properties for membranes in general, the ease of manufacturing, the superior flexibility, the good biocompatibility, and the tailored thermal, mechanical, and chemical properties with different synthetic approaches make nanoporous polymers excellent materials for filtration.

In the case of hydrogen adsorption, the major drawbacks of porous polymers are the relatively restricted number of synthetic strategies to achieve polymers with high surface areas (>1000 m^2/g) and the difficulty to achieve pores with sizes ideally lower than 2 nm. However, new systems, such as polymers of intrinsic microporosity (PIMs) (rigid macromolecules that form nanoporous organic materials because of their inability to pack space efficiently [175]) [176–179], hypercrosslinked polymers [180–182], amorphous conjugated microporous polymers (CMPs) [183], and polymeric cocrystalline forms [184], have emerged to overcome these problems. For instance, McKeown et al. [176] and later Budd and coworkers [177] developed different PIMs systems with pore widths between 0.6 and 0.7 nm (the density and membrane thickness were not specified). These systems exhibited BET surface areas around 1050 m^2/g (in the best case) and H_2 uptakes up to 1.8 wt.% at 77 K and 1 bar, or up to 2.7 wt.% at 77 K and 10 bar. Similar values were achieved by Ghanem et al. [178], who prepared a triptycene-based PIM polymer membrane with pore widths around 0.6 nm (the porosity and membrane thickness were not specified). This material presented a BET value around 1065 m^2/g and H_2 uptakes up to 1.65 wt.% at 77 K and 1 bar or up to 2.7 wt.% at 77 K and 10 bar.

The H_2 storage capacity of hypercrosslinked PS nanoporous membranes with pore widths around 4 nm were analyzed by Germain et al. [180] (the porosity and membrane thickness were not specified). In this case, BET surface areas up to 1200 m^2/g and H_2 uptakes up to 1.3 wt.% at 77 K and 1 bar were obtained. These results are consistent with those obtained by Lee et al. [181] in hypercrosslinked nanoporous PS (a broad pore size width distribution centered around 0.7 nm), which showed BET surface areas around 1466 m^2/g and H_2 uptakes up to 1.3 wt.% at 77 K and 1 bar or up to 2.7 wt.% at 77 K and 10 bar. In both cases, the values reached were lower than in the case of nanoporous PIMs.

Although these results are promising, there are fewer studies on nanoporous membranes than on the best carbon-based materials (see Fig. 22). However, the H_2 sorption capacity measured for these nanoporous polymers at 1 bar is comparable with that reported for AC and MOFs of equivalent surface areas and similar pore volumes. Thus, if the BET values could be increased, then the H_2 capacities could be similar.

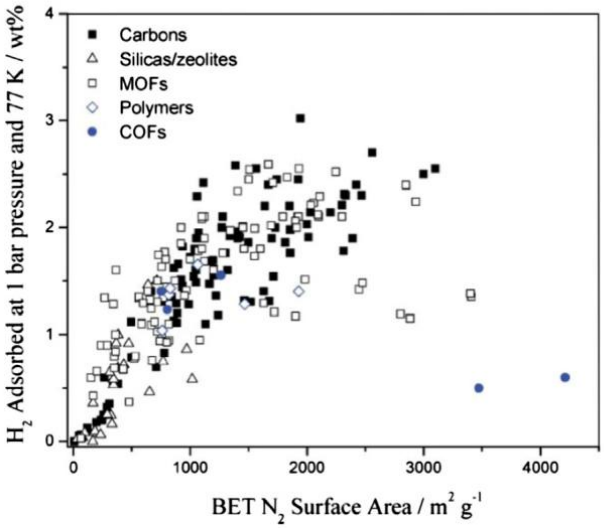

Fig. 22. Hydrogen adsorption at 1 bar and 77 K versus BET surface area for different nanoporous materials: carbon, silicas/zeolites, polymers, COFs, and MOFs. This figure is included with permission from Thomas [158].

Polymeric membranes have traditionally had limited application to gas and liquid transport because of the wide distribution of pore sizes achieved, which leads to a broad molecular weight cut off. However, the ion track etching technique and, more recently, the block copolymer approach [185] have allowed the manufacture of nanoporous polymeric membranes with narrow pore size distributions and higher pore densities.

The gas and liquid transport of polydicyclopentadiene nanoporous membranes with a porosity of 40%, a pore size around 14 nm, and a membrane thickness of 100 μm was studied by Phillip et al. [186]. The effective diffusion coefficients obtained varied according to the gas employed: for instance, it was 0.0184 cm^2/s for H_2 or 0.0047 cm^2/s for Ar. These results were in good agreement with those predicted by Knudsen diffusion. These membranes presented a more precise molecular weight cut off (MWCO) for liquid transport of dextrans than phase inversion membranes. Nevertheless, the water flux values obtained at 30 kPa ($1 \cdot 10^{-6}$ m^3/m^2 s) were smaller than the typical flux values of commercial phase inversion membranes (between $3 \cdot 10^{-5}$ and $4 \cdot 10^{-4}$ m^3/m^2 s). However, this water flux was greater than that achieved in the same conditions by the same author [187] using a nanoporous PS membrane (water flux $\approx 0.67 \cdot 10^{-7}$ m^3/m^2 s) with a porosity of 27%, a pore size around 24 nm, and a thickness of 4 μm. The differences in porosity and pore size could be the reasons for this difference.

CO_2 diffusivity through 50-μm-thick syndiotactic PS (s-PS) films (porosity = 7%; pore size ≈ 1 nm) was studied by Milano and Guerra [188], who obtained diffusivity values around 10^{-8} cm^2/s.

The liquid transport across nanoporous PS membranes has been widely analyzed in several works [187,189–191]. For instance, Yang and coworkers [189] created a PS nanoporous membrane with cylindrical pores (diameters around 15 nm), a porosity around 20%, and a membrane thickness of 100 nm. This system, which was supported on a polysulfone (PSU) membrane, showed ultrahigh selectivity and flux for the separation of viruses ($\approx 12 \cdot 10^{-6}$ m^3/m^2 s, a value 10 times higher than that obtained with a PC membrane). Later, good dimensional stability under high pressures and excellent solvent resistance was also reported for the same type of nanoporous membranes for virus filtration [190].

A novel approach using flash freezing was developed by Samitsu et al. [192] to produce nanoporous polymer (PS, PC, polyvinyl chloride (PVC), etc.) nanofiber networks with pore diameters ranging from 12 to 21 nm (the porosity was only specified for the PS system and was equal to 56%). These nanoporous polymers were able to separate toluene from aqueous solutions a few tens of ppm in concentration and could also adsorb a significant quantity of tetrahydrofuran from aqueous solution. However,

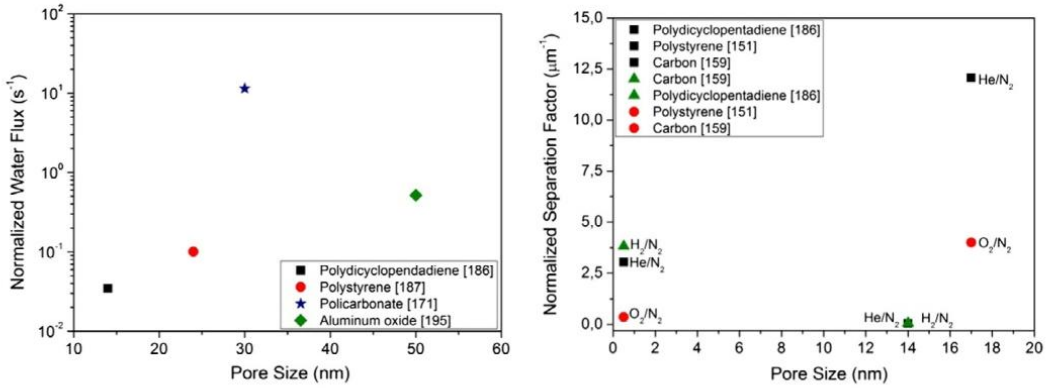

Fig. 23. Left: Normalized water flux measured at 1 bar for different polymeric and non-polymeric nanoporous membranes [171,186,187,195]. Right: Normalized separation factor for different polymeric and non-polymeric nanoporous membranes [151,159,186].

the mechanical stability of these porous systems was poor compared to that of the solid ($n = 3$ for the Young modulus of the PS system).

Other nanoporous polymeric systems such as polyimide [193], polyethylene [194], or polycarbonate (PC) [195] have also been investigated. Smuleac and coworkers [195] developed a nanoporous track-etched PC membrane (pore size: 30–100 nm; porosity: 0.47%; membrane thickness: 6–10 μm) which showed higher water fluxes (measured at 0.8 bar) as the pore size increased: $250 \cdot 10^{-2}$ m^3/m^2 s for a pore size of 100 nm and $42 \cdot 10^{-2}$ m^3/m^2 s for a pore size of 30 nm. Furthermore, they also demonstrated that the MWCO of Na_2SO_4 salt was higher in the membranes with lower pore sizes (a difference up to 800% for a feed concentration of 2 mM).

In conclusion, theoretical models for gas storage and solute transport (both gas and liquid) are well established both in polymeric and non-polymeric nanoporous membranes. All models agree that a reduction in pore size leads to enhanced storage and filtration capacities.

According to the results, the amount of gas stored, in particular of H_2, in nanoporous polymers is far from values obtained with porous carbon-based systems. However, if it is possible to increase the BET specific surface area of polymeric materials by optimizing the current production processes or developing new ones, it will be possible to achieve higher values of hydrogen uptake. This opens a new line of research into the use of polymers as gas storage devices.

Fig. 23 illustrates a comparison of the normalized water flux and gas separation values obtained with polymeric and non-polymeric nanoporous membranes (not all results of the articles mentioned in this review are included, since many of them do not give a porosity value). In both cases, the values obtained have been divided by the membrane thickness and by the relative density in order to observe only the influence of the pore size on solute transport. With the exception of some cases, solute transport (both gas and liquid) increases as pore size increases, independent of the material used. Thus, the technical requirements of each application will determine what type of material (polymeric or not) is most appropriate. In this situation, the mechanical, thermal, and chemical resistances will play an important role.

Therefore, according to the theoretical and experimental results, nanoporous polymers could achieve filtration and gas storage performances similar to those of non-polymeric materials as long as they exhibit similar structural parameters: porosity, pore size, a narrow pore size distribution, a high BET specific surface area, etc. Even though they have not yet reached those yields, nanoporous polymers present other advantages (ease of manufacturing, superior flexibility, good biocompatibility, and tailored thermal, mechanical, and chemical properties). Furthermore, recently, nanoporous polymeric materials with acceptable structures (a Knudsen number around 1 for Knudsen diffusion) have begun to be developed by physical processes (the gas dissolution foaming process [60]). However, more work is needed to obtain finer porous structures and to carry out experimental measurements to confirm their applicability.

6. Other properties (sensors and optical and multifunctional materials)

Apart from all the aforementioned features of nanoporous polymers, there other properties of emerging interest, such as sensing or optical properties, and uses of these materials as multifunctional materials.

There are two main sensor applications for which nanoporous materials have been studied: the stabilization of enzymes (biosensors) and humidity detection (humidity sensors).

In the field of biosensors, the stabilization of enzymes is crucial for the development of more reliable analytical devices. Several stabilization approaches (use of additives [196], covalent bonding on solid materials [197], or entrapment in different solid matrices [198]) have been developed for this purpose, and all of them are based on increasing the rigidity of the enzyme by reducing its tendency to open out. Recently, theoretical studies [199] have suggested that this tendency to unfold can also be avoided by introducing the enzyme within very small pores. In this case, the unfolded configurations of the enzyme are not thermodynamically favored. According to theoretical results, the maximum stabilization of enzymes occurs with pores with a spherical morphology whose size is 2–6 times the diameter of the original enzyme. Considering that the diameter of such a protein is about 10 nm, it can be demonstrated that nanoporous materials are a perfect fit for this application.

This theoretical approach has been experimentally demonstrated in non-polymeric nanoporous materials (mainly carbon materials); however, because of the novelty of polymer-based materials, there is a lack of studies specifically on polymers (both theoretical and experimental). In any case, results concerning nanoporous carbons will be briefly summarized to give an idea of the initial results that have been obtained to date.

For instance, Sotiropoulou and coworkers [200] were able to decrease the leaching rate of the protein *m-AChE* (2.5 and 11.5 times lower than the free enzyme for AC and silica beads, respectively) and increase the operational stability of the resulting sensor by using two different nanoporous systems: activated carbons (pore size: 100–300 nm; thickness: 0.1 mm; porosity: not specified) and porous silica beads (pore diameter: 10 nm). The lower pore diameter of the silica beads could justify the higher performance obtained. Other authors such as Gavalas and Chaniotakis [201,202] and Sotiropoulou et al. [203] studied the effect of introducing a mediator (fullerenes, diethylaminoethyl-dextran, and carbon nanotubes) into a nanoporous carbon matrix (porous structure parameters were not specified in detail) to improve the capacity to immobilize enzymes (glucose, lactate oxidase, and peroxide). In all cases, the use of a mediator led to an enhanced enzyme stabilization capacity.

Thus, experimental results on nanoporous carbon materials are in agreement with theoretical predictions, showing that the use of nanoporous materials may be very useful for the development of biosensors. However, further theoretical and experimental studies are needed, particularly for polymers, to show whether these nanoporous systems are suitable for the development of biosensors.

The use of humidity sensors for moisture detection is widespread in applications such as meteorological service, food processing, air conditioning, or electronics processing. Currently, most typical sensors have varying resistivity and capacity values with water adsorption. Nanoporous materials, characterized by a high surface-area-to-volume ratio, are a promising humidity sensor, since they can accurately detect resistance and/or capacitance changes owing to water adsorption inside the nanopores. Furthermore, nanoporous materials allow the optimization of the pore size according to the specific working conditions (temperature and relative humidity) in order to obtain the maximum performance of the sensor. For this purpose, the optimum pore size diameter can be calculated using Kelvin's relation [204]:

$$\Phi = \frac{4\gamma_L V}{RT \log\left(P/P_s\right)} \tag{21}$$

where P/P_s represents the relative humidity, γ_L is the water surface tension, R is the universal gas constant, T is the temperature in K, and V is the volume of water.

For instance, Varghese and coworkers [205] studied the effect of pore size on the response of a nanoporous alumina sensor (pore size: 13–45 nm; porosity and thickness: not specified) to humidity. They observed that, as the pore size increased, the humidity range over which the sensors had high

sensitivity decreased (see Fig. 24). Fig. 24 shows that the humidity range for the porous material with a pore size of 13.6 nm ranged from 20% to 90% RH, whereas this range was reduced to 65–75% RH for the nanoporous materials with pore sizes greater than 38.4 nm.

Thus, the theoretical basis underlying the use of nanoporous materials as humidity sensors has been established, though the number of theoretical works is still low, especially for polymeric systems. Although the sensory characterization of nanoporous polymeric materials is a recent topic, there are other experimental works related to the use of different nanoporous systems based on ceramics, which will be discussed below briefly for comparison.

The use of nanoporous ceramics as humidity sensors has been studied extensively in recent years [206–209] because of their high thermal capacity to withstand thermal fluctuations as well as their high capacity to operate under harsh environments. Nitta and Hayakawa [206] developed a resistive nanoporous ceramic sensor (formula $MgCr_2O_4$–TiO_2) with a porosity between 30% and 40%, a pore size ranging from 10 to 30 nm, and a thickness of 200 μm. These sensors exhibited a sensitivity around 0.22 MΩ/% relative humidity (RH) with a high linear response for the 1–90% RH range. In addition, two different nanoporous capacitive sensors, polysilicon and silicon carbide, were produced by Connolly et al. [207], with thicknesses of 0.4 and 0.5 μm, respectively (the porosity and pore size were not specified in the article). In this study, the normalized sensitivity capacity was higher for the nanoporous polysilicon system (0.025/% RH) than for the SiC system (0.01/% RH) in the 10–90% RH range. Differences in the pore size and porosity could be the reasons underlying this effect.

In general, the experimental results in nanoporous systems (at least in ceramics) indicated good moisture sensing capacity with the reduction of the pore size to the nanometer scale. Although there are several works showing this effect in ceramic systems, to date there has been only one experimental work related to the sensing behavior of nanoporous polymers because of the novelty of the use of nanoporous materials, and particularly of nanoporous polymers, as sensors.

Yang et al. [210] designed various types of resistive nanoporous polymer humidity sensors such as polycarbonate (pore size: 200 nm; thickness: 10 μm; porosity: not specified), cellulose acetate (pore size: 200 nm; thickness: 125 μm; porosity: 66%), and nylon (pore size: 100 nm; thickness: 110 μm; porosity: 55%). A highly linear response over a range of 40–100% RH with a sensitivity around 20 GΩ/% RH was obtained for nanoporous cellulose acetate and nylon systems. The response of PC was also linear for the same range of humidity, but the sensitivity value obtained was lower at around 4.5 GΩ/% RH (4.5 times lower than that obtained for the other porous polymers analyzed). Different porosities, thicknesses, and hydrophobicity values could be the reasons for this difference. However, even in the worst case, the sensitivity values obtained were better than those obtained by Nitta and

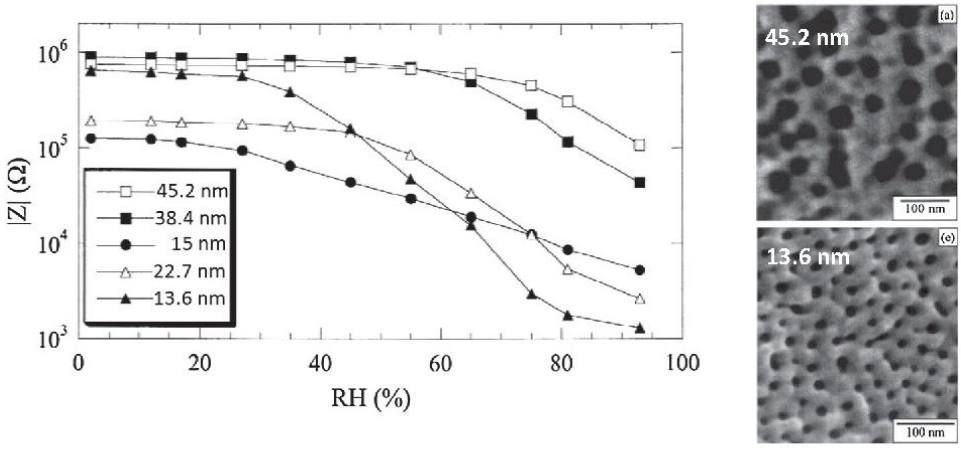

Fig. 24. Effect of pore size on the impedance of nanoporous alumina sensors measured at 5 kHz over different humidity levels. This figure has been adapted from Varghese et al. [205].

Table 2
Different effective medium approximations developed for the calculation of the effective index of refraction (n_{eff}), where n_s is the refractive index of the solid, n_g is the refractive index of the gas, and V_g is the porosity.

	Maxwell–Garnet Theory (MGT) [222]	Parallel model	Serial model
n_{eff}=	$n_s\left[1-\frac{3V_g\left(n_s^2-n_g^2\right)}{2n_s^2+n_g^2+V_g\left(n_s^2-n_g^2\right)}\right]^{1/2}$	$(1-V_g)n_s+V_g n_g$	$\left[\frac{1-V_g}{n_s}+\frac{V_g}{n_g}\right]^{-1}$
	Reciprocity model [223]	Volume Averaging Theory (VAT) [224,225]	
	$n_s\frac{1+V_g\left(\sqrt{\frac{n_g}{n_s}}-1\right)}{1+V_g\left(\sqrt{\frac{n_g}{n_s}}-1\right)}$	$\left[(1-V_g)n_s^2+V_g n_g^2\right]^{1/2}$	

Hayakawa [206] using a nanoporous ceramic (three orders of magnitude more sensitive). The higher porosity of nanoporous polymers could be the explanation for this difference.

Therefore, nanoporous polymers seem to exhibit better humidity detection capacity than nanoporous ceramics. Nevertheless, the number of theoretical and experimental works on either polymeric or non-polymeric materials is still limited. Thus, further studies are needed in order to determine whether nanoporous systems are actually appropriate for moisture sensors.

Last, but not least important, are nanoporous cocrystalline polymers, which seem to be good candidates for sensing elements in gravimetric sensors. These materials can detect organic compounds or low-molecular-mass substances present in gaseous and liquid environments. For instance, Pilla et al. [211] showed how 1-μm-thick s-PS films (porosity: 7%; pore size: not specified) can work as gravimetric sensors for the detection of chloroform in both vapor and liquid phases.

In the field of optics, the demand for materials with a low refractive index (n) has promoted great efforts to study the applicability of porous materials as waveguides [212,213], Fabry–Perot filters [214–216], Bragg reflectors [216,217], and antireflection coatings [218]. Porous materials can possess a very low value of n because of the introduction of air, which has a refractive index of $n = 1$. In this case, nanoporous materials are in demand because of the reduced dimensions of manufactured devices, where the pores must be much smaller than the thickness of the film. However, unlike dielectrics, in which the use of nanoporous materials is determined exclusively by the dimensions of the device, nanoporous materials for optics provide another advantage: if the pore size is much smaller than the wavelength of light, then light scattering from the pores is reduced [219]. Using this theoretical assumption, it has been speculated that nanoporous materials produced from amorphous polymers with a well-defined pore structure and pore sizes less than the wavelength of visible radiation could be transparent.

Therefore, understanding the effects of porosity, pore size and shape, and pore size distribution on the optical properties of nanoporous systems is crucial for better device performance. For this purpose, numerous effective medium theories have been developed. All of them treat heterogeneous media as homogeneous media with some effective properties. The most common models used to calculate the effective index of refraction are summarized in Table 2, although variations of them can also be found in the literature [220,221]. All the models mentioned consider only the porosity as a structural parameter of the foam, regardless of other important parameters such as pore size, shape, and pore distribution. Likewise, some of these models have been used to analyze the refractive index though they were not necessarily developed for this purpose (i.e., the MGT model was developed to calculate the electric permittivity). Thus, although the number of existing models is high, it is not clear which model is the most accurate in a given situation.

In order to clarify some of the aforementioned problems, Braun and Pilon [226] solved numerically the two-dimensional Maxwell's equations in non-absorbing nanoporous thin films with different morphologies for transverse electric (TE) absorbing electromagnetic waves. The effect of the film thickness (L) (Fig. 25(a)), pore size (Φ) (Fig. 25(a)), pore shape (Fig. 25(b)), pore distribution (Fig. 25(c)), and porosity (Fig. 25(d)) on the effective index of refraction was studied in detail. It was found that, below a certain critical film thickness, the effective index of refraction depends on the pore size and shape, porosity, and pore distribution. However, beyond this critical thickness, effective medium approaches

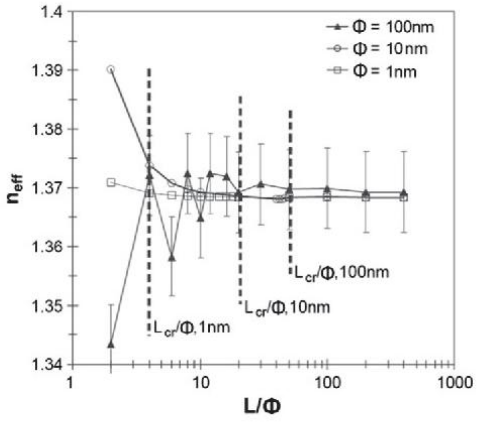

(a) Variation of n_{eff} as a function of L/Φ for films with 19.63% porosity and different pore diameters.

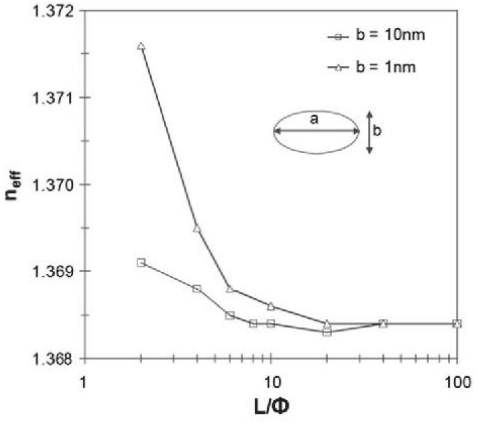

(b) Variation of n_{eff} as a function of L/Φ for elliptical pores with an aspect ratio a/b = 2, and a porosity of 19.63%.

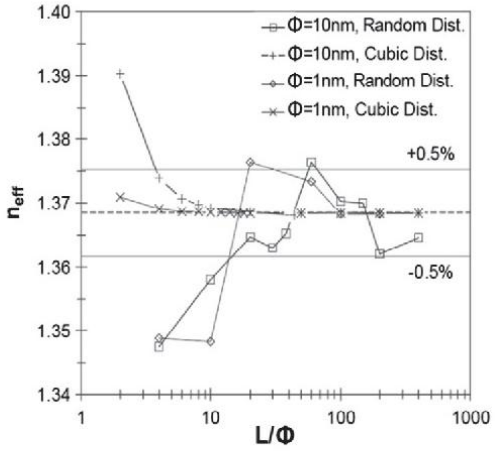

(c) Variation of n_{eff} as a function of L/Φ for regular and random pore size distribution with a porosity of 19.63%.

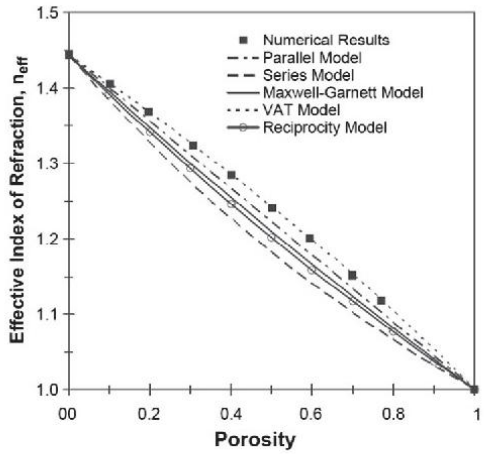

(d) Variation of n_{eff} as a function of porosity for nanoporous SiO_2 (Φ = 10 nm) at λ = 1.55 μm.

Fig. 25. Variation of the effective index of refraction of a nanoporous film as a function of film thickness (a), pore shape (b), pore size distribution (c), and porosity (d). Images have been adapted from Braun and Pilon [226]. (a) Variation of n_{eff} as a function of L/Φ for films with 19.63% porosity and different pore diameters. (b) Variation of n_{eff} as a function of L/Φ for elliptical pores with an aspect ratio a/b = 2, and a porosity of 19.63%. (c) Variation of n_{eff} as a function of L/Φ for regular and random pore size distribution with a porosity of 19.63%. (d) Variation of n_{eff} as a function of porosity for nanoporous SiO_2 (Φ = 10 nm) at λ = 1.55 μm.

are valid, and the effective index of refraction depends only on the porosity and the index of refraction of each of the constituent phases (solid and gas) (see Fig. 25 from (a) to (d)).

Similarly, Navid and Pilon [227] carried out another study to improve and better understand the theoretical models given in Table 2. The index of refraction of nanoporous films with different morphologies for normally incident transverse magnetic (TM) and transverse electric (TE) absorbing electromagnetic waves was determined by numerically solving the two-dimensional Maxwell's equations. They found that, for uniform pore distributions and spherical pores, the effective index of refraction for TE and TM waves is independent of both pore size and film thickness for $1 < \Phi < 10$ nm and $L/$

$\Phi \geqslant 300$. This result is in good agreement with the work of Braun and Pilon [226], since the regime they considered is above the critical film thickness given above. In this situation, the TM numerical data agree well with the parallel model, whereas the TE numerical data are consistent with the VAT theory. In the case of a random pore distribution and different pore shapes, it was found that TE waves are independent of the porous morphology and can be appropriately described by the VAT model (this result is consistent with predictions from Braun and Pilon [226]). However, for TM waves, the index of refraction depends on the porosity, pore distribution, and pore shape.

Therefore, theoretical models developed for nanoporous materials in general (and thus valid for both polymeric and non-polymeric systems) are well established, although the application limits of each model have not yet been well defined. All of them agree that the enhancement of the effective optical properties (i.e., the achievement of a lower value of the effective index of refraction) of a nanoporous material is mainly determined by the porosity for film thicknesses above a certain critical value; however, for film thicknesses below this value, the improvement in the optical properties is also determined by the pore size and shape and pore distribution [226].

Although the modification of the index of refraction by varying the morphology of the porous system is a recent topic in the field of nanoporous polymers, there are other experimental works related to the use of different nanoporous systems, such as TiO_2 [228], GaN [229], SiO_2 [218], and silicon [213,215–217], which will be discussed below briefly for comparison.

Silicon-based multilayer porous systems have been widely used in the manufacture of antireflection coatings [218], waveguides [213], Bragg reflectors [215–217], and Fabry–Perot devices [215]. Depth variations in porosity are created to obtain regions with different refractive indices that allow tuning of the optical properties of the system. For instance, Zhang and coworkers [218] developed an antireflection coating by means of a two-layer refractive index gradient. For this purpose, they use a SiO_2 aerogel nanoporous film (pore size: not specified; thickness: 220 nm; porosity: not specified) as the low-refractive-index layer ($n = 1.16$) and a TiO_2 film as the high-refractive-index layer ($n = 1.40$). This anti-reflective coating provided an average reflectance <2% in the wavelength range from 1000 to 2000 nm, which represents a reduction of 70% with respect to the solid system.

Other applications of nanoporous films in optics can be found in the work of Lee and Kang [228]. These researchers were able to improve the efficiency (measured under 100 mW/cm^2 simulated light) of a dye-sensitized solar cell (DSSC) through the incorporation of a nanoporous TiO_2 film (pore size: 10 nm; thickness: 4 μm; porosity: not specified). The efficiency value obtained was two times higher than that of a commercial DSSC also based on TiO_2. The cause of this improvement lies in the lower reflective Fresnel loss for incident light at its outer surface, which allowed more light to reach the active layer.

Another study was that carried out by Vajpeyi et al. [229], who obtained a considerable photoluminescence (PL) intensity improvement at 77 K (2.3 times higher than as-grown GaN films) in a nanoporous GaN film with cylindrical pores (pore size: ≈85 nm; thickness: 400 μm; porosity: not specified). They observed that the higher the pore length, the higher the PL intensity was. This system could be used as an intermediate layer for high-brightness light emitting devices.

Thus, experimental results obtained in non-polymeric nanoporous materials showed an improved optical response with respect to the solid or to the materials currently on the market. This improvement is in general governed by the porosity and not by the pore size. Although this apparent enhancement has been well demonstrated in non-polymeric systems, studies on nanoporous polymers are still scarce.

Cho et al. [230] introduced a novel method to produce highly antireflective coatings by means of nanoporous block copolymer (polystyrene-*block*-poly(4-vinylpyridine) (PS-*b*-P4VP) and polystyrene-*block*-poly(acrylic acid) (PS-*b*-PAA)) multilayer films. These films, with a pore size around 10 nm and a film thickness that varied from 25 to 104 nm, presented an index of refraction that was strongly influenced by the porosity (refractive index: from 1.14 to 1.25; porosity: from 65.7% to 42.8%, respectively). For the films with a thickness around 100 nm, a high antireflective capacity with light transmissions around 99% at 540 nm was found.

Similarly, Hiller and coworkers [231] designed a new methodology (aqueous-based process) to produce poly(allylamine hydrochloride)/poly(acrylic acid) (PAH/PAA) anti-reflective nanoporous films with reversibly erasable porosity. These films, with a thickness ranging from 80 to 130 nm, a pore size

of 60 nm, and a refractive index from 1.15 to 1.55 (although the article mentions that this factor varied with the porosity, the value was not specified), exhibited a light transmission >98% at 540 nm, a value 7.7% higher than that of untreated glass.

Yokoyama et al. [54] and later Li and coworkers [232] calculated the porosity of several nanoporous polystyrene-b-poly(perfluorooctylethyl methacrylate) (PS-PFMA) films (thickness: 1 μm [54]/50 nm [232]; pore size: 15–30 nm) from measurements of the index of refraction. Using the Lorentz–Lorentz equation [233], Yokoyama et al. [54] obtained porosities between 16% and 50% for indices of refraction ranging from 1.4 to 1.23 (lower values than that of the solid, n_s = 1.50), respectively, whereas Li and coworkers [232] achieved porosities between 12 and 24% and indices of refraction ranging from 1.42 to 1.37 (also lower values than that of the solid, n_s = 1.50), respectively. Although the tendency observed in both studies was the same (the higher the porosity, the lower the index of refraction is), the maximum reduction obtained in the index of refraction in each case was different. The reason for this difference resides in the presence of a dense layer that covered the films developed by Yokoyama et al. [54].

Finally, Rizzo et al. [234] and Guerra and coworkers [184] found that s-PS films (thickness ≈ 20 μm; pore size ≈ 1 nm; porosity: 7%) exhibited chiral optical responses both in the infrared and in the UV–visible regions, opening the opportunity to achieve s-PS-based films with tunable chiral optical properties.

Thus, nanoporous polymers seem to present enhanced optical behavior compared to the solid, which is mainly governed by the porosity of the system and not by the pore size. However, the number of studies is still too limited to obtain definitive conclusions.

The use of a polymeric system or not will depend on the technical specifications of each application. However, further studies on the mechanical, thermal, or chemical resistances of both polymeric and non-polymeric materials are needed to verify whether these systems are potential candidates for use in optics.

According to experimental and theoretical results, the pore size has no influence on the optics of nanoporous materials for film thicknesses above a critical value in principle; the porosity is primarily responsible for the improvement of this property in this situation. Only for film thicknesses below this critical value does the pore size play an important role. It is possible that, in this situation, light scattering from pores will have more influence, and, consequently, the transparency of amorphous nanoporous polymers could be reached.

Finally, although it is very useful to have materials with specific improved properties (mechanical, thermal, dielectric, optical, etc.), the current trend in designed materials implies the achievement of a material that combines a set of well-defined and enhanced properties. For instance, Harbuzaru and coworkers [235] proposed lanthanide-based nanoporous metal–organic frameworks (Ln-MOFs) as a material with interesting multifunctional properties such as luminescence, magnetism, hydrophobicity, and high thermal stability (no specific data are provided for the cellular structure or for the properties mentioned). However, nanoporous silica aerogels films (thicknesses between 3 and 110 nm) with porosities higher than 75% (pore size not specified) have also been proposed by Hrubesh and Poco [236] as multifunctional materials because of the excellent optical, acoustical, thermal, and electronic properties exhibited by this system and demonstrated elsewhere [237,238]. Recently, Notario and coworkers [14,67] have demonstrated that PMMA-based nanoporous materials (pore size: <300 nm; porosity: ≈60%) exhibit improved thermal and mechanical properties as well as promising dielectric (unpublished work) and filtration [60] properties.

Therefore, nanoporous materials are promising candidates for use in multifunctional systems. Although studies in both polymeric and non-polymeric systems are still scarce, the first results obtained have created high expectations.

7. Conclusions

In this review, the influence of the reduction in pore size to the nanometer range on the key physical properties of porous polymeric materials (mechanical properties, thermal properties, etc.) are described and analyzed in detail.

It was expected that the reduction in the pore size to the nanoscale together with the modification of the porous architecture would produce a series of improvements in several physical properties of these novel materials (mechanical, thermal, dielectric, optical, sensing, filtration, etc.). However, it has been found that the confinement of the constituent phases (gas and solid) in the nanometer range also leads to unexpected modifications or effects.

It has been demonstrated that nanoporous polymeric materials exhibit superior mechanical behavior at high strain rates and superior shore hardness compared with both microporous and solid materials. However, the studies on the mechanical response at low strain rates were inconclusive.

A possible alteration of the fundamental properties of the base polymer due to the confinement of the polymer chains within the pore walls, or due to the stretching of the polymer chains induced during the manufacturing process, could be the reason for the different tensile behaviors obtained in different papers. Nevertheless, further studies with different polymeric matrices are needed to understand, confirm or discard the contradictory tensile results obtained.

Thermal conductivity measurements in nanoporous polymers have shown a reduction of the thermal conductivity when the pore size was below one micron. The confinement of both the gaseous phase (the Knudsen effect) and the solid phase (different phonon scattering mechanisms and increased tortuosity) are the phenomena underlying this effect. To date, studies on nanoporous polymers are still scarce; nevertheless, the Knudsen effect depends only on the morphology of the porous structure and is independent of the solid matrix. Thus, it can be stated that there is sufficient evidence to confirm its presence and potential advantages in nanoporous polymeric materials.

New low-k nanoporous polymers, with a lower dielectric constant than the solid, have been achieved by the introduction of air into the polymer matrix.

Moreover, it was demonstrated that the pore size does not provide an additional advantage to low-k nanoporous systems; this was only a requirement imposed by the dimensions of the devices to be developed. Nevertheless, the existence or future appearance of side effects due to the reduction of pore size to the nanoscale cannot be completely discarded.

Filtration and membrane studies showed that a reduction in pore size leads to enhanced storage and filtration capacities. It was demonstrated that nanoporous polymers could reach filtration and gas storage performances similar to those of non-polymeric materials as long as they exhibit similar structural parameters: porosity, pore size, narrow pore size distribution, high BET specific surface area, etc. Although nanoporous polymeric materials were not the most conventional materials in this field, they presented other advantages (ease of manufacturing, superior flexibility, good biocompatibility, and tailored thermal, mechanical, and chemical properties) that make them materials of significant interest.

Nanoporous polymers also have a promising future in emerging fields such as sensing and optics. Nanoporous materials have proven very useful for the development of biosensors, since they prevent the tendency of enzymes to unfold. Although there are no articles related to nanoporous polymers, the good results obtained with nanoporous carbon-based materials suggest that polymer systems may also be used in this application. Furthermore, nanoporous polymers can also be employed as humidity sensors, because they can accurately detect resistance and/or capacitance variations due to water adsorption inside the nanopores. Initial results demonstrated that nanoporous polymeric materials exhibited a better humidity detection capacity than nanoporous ceramics. Nevertheless, the number of articles is still limited, and thus further studies are required in order to determine whether nanoporous polymers are appropriate as sensors.

Nanoporous polymers present enhanced optical behavior (i.e., a reduced index of refraction) compared to the solid, which is mainly governed by the porosity of the system. It was demonstrated that the pore size has, in principle, no influence on the optics of nanoporous materials for film thicknesses above a critical value, and the porosity is primarily responsible for the improvement in this property in this situation. Only for film thicknesses below this critical value does the pore size play an important role. It is possible that, in this situation, the light scattering from the pores will play a key role in the light transmission through the films, and consequently transparent nanoporous polymer films could be produced from amorphous polymers.

Furthermore, nanoporous polymers are promising candidates for use in multifunctional systems. Although the number of studies is still low, the initial results obtained have led to high expectations.

The aforementioned results obtained with nanoporous polymers are consistent with those obtained in other non-polymeric nanoporous systems and with the theoretical predictions developed up to now. However, the different matrices employed (polymer against metal) make that the results found for mechanical properties not comparable. Likewise, most of the theoretical models developed to study the mechanical behavior of nanoporous materials have been tested on non-polymeric systems, and the development of more specific models for polymers is necessary.

Therefore, according to these results, significant progress has been made in last years in the development of nanoporous polymeric materials. Their improved thermal, mechanical, dielectric, optical, filtration, and sensing properties, among others, make these materials promising candidates for applications such as thermal insulation, cushioning, packaging, electronics, and filtration. However, significant technical challenges remain in the production of nanoporous polymers with adequate densities, pore sizes, and external dimensions that allow for characterization of their properties and their production as a scalable industrial process. In addition, a better understanding of the structure–property relationships for these materials is needed. Fortunately, nanoporous material production is becoming an area of increased interest for both academia and industry, leading to further progress towards this target.

Acknowledgments

Financial support from FPI Grant BES-2013-062852 (B. Notario) from the Spanish Ministry of Education is gratefully acknowledged. Financial assistance from the MINECO and FEDER Program (MAT 2012-34901) and the Junta of Castile and Leon (VA035U13) is gratefully acknowledged.

References

[1] Gibson LJ, Ashby MF. Cellular solids: structure and properties. 2nd ed. Cambridge: Cambridge University Press; 1997.
[2] Weaire D, Hutzler S. The physics of foams. Oxford, UK: Oxford University Press; 1999.
[3] Klempner D, Sendijarevi'c V, Aseeva RM. Handbook of polymeric foams and foam technology. Munich: Hanser Publishers; 2004.
[4] Eaves D. Handbook of polymer foams. Rapra Technology; 2004.
[5] Business Communications Company Inc. RP-120X polymeric foams. USA: Updated Edition; 2004.
[6] Martini-Vvedensky JE, Suh NP, Waldman FA. Microcellular closed cell foams and their method of manufacture. Massachusetts Institute of Technology; 1984.
[7] Kumar V. Process synthesis for manufacturing microcellular thermoplastic parts. Massachusetts Institute of Technology; 1988.
[8] Kumar V, Suh NP. A process for making microcellular thermoplastic parts. Polym Eng Sci 1990;30:1323–9.
[9] Shimbo M, Higashitani I, Miyano Y. Mechanism of strength improvement of foamed plastics having fine cell. J Cell Plast 2007;43:157–67.
[10] Nadella K, Kumar V. Tensile and flexural properties of solid-state microcellular Abs panels. In: Gdoutos EE, editor. Experimental analysis of nano and engineering materials and structures. Netherlands: Springer; 2007. p. 765–6.
[11] Kumar V, Seeler KA, Vander Wel M, Weller J. Experimental characterization of the tensile behavior of microcellular polycarbonate foams. J Eng Mater Technol 1994;116:439–45.
[12] Kumar V, Weller JE, Ma M, Montecillo R, Kwapisz RR. The effect of additives on microcellular PVC foams: Part II. Tensile behaviour. Cell Polym 1998;17:350–61.
[13] Miller D, Kumar V. Microcellular and nanocellular solid-state polyetherimide (PEI) foams using sub-critical carbon dioxide II. Tensile and impact properties. Polymer 2011;52:2910–9.
[14] Notario B, Pinto J, Solorzano E, Saja JAd, Dumon M, Rodriguez-Perez MA. Experimental validation of the Knudsen effect in nanocellular polymeric foams. Polymer 2015;56:57–67.
[15] Hentze HP, Antonietti M. Porous polymers and resins for biotechnological and biomedical applications. Rev Mol Biotechnol 2002;90:27–53.
[16] Li L, Shen X, Hong SW, Hayward RC, Russell TP. Fabrication of co-continuous nanostructured and porous polymer membranes: spinodal decomposition of homopolymer and random copolymer blends. Angew Chem Int Ed Engl 2012;51:4089–94.
[17] Park SH, Xia YN. Macroporous membranes with highly ordered and three-dimensionally interconnected spherical pores. Adv Mater 1998;10:1045–8.
[18] du Fresne von Hohenesche C, Schmidt DF, Schädler V. Nanoporous melamine-formaldehyde gels by microemulsion templating. Chem Mater 2008;20:6124–9.
[19] Hedrick JL, Miller RD, Hawker CJ, Carter KR, Volksen W, Yoon DY, et al. Templating nanoporosity in thin-film dielectric insulators. Adv Mater 1998;10:1049–53.
[20] Costeux S, Zhu L. Low density thermoplastic nanofoams nucleated by nanoparticles. Polymer 2013;54:2785–95.
[21] Miller D, Chatchaisucha P, Kumar V. Microcellular and nanocellular solid-state polyetherimide (PEI) foams using sub-critical carbon dioxide I. Processing and structure. Polymer 2009;50:5576–84.

[22] Cheng LP, Dwan AH, Gryte CC. Membrane formation by isothermal precipitation in polyamide-formic acid-water systems I. Description of membrane morphology. J Polym Sci Part B Polym Phys 1995;33:211–22.
[23] Cheng LP, Dwan AH, Gryte CC. Membrane formation by isothermal precipitation in polyamide-formic acid-water systems II. Precipitation dynamics.. J Polym Sci Part B Polym Phys 1995;33:223–35.
[24] Kiefer J, Hilborn JG, Hedrick JL. Chemically induced phase separation: a new technique for the synthesis of macroporous epoxy networks. Polymer 1996;37:5715–25.
[25] Nam YS, Park TG. Biodegradable polymeric microcellular foams by modified thermally induced phase separation method. Biomaterials 1999;20:1783–90.
[26] Schugens C, Maquet V, Grandfils C, Jerome R, Teyssie P. Biodegradable and macroporous polylactide implants for cell transplantation. 1. Preparation of macroporous polylactide supports by solid–liquid phase separation. Polymer 1996;37:1027–38.
[27] Walheim S, Schäffer E, Mlynek J, Steiner U. Nanophase-separated polymer films as high-performance antireflection coatings. Science 1999;283:520–2.
[28] Hentze HP, Antonietti M. Template synthesis of porous organic polymers. Curr Opin Solid State Mater Sci 2001;5:343–53.
[29] Lazzari M, López-Quintela MA. Block copolymers as a tool for nanomaterial fabrication. Adv Mater 2003;15:1583–94.
[30] Lin JM, Uchiyama K, Hobo T. Enantiomeric resolution of dansyl amino acids by capillary electrochromatography based on molecular imprinting method. Chromatographia 1998;47:625–9.
[31] Mayes AG, Andersson LI, Mosbach K. Sugar binding polymer showing high anomeric and empimeric discrimination obtained by non-covalent molecular imprinting. Anal Biochem 1994;222:483–8.
[32] Cheong SH, Rachkov AE, Park JK, Yano K, Karube I. Synthesis and binding properties of a noncovalent molecularly imprinted testosterone-specific polymer. J Polym Sci Part A Polym Chem 1998;36:1725–32.
[33] Park SH, Xia Y. Fabrication of three-dimensional macroporous membranes with assemblies of microspheres as templates. Chem Mater 1998;10:1745–7.
[34] Olson DA, Chen L, Hillmyer MA. Templating nanoporous polymers with ordered block copolymers†. Chem Mater 2007;20:869–90.
[35] Zalusky AS, Olayo-Valles R, Wolf JH, Hillmyer MA. Ordered nanoporous polymers from polystyrene-polylactide block copolymers. J Am Chem Soc 2002;124:12761–73.
[36] Hedrick JL, Russell TP, Labadie J, Lucas M, Swanson S. High temperature nanofoams derived from rigid and semi-rigid polyimides. Polymer 1995;36:2685–97.
[37] Kazarian SG. Polymer processing with supercritical fluids. Polym Sci Series C 2000;42:78–101.
[38] Tsivintzelis I, Angelopoulou AG, Panayiotou C. Foaming of polymers with supercritical CO_2: an experimental and theoretical study. Polymer 2007;48:5928–39.
[39] Reverchon E, Cardea J. Production of controlled polymeric foams by supercritical CO_2. J Supercrit Fluids 2007;40:144–52.
[40] Jacobs LJM, Kemmere MF, Keurentjes JTF. Sustainable polymer foaming using high pressure carbon dioxide: a review on fundamentals, processes and applications. Green Chem 2008;10:731–8.
[41] Wells SL, DeSimone J. CO_2 technology platform: an important tool for environmental problem solving. Angew Chem Int Ed 2001;40:518–27.
[42] Kumar V, Weller J. Production of microcellular polycarbonate using carbon dioxide for bubble nucleation. J Eng Ind 1994;116:413–20.
[43] Reglero Ruiz JA, Viot P, Dumon M. Microcellular foaming of polymethylmethacrylate in a batch supercritical CO_2 process: effect of microstructure on compression behavior. J Appl Polym Sci 2010;118:320–31.
[44] Goel SK, Beckman EJ. Generation of microcellular polymeric foams using supercritical carbon dioxide. I: effect of pressure and temperature on nucleation. Polym Eng Sci 1994;34:1137–47.
[45] Guo Q, Wang J, Park CB. A microcellular foaming simulation system with a high pressure-drop rate. Ind Eng Chem Res 2006;45:6153–61.
[46] Krause B, Sijbesma HJP, Münüklü P, Van der Vegt NFA, Wessling M. Bicontinuous nanoporous polymers by carbon dioxide foaming. Macromolecules 2001;34:8792–801.
[47] Pinto J, Dumon M, Pedros M, Reglero JA, Rodriguez-Perez MA. Nanocellular CO_2 foaming of PMMA assisted by block copolymer nanostructuration. Chem Eng J 2014;243C:428–35.
[48] Janani H, Famili MHN. Investigation of a strategy for well controlled inducement of microcellular and nanocellular morphologies in polymers. Polym Eng Sci 2010;50:1558–70.
[49] Siripurapu S, DeSimone JM, Khan SA, Spontak RJ. Controlled foaming of polymer films through restricted surface diffusion and the addition of nanosilica particles or CO_2-philic surfactants. Macromolecules 2005;38:2271–80.
[50] Fujimoto Y, Ray SS, Okamoto M, Ogami A, Yamada K, Ueda K. Well-controlled biodegradable nanocomposite foams: from microcellular to nanocellular. Macromol Rapid Commun 2003;24:457–61.
[51] Ema Y, Ikeya M, Okamoto M. Foam processing and cellular structure of polylactide-based nanocomposites. Polymer 2006;47:5350–9.
[52] Urbanczyk L, Calberg C, Detrembleur C, Jérôme C, Alexandre M. Batch foaming of SAN/clay nanocomposites with $scCO_2$: a very tunable way of controlling the cellular morphology. Polymer 2010;51:3520–31.
[53] Ruckdäschel H, Gutmann P, Altstädt V, Schmalz H, Müller AHE. Foaming of microstructured and nanostructured polymer blends. In: John A, editor. Complex macromolecular systems I. Springer; 2010. p. 199–252.
[54] Yokoyama BH, Li L, Nemoto T, Sugiyama K. Tunable nanocellular polymeric monoliths using fluorinated block copolymer templates and supercritical carbon dioxide. Adv Mater 2004;16:1542–6.
[55] Spitael P, Macosko CW, McClurg RB. Block copolymer micelles for nucleation of microcellular thermoplastic foams. Macromolecules 2004;37:6874–82.
[56] Nemoto T, Takagi J, Ohshima M. Nanoscale cellular foams from a poly(propylene)-rubber blend. Macromol Mater Eng 2008;293:991–8.
[57] Otsuka T, Taki K, Ohshima M. Nanocellular foams of PS/PMMA polymer blends. Macromol Mater Eng 2008;293:78–82.
[58] Costeux S, Khan I, Bunker SP, Jeon HK. Experimental study and modeling of nanofoams formation from single phase acrylic copolymers. J Cell Plast 2014.

[59] Costeux S, Bunker SP, Jeon HK. Homogeneous nanocellular foams from styrenic-acrylic polymer blends. J Mater Res 2013;28:2351–65.
[60] Pinto J, Dumon M, Rodriguez-Perez MA, Garcia R, Dietz C. Block copolymers self-assembly allows obtaining tunable micro or nanoporous membranes or depth filters based on PMMA; fabrication method and nanostructures. J Phys Chem C 2014;118:4656–63.
[61] Handa YP, Zhang Z. A new technique for measuring retrograde vitrification in polymer–gas systems and for making ultramicrocellular foams from the retrograde phase. J Polym Sci Part B Polym Phys 2000;38:716–25.
[62] Costeux S. CO_2-blown nanocellular foams. J Appl Polym Sci 2014.
[63] Lu X, Caps R, Fricke J, Alviso CT, Pekala RW. Correlation between structure and thermal conductivity of organic aerogels. J Non-Cryst Solids 1995;188:226–34.
[64] Schmidt D, Raman VI, Egger C, du Fresne C, Schädler V. Templated cross-linking reactions for designing nanoporous materials. Mater Sci Eng C 2007;27:1487–90.
[65] Pinto J, Notario B, Verdejo R, Dumon M, Costeux S, Rodriguez-Perez MA. Molecular confinement of solid and gaseous phases of self-standing nanoporous polymers inducing enhanced and unexpected physical properties. Adv Mater 2015 [submitted for publication].
[66] Reglero Ruiz JA, Dumon M, Pinto J, Rodriguez-Pérez MA. Low-density nanocellular foams produced by high-pressure carbon dioxide. Macromol Mater Eng 2011;296:752–9.
[67] Notario B, Pinto J, Rodriguez-Perez MA. Towards a new generation of polymeric foams: PMMA nanocellular foams with enhanced physical properties. Polymer 2015;63:116–26.
[68] Mandelbrot B. How long is the coast of Britain? Statistical self-similarity and fractional dimension. Science 1967;156:636–8.
[69] Ma X, Peyton AJ, Zhao YY. Eddy current measurements of electrical conductivity and magnetic permeability of porous metals. NDT & E Int 2006;39:562–8.
[70] Collias DI, Baird DG. Impact toughening of polycarbonate by microcellular foaming. Polymer 1994;35:3978–83.
[71] Sun H, Sur GS, Mark JE. Microcellular foams from polyethersulfone and polyphenylsulfone. Preparation and mechanical properties. Eur Polym J 2002;38:2373–81.
[72] Juntunen RP, Kumar V, Weller JE. Impact strength of high density of microcellular of poly(vinyl chloride) foams. J Vinyl Add Tech 2000;6:93–9.
[73] Hodge AM, Biener J, Hayes JR, Bythrow PM, Volkert CA, Hamza AV. Scaling equation for yield strength of nanoporous open-cell foams. Acta Mater 2007;55:1343–9.
[74] Fan HL, Fang DN. Modeling and limits of strength of nanoporous foams. Mater Des 2009;30:1441–4.
[75] Xia R, Li X, Qin Q, Liu J, Feng XQ. Surface effects on the mechanical properties of nanoporous materials. Nanotechnology 2011;22:265714.
[76] Zhang WX, Wang TJ. Effect of surface energy on the yield strength of nanoporous materials. Appl Phys Lett 2007;90.
[77] Duan HL, Wang J, Karihaloo BL, Huang ZP. Nanoporous materials can be made stiffer than non-porous counterparts by surface modification. Acta Mater 2006;54:2983–90.
[78] Pande CS, Masumura RA, Armstrong RW. Pile-up based Hall–Petch relation for nanoscale materials. Nanostruct Mater 1993;2:323–31.
[79] Biener J, Hodge AM, Hayes JR, Volkert CA, Zepeda-Ruiz LA, Hamza AV, et al. Size effects on the mechanical behavior of nanoporous Au. Nano Lett 2006;6:2379–82.
[80] Hodge AM, Hayes JR, Caro JA, Biener J, Hamza AV. Characterization and mechanical behavior of nanoporous gold. Adv Eng Mater 2006;8:853–7.
[81] Weissmuller J, Newman RC, Jin HJ, Hodge AM, Kysar JW. Nanoporous metals by alloy corrosion: formation and mechanical properties. MRS Bull 2009;34:577–86.
[82] Xia R, Xu C, Wu W, Li X, Feng X-Q, Ding Y. Microtensile tests of mechanical properties of nanoporous Au thin films. J Mater Sci 2009;44:4728–33.
[83] Seker E, Gaskins JT, Bart-Smith H, Zhu J, Reed ML, Zangari G, et al. The effects of post-fabrication annealing on the mechanical properties of freestanding nanoporous gold structures. Acta Mater 2007;55:4593–602.
[84] Xia Z, Riester L, Sheldon BW, Curtin WA, Liang J, Yin A, et al. Mechanical properties of highly ordered nanoporous anodic alumina membranes. Rev Adv Mater Sci 2004;6:131–9.
[85] Sharudin RWB, Ohshima M. CO_2-induced mechanical reinforcement of polyolefin-based nanocellular foams. Macromol Mater Eng 2011;296:1046–54.
[86] Sue HJ, Yee AF. Micromechanical modeling of crack-tip rubber particle cavitational process in polymer toughening. Polym Eng Sci 1996;36:2320–6.
[87] Sue HJ, Huang J, Yee AF. Interfacial adhesion and toughening mechanisms in an alloy of polycarbonate/polyethylene. Polymer 1992;33:4868–71.
[88] Borggreve RJM, Gaymans RJ, Eichenwald HM. Impact behaviour of nylon-rubber blends: 6. Influence of structure on voiding processes; toughening mechanism. Polymer 1989;30:78–83.
[89] Barlow C, Kumar V, Flinn B, Bordia RK, Weller J. Impact strength of high density solid-state microcellular polycarbonate foams. J Eng Mater Technol 2001;123:229–33.
[90] Ikeda-Fukazawa T, Kita D, Nagashima K. Raman spectroscopic study of CO_2 sorption process in poly methyl methacrylate. J Polym Sci Part B Polym Phys 2008;46:831–42.
[91] Solorzano E, Rodriguez-Perez MA, Lázaro J, de Saja JA. Influence of solid phase conductivity and cellular structure on the heat transfer mechanisms of cellular materials: diverse case Studies. Adv Eng Mater 2009;11:818–24.
[92] Russell HW. Principles of heat flow in porous insulators*. J Am Ceram Soc 1935;18:1–5.
[93] Bedeaux D, Kapral R. The effective reaction rate and diffusion coefficients for a two-phase medium. J Chem Phys 1983;79.
[94] Collishaw PG, Evans JRG. An assessment of expressions for the apparent thermal conductivity of cellular materials. J Mater Sci 1994;29:2261–73.
[95] Holman JP. Heat transfer. New York: McGraw-Hill; 1981.

[96] Alvarez-Lainez M, Rodriguez-Perez MA, De Saja JA. Thermal conductivity of open-cell polyolefin foams. J Polym Sci Part B Polym Phys 2008;46:212–21.
[97] Glicksman LR. Heat-transfer and aging of cellular foam insulation. Cell Polym 1991;10:276–93.
[98] Ferkl P, Pokorný R, Bobák M, Kosek J. Heat transfer in one-dimensional micro- and nano-cellular foams. Chem Eng Sci 2013;97:50–8.
[99] Hrubesh LW, Pekala RW. Thermal properties of organic and inorganic aerogels. J Mater Res 1994;9:731–8.
[100] Forest C, Chaumont P, Cassagnau P, Swoboda B, Sonntag P. Polymer nano-foams for insulating applications prepared from CO_2 foaming. Prog Polym Sci 2014.
[101] Sundarram SS, Li W. On thermal conductivity of micro-and nanocellular polymer foams. Polym Eng Sci 2013;53:1901–9.
[102] Lee JH, Grossman JC, Reed J, Galli G. Lattice thermal conductivity of nanoporous Si: molecular dynamics study. Appl Phys Lett 2007;91.
[103] Bera C, Mingo N, Volz S. Marked effects of alloying on the thermal conductivity of nanoporous materials. Phys Rev Lett 2010;104.
[104] Tsui BY, Yang CC, Fang KL. Anisotropic thermal conductivity of nanoporous silica film. IEEE Trans Electron Devices 2004;51:20–7.
[105] Solórzano E, Reglero JA, Rodríguez-Pérez MA, Lehmhus D, Wichmann M, de Saja JA. An experimental study on the thermal conductivity of aluminium foams by using the transient plane source method. Int J Heat Mass Transfer 2008;51:6259–67.
[106] Lee OJ, Lee KH, Yim TJ, Kim SY, Yoo KP. Determination of mesopore size of aerogels from thermal conductivity measurements. Non-Cryst Solids 2002;298:287–92.
[107] Reichenauer G, Heinemann U, Ebert HP. Relationship between pore size and the gas pressure dependence of the gaseous thermal conductivity. Colloids Surf A 2007;300:204–10.
[108] Cuce E, Cuce PM, Wood CJ, Riffat SB. Toward aerogel based thermal superinsulation in buildings: a comprehensive review. Renew Sustain Energy Rev 2014;34:273–99.
[109] Song DW, Shen WN, Dunn B, Moore CD, Goorsky MS, Radetic T, et al. Thermal conductivity of nanoporous bismuth thin films. Appl Phys Lett 2004;84.
[110] Nait-Ali B, Haberko K, Vesteghem H, Absi J, Smith DS. Thermal conductivity of highly porous zirconia. J Eur Ceram Soc 2006;26:3567–74.
[111] (ATEPA) ATdPA. Libro Blanco del Poliuretano Proyectado. Madrid; 2010.
[112] Glassbrenner C, Slack G. Thermal conductivity of silicon and germanium from 3°K to the melting point. Phys Rev 1964;134:A1058–69.
[113] Costeux S, Zhu L, Jeon H, Bunker S, Kalantar T. Nanoporous polymeric foam having high cell density without nanofiller. Dow Global Technologies LLC; 2011.
[114] Costeux S, Bunker SP, Jeon HK, Jog PK. Polymeric nanofoam. Dow Global Technologies LLC; 2013.
[115] Liu S, Duvigneau J, Vancso GJ. Nanocellular polymer foams as promising high performance thermal insulation materials. Eur Polymer J 2015;65:33–45.
[116] Association SI. National technology roadmap for semiconductors. San Jose, California; 1997.
[117] Miller RD. In search of low-K dielectrics. Science 1999;286:421–3.
[118] Ro HW, Kim KJ, Theato P, Gidley DW, Yoon DY. Novel inorganic–organic hybrid block copolymers as pore generators for nanoporous ultralow-dielectric-constant films. Macromolecules 2005;38:1031–4.
[119] Wu Y, Zhao X, Li F, Fan Z. Evaluation of mixing rules for dielectric constants of composite dielectrics by MC-FEM calculation on 3D cubic lattice. J Electroceram 2003;11:227–39.
[120] Krause B, Koops G-H, van der Vegt NFA, Wessling M, Wübbenhorst M, van Turnhout J. Ultralow-k dielectrics made by supercritical foaming of thin polymer films. Adv Mater 2002;14:1041–6.
[121] Jin C, Luttmer JD, Smith DM, Ramos TA. Nanoporous silica as an ultralow-k dielectric. MRS Bull 1997;22:39–42.
[122] Baskaran S, Liu J, Domansky K, Kohler N, Li X, Coyle C, et al. Low dielectric constant mesoporous silica films through molecularly template synthesis. Adv Mater 2000;12:291–4.
[123] Ramos T, Wallace S, Smith DM. Nanoporous silica for low k dielectrics. MRS Proc 1997;495.
[124] Yang S, Mirau PA, Pai CS, Nalamasu O, Rechmanis E, Pai JC, et al. Nanoporous ultralow dielectric constant organosilicates template by triblock copolymers. Chem Mater 2002;14:369–74.
[125] Yang S, Mirau PA, Pai CS, Nalamasu O, Rechmanis E, Lin EK, et al. Molecular templating of nanoporous ultralow dielectric constant (1.5) organosilicates by tailoring the microphase separation of triblock copolymers. Chem Mater 2001;13:2762–4.
[126] Nguyen CY, Carter KR, Hawker CJ, Hedrick JL, Jaffe RL, Miller RD, et al. Low-dielectric, nanoporous organosilicate films prepared via inorganic/organic polymer hybrid templates. Chem Mater 1999;11:3080–5.
[127] Lee B, Park YH, Hwang YT, Oh W, Yoon J, Ree M. Ultralow-k nanoporous organosilicate dielectric films imprinted with dendritic spheres. Nat Mater 2005;4:147–50.
[128] Flannery CM, Wittkowski T, Jung K, Hillebrands B, Baklanov MR. Critical properties of nanoporous low dielectric constant films revealed by Brillouin light scattering and surface acoustic wave spectroscopy. Appl Phys Lett 2002;80:4594–6.
[129] Hawker CJ, Hedrick JL, Miller RD, Volksen W. Supramolecular approaches to nanoscale dielectric foams for advanced microelectronic devices. MRS Bull 2000;25:54–8.
[130] Lee Y-J, Huang J-M, Kuo S-W, Chang F-C. Low-dielectric, nanoporous polyimide films prepared from PEO–POSS nanoparticles. Polymer 2005;46:10056–65.
[131] Hedrick JL, Carter KR, Cha HJ, Hawker CJ, DiPietro RA, Labadie JW, et al. High-temperature polyimide nanofoams for microelectronic applications. React Funct Polym 1996;30:43–53.
[132] Carter KR, DiPietro RA, Sanchez MI, Swanson SA. Nanoporous polyimides derived from highly fluorinated polyimide/poly (propylene oxide) copolymers. Chem Mater 2001;13:213–21.
[133] Zhang Y, Ke S, Huang H, Zhao L, Yu L, Chan HLW. Dielectric relaxation in polyimide nanofoamed films with low dielectric constant. Appl Phys Lett 2008;92:052910.
[134] Fu GD, Zong BY, Kang ET, Neoh KG, Lin CC, Liaw DJ. Nanoporous low-dielectric constant polyimide films via poly(amic acid)s with RAFT-Graft copolymerized methyl methacrylate side chains. Ind Eng Chem Res 2004;43:6723–30.

[135] Mehdipour-Ataei S, Aram E. New polyimide and nanoporous structures with low dielectric constant. Adv Polym Technol 2014;33.
[136] Li X, Zou H, Liu P. Structure and dielectric properties of polyimide/silica nanocomposite nanofoam prepared by solid-state foaming. J Appl Polym Sci 2015;132:42355.
[137] Fu GD, Yuan Z, Kang ET, Neoh KG, Lai DM, Huan ACH. Nanoporous ultra-low dielectric constant fluoropolymer films via selective UV decomposition of poly(pentafluorostyrene)-block-poly(methyl methacrylate) copolymers prepared using atom transfer radical polymerization. Adv Funct Mater 2005;15:315–22.
[138] Fu GD, Shang Z, Hong L, Kang ET, Neoh KG. Nanoporous, ultralow-dielectric- constant fluoropolymer films from agglomerated and crosslinked hollow nanospheres of poly(pentafluorostyrene)-block-poly(divinylbenzene). Adv Mater 2005;17:2622–6.
[139] Xu Y, Tsai YP, Tu KN, Zhao B, Liu QZ, Brogo M, et al. Dielectric property and microstructure of a porous polymer material with ultralow dielectric constant. Appl Phys Lett 1999;75:853.
[140] Su Y-C, Chen W-C, Ou K-l, Chang F-C. Study of the morphologies and dielectric constants of nanoporous materials derived from benzoxazine-terminated poly(ε-caprolactone)/polybenzoxazine co-polymers. Polymer 2005;46:3758–66.
[141] Energy Do. DOE hydrogen program 2006 annual program report; 2006. p. 273.
[142] Cabria I, López MJ, Alonso JA. The optimum average nanopore size for hydrogen storage in carbon nanoporous materials. Carbon 2007;45:2649–58.
[143] Bênard P, Chahine R, Chandonia PA, Cossement D, Dorval-Douville G, Lafi L, et al. Comparison of hydrogen adsorption on nanoporous materials. J Alloys Compd 2007;446–447:380–4.
[144] Bénard P, Chahine R. Determination of the adsorption isotherms of hydrogen on activated carbons above the critical temperature of the adsorbate over wide temperature and pressure ranges. Langmuir 2001;17:1950–5.
[145] Li L. Nanoporous polymers for membrane applications. Technical University of Denmark; 2012.
[146] Mulder M. Basic principles of membrane technology. 2nd ed. USA: Kluwer Academic Publishers; 1996.
[147] Baker RW. Membrane technology and applications. 2nd ed. Chichester, UK; 2004.
[148] Bhatia SK. Modeling pure gas permeation in nanoporous materials and membranes. Langmuir 2010;26:8373–85.
[149] Derouane EG, Andre JM, Lucas AA. Surface curvature effects in physisorption and catalysis by microporous solids and molecular sieves. J Catal 1988;110:58–73.
[150] Yashonath S, Santikary P. Diffusion of sorbates in zeolites Y and A: novel dependence on sorbate size and strength of sorbate–zeolite interaction. J Phys Chem 1994;98:6368–76.
[151] Phillip WA, Rzayev J, Hillmyer MA, Cussler EL. Gas and water liquid transport through nanoporous block copolymer membranes. J Membr Sci 2006;286:144–52.
[152] Epstein N. On tortuosity and the tortuosity factor in flow and diffusion through porous media. Chem Eng Sci 1989;44:777–9.
[153] Li L, Schulte L, Clausen LD, Hansen KM, Jonsson GE, Ndoni S. Gyroid nanoporous membranes with tunable permeability. ACS Nano 2011;5:7754–66.
[154] Adiga SP, Curtiss LA, Elam JW, Pellin MJ, Shih CC, Shih CM, et al. Nanoporous materials for biomedical devices. Biol Mater Sci 2008:26–32.
[155] Pappenheimer JR. Passage of molecules through capillary walls. Physiol Rev 1953;33:387–423.
[156] Renkin EM. Filtration, diffusion, and molecular sieving through porous cellulose membranes. J General Physiol 1954;38:225–43.
[157] Morris RE, Wheatley PS. Gas storage in nanoporous materials. Angew Chem Int Ed Engl 2008;47:4966–81.
[158] Thomas KM. Adsorption and desorption of hydrogen on metal–organic framework materials for storage applications: comparison with other nanoporous materials. Dalton Trans 2009:1487–505.
[159] Shiflett MB, Foley HC. Ultrasonic deposition of high-selectivity nanoporous carbon membranes. Science 1999;285:1902–5.
[160] Shiflett MB, Pedrick JF, McLean SR, Subramoney S, Foley HC. Characterization of supported nanoporous carbon membranes. Adv Mater 2000;12:21–5.
[161] Han S, Sohn K, Hyeon T. Fabrication of new nanoporous carbons through silica templates and their application to the adsorption of bulky dyes. Chem Mater 2000;12:3337–41.
[162] Rösler J, Mukherji D. Design of nanoporous superalloy membranes for functional applications. Adv Eng Mater 2003;5:916–8.
[163] Park HB, Lee YM. Fabrication and characterization of nanoporous carbon/silica membranes. Adv Mater 2005;17:477–83.
[164] Newsam JM. The zeolite cage structure. Science 1986;231:1093–9.
[165] Bein T. Synthesis and applications of molecular sieve layers and membranes. Chem Mater 1996;8:1636–53.
[166] Daniel C, Longo S, Ricciardi R, Reverchon E, Guerra G. Monolithic nanoporous crystalline aerogels. Macromol Rapid Commun 2013;34:1194–207.
[167] Adiga SP, Jin C, Curtiss LA, Monteiro-Riviere NA, Narayan RJ. Nanoporous membranes for medical and biological applications. Nanomed Nanobiotechnol 2009;1:568–81.
[168] Gultepe E, Nagesha D, Sridhar S, Amiji M. Nanoporous inorganic membranes or coatings for sustained drug delivery in implantable devices. Adv Drug Delivery Rev 2010;62:305–15.
[169] Swan EE, Popat KC, Desai TA. Peptide-immobilized nanoporous alumina membranes for enhanced osteoblast adhesion. Biomaterials 2005;26:1969–76.
[170] La Flamme KE, Popat KC, Leoni L, Markiewicz E, La Tempa TJ, Roman BB, et al. Biocompatibility of nanoporous alumina membranes for immunoisolation. Biomaterials 2007;28:2638–45.
[171] Thormann A, Teuscher N, Pfannmoller M, Rothe U, Heilmann A. Nanoporous aluminum oxide membranes for filtration and biofunctionalization. Small 2007;3:1032–40.
[172] Desai TA, Hansford DJ, Leoni L, Essepreis M, Ferrari M. Nanoporous anti-fouling silicon membranes for biosensor applications. Biosens Bioelectron 2000;15:453–62.
[173] Rosenbloom AJ, Sipe DM, Shishkin Y, Ke Y, Devaty RP, Choyke WJ. Nanoporous SiC: a candidate semi-permeable material for biomedical applications. Biomed Microdevices 2004;6:261–7.

[174] Ng E-P, Mintova S. Nanoporous materials with enhanced hydrophilicity and high water sorption capacity. Microporous Mesoporous Mater 2008;114:1–26.
[175] Budd PM, McKeown NB, Fritsch D. Free volume and intrinsic microporosity in polymers. J Mater Chem 2005;15:1977–86.
[176] McKeown NB, Gahnem B, Msayib KJ, Budd PM, Tattershall CE, Mahmood K, et al. Towards polymer-based hydrogen storage materials: engineering ultramicroporous cavities within polymers of intrinsic microporosity. Angew Chem Int Ed Engl 2006;45:1804–7.
[177] Budd PM, Butler A, Selbie J, Mahmood K, McKeown NB, Ghanem B, et al. The potential of organic polymer-based hydrogen storage materials. Phys Chem Chem Phys 2007;9:1802–8.
[178] Ghanem BS, Msayib KJ, McKeown NB, Harris KD, Pan Z, Budd PM, et al. A triptycene-based polymer of intrinsic microposity that displays enhanced surface area and hydrogen adsorption. Chem Commun (Camb) 2007:67–9.
[179] Mckeown NB, Budd PM. Polymers of intrinsic microporosity (PIMs): organic materials for membrane separations, heterogeneous catalysis and hydrogen storage. Chem Soc Rev 2006;35:675–83.
[180] Germain J, Hradil J, Fréchet JMJ, Svec F. High surface area nanoporous polymers for reversible hydrogen storage. Chem Mater 2006;18:4430–5.
[181] Lee JY, Wood CD, Bradshaw D, Rosseinsky MJ, Cooper AI. Hydrogen adsorption in microporous hypercrosslinked polymers. Chem Commun 2006;25:2670–2.
[182] Germain J, Fréchet JMJ, Svec F. Hypercrosslinked polyanilines with nanoporous structure and high surface area: potential adsorbents for hydrogen storage. J Mater Chem 2007;17:4989–97.
[183] Jiang JX, Su F, Trewin A, Wood CD, Niu H, Jones JTA, et al. Synthetic control of the pore dimension and surface area in conjugated microporous polymer and copolymer networks. J Am Chem Soc 2008;130:7710–20.
[184] Guerra G, Daniel C, Rizzo P, Tarallo O. Advanced materials based on polymer cocrystalline forms. J Polym Sci Part B Polym Phys 2012;50:305–22.
[185] Schulte L, Grydgaard A, Jakobsen MR, Szewczykowski PP, Guo F, Vigild ME, et al. Nanoporous materials from stable and metastable structures of 1,2-PB-b-PDMS block copolymers. Polymer 2011;52:422–9.
[186] Phillip WA, Amendt M, O'Neill B, Chen L, Hillmyer MA, Cussler EL. Diffusion and flow across nanoporous polydicyclopentadiene-based membranes. ACS Appl Mater Interfaces 2009;1:472–80.
[187] Phillip WA, O'Neill B, Rodwogin M, Hillmyer MA, Cussler EL. Self-assembled block copolymer thin films as water filtration membranes. ACS Appl Mater Interfaces 2010;2:847–53.
[188] Milano G, Guerra G. Understanding at molecular level of nanoporous and co-crystalline materials based on syndiotactic polystyrene. Prog Mater Sci 2009;54:68–88.
[189] Yang SY, Ryu I, Kim HY, Kim JK, Jang SK, Russell TP. Nanoporous membranes with ultrahigh selectivity and flux for the filtration of viruses. Adv Mater 2006;18:709–12.
[190] Yang SY, Park J, Yoon J, Ree M, Jang SK, Kim JK. Virus filtration membranes prepared from nanoporous block copolymers with good dimensional stability under high pressures and excellent solvent resistance. Adv Funct Mater 2008;18:1371–7.
[191] Jackson EA, Hillmyer MA. Nanoporous membranes derived from block copolymers: from drug delivery to water filtration. ACS Nano 2010;4:3548–53.
[192] Samitsu S, Zhang R, Peng X, Krishnan MR, Fujii Y, Ichinose I. Flash freezing route to mesoporous polymer nanofibre networks. Nat Commun 2013;4:2653.
[193] Metz S, Trautmann C, Bertsch A, Renaud P. Flexible microchannels with integrated nanoporous membranes for filtration and separation of molecules and particles. Micro Electro Mech Syst 2002:81–4.
[194] Uehara H, Kakiage M, Sekiya M, Sakuma D, Yamonobe T, Takano N, et al. Size selective diffusion in nanoporous but flexible membranes for glucose sensors. ACS Nano 2009;3:924–32.
[195] Smuleac V, Butterfield DA, Bhattacharyya D. Permeability and separation characteristics of polypeptide-functionalized polycarbonate track-etched membranes. Chem Mater 2004;16:2762–71.
[196] Chaniotakis NA. Enzyme stabilization strategies based on electrolytes and polyelectrolytes for biosensor applications. Anal Bioanal Chem 2004;378:89–95.
[197] Abad JM, Velez M, Santamaria C, Guisan JM, Matheus PR, Vazquez L, et al. Immobilization of peroxidase glycoprotein on gold electrodes modified with mixed epoxy-boronic acid monolayers. J Am Chem Soc 2002;124:12845–53.
[198] Besanger TR, Chen Y, Deisingh AK, Hodgson R, Jin W, Mayer S, et al. Screening of inhibitors using enzymes entrapped in sol–gel-derived materials. Anal Chem 2003;75:2382–91.
[199] Zhou HX, Dill KA. Stabilization of proteins in confined spaces. Biochemistry 2001;40:11289–93.
[200] Sotiropoulou S, Vamvakaki V, Chaniotakis NA. Stabilization of enzymes in nanoporous materials for biosensor applications. Biosens Bioelectron 2005;20:1674–9.
[201] Gavalas VG, Chaniotakis NA. [60]Fullerene-mediated amperometric biosensors. Anal Chim Acta 2000;409:131–5.
[202] Gavalas VG, Chaniotakis NA. Polyelectrolyte stabilized oxidase based biosensors: effect of diethylaminoethyl-dextran on the stabilization of glucose and lactate oxidases into porous conductive carbon. Anal Chim Acta 2000;404:67–73.
[203] Sotiropoulou S, Gavalas V, Vamvakaki V, Chaniotakis NA. Novel carbon materials in biosensor systems. Biosens Bioelectron 2003;18:211–5.
[204] Dickey EC, Varghese OK, Ong KG, Gong D, Paulose M, Grimes CA. Room temperature ammonia and humidity sensing using highly ordered nanoporous alumina films. Sensors 2002;2:91–110.
[205] Varghese OK, Gong D, Paulose M, Ong KG, Grimes CA, Dickey EC. Highly ordered nanoporous alumina films: effect of pore size and uniformity on sensing performance. J Mater Res 2002;17:1162–71.
[206] Nitta T, Hayakawa S. Ceramic humidity sensors. IEEE Trans Compon Hybrids Manuf Technol 1980;3:237–43.
[207] Connolly EJ, French PJ, Pham HTM, Sarro PM. Relative humidity sensors based on porous polysilicon and porous silicon carbide. In: Sensors, 2002 proceedings of IEEE, vol. 1; 2002. p. 499–502.
[208] An DK, Mai LH. Surface effect humidity sensor based on alumina and porous silicon materials some electrical parameters, sensitivity and internal noises in comparison. In: Sensors, 2002 proceedings of IEEE, vol. 1; 2002. p. 633–40.
[209] Kim SJ, Park JY, Lee SH, Yi SH. Humidity sensors using porous silicon layer with mesa structure. J Phys D Appl Phys 2000;33:1781–4.

[210] Yang B, Aksak B, Lin Q, Sitti M. Compliant and low-cost humidity nanosensors using nanoporous polymer membranes. Sens Actuators B Chem 2006;114:254–62.
[211] Pilla P, Cusano A, Cutolo A, Giordano M, Mensitieri G, Rizzo P, et al. Molecular sensing by nanoporous crystalline polymers. Sensors 2009;9:9816–57.
[212] Arrand HF, Benson TM, Loni A, Krueger MG, Thoenissen M, Lueth H. Self-aligned porous silicon optical waveguides. Electron Lett 1997;33:1724–5.
[213] Loni A, Canham LT, Berger MG, Arens-Fischer R, Munder H, Luth H, et al. Porous silicon multilayer optical waveguides. Thin Solid Films 1996;276:143–6.
[214] Zangooie S, Jansson R, Arwin H. Ellipsometric characterization of anisotropic porous silicon Fabry-Pérot filters and investigation of temperature effects on capillary condensation efficiency. J Appl Phys 1999;86:850.
[215] Berger MG, Thönissen M, Arens-Fischer R, Münder H, Lüth H, Arntzen M, et al. Investigation and design of optical properties of porosity superlattices. Thin Solid Films 1995;255:313–6.
[216] Kordás K, Beke S, Pap AE, Uusimäki A, Leppävuori S. Optical properties of porous silicon. Opt Mater 2004;25:257–60.
[217] Zangooie S, Schubert M, Trimble C, Thompson DW, Woollam JA. Infrared ellipsometry characterization of porous silicon Bragg reflectors. Appl Opt 2001;40:906–12.
[218] Zhang Q, Wang J, Wu G, Shen J, Buddhudu S. Interference coating by hydrophobic aerogel-like SiO_2 thin films. Mater Chem Phys 2001;72:56–9.
[219] Macleod HA. Thin-film optical filters. New York; 1969.
[220] Bruggeman DAG. Dielectric constant and conductivity of mixtures of isotropic materials. Ann Phys (Leipzig) 1935;24:636–79.
[221] Garahan A, Pilon L, Yin J, Saxena I. Effective optical properties of absorbing nanoporous and nanocomposite thin films. J Appl Phys 2007;101:014320.
[222] Garnett JCM. Colours in metal glasses and in metallic films. Phil Trans R Soc London A 1904;203:385–420.
[223] Choy TC. Effective medium theory: principles and applications. Oxford: Oxford University Press; 1999.
[224] Río JAd, Whitaker S. Maxwell's equations in two-phase systems I: local electrodynamic equilibrium. Transp Porous Media 2000;39:159–86.
[225] Rio JAd, Whitaker S. Maxwell's equation in two-phase systems II: two-equation model. Transp Porous Media 2000;39:259–87.
[226] Braun MM, Pilon L. Effective optical properties of non-absorbing nanoporous thin films. Thin Solid Films 2006;496:505–14.
[227] Navid A, Pilon L. Effect of polarization and morphology on the optical properties of absorbing nanoporous thin films. Thin Solid Films 2008;516:4159–67.
[228] Lee Y, Kang M. The optical properties of nanoporous structured titanium dioxide and the photovoltaic efficiency on DSSC. Mater Chem Phys 2010;122:284–9.
[229] Vajpeyi AP, Tripathy S, Chua SJ, Fitzgerald EA. Investigation of optical properties of nanoporous GaN films. Physica E 2005;28:141–9.
[230] Cho J, Hong J, Char K, Caruso F. Nanoporous block copolymer micelle/micelle multilayer films with dual optical properties. J Am Chem Soc 2006;128:9935–42.
[231] Hiller JA, Mendelsohn JD, Rubner MF. Reversible erasable nanoporous anti-reflection coatings from polyelectrolyte multilayers. Nat Mater 2002;1:59–63.
[232] Li L, Nemoto T, Sugiyama K, Yokoyama H. CO_2 foaming in thin films of block copolymer containing fluorinated blocks. Macromolecules 2006;39:4746–55.
[233] Born M, Wolf E. Principles of optics: electromagnetic theory of propagation, interference and diffraction of light. Cambridge, United Kingdom: Cambridge University Press; 1999.
[234] Rizzo P, Montefusco T, Guerra G. Chiral optical films based on achiral chromophore guests. J Am Chem Soc 2011;133:9872–7.
[235] Harbuzaru BV, Corma A, Rey F, Atienzar P, Jorda JL, Garcia H, et al. Metal–organic nanoporous structures with anisotropic photoluminescence and magnetic properties and their use as sensors. Angew Chem Int Ed Engl 2008;47:1080–3.
[236] Hrubesh LW, Poco JF. Thin aerogel films for optical, thermal, acoustic and electronic applications. J Non-Cryst Solids 1995;188:46–53.
[237] Fricke J. In: Aerogels, editor. Springer proceedings in physics; 1986.
[238] Vacher R, Phalippou J, Pelous J, Woignier T. 2nd International symposia on aerogels. Rev Phys Appl; 1989.

0.4 Objectives

Traditionally, there are four main areas on the study of a new cellular material: its production route, cellular structure, properties, and potential applications. These topics are strongly interrelated, as the materials tetrahedron of Figure 0.6 shows.

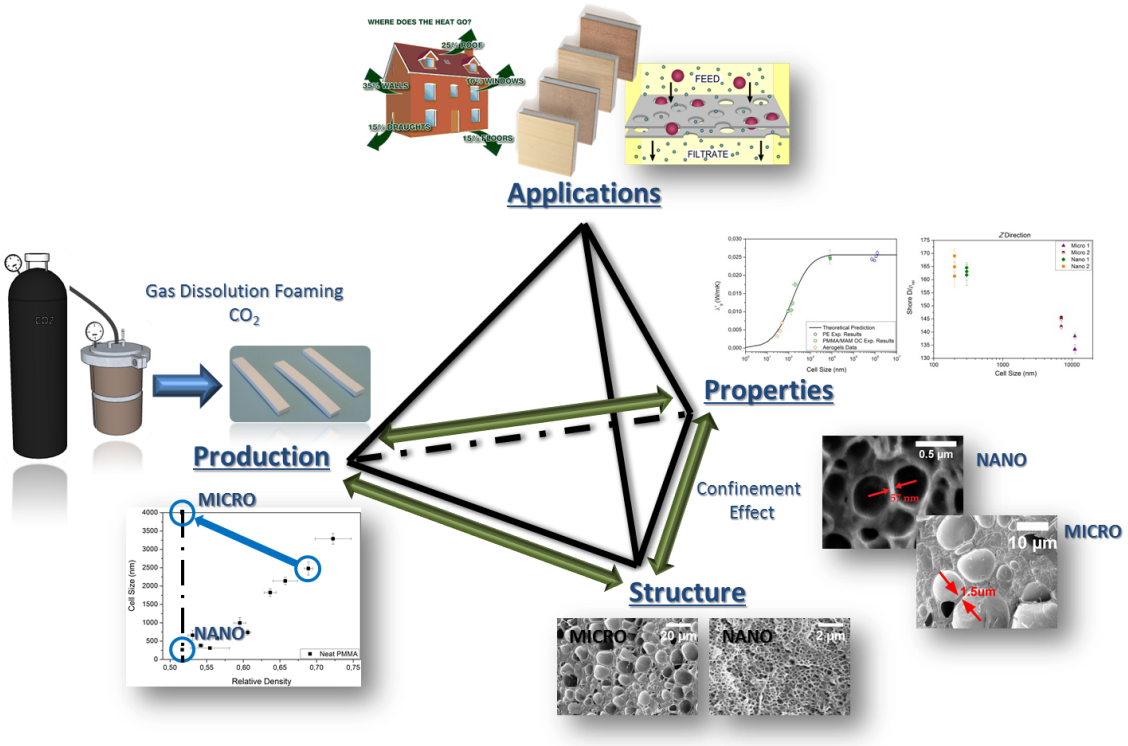

Figure 0.6. Tetrahedron of research areas and their relationships for foamed materials

Based on this concept, the goal of this work has been to study systematically the transition of the physical properties between microcellular and nanocellular polymers. For this purpose the production processes were optimized to obtain both micro and nanocellular polymers with similar relative densities and with appropriate dimensions and geometries for their further characterization. The precursor systems used for this purpose are PMMA and blends of PMMA/MAM. These systems has been previously studied regarding the production and foaming mechanisms, therefore this study has been focused on the performing of a systematic study of the physical properties of nanocellular polymers in comparison with microcellular ones and in understanding the key differences taking into account the structural differences between the materials.

Then, the three main scientific and technical objectives are as follows:

1. To solve the existing limitation of producing micro and nanocellular polymers with appropriate dimensions, geometries, and similar densities to perform a characterization of the physical properties using standard procedures ("Production").

2. To provide a better understanding of the mechanisms involved in the improvements of several physical properties of nanocellular systems ("Structure ↔ Properties").

3. To study whether there is a transition in the properties of these materials when cell size goes from the microcellular to the nanocellular range, and to determine the validity of the assumptions made in that respect in recent years..

Likewise, some partial objectives have been defined inside each of the main objectives to define precisely the scope and extent of each of them.

From the production and technical point of view, we aim at obtaining nanocellular polymers with the following requisites:

- Raw polymers should be easily accessible, and preferably being commercial polymers.
- Solid blends of PMMA/MAM should show a self-assembly nanostructuration.
- Foamed samples with micro and nanocellular structures should have appropriate dimensions and geometries enabling further characterization using standard protocols.
- Foamed samples should be obtained with similar relative densities, showing a significant reduction of the density (around 50 % in comparison with the solid material). Furthermore, the degree of density reduction should not depend on the presence of micro or nano cellular structures.
- Production route should be industrially scalable, avoiding requirements as extremely high pressures, high pressure drop rates, low saturation temperatures (below room temperature), etc.

From the scientific point of view, we have focused a key part of our research on the underlying mechanisms that lead to physical properties modification or to the occurrence of unexpected phenomena. In particular we wonder:

- Does the reduction of the cell size to the nanometer range produce a confinement of the polymer macromolecules?
- What influence does the confinement of the gaseous phase have in the physical properties?
- How does tortuosity influence on the physical properties when the size of both solid and gaseous phase change from sizes in the microscale to sizes in the nanoscale?

And finally, from the point of view of the analysis of the expected improvements of the physical properties of nanocellular polymers as compared to microcellular ones, the work has been focused on:

- Thermal conductivity: it is expected a significant decrease of the thermal conductivity of the gaseous phase when pore size falls in the nanometric range due to an effect known as Knudsen Effect [97] (see section *0.3 Summary of the State of the Art*).

- Mechanical properties: traditionally microcellular polymers have exhibited improved mechanical properties as compared with conventional foams due to the reduction of cell size [98]. Therefore, it is expected that a further reduction of the cell size (nanocellular polymers) will lead to enhance mechanical properties in comparison with microcellular ones.

- Dielectric properties: it is expected that the dielectric behavior of nanocellular polymers will be different in comparison with that of microcellular ones due to the confinement of the solid and gas phases.

- Acoustic properties: it is expected that the acoustic behavior of nanocellular polymers differs from microcellular ones owing to the structural change of one with respect to the other.

0.5 Structure of this Thesis

The research presented on this thesis is presented to obtain the degree of *Doctor in Philosophy* (Ph.D.) with an *International Mention*. For this reason the main body of the thesis is written in English.

Moreover, this thesis is written as a compendium of publications. Six regular papers sent to international journals (four of them already published and two of them under revision). Likewise some unpublished results have been included in several chapters in order to provide a better understanding of the work and cover the objectives previously defined (see section *0.4 Objectives*). Table 0-1 summarizes the papers included in this thesis, with their enclosing chapter in the right column.

Other peer-reviewed publications, contributions to international conferences (related to the thesis and to other topics), research stages in other institutions, and participation in research projects during the last four years are summarized in tables 0-2, 0-3, 0-4, 0-5, and 0-6, respectively.

The manuscript is divided into seven chapters including the following information:

The introduction describes the state of the art concerning the different physical properties of nanocellular polymers, comparing it with other non-polymeric nanocellular materials. In this introduction the different production techniques of nanocellular polymers, the parameters that can be affected by the change of scale, and the potential applications that these cellular polymers can have in the near future are also briefly described.

Chapter 1 describes the raw polymers used in this research, PMMA and MAM, and the production route of PMMA/MAM solid blends as well as the production route of microcellular

and nanocellular polymers. The characterization techniques used are described and the cellular structure of the foams produced is included.

Chapter 2 shows the new effects that appear as a consequence of the reduction of the cell size to the nanometer range and the increase of cell density. This chapter demonstrates the confinement of both the solid and gaseous phases of nanoporous PMMA-based materials. Regarding to the solid phase, this effect implies conformational changes and immobilization of the PMMA chains, which results in an increment of 11º C of the glass transition temperature. Related to the confinement of the gaseous phase, an unexpected capacitor-like behavior appears in polymeric nanopores due to the appearance of a Maxwell Wagner Sillars (MWS) phenomenon. Finally this paper also illustrates an increase of the tortuosity of the porous architecture when the cell size goes from the micro to the nanometer scale.

Chapter 3 studies the thermal conductivity of nanocellular polymers in comparison with that of microcellular ones. In this case, it is demonstrated how the confinement of the constituent phases of the foam (gas and solid) allow reducing the overall thermal conductivity even for medium density samples.

Chapter 4 carries out a comparative study of the mechanical properties between microcellular and nanocellular polymers with similar relative densities. In this section, it is demonstrated that nanocellular polymers exhibit higher Young´s modulus, impact resistance, and shore hardness than microcellular polymers.

Chapter 5 studies the dielectric properties of both micro and nanocellular PMMA, showing an evident transition from a capacitive to a combination of a resistive and a capacitive behavior when cell size shift from the micro to the nanoscale.

Chapter 6 analyzes the acoustic properties of PMMA nanocellular polymers in comparison with that of microcellular PMMA foams with similar relative densities. Moreover, a comparative study of the different theoretical models that could be used to understand the results is presented.

Last chapter collects the main conclusions of this work, and includes several research topics for future research. Furthermore, it also includes a general discussion of the influence that each of the parameters (confinement of the solid and gaseous phases, tortuosity, etc.) have on nanocellular polymers properties.

To provide a better understanding of the thesis structure a schematic view can be found in Figure 0.7.

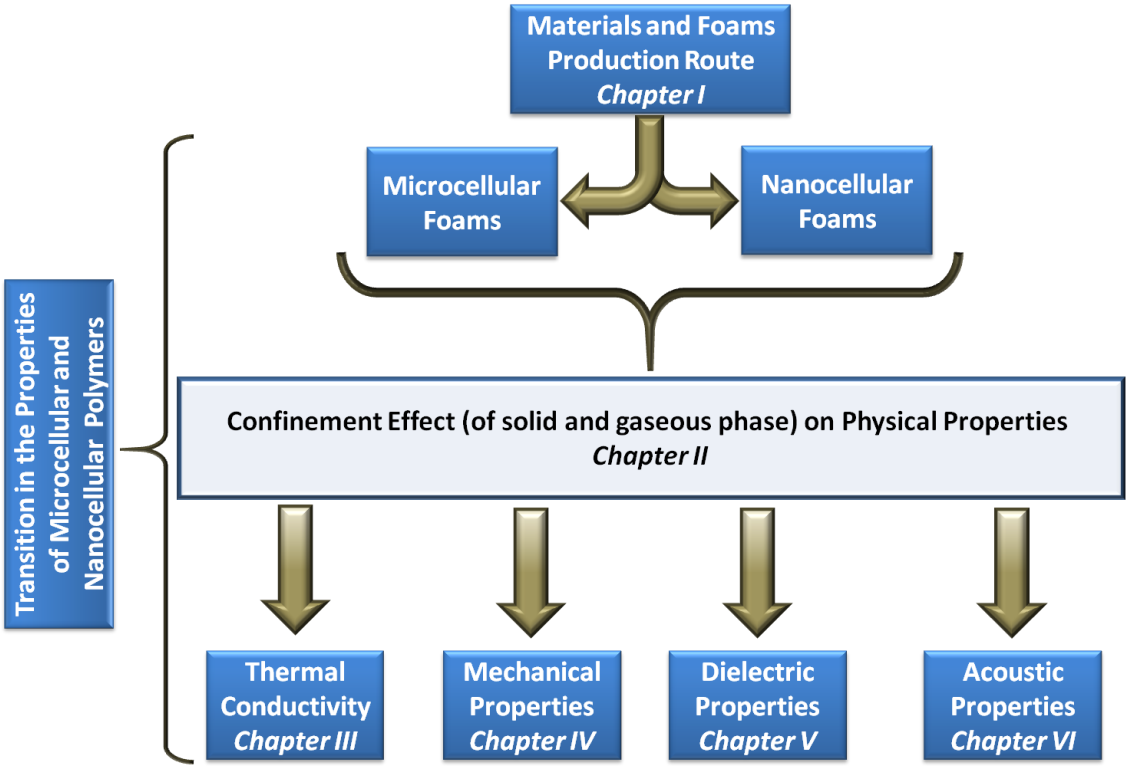

Figure 0.7. Scheme of the thesis structure

Table 0-1. Publications in international journals included in this dissertation; the PhD is main author or main participant

Publications submitted to international journals	Chapter
B. Notario, J. Pinto, E. Solórzano, J. A. de Saja, M. Dumon, M. A. Rodríguez-Pérez **Experimental Validation of the Knudsen Effect in Nanocellular Polymeric Foams** *Polymer 56, 57-67 (2015)* ***Invited Article***	III
B. Notario, J. Pinto, M. A. Rodríguez-Pérez **Towards a New Generation of Polymeric Foams: PMMA Nanocellular Foams with Enhanced Physical Properties** *Polymer 63, 116-126 (2015)*	IV
J. Pinto, B. Notario, R. Verdejo, M. Dumon, S. Costeux, M. A. Rodríguez-Pérez **Molecular Confinement of Solid and Gaseous Phases of Self-Standing Nanoporous Polymers Inducing Enhanced and Unexpected Physical Properties** *The Journal of Physical Chemistry Letters (2016) Submitted*	II
B. Notario, J. Pinto, M. A. Rodríguez-Pérez **Nanoporous Polymeric Materials: a New Class of Materials with Enhanced Properties** *Progress in Materials Science 78-79, 93-139 (2016)*	0
B. Notario, J. Pinto, R. Verdejo, M. A. Rodríguez-Pérez **Dielectric Behavior of Porous PMMA: from the Micrometer to the Nanometer Scale** *Polymer (2015) Submitted*	V
B. Notario, A. Ballesteros, J. Pinto, M. A. Rodríguez-Pérez **Nanoporous PMMA: a Novel System with Different Acoustic Properties** *Materials Letters 168, 76-79 (2016)*	VI

Table 0-2. Other publications in international journals; the PhD is main author or co-author

Other publications submitted to international journals
B. Notario, J. Pinto, E. Solórzano, J. Escudero, J. Martín-de León, D. Velasco, M. A. Rodríguez-Pérez **In-Situ Optical Analysis of Structural Changes in Polylactic Acid (PLA) during the Gas Dissolution Process** *Defect and Diffusion Forum 353, 131-136 (2014)*
J. Escudero, B. Notario, C. Jiménez, M. A. Rodríguez-Pérez **Characterization of Nanoclays Intercalation during Foaming by Using in Situ Energy-Dispersive X-Ray Diffraction** *Journal of Applied Polymer Science 133, 43432-43440 (2016)*

Table 0-3. Communications in international conferences related to the thesis work

Communications presented in international conferences related to the thesis
B. Notario, J. Pinto, E. Solórzano, J. Escudero, J. Martín-de León, D. Velasco, M. A. Rodríguez-Pérez **Analysis of Structural Changes in Amorphous Polymers during the Gas Dissolution Process** **Oral**. *DSL 2013, Madrid (Spain) (2013)*
B. Notario, J. Pinto, E. Solórzano, A. Martín-Cid, M. A. Rodríguez-Pérez, M. Dumon **Physical Properties of Nanocellular Foams: the Transition from the Micro to the Nano Scale** **Oral**. *International Conference on Foams and Foams Technology, FOAMS 2014, New Jersey (USA) (2014)*
S. Perez-Tamarit, B. Notario, E. Solorzano, M. A. Rodríguez-Pérez **Cell Size Determination by means of Light Scattering Methodologies in Micro and Nanoporous Foams** **Oral**. *7th European School on Molecular Nanoscience (ESMolNa), Gandía (Spain) (2014)*
M. A. Rodríguez-Pérez , B. Notario, J. Pinto **Physical Properties of Nanocellular Foams: the Transition from the Micro to the Nano Scale** **Invited Talk**. *IMP Workshops, Processing and Applications of Polymer Foams, Lyon-Villeurbanne (France) (2015)*
B. Notario, J. Pinto, M. A. Rodríguez-Pérez **The Influence of Reducing the Cell Size to the Nanoscale on the Physical Properties of Polymeric Nanocellular Foams** **Oral**. *International Conference on Composite Materials, Copenhagen (Denmark) (2015)*
B. Notario, J. Pinto, M. A. Rodríguez-Pérez **Improving the Properties of Polymer Foams by Reducing the Cell Size to the Nanoscale** **Oral**. *Polymer Foams Conference, Colonia (Germany) (2015*)

Table 0-4. Other communications in international conferences

Other communications presented in international conferences
B. Notario, C. Jiménez, J. Escudero, M. A. Rodríguez-Pérez, M. Klaus **Seguimiento In-Situ de la Exfoliación de Nanoarcillas mediante ED-XRD durante el Espumado de Materiales Termoplásticos** **Oral**. *XIII Escuela Nacional de Materiales Moleculares, El Escorial, Madrid (Spain) (2012)*
A. Esteban-Cubillo, J. Santaren, A. Alvarez, B. Notario, D. Velasco, M. A. Rodríguez-Pérez **Improving the Cellular Structure and Thermal Conductivity of Polystyrene Foams by Using Sepiolite** **Oral**. *International Conference on Foams and Foams Technology, FOAMS 2012, Barcelona (Spain) (2012)*
B. Notario, J. Escudero, M. A. Rodríguez-Pérez **In-Situ Study of the Foaming Process of Polyethylene Reinforced with Nanoclays** **Poster**. *International Conference on Foams and Foams Technology, FOAMS 2012, Barcelona (Spain) (2012)*
B. Notario, J. Escudero, A. López, M. A. Rodríguez-Pérez **Foaming Induces Exfoliation in Polyolefins containing Clay Nanoparticles: In-Situ Evolution of the Process by using XRD of Synchrotron Light and Applicability to the Production of Foams with Improved Properties** **Oral**. *International Conference on Foams and Foams Technology, FOAMS 2013, Seattle (USA) (2013)*
B. Notario, J. Escudero, M. A. Rodríguez-Pérez, C. Jiménez, M. Klaus **Characterization by Synchrotron Radiation of the Foaming Process of Polyethylene Reinforced with Nanoclays: Analysis of the Exfoliation induced by Foaming Phenomenon** **Poster**. *International Conference on Foams and Foams Technology, FOAMS 2014, New Jersey (USA) (2014)* ***Best Poster Award***
B. Notario, J. Escudero, M. A. Rodríguez-Pérez, C. Jiménez, M. Klaus **Characterization by Synchrotron Radiation of the Foaming Process of Polyethylene Reinforced with Nanoclays: Analysis of the Exfoliation induced by Foaming Phenomenon** **Poster**. *HZB User Meeting, Berlin (Germany) (2014)*
C. Jimenez, M. Paeplow, Ch. Fella, A. Balles, W. Wiest, B. Notario, S. Zabler, F. García-Moreno **Possibilities for In-Situ Imaging of Metallic and Polymeric Foams using Laboratory Liquid Metal Jet and Microfocus X-Ray Sources** **Poster**. *Metfoam 2015, Barcelona (Spain) (2015)*
B. Notario, E. Laguna-Gutiérrez, J. Pinto, M. A. Rodríguez-Pérez **Final Year Project in Physics´s Degree: a New Challenge for the Scientific and Technical Training of Students in their Last Year of the Physics' Degree** **Virtual**. *7th International Conference on Education and New Learning Technologies (EDULEARN15), Barcelona (Spain) (2015)*
E. Laguna-Gutiérrez, B. Notario, J. Pinto, M. A. Rodríguez-Pérez **Preparing Students of Scientific and Technical Degrees for their Future Professional Careers** **Virtual**. *7th International Conference on Education and New Learning Technologies (EDULEARN15), Barcelona (Spain) (2015)*

Table 0-5. Stages in other research institutions

Stages in other research institutions
Two months in the Helmholtz-Zentrum Berlin (HZB) of Berlin (Germany) in 2011 **Topic: Comparative study of polymer and metal foaming by in-sity techniques**
Three months in the Microcellular Plastics Laboratory (Mechanical Engineering Department) of the University of Washington (USA) in 2015 **Topic: Production of nanocellular PMMA by gas dissolution foaming at low saturation temperatures. Study of the thermal conductivity of microcellular polymers: PEI, PC, and ABS.**

Table 0-6. Participation to other research funded projects in the course of the 4 years

Research funded projects
Ministerio de Ciencia e Innovación (National Materials Plan). **MAT2012-34901**
Junta of Castile and Leon. **VA035U13**
Ministerio de Ciencia e Innovación (Impact Program). **IPT-2011-0725-310000**
Junta of Castile and Leon. **VA174A12-2**
Ministerio de Ciencia e Innovación (National Materials Plan). **MAT209-14001-C02-01**
FP7 European Commission. **NANCORE 214148**
European Spatial Agency. **UGFOAM 14308/00/NL/SH**
ABN PIPE SYSTEMS SLU. **PRIVATE FUNDED**
Dow Chemical. **PRIVATE FUNDED**
Tolsa S.A. **PRIVATE FUNDED**
FERRO SPAIN. **PRIVATE FUNDED**

0.6 Main Results

To conclude this introduction the main results obtained in this research work are summarized:

- The initial precursor materials for the production of nanocellular polymers are commercial, easily accessible, and well defined polymers.

- Nanocellular polymers (with relative densities around 0.5 and cell sizes in the range of 200 nm and several millimeters thick) have been obtained using processing parameters that do not use extreme conditions. For instance saturation pressures above 30 MPa and temperatures above 23 ºC have not been used.

- Microcellular and nanocellular polymers with similar densities (around 0.5) were obtained in a controlled manner, with macroscopic dimensions and appropriate geometries to conduct a proper characterization of the physical properties using standard techniques. The desired final cellular polymer (micro or nanocellular) can be obtained by adjusting the saturation pressure and the foaming conditions (temperature and time).

- New effects or non-expected behaviors have been found due to the confinement of the constituent elements of the cellular polymer in the nanometer regime such as: an increment of the glass transition temperature, a reduction of the thermal conductivity of the solid phase, an increase of the stiffness of the polymer matrix, an increase of the loss permittivity at low frequencies (MWS phenomenon), etc.

- A clear reduction of the thermal conductivity of the gaseous phase has been found in PMMA based foams for cell sizes below the micron, validating experimentally for the first time the Knudsen effect on cellular polymeric materials.

- A clear improvement in some mechanical properties at high strain rates (Charpy impact), and low strain rates (shore hardness, and Young´s modulus) has been found. On the contrary, for several specific characteristics also measured at low strain rates (the strain at break and the yield strength) the nanocellular polymers present lower properties.

- An evident transition from a capacitive to a combination of a resistive and a capacitive behavior has been detected when cell size shift from the micro to the nanoscale. A strong reduction of the dielectric constant of nanocellular PMMA as compare to the solid was found. Furthermore, it was demonstrated that the confinement effect of the polymeric macromolecules is stable in the temperature domain (from -20 ºC to 110 ºC).

- A different acoustic behavior, both in absorption and transmission, has been detected between microcellular and nanocellular polymers. Experimental differences may be explained by the different wave propagation mechanism in the micro and nanoscale, which is influenced by the confinement of both the gas and solid phases.

0.7 References

1. EU EU. Horizon 2020. Work Programme 2014-2015. 2013.
2. Gibson LJ and Ashby MF. Cellular Solids: Structure and Properties, 2nd ed. Cambridge: Cambridge University Press, 1997.
3. Klempner D, Sendijarevi'c V, and Aseeva RM. Handbook of Polymeric Foams and Foam Technology. Munich: Hanser Publishers, 2004.
4. Gibson LJ, Ashby MF, and Harley BA. Cellular Materials in Nature and Medicine. Cambridge, U.K.: Cambridge University Press, 2010.
5. Weaire D and Hutzler S. The Physics of Foams. Oxford, U.K.: Oxford University Press, 1999.
6. Davies GJ and Zhen S. Journal of Materials Science 1983;18(7):1899-1911.
7. Eaves D. Handbook of Polymer Foams: Rapra Technology, 2004.
8. Bhaduri SB. Advanced Performance Materials 1994;1(3):205-220.
9. Solórzano E and Rodriguez-Perez MA. Polymer Foams. In: Busse M, Herrmann AS, Kayvantash K, and Lehmhus D, editors. Structural Materials and Processes in Transportation. Weinheim (Germany): Wiley-VCH, 2013.
10. Papadopoulos AM. Energy and Buildings 2005;37(1):77-86.
11. Díez-Gutiérrez S, Rodriguez-Perez MA, Machimbarranea M, González J, and De Saja JA. Journal of Building and Acoustics 2003;10(3):261-271.
12. Twigg MV and Richardson JT. Chemical Engineering Research and Design 2002;80(2):183-189.
13. Ulbricht M. Polymer 2006;47(7):2217-2262.
14. Schmidt D, Raman VI, Egger C, du Fresne C, and Schädler V. Materials Science and Engineering: C 2007;27(5–8):1487-1490.
15. Pajonk GM. Journal of non-crystalline solids 1998;225:307-314.
16. Hentze HP and Antonietti M. Reviews in molecular biotechnology 2002;90(1):27-53.
17. Madou MJ. Fundamentals of Microfabrication: The Science of Miniaturization, Second Edition. Boca Raton: CRC, 2002.
18. Hillmyer MA. Nanoporous materials from block copolymer precursors. Block Copolymers II: Springer, 2005. pp. 137-181.
19. Olson DA, Chen L, and Hillmyer MA. Chemistry of materials 2007;20(3):869-890.
20. Hedrick JL, Miller RD, Hawker CJ, Carter KR, Volksen W, Yoon DY, and Trolls\aas M. Advanced Materials 1998;10(13):1049-1053.
21. Hentze HP and Antonietti M. Current Opinion in Solid State and Materials Science 2001;5(4):343-353.
22. Jackson EA and Hillmyer MA. ACS nano 2010;4(7):3548-3553.
23. Hedrick JL, Carter KR, Labadie JW, Miller RD, Volksen W, Hawker CJ, Yoon DY, Russell TP, McGrath JE, and Briber RM. Nanoporous polyimides. Progress in Polyimide Chemistry II: Springer, 1999. pp. 1-43.
24. Lazzari M and López-Quintela MA. Advanced Materials 2003;15(19):1583-1594.
25. Park C, Yoon J, and Thomas EL. Polymer 2003;44(22):6725-6760.
26. Vieth WR and Sladek KJ. Journal of Colloid Science 1965;20(9):1014-1033.
27. Crank J. The Mathematics of Diffusion. London, England: Oxford University Press, 1956.
28. Goel SK and Beckman EJ. Polymer Engineering & Science 1994;34(14):1137-1147.
29. Colton JS. Polymer Engineering & Science 1987;34(14):1137-1147.
30. Goel SK and Beckman EJ. Polymer Engineering & Science 1994;34(14):1148-1156.
31. Zhang Z and Handa YP. Journal of Polymer Science Part B: Polymer Physics 1998;36(6):977-982.
32. Dong Hwang Y and Woon Cha S. Polymer Testing 2002;21(3):269-275.

33. Alessi P, Cortesi A, Kikic I, and Vecchione F. Journal of Applied Polymer Science 2003;88(9):2189-2193.
34. Reglero Ruiz JA, Viot P, and Dumon M. Journal of Applied Polymer Science 2010;118(1):320-331.
35. Tsivintzelis I, Angelopoulou AG, and Panayiotou C. Polymer 2007;48(20):5928-5939.
36. Kumar V and Suh NP. Polymer Engineering & Science 1990;30(20):1323-1329.
37. Guo Q, Wang J, and Park CB. Industrial & Engineering Chemistry Research 2006;45(18):6153-6161.
38. Spitael P, Macosko CW, and McClurg RB. Macromolecules 2004;37(18):6874-6882.
39. Ruckdäschel H, Gutmann P, Altstädt V, Schmalz H, and Müller AHE. Foaming of microstructured and nanostructured polymer blends. Complex Macromolecular Systems I: Springer, 2010. pp. 199-252.
40. Kim Y. Study of Cell Nucleation in Nano Polymer Foams: An SCFT Approach. University of Waterloo, 2012.
41. Pinto J, Dumon M, Pedros M, Reglero JA, and Rodriguez-Perez MA. Chemical Engineering Journal 2014;243C:428-435.
42. Costeux S, Bunker SP, and Jeon HK. Journal of Materials Research 2013;28(17):2351-2365.
43. Yokoyama BH, Li L, Nemoto T, and Sugiyama K. Advanced Materials 2004;16(17):1542-1546.
44. Yokoyama H and Sugiyama K. Macromolecules 2005;38(25):10516-10522.
45. Rodriguez-Perez MA. Propiedades Térmicas y Mecánicas de Espumas de Poliolefinas. Universidad de Valladolid, 1998.
46. Almanza O. Caracterización y Modelización de las Propiedades Térmicas y Mecánicas en Espumas de Poliolefinas. Universidad de Valladolid, 2000.
47. Arcos y Rábado LO. Propiedades Térmicas y Mecánicas de Espumas de Poliolefinas Fabricadas en un Proceso de Moldeo por Compresión. Universidad de Valladolid, 2002.
48. Ruiz-Herrero JL. Impacto y Fluencia de Espumas con Base Polietileno. Universidad de Valladolid, 2004.
49. González-Peña JI. Efecto de los Tratamientos Térmicos en Bloques de Espuma de Polietileno de Baja Densidad Producidos Mediante Moldeo por Compresión. Universidad de Valladolid, 2006.
50. Álvarez-Laínez M. Propiedades Térmicas, Mecánicas y Acústicas de Espumas de Poliolefina de Celda Abierta. Universidad de Valladolid, 2007.
51. Reglero Ruiz JA. Manufacture and characterization of aluminium foams: Applications in the aeronautical sector. Universidad de Valladolid, 2007.
52. Solórzano E. Aluminium foams: Foaming process, cellular structure & properties. Universidad de Valladolid, 2008.
53. Hidalgo-González F. Diseño Optimizado de los Parámetros de Proceso de Fabricación de Espuma de Poliolefina Reticulada mediante Moldeo por Compresión. Universidad de Valladolid, 2008.
54. Román-Lorza S. Fabrication and characterization of flame retardant halogen free polyolefin based cellular materials. Universidad de Valladolid, 2010.
55. Campo-Arnáiz R. Aplicación de Técnicas Espectroscópicas al Estudio de la Morfología Polimérica, Propiedades Térmicas y de Emisión de Espumas de Baja Densidad con Base Poliolefina. Universidad de Valladolid, 2011.
56. Saiz-Arroyo C. Fabricación de materiales celulares mejorados basados en poliolefinas. Relación procesado-composición-estructura-propiedades. Universidad de Valladolid, 2012.
57. Lobos Martín J. Improving the stiffness and strength of porous materials by enhancement of the matrix microstructure and cellular morphology. Universidad de Valladolid, 2013.

58. Pinto J. Fabrication and characeterization of nanocellular polymeric materials from nanostructured polymers. University of Valladolid & University of Bordeaux, 2014.
59. Pardo-Alonso S. X-Ray Imaging Applied to the Characterization of Polymer Foams' Cellular Structure and Its Evolution. University of Valladolid, 2014.
60. Estravis S. CELLULAR NANOCOMPOSITES BASED ON RIGID POLYURETHANE AND NANOCLAYS: FABRICATION, CHARACTERIZATION AND MODELING OF THE MECHANICAL AND THERMAL PROPERTIES. University of Valladolid, 2014.
61. Oliveira-Salmazo L. CINÉTICAS DE ESPUMACIÓN Y CONTROL DE LA ESTRUCTURA CELULAR EN MATERIALES BASADOS EN CAUCHO NATURAL Y POLIOLEFINAS University of Valladolid & Universidad Estadual Paulista "Julio de Mesquita Filho", 2015.
62. Lázaro J. Optimización de la Estructura Celular en Espumas de Aluminio. University of Valladolid, 2014.
63. Velasco JI, Martínez AB, Arencón D, Pérez MAR, and Saja JAD. Journal of materials science 1999;34(3):431-438.
64. Rodriguez-Perez MA, Ruiz-Herrero JL, Solorzano E, and De Saja JA. Cellular polymers 2006;25(4):221-236.
65. Rodríguez-Pérez MA, Duijsens A, and De Saja JA. Journal of Applied Polymer Science 1998;68(8):1237-1244.
66. Rodríguez-Pérez MA, Díez-Gutiérrez S, and De Saja JA. Polymer Engineering & Science 1998;38(5):831-837.
67. Rodriguez-Perez MA and De Saja JA. Cellular polymers 1999;18(1):1-20.
68. Rodríguez-Pérez MA, Campo-Arnáiz RA, Aroca RF, and de Saja JA. Polymer 2005;46(26):12093-12102.
69. Rodriguez-Perez MA, Álvarez-Láinez M, and de Saja JA. Journal of Applied Polymer Science 2009;114(2):1176-1186.
70. Rodríguez-Pérez MA, Alonso O, Souto J, and de Saja JA. Polymer Testing 1997;16(3):287-298.
71. Rodriguez-Perez MA, Almanza O, Ruiz-Herrero JL, and De Saja JA. Cellular polymers 2008;27(3):179-200.
72. Rodríguez-Pérez MA, Almanza O, and De Saja JA. Journal of Applied Polymer Science 1999;73(14):2825-2835.
73. Mills NJ and Rodriguez-Perez MA. Cellular polymers 2001;20(2):79-100.
74. Alvarez-Lainez M, Rodriguez-Perez MA, and De Saja JA. Journal of Polymer Science Part B: Polymer Physics 2008;46(2):212-221.
75. Almanza O, Rodrıguez-Pérez MA, and De Saja JA. Polymer 2001;42(16):7117-7126.
76. Almanza O, Rodríguez-Pérez MA, Chernev B, de Saja JA, and Zipper P. European Polymer Journal 2005;41(3):599-609.
77. Almanza O, Arcos y Rábago LO, Rodíguez-Pérez MA, González A, and de Saja JA. Journal of Macromolecular Science, Part B 2001;40(3-4):603-613.
78. Rodriguez-Perez MA, Lobos J, Perez-Muñoz CA, and Saja JAd. Journal of Cellular Plastics 2009;45(5):389-403.
79. Reglero Ruiz JA, Saiz-Arroyo C, Dumon M, Rodríguez-Perez MA, and Gonzalez L. Polymer international 2011;60(1):146-152.
80. Pinto J, Reglero-Ruiz JA, Dumon M, and Rodriguez-Perez MA. The Journal of Supercritical Fluids 2014;94:198-205.
81. Pinto J, Dumon M, Rodriguez-Perez MA, Garcia R, and Dietz C. The Journal of Physical Chemistry C 2014;118(9):4656-4663.
82. Verdejo R, Saiz-Arroyo C, Carretero-Gonzalez J, Barroso-Bujans F, Rodriguez-Perez MA, and Lopez-Manchado MA. European Polymer Journal 2008;44(9):2790-2797.
83. Velasco JI, Antunes M, Ayyad O, Saiz-Arroyo C, Rodríguez-Pérez MA, Hidalgo F, and de Saja JA. Journal of Applied Polymer Science 2007;105(3):1658-1667.

84. Román-Lorza S, Rodriguez-Perez MA, Sáez JADS, and Zurro J. Journal of Cellular Plastics 2010;46(3):259-279.
85. Ma Y, Pyrz R, Rodriguez-Perez MA, Escudero J, Rauhe JC, and Su X. Cellular polymers 2011;30(3):95-109.
86. Wang Y, Rodriguez-Perez MA, Reis RL, and Mano JF. Macromolecular Materials and Engineering 2005;290(8):792-801.
87. Simoes RD, Rodriguez-Perez MA, De Saja JA, and Constantino CJL. Polymer Engineering & Science 2009;49(11):2150-2157.
88. Rodriguez-Perez MA, Simoes RD, Roman-Lorza S, Alvarez-Lainez M, Montoya-Mesa C, Constantino CJL, and de Saja JA. Polymer Engineering & Science 2012;52(1):62-70.
89. Solórzano E, Rodríguez-Perez MA, Reglero JA, and de Saja JA. Advanced Engineering Materials 2007;9(11):955-958.
90. Solórzano E, Rodriguez-Perez MA, and de Saja JA. Advanced Engineering Materials 2008;10(4):371-377.
91. Lázaro J, Solórzano E, Saja JAd, and Rodríguez-Pérez MA. Journal of materials science 2013;48(14):5036-5046.
92. Garcia-Moreno F, Solórzano E, and Banhart J. Soft Matter 2011;7(19):9216-9223.
93. Solórzano E, Pinto J, Pardo S, Garcia-Moreno F, and Rodriguez-Perez MA. Polymer Testing 2013;32(2):321-329.
94. Solórzano E, Pardo-Alonso S, Saja JAd, and Rodriguez-Perez MA. Colloids and Surfaces A: Physicochemical and Engineering Aspects 2013;438:167-173.
95. Solórzano E, Antunes M, Saiz-Arroyo C, Rodríguez-Pérez MA, Velasco JI, and de Saja JA. Journal of Applied Polymer Science 2012;125(2):1059-1067.
96. Pardo-Alonso S, Solórzano E, Brabant L, Vanderniepen P, Dierick M, Van Hoorebeke L, and Rodríguez-Pérez MA. European Polymer Journal 2013;49(5):999-1006.
97. Lu X, Caps R, Fricke J, Alviso CT, and Pekala RW. Journal of non-crystalline solids 1995;188(3):226-234.
98. Weller E and Kumar V. Handbook of Polymeric Foams. UK: Rapra Technology, 2004.

MATERIALS AND FOAMS PRODUCTION

Belén Notario Collado

Chapter I. Materials and Foams Production

In this chapter the characteristics of the polymers employed, the production routes used, and the characterization techniques employed are presented.

First, the main characteristics of PMMA and MAM, and the features of PMMA/ MAM blends are described.

Secondly, the production route of microcellular and nanocellular PMMA cellular polymers is explained. These cellular polymers were produced by gas dissolution foaming at different saturation pressures. This chapter includes a selection of SEM micrographs of the PMMA cellular structures, analyzing general aspects of the cellular structure such as the cell size and the homogeneity of the cellular structure. Furthermore, representative SEM micrographs of PMMA/MAM cellular polymers have been also included.

Finally, the different experimental techniques used to characterize the cellular structure of the cellular polymers and the properties of foamed and solid samples are summarized. Each publication describes the specific experimental procedures employed, however, in this chapter a brief explanation is provided to have a general view of the characterizing methods used. In particular, the experimental methods that are not conventional have been described in more detail.

I.1 Materials

This research was carried out using PMMA and MAM as raw materials, both polymers are optically transparent, and were kindly supplied by Arkema Company (France) in the form of pellets.

I.1.1 Poly(methyl methacrylate) (PMMA)

PMMA is an amorphous polymer, whose chemical formula is shown in Figure I.1.

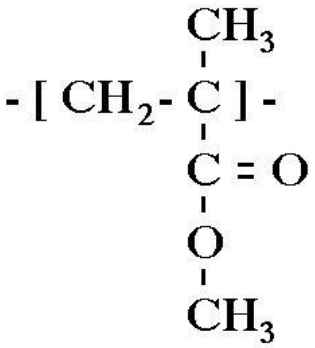

Figure I.1. Chemical formula of PMMA

The particular PMMA used in our study (Plexiglas® V825 from Arkema Company (France)) is a pure homopolymer (without impact modifier), with a density (ρ) of 1.18 g/cm^3, glass transition temperature (T_g) about 112° C, melt flow rate (at 230 ºC/3.8 kg) of 3.7 g/10 min, and the

following characteristics $M_w \approx 83000$ g/mol, $M_n \approx 43000$ g/mol, $I_p \approx 1.9$ (where M_w is the weight average molecular weight, M_n is the number average molecular weight, and $I_p = M_w/M_n$ is the polydispersity index. Molar mass values are related to polystyrene standards).

I.1.2 Poly(methyl methacrylate)/ Poly(methyl methacrylate)-co-poly(butyl acrylate)-co-poly(methyl methacrylate) (MAM) blends

MAM copolymers are a family of "ABA" block copolymers synthesized by controlled radical polymerization with a DEPN (N-tert-butyl-N-(1-diethylphosphono-2,2-dimethylpropyl) nitroxide) [1, 2]. They have a rather high dispersity index (I_p around 1.9 to 2.2), and average molar masses $65000 \leq M_n \leq 90000$ g/mol. Depending upon the "grade", the number average molar mass M_n of the middle Poly(Butyl Acrylate) (PBA) block is ranging from 20000 to 27000 g/mol with a low dispersity $I_p \leq 1.2$. Chemical formula of PBA homopolymer is shown in Figure I.2. T_g of PBA homopolymer is around -45° C.

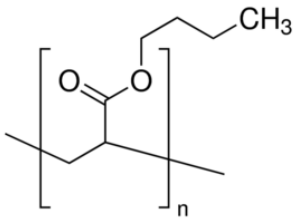

Figure I.2. Chemical formula of PBA

The particular MAM in our study, 36 wt.% PBA, has the following characteristics: ρ = 1.08 g/cm^3, $M_w^{MAM} \approx 180000$ g/mol, $M_n^{MAM} \approx 85000$ g/mol, thus $I_p^{MAM} \approx 2$, and $M_n^{PMMAblock} \approx 27000$ g/mol (molar mass values are related to polystyrene standards).

I.1.3 Production of PMMA/MAM Blends

Blends of PMMA/MAM with different MAM amounts (from 5 to 75 wt.%) were produced by extrusion using a Scamex CE02 single screw extruder (IUT Bordeaux 1, France). The extruder had a diameter of 45 mm and a length/diameter ratio (*L/D*) of 28.

Both materials, PMMA and MAM, were dried in vacuum (680 mm Hg) at 80° C during 4 h prior to the extrusion. Then, they were introduced in the extruder at the appropriate proportions, and processed with a temperature profile from 165 to 225° C and a screw speed of 60 rpm. Pellets from each blend were obtained using a continuous cutting machine operating at the end of the extrusion line.

PMMA/MAM blends generated following this procedure were transparent and macroscopically homogeneous.

Main characteristics (density and glass transition temperature) of these PMMA/MAM blends are shown in Table I-1. It should be noticed that in our DSC experiments, carried out with a DSC 862 (Mettler) at 10° C/min and N_2 flow of 60 ml/min, temperature range was from 20 to

160° C; and therefore the T_g of the PBA (around -45° C) was not detected. Thus only the T_g (midpoint) of the PMMA phase (that includes the homopolymer PMMA and the part of PMMA phase in the copolymer) was measured.

Table I-1. Density and glass transition temperature (T_g) of the pellets of PMMA/MAM blends.

PMMA/MAM wt.%	Density / g/cm^3	T_g / ° C
95/5	1.18	115
90/10	1.17	115
50/50	1.16	108
25/75	1.14	104

I.1.4 Solid Samples Production Route

Solid samples of neat PMMA and PMMA/MAM blends were produced by compression molding (PMMA) or by injection molding (PMMA/MAM blends) (Figure I.3). In both cases, pellets, both of the raw materials and blends, were first dried in the same conditions as those used before the extrusion process.

In the case of injection molded samples (PMMA/MAM blends), dried pellets were injected into bulk pieces (50 x 15 x 3 mm^3) using a small scale injection molding machine (DSM Xplore). Process parameters were set at 240° C for the melt temperature, 60° C for the mold temperature, and 1 MPa for the injection pressure during 8 seconds.

With respect to compression molded samples (PMMA samples); dried pellets were molded into precursors of 155 mm x 75 mm and 4 mm in thickness using a two-hot plates press. The temperature of the press was fixed at 250 ºC. The material was first molten without pressure for 9 minutes, then it was compacted under a constant pressure of 2.18 MPa for another minute and finally it was cooled down under the same pressure. Then, these molded precursors were cut at the desired dimensions (depending on the test to be performed).

Pieces obtained (following one process or another) were optically transparent, both for raw materials and blends, and with no presence of air bubbles inside the parts (Figure I.3).

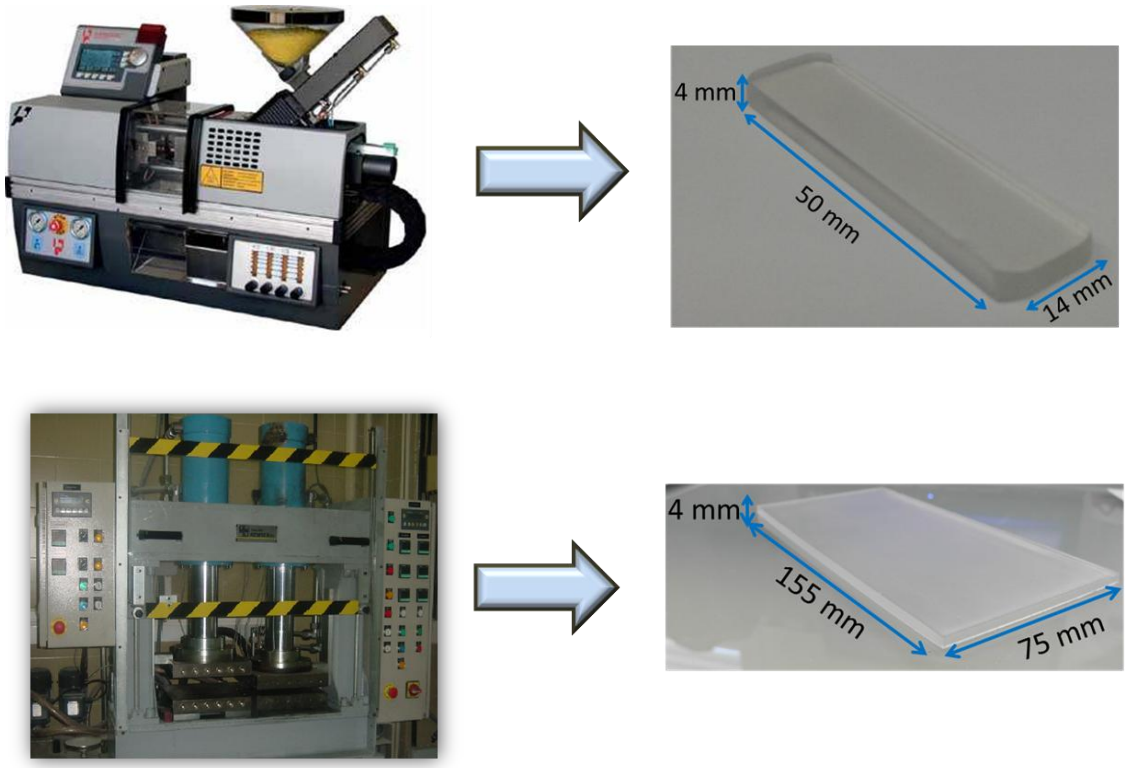

Figure I.3.Top: Injection molding machine together with an injection molded sample of a PMMA /MAM (95/5) blend. Bottom: Two-hot plates press along with a compression molded sample of neat PMMA.

I.2 Foams Production Route

Cellular polymers from neat PMMA and PMMA/MAM blends with different MAM amounts (from 5 to 75 wt.%) were produced by gas dissolution foaming using CO_2 as physical blowing agent.

PMMA/MAM cellular polymers were manufactured in a previous study in collaboration with the University of Bordeaux [3], and characterized in detail in this work; whereas neat PMMA cellular polymers have been produced and characterized entirely in this thesis.

To produce the PMMA cellular polymers, a high pressure vessel provided by Parr Instrument Company (model PARR 4681), with a capacity of 1 liter, and capable of operating at a maximum temperature of 350° C and a maximum pressure of 41 MPa (Figure I.4) was employed. The reactor is equipped with an accurate pressure pump controller (model SFT-10) provided by Supercritical Fluid Technologies Inc., and it is controlled automatically to keep the pressure at the desired values (Figure I.4). The vessel is equipped with a clamp heater of 1200 watts, and its temperature is controlled via a CAL 3300 temperature controller. The temperature and pressure were monitored in the course of the process. This vessel was used to produce both microcellular and nanocellular neat PMMA cellular polymers. The production route employed to obtain them is detailed below.

Figure I.4. Parr Instrument Company high pressure vessel (left) and Supercritical Fluid Technologies pressure pump (right).

I.2.1 Microcellular and Nanocellular PMMA Foams Production Route

Prior to this thesis, it was observed that cell size of PMMA presents a strong dependence with saturation pressure (Figure I.5). In fact, it was possible to obtain both micro and nanocellular polymers using the same raw material [4]. However, the final density of the foams was also related to the cell size and/ or to the saturation pressure (Figure I.5), and therefore microcellular and nanocellular polymers with comparable densities were not obtained.

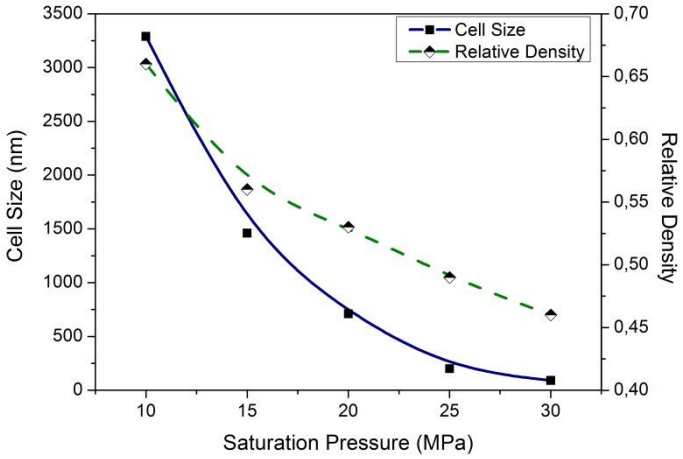

Figure I.5. Variation of the cell size and relative density with the saturation pressure for neat PMMA [4].

According to these results, in this investigation it was decided to work at room temperature during the saturation stage and used four different pressures to obtain two different sets of microcellular polymers (using 13 and 15 MPa as saturation pressures) and two different sets of nanocellular ones (using 31 and 32 MPa). All samples were saturated during 20 h to assure equilibrium dissolution of CO_2 in the polymer. After the saturation process, the pressure inside the vessel was released. During the desorption step, the samples temperature decrease to values clearly below room temperature (adiabatic depressurization), so when samples are removed from the pressure vessel they are cooled and solid [5]. Unlike previous studies, a step of controlled foaming is introduced in order to control the final density of the samples (see

Figure I.6 in which the controlled foaming step is represented by green arrows). The introduction of this controlled step allows achieving the desired density for the foams (Figure I.6. The density of the cellular polymers without the foaming step (represented by black squares) is reduced up to the desired values (orange squares) after the foaming process). Foaming of the samples was carried out in a thermostatic water bath at temperatures between 25 and 60 ºC and times between 40 seconds and 5 minutes (Table I-2). Low temperatures were used to produce the cellular polymers saturated at high pressures and high temperatures were used to produce the cellular polymers saturated at low pressure. The elapsed time between the pressure release and introduce the sample in the water bath (desorption time) was of three and 30 seconds, remaining the samples cooled and in a solid state during this time. It should be noticed that the temperatures used in the foaming step were lower than the glass transition temperature of PMMA (section *I.1.1 Poly(methyl methacrylate) (PMMA)*), because of the low values of the effective glass transition temperature of PMMA plasticized with CO_2 [6, 7].

As it can be observed in Figure I.6, nanocellular polymers without foaming showed a density value close to the density of microcellular polymers with controlled foaming. But these nanocellular polymers present a thicker solid skin that makes difficult to obtain homogeneous samples with appropriate dimensions for their characterization. For this reason, a controlled foaming step was also applied to nanocellular samples obtaining specimens more appropriate for their characterization.

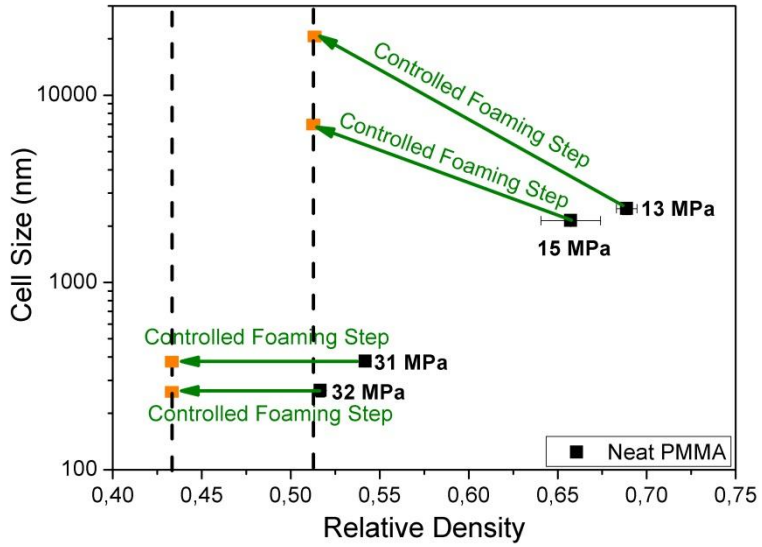

Figure I.6. Variation of the relative density and cell size of the cellular polymers with or without the introduction of the controlled foaming step. Black squares represent the density of the cellular polymers without the foaming step, whereas the orange squares represent the final density of the cellular materials achieved after carrying out the controlled foaming step.

Table I-2. Foaming parameters together with the final relative density achieved of the cellular polymers after performing the controlled foaming step

Name	Saturation Pressure (MPa)	Foaming Temperature (° C)	Foaming Time (s)	Relative Density
PMMA solid	-	-	-	1
Micro 1 PMMA foam	13	60	40	0.52
Micro 2 PMMA foam	15	60	45	0.49
Nano 1 PMMA foam	31	25	300	0.43
Nano 2 PMMA foam	32	25	300	0.42

Then by controlling the saturation pressure and the foaming temperature it is possible to obtain samples with comparable densities in the microcellular and nanocellular range (Table I-2). As a result, differences between density values of micro and nanocellular polymers are significantly reduced, obtaining in all cases cellular polymers in a range of relative densities between 0.4 and 0.5. This fact has allowed us to perform an accurate comparative study of the transition of the physical properties from the micrometer to the nanometer scale at almost constant relative density.

Prior to the study of the physical properties, removing of the solid dense skin as well as a detail characterization of the cellular structure of the samples produced following this route was carried out.

A main characteristic of the cellular materials produced by solid state foaming is the presence of a foamed core and an outer solid skin (Figure I.7). This structure appears due to the changes in the gas concentration profile inside the polymer sample during the desorption step, and the existence of a minimum gas concentration needed to trigger the homogeneous cell nucleation [ref. 12 Pinto]. In our study, the average thickness of this skin was study by means of X-ray radiography (section *I.3.2 X- Ray Radiography*) and varied from 0.4 mm in the case of microcellular PMMA up to 0.1 mm in the case of nanocellular PMMA. With the aim of obtaining homogeneous samples and of avoiding an influence of the solid skin in the study of the physical properties, dense skin of PMMA foamed samples were polished using a polishing machine (model LaboPO12-LaboForce3, Struers) equipped with a silicon carbide grinding paper (P 180). After polishing, samples had an average thickness of around 5 mm.

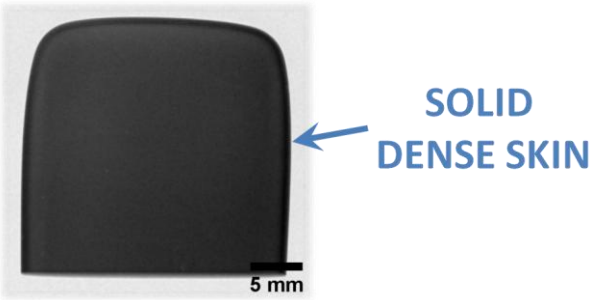

Figure I.7. Radioscopy image of a PMMA sample used in the study of the thermal conductivity (*Chapter III*). The arrow points to the darker area of the X-ray image, which corresponds to the solid dense skin produced as a consequence of the solid state foaming process.

The average cell size in the different planes of the sample as well as the homogeneity and other important parameters of the cellular structure (cell nucleation density, anisotropy ratio, asymmetry coefficient, and standard deviation) were analyzed (see *Chapter IV, Section "Towards a New Generation of Polymeric Foams: PMMA Nanocellular Foams with Enhanced Physical Properties"*). In this section a scheme of the planes of the samples studied (Figure I.8) and representative SEM micrographs of the microcellular and nanocellular polymers are shown; providing an overview of the different structures obtained. Figure I.9 shows the SEM images in the *ZY* plane whereas Figure I.10 illustrates the SEM micrographs in the *ZX* plane.

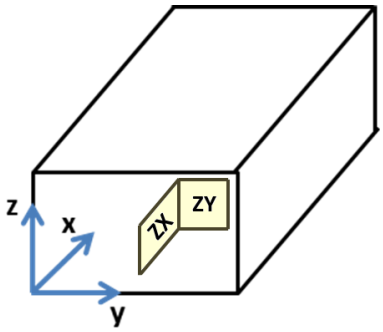

Figure I.8. Scheme of the planes analyzed in the cellular structure, where Z is the compression molding direction during the production of the solid precursors and also the thickness direction of the cellular polymers

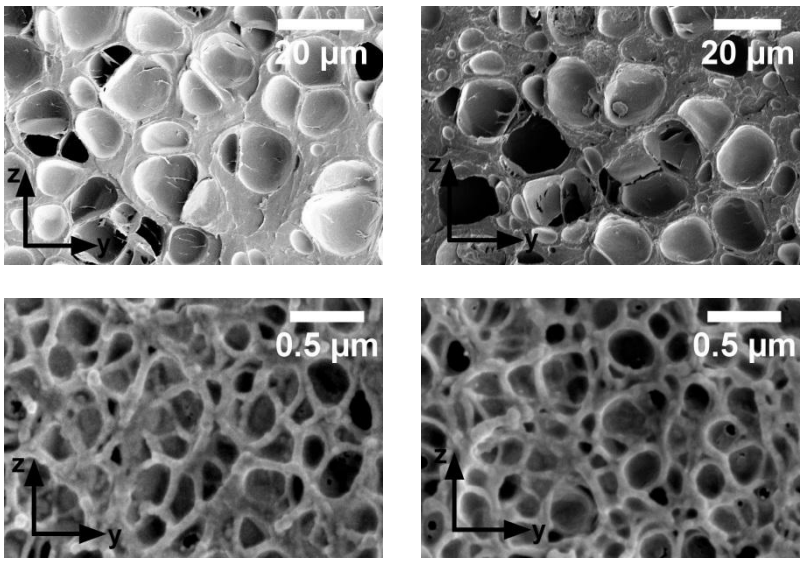

Figure I.9. SEM micrographs of the cellular structure of a) Micro 1 PMMA foam (top left), b) Micro 2 PMMA foam (top right), c) Nano 1 PMMA foam (bottom left), and d) Nano 2 PMMA foam (bottom right) in the *ZY* plane.

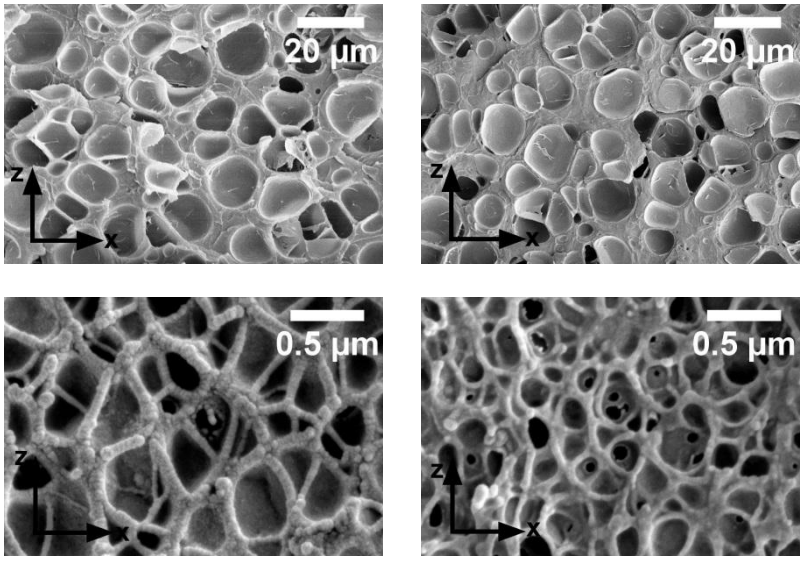

Figure I.10. SEM micrographs of the cellular structure of a) Micro 1 PMMA foam (top left), b) Micro 2 PMMA foam (top right), c) Nano 1 PMMA foam (bottom left), and d) Nano 2 PMMA foam (bottom right) in the *ZX* plane.

As it can be observed there are clearly two groups of cellular polymers: microcellular (top micrographs of both Figure I.9 and Figure I.10) and nanocellular (bottom micrographs of both Figure I.9 and Figure I.10) PMMA foams. All of them present closed cell morphologies, homogeneous cell size distributions, and a reduction of the cell size (Table I-3) when the saturation pressure is increased (i.e. Micro 2 with respect to Micro 1, and Nano 2 with respect to Nano 1). These parameters will be studied in more detail in *Chapter IV* as it was mentioned before.

Table I-3. Cell size results for the microcellular (denoted as Micro 1 and Micro 2) and nanocellular (denoted as Nano 1 and Nano 2) PMMA cellular polymers

Name	Plane	Cell Size (nm)	Relative Density	Saturation Pressure (MPa)
Micro 1	ZY	11880	0.52	13
Micro 1	ZX	11330		
Micro 2	ZY	7190	0.49	15
Micro 2	ZX	7540		
Nano 1	ZY	300	0.43	31
Nano 1	ZX	360		
Nano 2	ZY	210	0.42	32
Nano 2	ZX	205		

PMMA cellular polymers produced following this route were used to characterize the possible transition between microcellular and nanocellular polymers in the mechanical (*Chapter IV*) and acoustic (*Chapter VI*) properties.

I.2.2 PMMA/MAM Foams

As it was mentioned in section "*I.2 Foams Production Route*", PMMA/MAM foams were produced previously [8] in collaboration with the University of Bordeaux and used in this work to characterize some of their physical properties.

These samples were saturated at different pressures (from 20 to 30 MPa), and at different temperatures (from 0 to 70º C) during 24 h to assure the complete dissolution of CO_2 in the polymer.

In this section, some representative SEM micrographs of the samples analyzed are shown to show of the different structures obtained. Figure I.11 shows a scheme of the planes analyzed, whereas Figure I.12 illustrates some representative SEM micrographs of the different PMMA/MAM blends employed in this work (left: SEM images of the V plane; right: SEM images of the H plane).

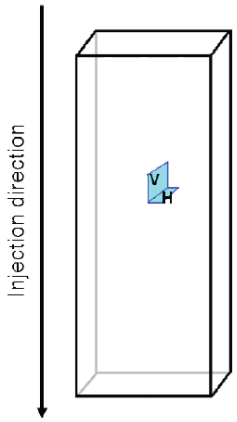

Figure I.11. Location and nomenclature of SEM samples taken from foamed samples. The injection direction used during the production of the solid precursors is showed.

PMMA/MAM (95/5)

V Plane *H Plane*

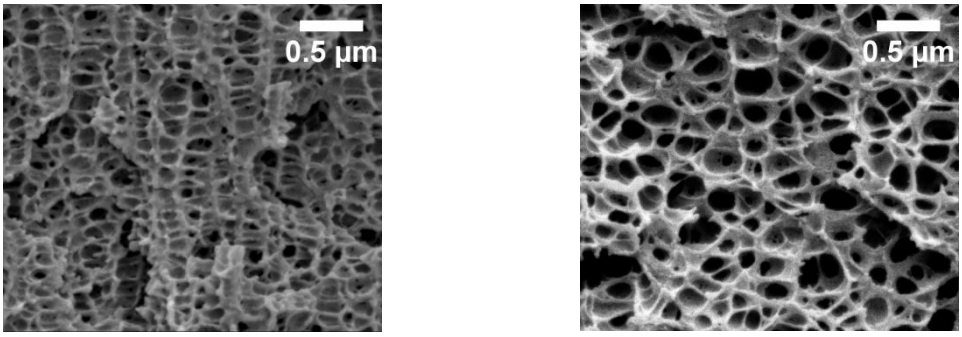

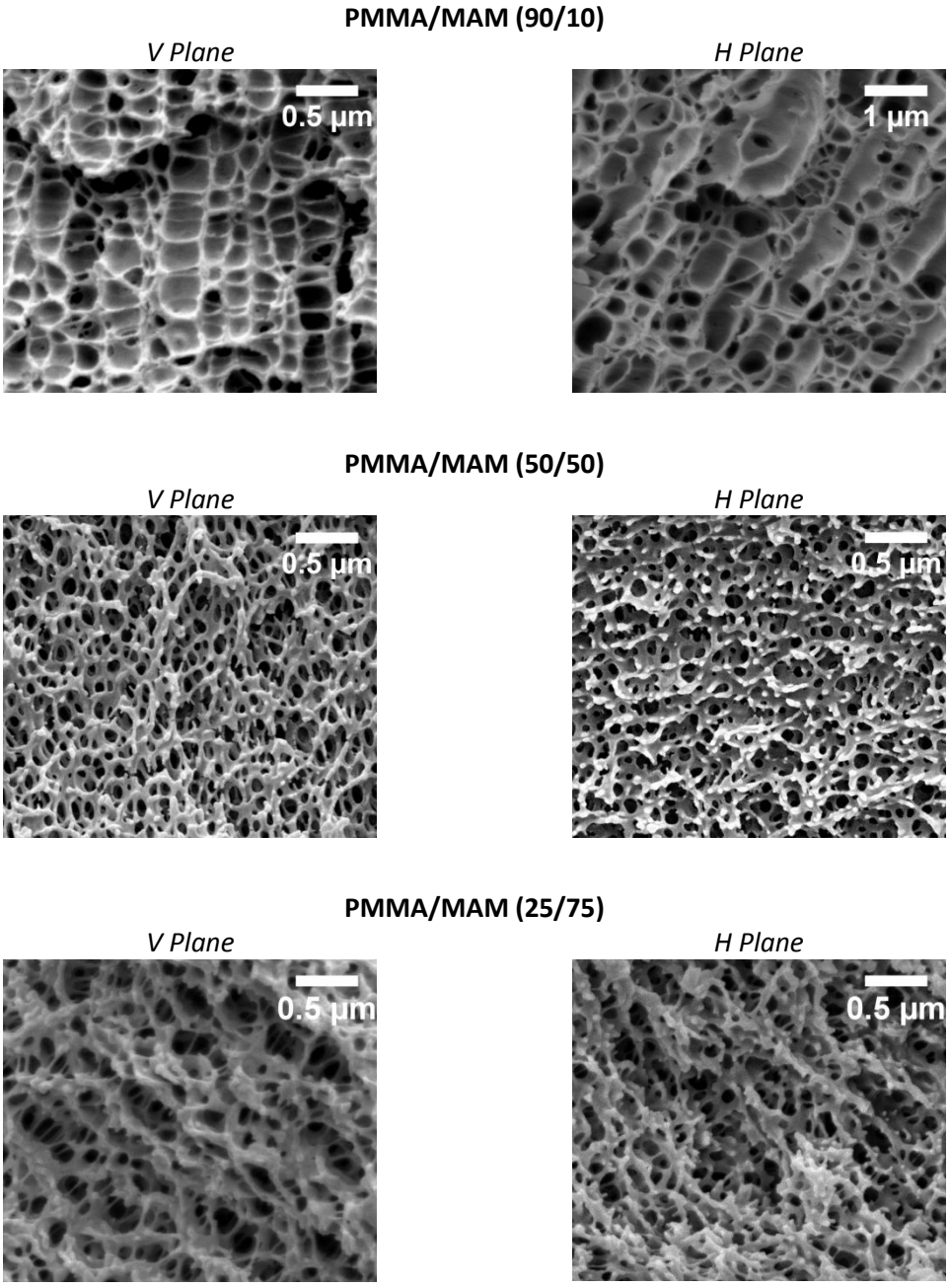

Figure I.12. SEM micrographs of the cellular structure of the PMMA/MAM cellular polymers used in this work. Left) SEM images belonging to the V plane. Right) SEM images belonging to the H plane. All these cellular materials were foamed at room temperature and at different saturation pressures: 95/5: 30 MPa; 90/10: 30 MPa; 50/50: 20 MPa; and 25/75: 30 MPa

As it can be observed, the higher the MAM amount, the higher the open cell content is [9]. It was found that in general the cellular structure of the selected PMMA/MAM blends present good homogeneity and in general negligible anisotropy, with the exception of 90/10 PMMA/MAM cellular polymers which exhibited an anisotropic cellular structure. A more detailed characterization of these cellular structures can be found elsewhere [8] and in *Chapters III* and *V* of this thesis.

These PMMA/MAM cellular polymers will be employed to analyze the existence of possible confinement effects due to the reduction of the cell size to the nanometer range (*Chapter II*), and the transition between microcellular and nanocellular polymers in the thermal conductivity (*Chapter III*) as well as in the dielectric behavior (*Chapter V*).

I.3 Experimental Techniques

Several standard and well-known experimental techniques were used to characterize the cellular structure of the foams and the properties of foamed and solid samples. Table I-4 lists them in order to provide a general view of the characterizing methods used as well as the purpose of each one. Although each publication describes them later, in this chapter further explanations about experimental techniques that have not been conventionally used to characterize this type of materials (DC electrical resistivity, X-ray radiography, and thermal conductivity under vacuum conditions) are provided.

Table I-4. Experimental techniques employed in this work, purpose of their use, and chapter in which they are used.

Experimental technique	Purpose	Chapter
Archimedes densimetry	Obtain the foam density	II-III-IV-V-VI
Scanning electron microscopy (SEM)	Analyze the cellular structure	II-III-IV-V-VI
Cell structure characterization assisted by software (image analysis)	Characterize the average cell size, cell size distribution, cell nucleation density (N_0), and anisotropy ratio of the samples manufactured	II-III-IV-V-VI
Differential scanning calorimetry (DSC)	Detect variations in the glass transition temperature	II
CO_2 uptake gravimetric measurement	Measure the differences of CO_2 uptake as a function of saturation pressure	II
Raman spectroscopy	Detect variations in the Raman spectra between nanocellular and microcellular polymers due to the confinement of the polymer macromolecules	II
DC electrical resistivity	Measure differences in the DC electrical response between microcellular and nanocellular polymers	II & V
Broadband dielectric spectroscopy (BDS)	Measure differences in the dielectric behavior between microcellular and nanocellular polymers	II & V

X-ray radiography	Exclude of the characterizations those samples presenting internal defects or inhomogeneities	III-IV-VI
Thermal conductivity: Transient plane source (TPS)	Measuring the thermal conductivity and analyzing the contribution of the gaseous and solid phase	III
Dynamic mechanical analysis (DMA) (Bending test)	Analyze the viscoelastic behavior of foamed samples	IV
Universal testing machine Instron (Tensile test)	Characterize the mechanical behavior at low strain rates of both solid and microcellular and nanocellular polymers	IV
Charpy impact testing	Characterize the mechanical response at high strain rates of both solid and foamed samples	IV
Shore hardness D	Analyze the difference in the shore hardness of micro and nanocellular polymers	IV
Impedance tube	Characterize the acoustic behavior of microcellular and nanocellular foamed samples	VI

I.3.1 DC Electrical Resistivity

Resistivity measurements of solid and microcellular and nanocellular polymers were determined by means of a Keithley Resistivity Adapter model 6105. The DC is a standard technique for electrical properties characterization [10].

I.3.1.1 Introduction to the DC Electrical Resistivity

The basic principle of the DC electrical resistivity is that when a voltage is applied across a polymeric material, the current that flows through it depends upon the number of electrons that crosses the cross-section per unit time. This number of electrons crossing the cross-section is a function of the free electrons available in the polymer. However, for heterogeneous materials such as cellular materials, the current through the material not only depends on the number of free electrons in it, but also depends on the length of the path that an electron has to travel to reach from the lower potential end to the higher potential end of the material (i.e. depends on the tortuosity of the path. The higher the tortuosity of the path, the higher the length of the path is, and therefore the difficult to reach the higher potential end rises).

Then, as the measurement of the DC electrical resistivity provides information on the resistivity of the material, it would be possible to establish qualitative relations between the measured resistivity and the tortuosity of the cellular structure.

I.3.1.2 Experimental Procedure

The CellMat DC device is composed by the DC electrodes, a voltage source (power supply), an ammeter, and a multimeter (Figure I.13).

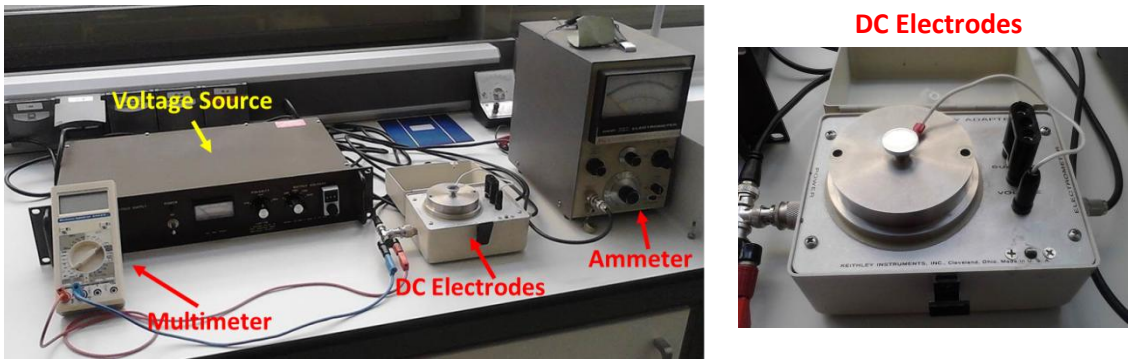

Figure I.13. Experimental set-up to perform DC electrical measurements (left). Detail of the DC electrodes (right)

Samples preparation and measurements were carried out following the next steps:

1º Samples were polished using a polishing machine (mod. LaboPol2-LaboForce3, Struers) equipped with a silicon carbide grinding paper (P 180) to assure an appropriate contact with the electrode faces and to remove the outer solid or densified skin (if any). After polishing, samples had an average thickness of about 5 mm.

2º Solid and polished foamed samples were machined using a precision cutting machine (Mod. 1000 from IsoMet). The test pieces were prepared to be approximately 10 x 10 mm^2 and 1 mm in thickness.

3º Samples were dried during 4 h at 50º C.

4º Samples were stored at controlled temperature and humidity (23º C and 50 % humidity) during at least 3 days before the measurements.

5º Samples were measured 4 times at +500 V, -500 V, +500 V, and -500 V. Time of electrification was 60 seconds, and the time of discharge before making a measurement with reversed voltage was 4 minutes.

6º Resistivity (*R*, ohms·cm) of foamed and solid samples was calculated using the following expression:

$$R = \frac{A \times V}{t \times I} \quad \text{(I-1)}$$

Where *A* and *t* are the area and thickness of the sample respectively, *V* the voltage applied, and *I* the current intensity measured.

I.3.2 X-Ray Radiography

Study of the presence of structural defects or inhomogeneities on polymeric cellular materials can provide valuable information about the reduction of the expected properties of these materials (e.g. structural defects can reduce the mechanical properties of a cellular material providing starting points for a mechanical failure).

The presence of these internal defects or density inhomogeneities is usually studied by destructive methods. Internal defects can be detected by cutting the sample to reveal the internal structure, and the homogeneity of the sample is studied by measuring the density of several samples extracted from different areas of the studied foam.

An alternative to these destructive methods is the X-ray radiography technique (or X-ray radioscopy technique if the study also has time resolution). This technique allows studying the internal structure and density distribution of the samples preserving their integrity. Application of this non-destructive technique to the study of microcellular and nanocellular materials has been widely employ throughout this thesis. Figure I.14 shows examples of how this technique is able to detect defects in the produced samples. Only those samples that were free from defects or inhomogeneities visible through X-rays (pixel size = 50 µm) were selected for further studies.

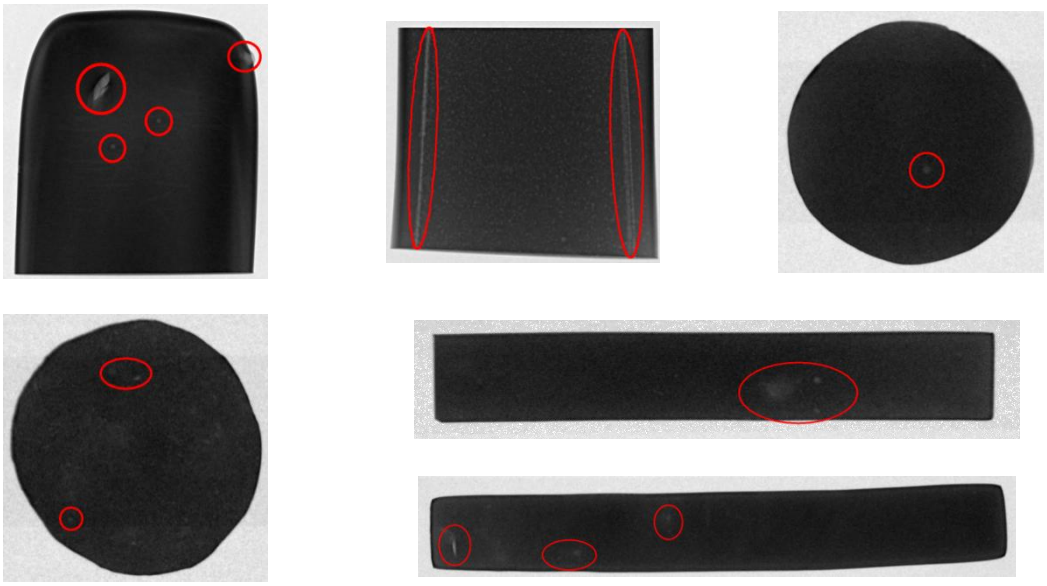

Figure I.14. X-ray radiographs of some of the produced foams. Detection of internal defects (identified with red circles) on polymeric foams by X-ray radiography

Basic fundamentals of this technique and a description of the experimental device used on this research are summarized in the following subsections.

I.3.2.1 X-Ray Imaging Fundamentals

The typical energy of X-rays photons ranges from 100 eV up to 20 MeV (i.e. from 10^{-8} to 10^{-12} m) (see Figure I.15). Therefore this penetrating radiation seems to be appropriate for obtaining structural information of matter since the distance between atoms is 10^{-10} m approximately. The penetration power of X-rays is rather high and thus it allows for transmission imaging. However, for imaging purposes the useful energies are 5 – 150 KeV. Too soft X-rays do not penetrate deeply enough and too hard X-rays simply are not absorbed leading to poor contrast.

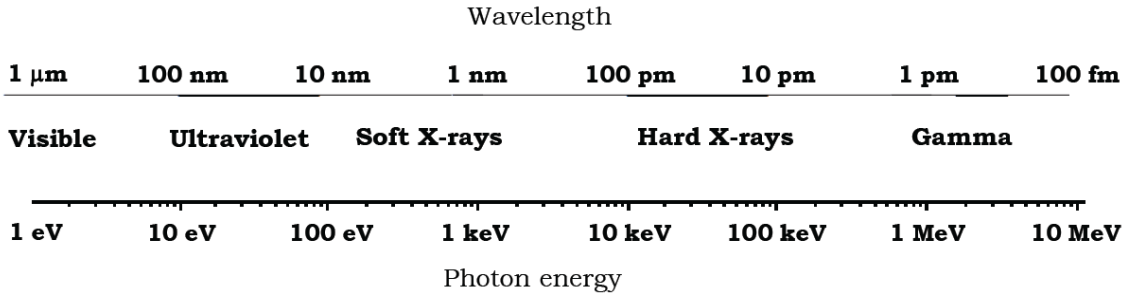

Figure I.15. Electromagnetic spectrum of energies and wavelengths

I.3.2.2 Matter Beam Interaction

X-rays interact with matter in a number of different ways that can be used for imaging: electron photoemission, elastic and inelastic scattering fluorescence, etc. (see Figure I.16). Hence, X-ray detection techniques can be classified based on the particle-matter interaction that is used to form the image. Conventional X-ray imaging relies on transmission measurement that is determined by object beam absorption. Photoelectric absorption and inelastic scattering are mainly contributing to absorption. Elastic scattering is also contributing to absorption although it is more related to macroscopic refraction effect.

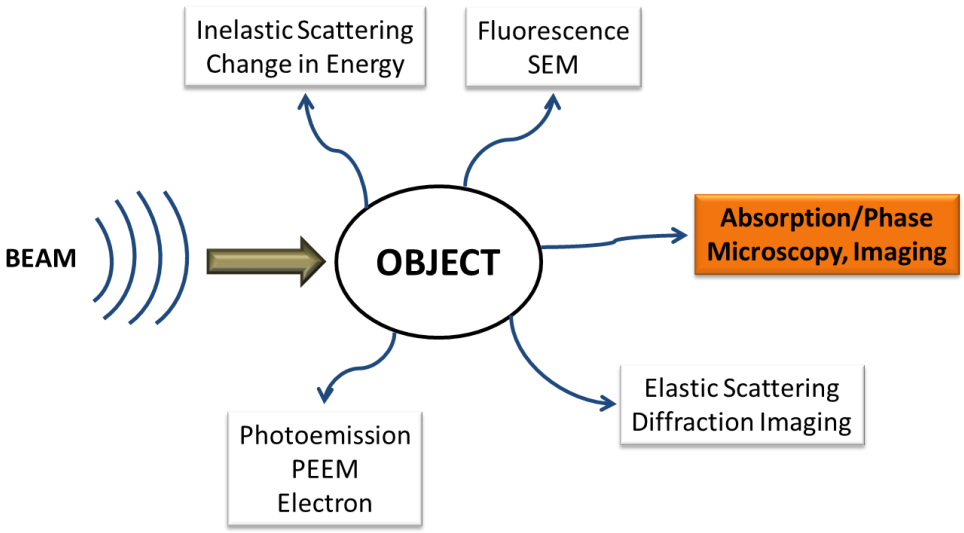

Figure I.16. X-ray and matter interaction producing elastic and inelastic phenomena as a result

The physical fundamentals of radiation absorption are based on the Beer-Lambert equation shown in Equation I-2. This expression predicts the attenuation of incident monochromatic (it is usually not true in this simple form for polychromatic beams) X-ray radiation by an exponential function of the linear absorption coefficient (μ), the element concentration (c) and the thickness (t). Additionally, it is possible to estimate an effective linear attenuation coefficient, μ_{eff}, if several elements are contained in the irradiated material and for polychromatic beam, as shown in Eq. I-3. Finally, it is sometimes used more conveniently mass attenuation coefficient by defining $\mu_m=\mu_{eff}/c$.

$$I = I_0 e^{-\mu c t} \tag{I-2}$$

$$I = I_0 e^{-\mu_{eff} c t} \tag{I-3}$$

The attenuation coefficient, μ, also varies with incident radiation wavelengths and energy. It is also important to note that a relationship of the captured intensity (non-absorbed by the material) and the density (ρ) can be established. In the specific case of monochromatic beam and pure element, the attenuation coefficient can be further extended and related to atomic number, Z. High atomic weight (Z) materials such as metals will stop X-ray radiation immediately (either by absorbing, reflecting or dispersing it), whereas materials with light molecular weight made for instance from carbon and hydrogen (polymers) will let almost all light to pass.

I.3.2.3 Microfocus X-Ray System at CellMat

The X-ray imaging device used in this work has been recently built in CellMat. It is a valuable tool able to obtain information about polymer foaming processes. Both the X-ray tube and the flat panel detector needed careful selection since polymers present low X-rays absorption coefficient and foaming is a process evolving rapidly. In this sense low energies of the emitted

X-rays are suitable for imaging polymers although detectors are not conceived for low energies. The high sensitivity of the detector response is thus of extreme importance. Moreover, dimensions of cellular structure are in the order of microns and therefore high resolution is also relevant, thus needed small spot focus size and small pixel size in the detector.

System configuration:

X-ray tube and flat panel detector are settled on in front of each other inside a X-ray shielded lead cabinet, as seen in Figure I.17. In principle, it is possible to position them at any distance, *SDD*, but in general optimum distances are in the range of 0.3 to 1.2 m As the beam is cone-spread the more distant the less radiation the FP-detector receives, which, in principle, is positive for its lifetime but reduces image quality since different artifacts effects increase with distance. In this particular device, the box dimensions limit this distance and it was chosen at 580 mm, becoming a compromise distance for all the involved factors. The objects to be imaged can be placed at any position in between the detector and the source. The fact of having diverging (cone-beam) X-ray beam allows for object magnification. Magnification factor (*M*) is a function of the object to source distance (*OSD*) compared to the total distance from the source to the detector (*SDD*). Thus magnification is defined as indicated in Eq. I-4.

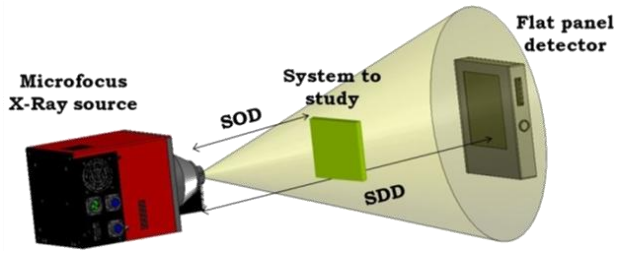

Figure I.17. Magnification scheme obtained thanks to cone-beam geometry

$$M = \frac{SDD}{SOD} \tag{I-4}$$

I.3.2.4 Acquisition of Radiographs

Acquisition of the X-ray radiographs of cellular polymers requires samples with a homogeneous thickness. Appropriate samples from PMMA and PMMA/MAM foams were obtained using a precision saw (mod. 1000, Isomet) with a thickness of about 4 mm.

X-ray radiographies from these samples were taken using the following parameters: *V* = 45 KV, *I* = 150 µA, and *t* = 1500 ms (*V* and *I* are the voltage and current intensity of the X-ray source, and *t* is the exposition time of the detector used to take the image). Moreover, a *background* and *brigthfield* images were taken with the same parameters (the *background* is taken with the X-ray source off, while the *brigthfield* is taken without sample and with the X-ray source on) to be used in the correction of the images.

I.3.3 Thermal Conductivity: Transient Plane Source (TPS)

Thermal conductivity of microcellular and nanocellular polymers was measured by the Transient Plane Source (TPS) technique using a thermal conductivimeter mod. HDMD (Hotdisk). The TPS is a standard technique for thermal properties characterization of different materials (metals, ceramics, polymers, liquids, etc.) [11].

I.3.3.1 Introduction to the TPS Method

Measurement of thermal conductivity by means of the TPS method has been demonstrated elsewhere [12-17]. The basic principle of this method relies on a plane element which acts both as temperature sensor and heat source. This element consists of an electrically conducting pattern of thin nickel foil (10 µm) spiral-shaped, embedded in an insulation layer usually made of Kapton (70 µm thick). The TPS element is located between two samples with both sensor faces in contact with the two surfaces as Figure I.18 depicts. Two samples of similar characteristics and appropriate surfaces to ensure good contact with the sensor are required for this purpose.

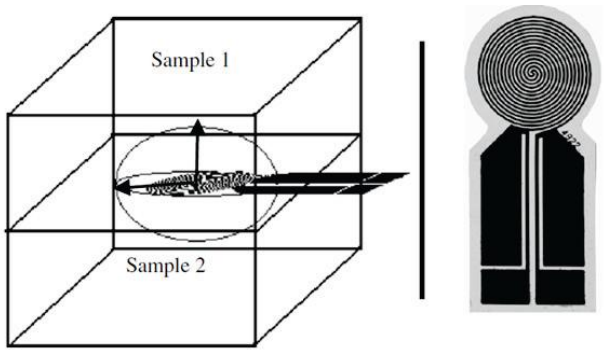

Figure I.18. Experimental set-up to perform TPS measurements and sensor shape

This method offers some advantages in comparison with other standard methods, such as fast and easy experiments, wide ranges of measurement temperatures (50 K < *T* < 1000 K) and thermal conductivities accessible (from 0.01 to 500 W/m·K), measurement can be carried out at atmospheric pressure or under vacuum conditions, marginal effort needed in sample preparation, flexibility in sample size and the possibility to perform local or bulk measurements only changing the sensor diameter.

It is important to remark that this is a contact method, so special care has to be taken to minimize thermal contact resistance. The good heat transition through two different materials is mainly associated to contact pressure and surface roughness [18, 19].

Moreover, the TPS equipment is able to compensate the heat capacity of the sensor and other thermal delays of the heat flow by introducing a time correction. Nevertheless, it is necessary to suppress the first 20-30 points of each measurement (of a total of 200 points of the heating

curve) to eliminate the heat capacity of the sensor that cannot be fully compensated by the time correction [14, 15, 20].

Finally, to avoid residual temperature drifts on the samples, it is necessary to fix a time spam between individual experiments on each specimen.

I.3.3.2 Experimental Procedure

The CellMat TPS device is composed by the TPS sensor, TPS controller unit associated to a computer, a vacuum chamber, a rotary vacuum pump (Edwards, mod. RV3 A65201903), and a vacuum sensor (BOC Edwards, mod. WRG-S) (Figure I.19).

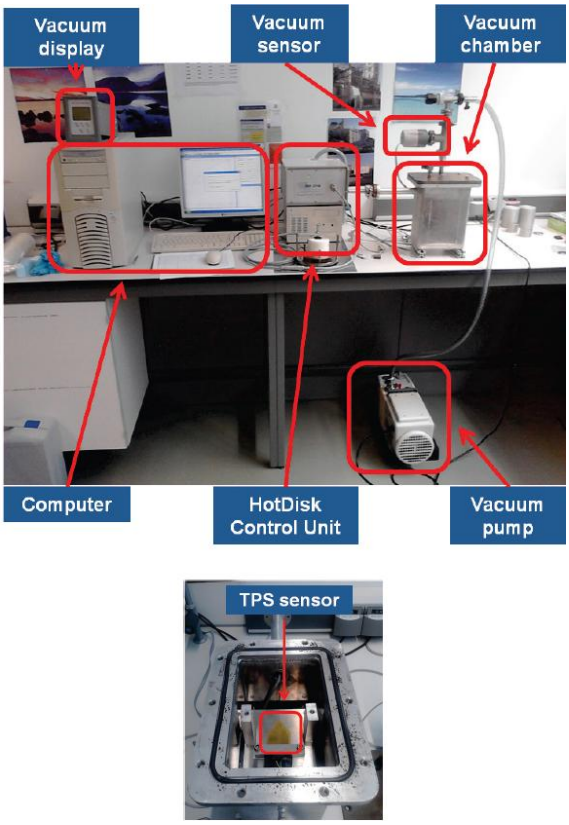

Figure I.19. General view of the CellMat TPS device (up). Detail of the TPS sensor inside the vacuum chamber (down)

Samples preparation and measurement were carried out following the next steps:

1º Samples were studied by X-ray radiography to exclude those cellular polymers presenting defects or inhomogeneities that could be an important source of inaccuracy in the thermal conductivity measurements.

2º Samples were polished using a polishing machine (mod. LaboPol2-LaboForce3, Struers) equipped with a silicon carbide grinding paper (P 180) to assure an appropriate contact with the sensor faces and to remove the outer solid or densified

skin. After polishing, samples had an average thickness about 5 mm and dimensions of 25 mm x 25 mm.

3º Samples were dried during 4 h at 50º C.

4º Samples were stored at controlled temperature and humidity (23º C and 50 % humidity) during at least 3 days before the measurements.

5º Samples were placed in the experimental set-up, inside the vacuum chamber, with a constant applied pressure between the two pieces, using a TPS sensor of radius 3.189 mm. After samples placement the vacuum chamber was closed.

6º Samples and experimental set-up were allowed to reach an equilibrium temperature (23 ºC) (experiments were carried out in an environment with controlled temperature) before the beginning of the measurements (typically 30 minutes).

7º Measurement parameters (power and time) were adjusted to ensure accurate results. Typical parameters to measure PMMA-based foams are about 0.006 watts and 55 seconds.

8º Samples were measured five times at atmospheric pressure. Time span to avoid temperature drift was fixed on 5 minutes. The conductivity of the sample was taken as the average value of these five measurements.

9º After the measurement under atmospheric pressure the rotary vacuum pump was activated.

10º After reaching the desired vacuum conditions ($5 \cdot 10^{-2}$ mbar approximately), samples and experimental set-up were allowed again to reach an equilibrium temperature before the beginning of the measurements (typically during 60 minutes).

11º Measurement parameters (power and time) were adjusted to ensure accurate results. It should be noticed that measurement parameters usually change between atmospheric pressure and vacuum conditions. Parameters used at atmospheric pressure can damage the sample and the sensor due to the lower heat dissipation under vacuum conditions. In general, measurements under vacuum conditions require lower power and higher measuring time (e.g., atmospheric pressure: w = 0.006 watts and t = 55 s; vacuum: w = 0.005 watts and t = 60 s).

12º Samples were measured twelve times at vacuum conditions. Time spam between consecutive experiments to avoid temperature drift was fixed on 60 minutes. Also these measurements performed during 12 hours allowed detecting if an evolution of the thermal conductivity occurs (due to a slow and progressive extraction of the gas inside the cellular polymer). The thermal conductivity of the sample in these conditions was taken as the average value of these twelve measurements.

13º Thermal conductivities of the samples, both measured at atmospheric pressure and under vacuum conditions, were calculated using the software provided with the

TPS device. Calculations were made selecting the "*Standard Analysis"* and neglecting the first 25 measured points to eliminate the effect of the heat capacity of the sensor.

14º Taking into account the average cell size and density of the measured foams, their total thermal conductivity (λ_t) is the addition of two contributions: the thermal conductivity through the solid (λ_s) and gaseous (λ_g) phases (more details can be found in *Chapter III*). Measurements carried out at atmospheric pressure allow obtaining λ_t; whereas measurements under vacuum conditions provide λ_s (assuming that the gas inside the voids of the cellular polymer is completely extracted); therefore, λ_g can be calculated from the previous values, obtaining by this way a complete characterization of the thermal conductivity of these foams (total conductivity (λ_t) and contributions of the solid (λ_s) and gas phase (λ_g)).

I.4 References

1. Lalande L, Plummer CJG, Manson J-AE, and Gérard P. Polymer 2006;47(7):2389-2401.
2. Lalande L, Plummer CJG, Manson J-AE, and Gérard P. Engineering fracture mechanics 2006;73(16):2413-2426.
3. Pinto J. Fabrication and characeterization of nanocellular polymeric materials from nanostructured polymers. University of Valladolid & University of Bordeaux, 2014.
4. Pinto J, Dumon M, Pedros M, Reglero JA, and Rodriguez-Perez MA. Chemical Engineering Journal 2014;243C:428-435.
5. Pinto J, Reglero-Ruiz JA, Dumon M, and Rodriguez-Perez MA. The Journal of Supercritical Fluids 2014;94:198-205.
6. Goel SK and Beckman EJ. Cellular polymers 1993;12(4):251-274.
7. Nawaby AV, Handa YP, Liao X, Yoshitaka Y, and Tomohiro M. Polymer international 2007;56(1):67-73.
8. Pinto J. Fabrication and Characterization of Nanocellular Polymeric Materials from Nanostructured Polymers. University of Valladolid & University of Bordeaux, 2014.
9. Pinto J, Dumon M, Rodriguez-Perez MA, Garcia R, and Dietz C. The Journal of Physical Chemistry C 2014;118(9):4656-4663.
10. ASTM. Standard Test Methods for DC Resistance or Conductance of Insulating Materials. vol. D 257-99: ASTM International, 2005. pp. 18.
11. UNE-EN ISO 22007-2 AC. Determinación de la conductividad térmica y la difusividad térmica. Parte 2: Método de la fuente de calor plana transitoria (disco caliente). Plásticos, vol. UNE-EN ISO 22007-2: AENOR, 2012. pp. 23.
12. Solórzano E, Reglero JA, Rodríguez-Pérez MA, Lehmhus D, Wichmann M, and de Saja JA. International Journal of Heat and Mass Transfer 2008;51(25–26):6259-6267.
13. Solórzano E, Rodriguez-Perez MA, and de Saja JA. Advanced Engineering Materials 2008;10(4):371-377.
14. Gustavsson M, Karawacki E, and Gustafsson SE. Review of Scientific Instruments 1994;65:3856-3859.
15. Log T and Gustafsson SE. Fire Materials 1995;19:39-43.
16. Reglero Ruiz JA, Saiz-Arroyo C, Dumon M, Rodríguez-Perez MA, and Gonzalez L. Polymer international 2011;60(1):146-152.
17. Almanza O, Rodríguez-Pérez MA, and De Saja JA. Journal of Polymer Science Part B: Polymer Physics 2004;42(7):1226-1234.

18. Singhal V, Litke PJ, Black AF, and Garimella SV. International journal of heat and mass transfer 2005;48:5446-5459.
19. Wolff EG and Schneider DA. International journal of heat and mass transfer 1998;41:3469-3482.
20. Gustafsson SE. Review of Scientific Instruments 1991;62:797-804.

CONFINEMENT EFFECT

Chapter II. Confinement Effect

The reduction of the cell size from the micrometer to the nanometer scale, maintaining constant the density, leads to a confinement of the gaseous phase into the nanometric cells and to a strong reduction of the thickness of the cell walls.

As a consequence of the confinement of the gaseous phase, a reduction of the thermal conductivity of the gas phase is expected (see *Chapter III*) because it is supposed that these nanocellular materials will present the well-known Knudsen effect [1, 2]. This effect implies that when cell size is comparable or smaller than the mean free path (l_g ≈ 70 nm for air at room temperature) of the gas, the molecules of the latter collide more often with the molecules forming the surrounding solid part than among them (Figure II.1). Thus, the energy transfer through the gas molecules is reduced.

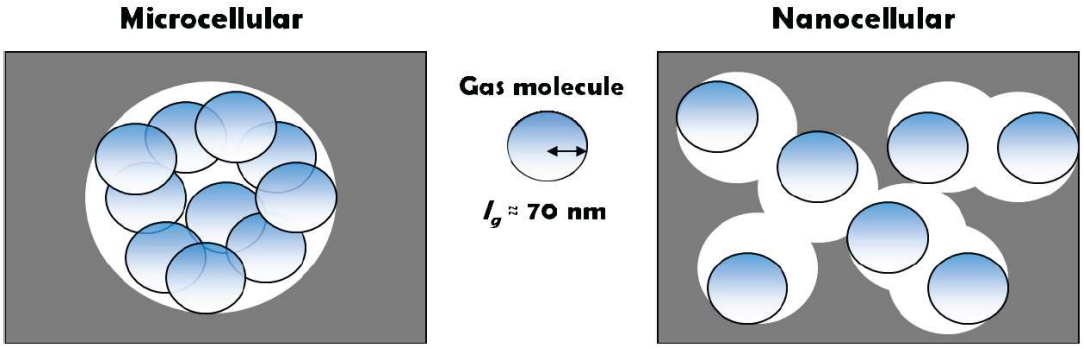

Figure II.1. Behavior of gas molecules of air in microcellular polymers (left) and in nanocellular polymers with a cell size similar to the mean free path l_g (right) of the gas. Gas molecules (represented assuming a radius equal to their mean free path in air at room temperature) interact between them in the microcellular polymers, allowing the heat transmission; whereas no interaction, or a reduced one, is found between the gas molecules on the nanocellular polymer.

Then, in gas-filled cellular structures, the effective gaseous thermal conductivity (λ'_g) can be described by the Knudsen equation [1]:

$$\lambda'_g = \lambda'_{go}/(1 + \beta Kn) \qquad \text{(II-1)}$$

Where λ'_{go} is the thermal conductivity of the gas (usually air, λ_{air} = 0.026 W/mK at room temperature and pressure), β is a parameter that takes into account the energy transfer between gas molecules and the limiting solid structure (about 2 for air), and *Kn* is the Knudsen number that is obtained by dividing the mean free path of the gas molecules between the average cell size (Φ):

$$Kn = l_g/\Phi \qquad \text{(II-2)}$$

Combining equations II-1 and II-2 is obtained that λ'_g decreases significantly when the cell size decreases below the micron. Thus for cellular materials with cells sizes in the nanometer scale, a reduction of the thermal conductivity of the gas phase should be expected.

On the other hand, cell size reduction also leads (as mentioned before) to a strong reduction of the thickness of the cell walls. An example of this reduction is shown in Figure II.2, in which the cell wall thickness of a porous PMMA is reduced from around 1.5 µm to 45 nm when the cell size switches from the micro (Figure II.2 left) to the nanometer range (Figure II.2 right).

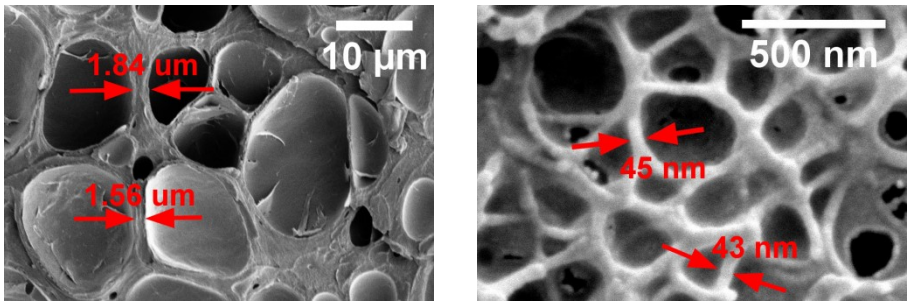

Figure II.2. Cell wall thickness of a microcellular PMMA (left) and a nanocellular PMMA (right)

This reduction of the cell wall thickness confines the polymer chains within the cell walls leading to a reduction of the mobility of the polymeric macromolecules (confinement effect). Previous studies on thin films have demonstrated that chain confinement modified the glass transition temperature (T_g) of the polymer, that can be either higher or lower than that of the bulk polymer [3], depending on the interfacial interactions between the polymer and the surrounding material (e.g. supporting substrate or nanoporous glass or alumina containers, etc.), surface mobility effects [4], and other mechanisms yet to be identified [5].

For instance, an increment of the glass transition temperature was detected by J. A. Reglero - Ruiz et al. [6] in PMMA based nanoporous materials (average cell size around 200 nm) by means of differential scanning calorimetry (DSC). They observed an increase of 11º C of the T_g of the nanocellular PMMA based foams with respect to the bulk polymer.

This effect was also detected later in nanocellular polyethylenimine (PEI) (average pore size between 30 and 120 nm) by D. Miller and coworkers [7]. They also studied the thermal behavior of foamed PEI by DSC, obtaining an increase of the glass transition temperature in the nanocellular system of 5º C with respect to both microcellular PEI and the solid material. Also, B. Notario et al. [8] (*Chapter IV*) showed this phenomenon in nanocellular PMMA (average cell size between 200 and 300 nm) both by DSC and by dynamic mechanical analysis (DMA). In this study, the nanocellular system exhibited a glass transition temperature 7º C higher than that of both the microcellular material and the solid matrix.

On the other side, J. A. Forrest and coworkers [9] found by means of Brillouin light scattering that in thin freely standing polystyrene (PS) films the T_g decreases linearly with film thickness for a thickness ≤ 70 nm. They achieved a reduction of 70 ºC for a film thickness of 29 nm.

A similar result was obtained by O. K. C. Tsui et al. [10] who studied the variation of the glass transition temperature in thin freely standing films of PS as a function of film thickness. For this purpose they measured the change in the thermal expansion using X-ray reflectivity. They showed that the T_g of PS decreased with decreasing film thickness (according to the work of J. A. Forrest et al. [9]).

The glass transition temperature of freely standing thin PS films was also characterized by J. A. Forrest et al. [11] as a function of the film thickness for two different molecular weights M_w. Brillouin light scattering and ellipsometry measurements revealed that T_g is decreased dramatically from the bulk value by a quantity that depends on both the film thickness and the M_w (in good agreement with the previous works).

Then, the main constraints found in the study of these phenomena are in general due to the interaction that the material under study have with the substrates. Furthermore, there are only studies conducted in depth in thin films, suggesting but not demonstrating the existence of the confinement effect on bulk samples with structures that can present this confinement (nanocellular materials).

A study about this phenomenon was carried out and submitted to **The Journal of Physical Chemistry (2016)**, with the title ***"Molecular Confinement of Solid and Gaseous Phases of Self-Standing Nanoporous Polymers Inducing Enhanced and Unexpected Physical Properties"***.

In this work, the first evidences of the molecular confinement of polymer chains on self-standing bulk nanocellular PMMA based materials are presented. A wide range of PMMA-based porous samples with cell sizes between 90 nm and 3 µm were produced by the gas dissolution foaming process.

Restriction of the polymer chains mobility on cellular materials with cell sizes below 200 nm is consistently demonstrated by different experimental techniques, such as differential scanning calorimetry (DSC), Raman spectroscopy, and broadband dielectric spectroscopy. In addition, several scale-reduction related phenomena on the constituent elements, both in the polymeric and in the gaseous phases, and on the porous architecture are discussed and identified, as well as their significant implications on the macroscopic physical properties of the nanocellular system, such as the electrical conductivity and permittivity.

Furthermore, these results will provide explanations to evidences of improved mechanical properties (*Chapter IV*) and thermal insulation (*Chapter III*) of these materials.

Molecular Confinement of Solid and Gaseous Phases of Self-standing Bulk Nanoporous Polymers Inducing Enhanced and Unexpected Physical Properties

Javier Pinto[¥]*, *Belen Notario*[δ], *Raquel Verdejo*[Φ], *Michel Dumon*[Δ], *Stephane Costeux*[γ], *and Miguel A. Rodriguez-Perez*[δ]*

¥: Nanophysics – Smart Materials Group, Istituto Italiano di Tecnologia (IIT), Via Morego, 30 16163 Genova, Italy

δ: Cellular Materials Laboratory (CellMat), Condensed Matter Physics Department, Paseo Belén nº7, University of Valladolid, 47011 Valladolid, Spain

Φ: Institute of Polymer Science and Technology (ICTP-CSIC), Juan de la Cierva, 3, Madrid 28006, Spain

Δ: Laboratoire de Chimie des Polymères Organiques (LCPO), Institut National Polytechnique de Bordeaux (INP), Université de Bordeaux, 16 Avenue Pey Berland, 33607 Pessac-Cedex, France

γ: The Dow Chemical Company, Dow Building Solutions, 1501 Larkin Center Dr., Midland, MI 48674

AUTHOR INFORMATION

Corresponding Author

* Javier Pinto. Email: Sanz.Pinto@iit.it

* Miguel A. Rodriguez-Perez. Email: marrod@fmc.uva.es

ABSTRACT

In this work it is provided the first evidence of the polymer chains confinement within self-standing pore walls of nanoporous materials based on poly(methyl methacrylate) (PMMA). This was made possible by producing a series of porous samples with a wide range of pore sizes between 90 nm and 3 μm using processes combining CO2 sorption, selective block copolymer swelling or homogeneous physical foaming. Mobility restrictions of the PMMA chains in the porous samples with pore size below 200 nm was consistently demonstrated with several experimental techniques, including differential scanning calorimetry, Raman spectroscopy, and broadband dielectric spectroscopy. In addition, several scale-reduction phenomena related to the constitutive elements of the porous materials, both in the polymeric and gaseous phases, and to the porous architecture are identified. The significance of these phenomena on macroscopic electrical conductivity and permittivity of the nanoporous materials is demonstrated, and the presented observations support previous explanations of improved mechanical properties and thermal insulation of this type of nano-materials.

TOC GRAPHICS

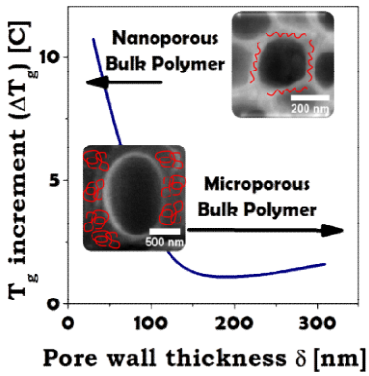

KEYWORDS nanoporous polymers, molecular chain confinement, dielectric properties, CO2 sorption

Nanoporous polymers are of great scientific and technological importance. Their tunable chemistry, high surface area, and improved mechanical properties offer promising new applications in catalysis, filtration,[1] hydrogen storage,[2] gas transport, while their superior thermal properties are suited for applications as high performance thermal insulators in building trade, aeronautics, or even space launch.[3-4] Several strategies have been developed for the production of these novel materials, often taking advantage of polymer blends or block copolymers self-assembly followed by swelling or removal of a dispersed nanometric phase.[5-7] In recent years, the use of physical blowing agents (e.g. CO_2) to induce the nucleation of pores inside homogeneous polymers with high chemical affinity for the blowing agent has gained popularity as this provides a pathway to exploit the unique properties of nanostructured porous polymers in advanced materials for large scale applications.[8-12] Here, we have employed both strategies to demonstrate that features in the nanometric architecture prevail in controlling the final properties over the procedure to develop the nanoporosity.

The nanometric architecture, defined by the presence of nanopores with sizes below 100 nm, provides polymeric materials with a high surface area, in which the confinement of a gaseous phase leads to a drastic reduction of thermal conductivity (i.e. the Knudsen effect already demonstrated in aerogels and porous ceramics),[13] as recently shown experimentally in bulk nanoporous materials (thick nanocellular foams) phase–separated poly(methyl methacrylate) (PMMA)-based systems.[14] Some indirect evidence of changes in the polymer phase behavior within these nanoporous materials were found, along with an enhancement of several mechanical properties compared to microcellular foams.[15] Such improvements were explained by a possible confinement of the polymer chains into pore walls with nanometric dimensions below 60 nm, by

analogy to thin films.[16] Yet no experimental evidence exists of a relation between a hypothetical polymer chains confinement in the nanometric polymer matrix and macroscopic physical properties of bulk nanoporous polymers (i.e. self-standing samples with significant thickness of about or over 1 mm, or thousands of times thicker than the size of the pores within), in particular when materials have a closed porous structure. To provide such experimental evidence of the confinement and scale-related effects, we first need to produce a series of bulk porous materials with various degrees of confinement, which is achieved by inducing porosity into homogeneous and nanostructured polymer matrices based on PMMA using CO_2 as physical blowing agent.

Scanning electron microscopy (SEM) (**Figure 1**) shows the distinct porous architecture of neat PMMA and of nanostructured blends of 90 wt.% PMMA and 10 wt.% poly(methyl methacrylate)-co-poly(butyl acrylate)-co-poly(methyl methacrylate) (MAM). CO_2 can induce porous structures in neat PMMA with increasing pore density and decreasing average pore sizes from 3 μm to 90 nm by modifying the saturation pressure during the production process (**Table 1**). In contrast, the same procedure with the 90/10 PMMA/MAM blend consistently leads to porous structures with pore sizes below 200 nm, due to the controlled swelling of the poly(butyl acrylate) dispersed domains,[1, 17] which results in rather constant pore densities that match the initial number density of dispersed domains. Details of the processing parameters and main characteristics of the porous structures obtained can be found in **Table 1** and elsewhere.[17] The thickness of the pore walls (δ) decreases with the decrease of the pore size, reaching values between 20 and 65 nm for nanoporous samples with pore sizes below 200 nm (**Table 1**).

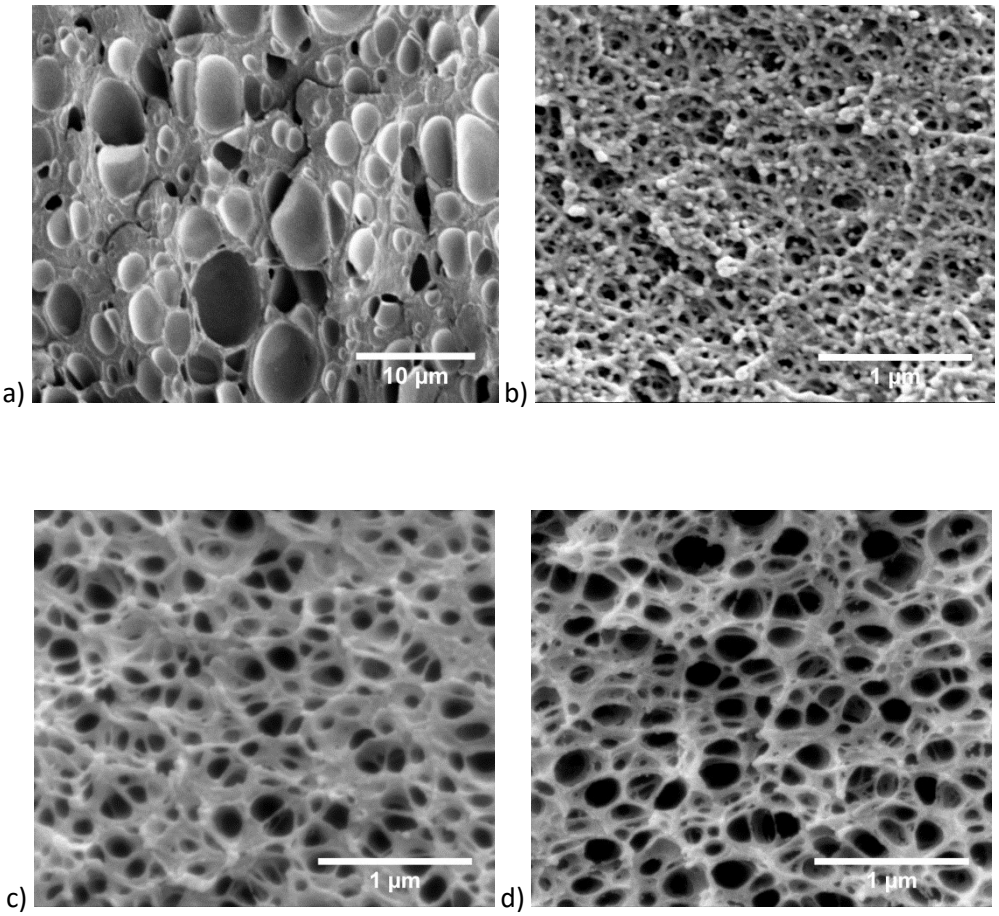

Figure 1. SEM micrographs of a) microporous neat PMMA produced at 10 MPa, b) nanoporous neat PMMA produced at 30 MPa, c) nanoporous 90/10 PMMA/MAM produced at 10 MPa, and d) nanoporous 90/10 PMMA/MAM produced at 25 MPa.

To make progress toward understanding the confinement effects of nanoporous structures on amorphous thermoplastics polymer chains (e.g. PS and PMMA), differential scanning calorimetry (DSC) and Raman spectroscopy measurements were carried out. Previous studies demonstrated that chain confinement modified the glass transition temperature (T_g) of the polymer, that can be either higher or lower than that of the bulk polymer,[18-19] depending on the interfacial interactions between the polymer and the surrounding material (e.g. supporting substrate or nanoporous glass or alumina containers...), surface mobility effects,[20] and other mechanisms yet to be identified.[21] Raman spectroscopy is a valuable technique to detect conformational changes of

polymer chains induced by confinement.[22] The nanoporous walls are considered as self-standing confined materials (i.e. not supported by a substrate or in a container) and therefore, are free of interfacial constraints as opposed to model systems previously studied[23-24] (see Supporting Information).

Figure 2.a shows the T_g increment between the bulk porous materials and solid polymer ($\Delta T_g = T_g^{porous} - T_g^{solid}$) for various wall thicknesses. A gradual increase of T_g is measured as the wall thickness decreases below 100 nm (i.e. nanoporous region), in contrast with the microporous region in which T_g remains constant and equal to that of bulk dense PMMA. This effect is a direct consequence of PMMA chain confinement in thin pore walls. The thickness corresponding to the transition between the two regions is set around 100-150 nm. A previous study has suggested the appearance of such confinement effect on thin films with thickness below six times the radius of gyration ($<r^2>$) of the polymer chains.[25] Here, the confinement region occurs at higher thicknesses than the suggested by Kraus *et al.* that corresponds to about 50 nm ($<r^2>_{PMMA}$ = 7.97 nm, see Supporting Information). It can be argued that such increase is due to the dynamic nature of the process used to make the materials, involving swelling by CO_2 and biaxial stresses during pore expansion. Effect of biaxial stretching of PMMA chains on T_g of the pore walls can be discarded according to literature.[26] However, CO_2 sorption can increase the radius of gyration of PMMA chains, thus inducing a local stretching of the molecules,[27] thereby raising the thickness boundary at which the confinement is first observed. It should be noted that CO_2 sorption effects alone cannot explain the increase in T_g, as several microporous PMMA samples made at high pressures experienced higher CO_2 uptakes than nanoporous 90/10 PMMA/MAM made at lower pressure (**Table 1**), and yet do not show a T_g increment. Therefore, our

experiments demonstrate that the T_g increase in nanoporous materials is directly related to polymer chains confinement (restriction of the molecular dynamics) in pore walls thinner than 100 nm.

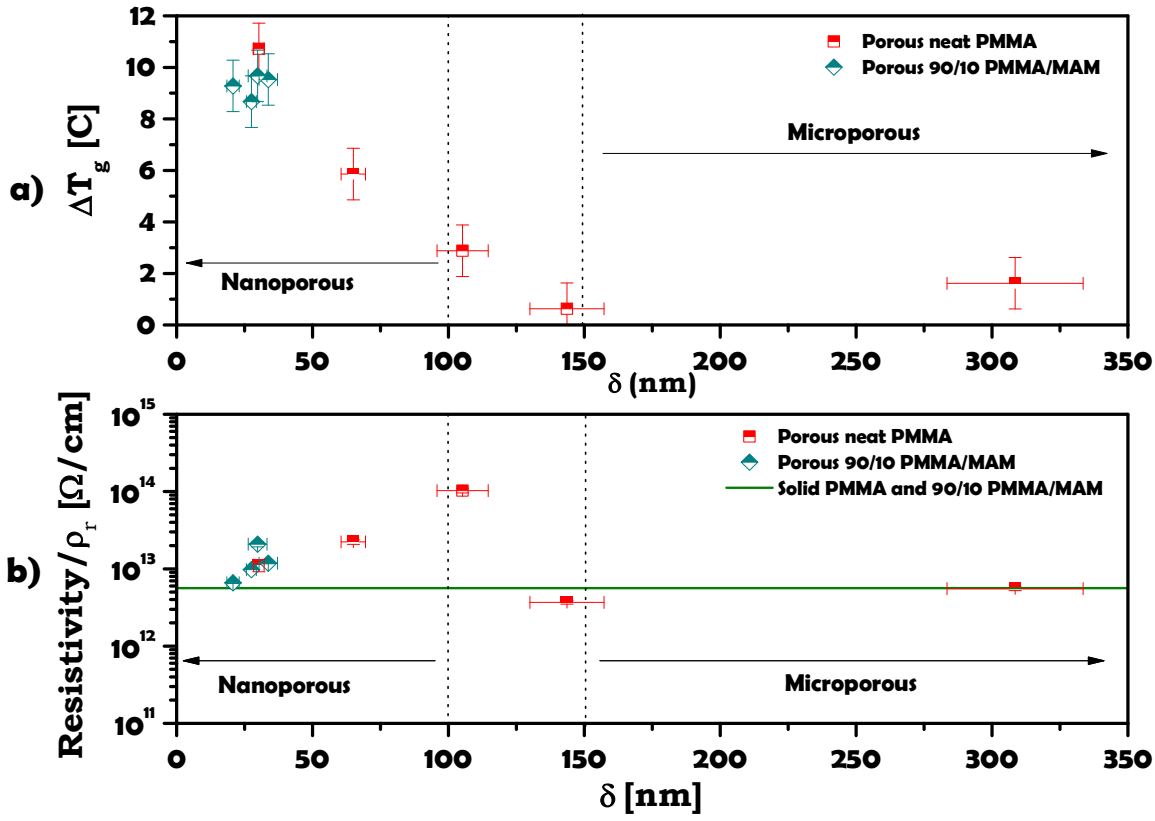

Figure 2. a) Increment of the T_g of porous neat PMMA and 90/10 PMMA/MAM samples due to the reduction of the pore wall thickness (δ); b) Evolution of the DC electrical resistivity of porous neat PMMA and 90/10 PMMA/MAM samples as a function of the pore wall thickness (δ), and compared to the resistivity of the solid PMMA and 90/10 PMMA/MAM samples.

Table 1. Processing parameters, CO_2 uptake, porous structure characteristics, and Raman spectra relative intensities of the neat PMMA and 90/10 PMMA/MAM solid and porous samples. Wave number of the Raman studied peaks are indicated as subscripts (Y_{nnnn}, where *nnnn* is the wavelength in cm^{-1}).

	Neat PMMA					
Saturation Pressure [MPa]	0 (Solid)	10	15	20	25	30
CO_2 Uptake [wt.%]	-	24.3 ± 0.2	26.7 ± 0.7	28.1 ± 0.7	29.7 ± 0.7	31.5 ± 0.1
Relative Density	1	0.66 ± 0.01	0.56 ± 0.01	0.53 ± 0.01	0.49 ± 0.01	0.46 ± 0.01
Average Pore Size [nm]	-	3290 ± 40	1460 ± 20	710 ± 13	200 ± 5	90 ± 2
Average Pore Wall Thickness [nm]	-	308 ± 25	143 ± 14	105 ± 9	65 ± 4	30 ± 2
Average Pore Density [pores/cm^3]	-	4.18×10^{10}	8.61×10^{11}	8.92×10^{12}	5.06×10^{14}	6.39×10^{15}
Raman Relative Intensities:						
Y_{812}/Y_{968}	3.18 ± 0.01	2.44 ± 0.01	2.50 ± 0.03	2.43 ± 0.01	2.60 ± 0.01	2.85 ± 0.02
Y_{812}/Y_{1452}	1.97 ± 0.01	1.41 ± 0.01	1.45 ± 0.01	1.45 ± 0.01	1.61 ± 0.03	1.79 ± 0.01
Y_{1736}/Y_{1452}	0.53 ± 0.01	0.40 ± 0.01	0.42 ± 0.01	0.41 ± 0.01	0.42 ± 0.01	0.47 ± 0.01
Y_{2954}/Y_{1452}	8.50 ± 0.02	6.30 ± 0.07	6.47 ± 0.01	6.41 ± 0.01	6.55 ± 0.12	7.28 ± 0.09

	90/10 PMMA/MAM				
Saturation Pressure [MPa]	0 (Solid)	10	15	20	25
CO_2 Uptake [wt.%]	-	24.9 ± 0.1	27.5 ± 0.1	28.9 ± 0.2	30.6 ± 0.2
Relative Density	1	0.58 ± 0.01	0.54 ± 0.01	0.49 ± 0.01	0.43 ± 0.01
Average Pore Size [nm]	-	150 ± 4	160 ± 4	170 ± 4	190 ± 4
Average Pore Wall Thickness [nm]	-	21 ± 2	27 ± 2	33 ± 3	30 ± 3
Average Pore Density [pores/cm^3]	-	6.72×10^{14}	7.06×10^{14}	7.78×10^{14}	8.56×10^{14}
Raman Relative Intensities:					
Y_{812}/Y_{968}	3.09 ± 0.02	2.62 ± 0.05	2.66 ± 0.04	2.63 ± 0.08	2.66 ± 0.08
Y_{812}/Y_{1452}	1.86 ± 0.03	1.57 ± 0.05	1.61 ± 0.04	1.61 ± 0.03	1.63 ± 0.06
Y_{1736}/Y_{1452}	0.52 ± 0.01	0.44 ± 0.01	0.45 ± 0.01	0.44 ± 0.01	0.44 ± 0.01
Y_{2954}/Y_{1452}	8.45 ± 0.13	6.40 ± 0.10	6.48 ± 0.14	6.43 ± 0.07	6.53 ± 0.22

The analysis of the Raman relative intensities of the pendant groups provides further evidences of the molecular chain conformational modifications (**Table 1**, details of the studied peaks and example of Raman spectra can be found in the Supporting Information). Extending the previous discussion, Raman analyses should account for both confinement effect inside the pore walls and the aforementioned influence of CO_2 exposure on the polymer chains conformation. We note that nanoporous 90/10 PMMA/MAM with comparable pore wall thicknesses but CO_2 uptakes ranging from 24.9 to 30.6 wt.% present comparable values of the relative Raman intensities (**Table 1**). Thus, effects of CO_2 uptake are negligible. Furthermore, the evolution of Raman relative peak intensities on neat PMMA porous samples indicates that ratios are rather constant for pore wall thicknesses above 100 nm (**Table 1**), but gradually increase by 10 to 20% as pore wall thicknesses fall below 100 nm.

According to the selected relative intensities (see Supplementary Information), such an increase is expected to relate to a vibrational mode hindrance of the larger pendant groups (e.g. here CH_3). This is consistent with conformational changes due to polymer chains confinement in pore walls with thickness below about 100 nm, in good agreement with the T_g results.

Such conformational changes of polymer chains can provide an explanation for the mechanical properties enhancement found in bulk nanoporous PMMA materials,[15] in the same way as the confinement of the gaseous phase provides the main explanation of the enhancement of the thermal insulation of these materials.[14] However, the reduction of the size of the constituent elements could modify the architecture of the porous material leading to modifications of their macroscopic properties. Such possibility was suggested as the result of the observed decrease of the solid phase contribution to the

thermal conductivity, which was ascribed to an expected increase of the tortuosity of the porous architecture.[14] With the aim of validating this hypothesis, the DC electrical resistivity of the samples was measured, as an increase of the solid phase tortuosity should also increase the electrical resistivity of the porous material.

Figure 2.b shows the evolution of the DC electrical resistivity as a function of the pore wall thickness. An unexpected behavior is found: the resistivity of the microporous samples corresponds to the resistivity of the solid samples, but for pore wall thickness between 150 and 100 nm the resistivity rises about two orders of magnitude, and then decreases to the initial values of the solid and microporous samples. Comparison between Figure 2.a and 2.b indicates that the evolution of the electrical conductivity is not directly related to the confinement effect of the solid PMMA phase. The sharp increment of the resistivity corresponds to a transition between micro and nanoporous materials (pore wall thickness from 150 to 100 nm, corresponding to pore sizes from 1.5 μm to 700 nm). This increment of the DC electrical resistivity due to the reduction of the pore size (e.g. transition micro to nano porous materials) can be explained by the increase in tortuosity of the porous architecture, also observed in previous results on microporous materials,[28] and the reduction of the thermal conductivity in this kind of samples.[14] However, this hypothesis alone cannot explain the later progressive decrease in DC electrical resistivity when the pore size is decreased in the nanoporous domain. This points to an additional phenomenon that takes place in the nanoporous domain and overlaps with the increment of tortuosity.

Figure 3.a shows the dielectric constant (ε') and the dielectric loss (ε'') at room temperature of neat PMMA solid and porous samples determined by broadband

dielectric spectroscopy over the frequency range from 10^{-2} to 10^{5} Hz. As expected, the dielectric constant decreases as the result of the increased free volume and the presence of entrapped air within the micro and nanopores. The solid and microporous samples present a dielectric relaxation, associated with local relaxation processes in amorphous polymers. This local relaxation is independent of the presence of the porous architecture and, hence, its relaxation time is the same in both the solid and the microporous materials. However, its intensity is drastically affected and decreases upon reduction of the pore size, disappearing for nanoporous materials. This intensity reduction and disappearance could be related to a progressive immobilization of the dipoles and polymer chains. Further evidence towards this argument is the decrease of the normalized dielectric strength as a function of the pore wall thickness (**Figure 3.b**). The dielectric strength ($\Delta\varepsilon$) provides information on the contribution of the orientational polarization towards the dielectric permittivity, i.e. it provides information on the capacity of the dipoles to orient themselves, and is proportional to the density of dipoles involved in the relaxation process. Hence, the decrease of $\Delta\varepsilon$ with wall thickness is ascribed to a progressive reduction of the number of free dipoles able to rotate, due to confined configuration of the nanoporous system. A similar dependency of the $\Delta\varepsilon$ with films thicknesses was reported by Napolitano et al. for thin films.[29]

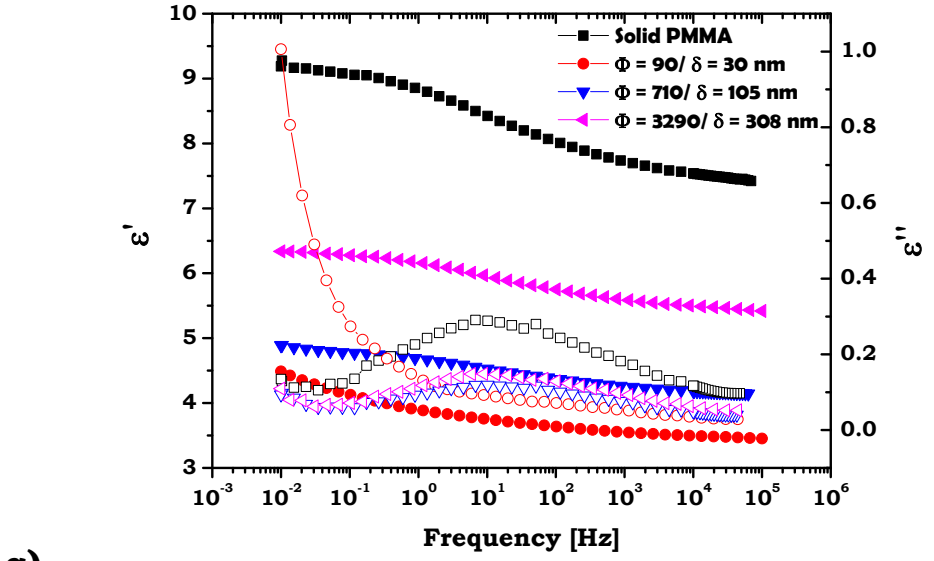

a)

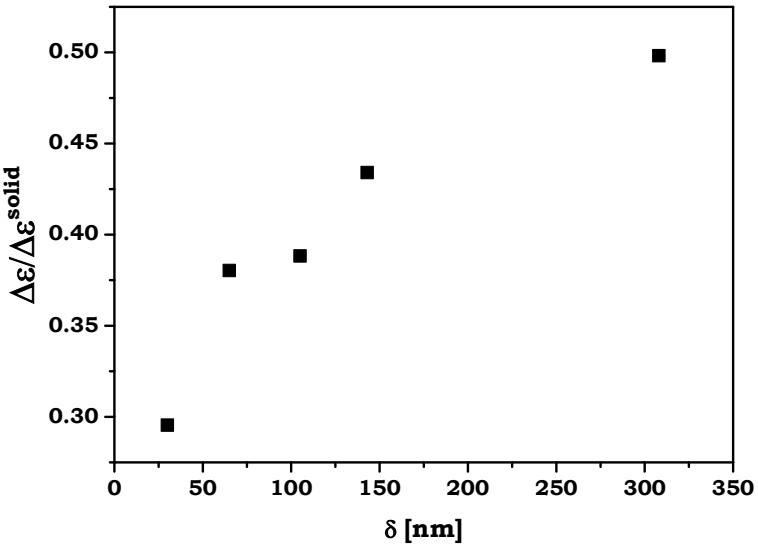

b)

Figure 3. a) Dielectric constant (ε', solid symbols) and dielectric loss (ε'', open symbols) as a function of frequency at room temperature (23º C). b) Normalized dielectric strength ($\Delta\varepsilon/\Delta\varepsilon^{solid}$) as a function of the pore wall thickness (δ).

Furthermore, nanoporous sample presents an abrupt increase of the loss permittivity at low frequencies, due to the presence of a conductivity component and an interfacial

polarization phenomena, or Maxwell Wagner Sillars (MWS). MWS arises in heterogeneous materials, such as composites or blends, and is related to the accumulation of charges at the interfaces. MWS is very weak in all microporous samples but it sharply rises in the nanoporous sample due to a combined effect of conductivity and MWS, visible as a change in the slope of ε'' at low frequencies. This conductivity could be the result of a possible capacitor-like behavior of opposing cell walls in nanopores presenting this accumulation of superficial charges. A classical explanation of this contribution of nanopores to the conductivity is the dielectric breakdown of the gas inside the capacitor-like nanopores due to the voltages employed in the characterization and the extremely small distances between the pore walls (between 90 and 200 nm in the samples that present this behavior). However, as previously demonstrated, the gas inside the nanopores presents a Knudsen diffusion regime due to the confinement,[14] instead of classical Fickian diffusion. Therefore the assumption of a conventional dielectric breakdown could be inaccurate, making further studies necessary to identify the conductive mechanism through the capacitor-like nanopores. At high frequencies, where MWS does not take place, the sole mechanism is the influence of the porous architecture (i.e. tortuosity), which is responsible for the resistivity increment between micro and nanoporous samples (see Supplementary Information). In summary, dielectric strength measurements demonstrate the polymer chains immobilization in the nanoporous materials. Moreover, the peculiar behavior of the electrical permittivity of PMMA-based nanoporous samples can be explained by the superposition of two phenomena: (1) a conductive mechanism through the confined gaseous phase of the nanopores detectable at low frequencies/DC, resulting in a reduction of the overall resistivity of the porous material proportional to the reduction of the pore size in the nanometer range; and (2) an increase in electrical resistivity of the

solid phase due to the increase of the tortuosity when the pore size is decreased independently of current frequency (i.e. modification of porous architecture).

In conclusion, we demonstrate the presence of a confinement effect both in solid and gaseous phases of bulk nanoporous PMMA-based materials, produced by a CO_2 sorption and selective swelling or foaming process. In the solid phase, this effect implies conformational changes and immobilization of the PMMA chains, which have been detected by Raman and Dielectric spectroscopy. As a consequence, the glass transition temperature of these materials presents an increase of up to 11º C in nanoporous samples with pore sizes about 90 nm. As far as we know, this is the first demonstration of the confinement effect on self-standing three-dimensional porous polymeric samples with thickness of about 3 mm and porous structures with constitutive elements below 200 nm, the results being independent of the pores generation mechanism (e.g. swelling of pre-existing self-assembled nanodomains or homogeneous pore nucleation in single phase PMMA). This confinement could be one of the key reasons explaining the improved mechanical properties of these materials previously observed. Moreover, we demonstrate the effect of a reduction of the scale of constituent elements (from micro to nano) on the tortuosity of the porous architecture, which in turn has a significant impact on macroscopic physical properties as their electric and thermal conductivity. Finally, we observe an unexpected capacitor-like behavior in polymeric nanopores due to the appearance of a MWS phenomenon related to the confinement of the gaseous phase, with a significant influence on the electrical conductivity of these materials. This offers the potential for the development of unique sensors with very high surface area based on nanoporous polymeric materials and higher electrical conductivity than the pristine solid polymer.

Experimental Methods

Fabrication of PMMA-based nanoporous polymers: Neat poly(methyl methacrylate) (PMMA) and a triblock copolymer poly(methyl methacrylate)-co-poly(butyl acrylate)-co- poly(methyl methacrylate) (MAM), both gently provided by Altuglas-Arkema Company (France), were employed for the production of bulk solid samples (50 x 15 x 3 mm^3) with PMMA/MAM contents in weight of 100/0 and 90/10. PMMA/MAM blends present a self-assembled nanostructure that acts as a pattern in the production of the porous structure.[1] Bulk porous polymeric structures with pore sizes in the micrometric and nanometric range for neat PMMA, and only in the nanometric range for PMMA/MAM blends were obtained respectively by conventional gas dissolution foaming and selective swelling of the soft phase, using CO_2 as physical blowing agent at room temperature and pressures between 10 and 30 MPa (Table 1, more details about the production of the porous polymers and photographs of the solid and porous bulk samples can be found in the Supporting Information).[17]

Characterization of solid and nanoporous PMMA-based materials: solid and porous polymers were analyzed by differential scanning calorimetry (DSC, Mod. 862 Mettler), Raman spectroscopy (He-Ne Horiba JY Induram Laser (633 nm), Kaiser Raman OSI head MKII, and Kaiser spectrometer OSI HoloSpec), DC electrical resistivity (Keithley 6105 Resistivity Adapter), and broadband dielectric spectroscopy (BDS, Alpha high-resolution dielectric analyzer). Porous polymers were studied by scanning electron microscope (SEM, model Quanta 200FEG, FEI) to measure the pore size, pore density, and polymer wall thickness. More details about the characterization procedures can be found in the Supporting Information.

ASSOCIATED CONTENT

Supporting Information. Detailed experimental methodology and fabrication route of the samples, photographs of the bulk nanoporous samples, Raman spectra of the PMMA and additional information about the peaks interpretation and selection for further study, graph of the resistivity at low frequencies, additional SEM micrographs of the nanoporous materials, and theoretical considerations about the confinement effect boundary, gyration radio of PMMA, and interfacial effects.

AUTHOR INFORMATION

Notes

J. Pinto and B. Notario contributed equally to this work. The authors declare no competing financial interests.

ACKNOWLEDGMENT

Financial support from The Dow Chemical Company USA, FPI grant BES-2013-062852 (B. Notario) from the Spanish Ministry of Education, MINECO (MAT 2012-34901), and the Junta of Castile and Leon (VA035U13) is gratefully acknowledged.

REFERENCES

1. Pinto, J.; Dumon, M.; Rodriguez-Perez, M. A.; Garcia, R.; Dietz, C. Block Copolymers Self-Assembly Allows Obtaining Tunable Micro or Nanoporous Membranes or Depth Filters Based on PMMA; Fabrication Method and Nanostructures. *The Journal of Physical Chemistry C* **2014,** *118* (9), 4656-4663.

2. Germain, J.; Frechet, J. M.; Svec, F. Nanoporous polymers for hydrogen storage. *Small* **2009,** *5* (10), 1098-111.

3. Fesmire, J. E. Aerogel insulation systems for space launch applications. *Cryogenics* **2006,** *46* (2-3), 111-117.

4. Forest, C.; Chaumont, P.; Cassagnau, P.; Swoboda, B.; Sonntag, P. Polymer nano-foams for insulating applications prepared from CO2 foaming. *Progress in Polymer Science* **2015,** *41*, 122–145.

5. Wang, Y.; Li, F. An emerging pore-making strategy: confined swelling-induced pore generation in block copolymer materials. *Advanced materials* **2011,** *23* (19), 2134-48.

6. Lazzari, M.; Lopez-Quintela, M. A. Block Copolymers as a Tool for Nanomaterial Fabrication. *Advanced materials* **2003,** *15* (19), 1583-1594.

7. Hentze, H.-P.; Antonietti, M. Porous polymers and resins for biotechnological and biomedical applications. *Reviews in Molecular Biotechnology* **2002,** *90*, 27-53.

8. Yokoyama, H.; Li, L.; Nemoto, T. Tunable Nanocellular Polymeric Monoliths Using Fluorinated Block Copolymer Templates and Supercritical Carbon Dioxide. *Advanced materials* **2004,** *16* (17), 1542-1546.

9. Yokoyama, H.; Sugiyama, K. Nanocellular Structures in Block Copolymers with CO2-philic Blocks Using CO2 as a Blowing Agent: Crossover from Micro- to Nanocellular Structures with Depressurization Temperature. *Macromolecules* **2005,** *38*, 10516-10522.

10. Costeux, S. CO2-Blown Nanocellular Foams. *Journal of Applied Polymer Science* **2014,** *131* (23).

11. Li, L.; Yokoyama, H.; Nemoto, T.; Sugiyama, K. Facile Fabrication of Nanocellular Block Copolymer Thin Films Using Supercritical Carbon Dioxide. *Advanced materials* **2004,** *16*, 1226-1229.

12. Krause, B.; Koops, G.-H.; Vegt, N. F. A. v. d.; Wessling, M.; Wubbenhorst, M.; Turnhout, J. V. Ultralow-k Dielectrics Made by Supercritical Foaming of Thin Films. *Advanced materials* **2002,** *14*, 1041-1046.

13. Hrubesh, L. W.; Pekala, R. W. Thermal properties of organic and inorganic aerogels. *Journal of Materials Research* **1994,** *9* (3), 731-738.

14. Notario, B.; Pinto, J.; Solorzano, E.; de Saja, J. A.; Dumon, M.; Rodríguez-Pérez, M. A. Experimental validation of the Knudsen effect in nanocellular polymeric foams. *Polymer* **2015,** *56*, 57-67.

15. Notario, B.; Pinto, J.; Rodríguez-Pérez, M. A. Towards a new generation of polymeric foams: PMMA nanocellular foams with enhanced physical properties. *Polymer* **2015,** *63*, 116-126.

16. Kim, S.; Mundra, M. K.; Roth, C. B.; Torkelson, J. M. Suppression of theTg-Nanoconfinement Effect in Thin Poly(vinyl acetate) Films by Sorbed Water. *Macromolecules* **2010,** *43* (11), 5158-5161.

17. Pinto, J.; Dumon, M.; Pedros, M.; Reglero, J.; Rodriguez-Perez, M. A. Nanocellular CO2 foaming of PMMA assisted by block copolymer nanostructuration. *Chemical Engineering Journal* **2014,** *243*, 428-435.

18. Keddie, J. L.; Jones, R. A. L.; Cory, R. A. Interface and surface effects on the glass-transition temperature in thin polymer films. *Faraday Discussions* **1994,** *98*, 219-230.

19. Keddie, J. L.; Jones, R. A. L.; Cory, R. A. Size-Dependent Depression of the Glass Transition Temperature in Polymer Films. *Europhysics Letters* **1994,** *27*, 59-64.

20. Yang, Z.; Clough, A.; Lam, C.-H.; Tsui, O. K. C. Glass Transition Dynamics and Surface Mobility of Entangled Polystyrene Films at Equilibrium. *Macromolecules* **2011,** *44* (20), 8294-8300.

21. Forrest, J. A.; Dalnoki-Veress, K.; Dutcher, J. R. Interface and chain confinement effects on the glass transition temperature of thin polymer films. *Physical Review E* **1997,** *56* (5), 5705-5716.

22. Blaszczyk-Lezak, I.; Hernández, M.; Mijangos, C. One Dimensional PMMA Nanofibers from AAO Templates. Evidence of Confinement Effects by Dielectric and Raman Analysis. *Macromolecules* **2013,** *46* (12), 4995-5002.

23. Teisseire, J.; Revaux, A.; Foresti, M.; Barthel, E. Confinement and flow dynamics in thin polymer films for nanoimprint lithography. *Applied Physics Letters* **2011,** *98* (1), 013106.

24. Ding, Y.; Ro, H. W.; Germer, T. A.; Douglas, J. F.; Okerberg, B. C.; Karim, A.; Soles, C. L. Relaxation Behavior of Polymer Structures Fabricated by Nanoimprint Lithography. *ACS Nano* **2007,** *1* (2), 84-92.

25. Kraus, J.; Müller-Buschbaum, P.; Kuhlmann, T.; D. W. Schubert; Stamm. Confinement effects on the chain conformation in thin polymer films. *Europhysics Letters* **2000,** *49* (2), 210-216.

26. Ube, T.; Aoki, H.; Ito, S.; Horinaka, J.-i.; Takigawa, T. Conformation of single PMMA chain in uniaxially stretched film studied by scanning near-field optical microscopy. *Polymer* **2007,** *48* (21), 6221-6225.

27. Ikeda-Fukazawa, T.; Kita, D.; Nagashima, K. Raman spectroscopic study of CO2sorption process in poly methyl methacrylate. *Journal of Polymer Science Part B: Polymer Physics* **2008,** *46* (8), 831-842.

28. Ma, X.; Peyton, A. J.; Zhao, Y. Y. Eddy current measurements of electrical conductivity and magnetic permeability of porous metals. *NDT & E International* **2006,** *39* (7), 562-568.

29. Napolitano, S.; Capponi, S.; Vanroy, B. Glassy dynamics of soft matter under 1D confinement: how irreversible adsorption affects molecular packing, mobility gradients and orientational polarization in thin films. *The European physical journal. E, Soft matter* **2013,** *36* (6), 61.

Supporting Information

Samples Production Route

Polymer blends of PMMA containing 10 wt.% of MAM were produced as follows. Both materials, PMMA and MAM, were dried in vacuum (680 mm Hg), at 80 °C during 4 h before processing. Mixing and extrusion were carried out using a Scamex CE02 single-screw extruder (L/D = 28, d = 45 mm), with a temperature profile from 165 to 225 °C at a screw speed of 60 rpm in the desired proportions. Pellets were produced using a continuous cutting machine operating at the end of the line at a constant speed of 240 rpm.

In a second step, neat PMMA and 90/10 PMMA/MAM were injected into pieces 50 × 15 mm^2 with 3 mm thickness, using a small scale injection molding machine developed by DSM Xplore. The working temperature was fixed at 240 °C, whereas mold temperature was set at 60 °C. The injection pressure was fixed at 1 MPa. All samples were transparent and showed a good surface appearance as well as a good injection behavior, without air bubbles inside the parts (Figure S1).

Foaming experiments were carried out in a high pressure vessel provided by TOP Industry (France), with a capacity of 300 cm^3 and capable of operating at maximum temperature of 250 °C and maximum pressure of 40 MPa. The reactor is equipped with an accurate pressure pump controller provided by Teledyne ISCO, and controlled automatically to keep the temperature and pressure at the desired values. The CO_2 vessel temperature and pressure were monitored in the course of the process. Thus a collection of experiments was performed in a modified solid state foaming process. The usual solid state foaming process with amorphous polymers has three stages: the saturation (under fixed gas pressure and temperature), gas desorption during and after

the pressure release (to room pressure and temperature), and foaming of the sample (at a temperature over or around the T_g of the plasticized polymer). However, the actual glass transition temperature of PMMA-CO_2 systems can reach values close to room temperature, even below room temperature in some particular conditions, so in this work the desorption (at room temperature) and foaming stages (also performed at room temperature) are not clearly separated.

In previous works it was stablished that the production of the porous structure in neat PMMA samples is obtained by a conventional gas nucleation and foaming process, whereas PMMA/MAM blends present a selective swelling of the soft phase (poly(butyl acrylate)) confined by the surrounding PMMA matrix.[1]

In this study, samples were saturated at different pressures, from 10 to 30 MPa, and at room temperature during 24 h to assure the complete dissolution of CO_2 in the polymer. After this saturation process, foaming was triggered by releasing the pressure inside the vessel at a pressure drop rate between 10 and 30 MPa/min and carried out at room temperature, obtaining bulk white porous samples (Figure S1).

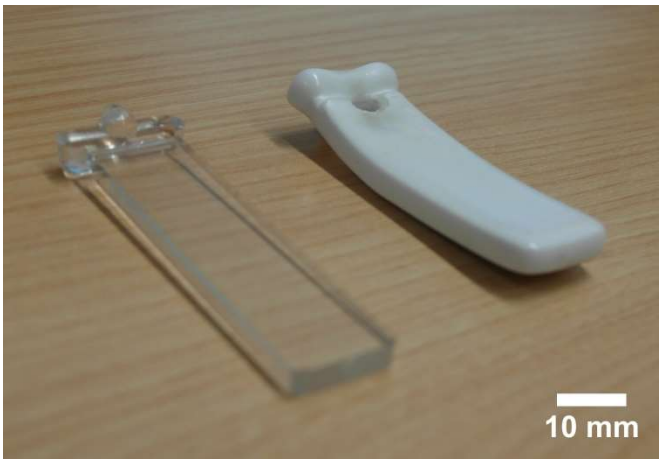

Figure S1. Photographs of the PMMA-based transparent solid injected samples and the white porous samples.

Characterization Procedures

1. Differential Scanning Calorimetry

Characteristic thermal properties of solid and foamed blends were determined by means of a Mettler DSC862 differential scanning calorimeter previously calibrated with Indium. Weight of the samples was around 5 mg. Samples were heated from 20 ºC to 160 ºC at a heating rate of 10 ºC/min in a nitrogen atmosphere. The glass transition temperature (T_g) was taken at the midpoint of the first heat flow-temperature curve.

Usually the determination of the T_g is performed in a second heating cycle, after a previous heating cycle to erase the thermal history of the material; and this procedure has been employed in the study of the confinement of polymers inside nanoporous glass.[2] However, in the present study the T_g of the nanoporous materials was measured in the first heating scan, because in the second heating ramp the T_g was modified due to the collapse of the nanoporous structure at temperatures over its T_g (as self-standing nanoporous materials, they do not have a supporting structure which keeps the

confinement of the polymer phase at temperatures over the confined polymer T_g). However, it can be assumed small or negligible differences between the thermal history of the different porous samples produced in this work, as the processing temperature and time have been the same for all of them.

2. Raman Spectroscopy

Raman spectra were recorded using the Kaiser OSI HoloSpec instrument. The excitation energy for Raman emission was produced by a Horiba JY Induram laser, using laser excitation at 633 nm He-Ne, and laser powers of 8 mW at the sample. The spectra were measured over the wave number range between 0 and 3800 cm^{-1}, with a spectral resolution of 5 cm^{-1}.

The incident laser beam was focused on the surface of the sample with a diameter of 40 microns through an optical system Kaiser Raman OSI head MKII coupled to a Nikon 50 X microscope objective of long focal length.

The Raman spectrum of PMMA has been extensively investigated and correlations between internal vibrational modes and observed bands have been published.[3-6] This spectrum is also valid for the blends of PMMA and MAM since the main chemical groups of these blends are those of PMMA. Moreover, a previous work about the interaction between CO_2 and the PMMA chains demonstrated that the relative intensities of vibrational modes are modified by the CO_2[4]; therefore, it is not possible to compare the relative intensities of solid PMMA samples (without interaction with CO_2) and foamed PMMA samples (after interaction with CO_2). The assignment of the Raman spectrum peaks is shown in Table S2.

Table S2. Poly(methyl methacrylate) Raman spectra and their assignments (vs = very strong; s = strong; m = medium; w = weak; vw = very weak; v_s denotes the symmetric stretching mode; v_a denotes asymmetric stretching mode)

Wave number of the Raman peaks reported previously (cm^{-1})[2-4]	Assignments
537 w	δ (C-C-C)
604 s	v (C-COO), v_s (C-C-O)
736 vw	v (C-C) skeletal mode
812 vs	v_s (C-O-C)
833 vw	v (CH_2)
968 ms	α·CH3 rock
991 ms	O-CH_3 rock
1234 w	v (C-O), v (C-COO)
1276 vw	v (C-O), v (C-COO)
1452 ms	δ_a (C-H) of α-CH_3
1490 w	δ (CH_2)

1736 mw	v (C=O) of (C-COO)
2849 vw	Combination band involving O-CH_3
2920 vw	Combination band involving O-CH_3 and v_s (CH_2)
2954 m	v_s (C-H) of O-CH_3, v_a (CH_2)
3002 m	Overtone involving O-CH_3

The observed spectrum can be split in two parts. The first one belongs to the C-H vibration, including the intense bands at 2954, and 1452 cm^{-1}, and some weak features, as those observable at 2920, 2849, and 3002 cm^{-1}. The other part is related to the C-$COOCH_3$ group (pendant group), including the strong peak at 812 cm^{-1}, which is associated to the vibration mode v_s (C-O-C). In addition, the peak at 3002 cm^{-1} is attributed to the overtone involving O-CH_3.

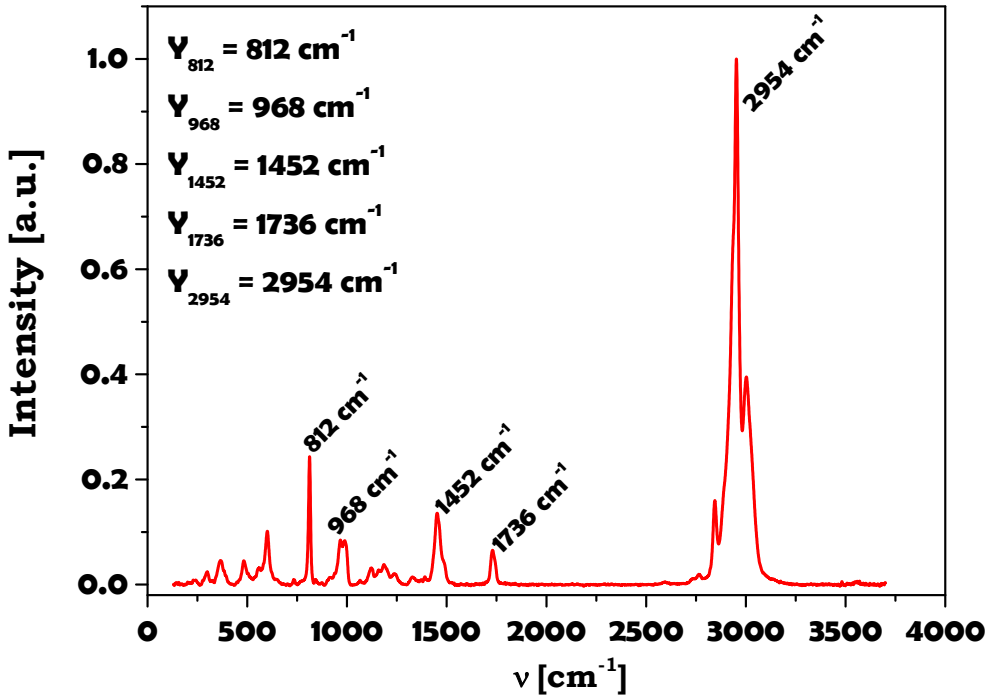

Figure S2. Raman spectra of porous PMMA and identification of peaks selected for the study

The analysis of the Raman spectra was carried out by analyzing the evolution of four relative intensities between six peaks corresponding to vibrational modes of the pendant groups. The peaks selected in this study corresponds to 812, 968, 1452, 1736, and 2954 cm^{-1} (Figure S2). Relative intensities under study were selected according to the following criteria: for each pair of peaks the intensity of the peak of the pendant group or vibrational mode that needs less volume is divided by the intensity of the peak of the pendant group or vibrational mode expected that needs more volume in the vibration. Pendant groups or vibrational modes that need more volume will be more sensible to the confinement (as they are going to be constrained first and before the others needing less volume), and therefore it can be expected that the studied ratios will be sensitive to

the chain conformational changes, increasing when the volume than the chain can occupy is reduced. The intensity ratios under study were Y_{812}/Y_{968} , Y_{812}/Y_{1452}, Y_{1736}/Y_{1452}, and Y_{2954}/Y_{1452}.

For instance, in the case of the relative intensity Y_{812}/Y_{968}, the CH_3 group occupies more volume than the C-O-C group. Likewise, more volume is required to carry out the rock vibration than to perform the stretching one. Thus, in the nanometer scale, where movements are limited due to the reduction of pore walls thickness, the ratio between the intensity of the C-O-C group is higher than the intensity of the CH_3 group should increase in the nanometer scale than in the micrometer scale.

3. DC Electrical Resistivity

Resistivity measurements of solid and foamed polymers were determined using a Keithley Resistivity Adapter model 6105 according to ASTM D257-99.[7]

Samples were first dried, and then conditioned at controlled temperature and humidity (23 ºC and 50% humidity) at least three days before being measured in order to avoid discrepancies in the measurements due to differences in temperature or humidity between the different samples. Then, samples were measured four times at +500 V, -500 V, + 500 V, -500 V. Time of electrification was 60 seconds, and the time of discharge before making a measurement with reversed voltage was 4 minutes.

Resistivity (R) was calculated using Equation S1.

$$R = \frac{A \cdot V}{t \cdot I} \qquad [S1]$$

Where A and t are the area and thickness of the sample respectively, V the voltage applied, and I the current intensity measured.

Graphical representation of the DC electrical resistivity results was done normalizing the resistivity values by the relative density of the porous materials, to remove the effect of the relative density on these measurements.

4. Broadband Dielectric Spectroscopy

Broadband dielectric spectroscopy (BDS) provides information on the molecular dynamics and conductivity processes. The molecular fluctuations of the dipoles in the polymer chains result in relaxation phenomena, which are observed as peaks in the dielectric loss with characteristic relaxation times and shapes. Meanwhile, conductivity phenomena are observed as an increase of the dielectric loss with decreasing frequency.[8]

These measurements were performed on an ALPHA high-resolution dielectric analyzer. Square-shaped samples were held in the dielectric cell between two parallel gold-plated electrodes. The thickness of the samples (around 1000 μm) was taken as the distance between the electrodes and determined using a micrometer gauge.

The dielectric response of each sample was assessed by measuring the complex capacity $C^*(w) = C'(w) - jC''(w)$ over a frequency range window of 10^{-2} to 10^5 Hz at 23 ºC. The amplitude of the alternating current (ac) electric signal applied to the samples was 1 V.

Electrical resistivity results were analyzing by normalizing by the relative density of the porous materials, to remove the effect of the relative density on these measurements.

Dielectric strength (Δε) was obtained by adjusting the experimental results obtained at 23º C to the equation of Havriliak-Negami.

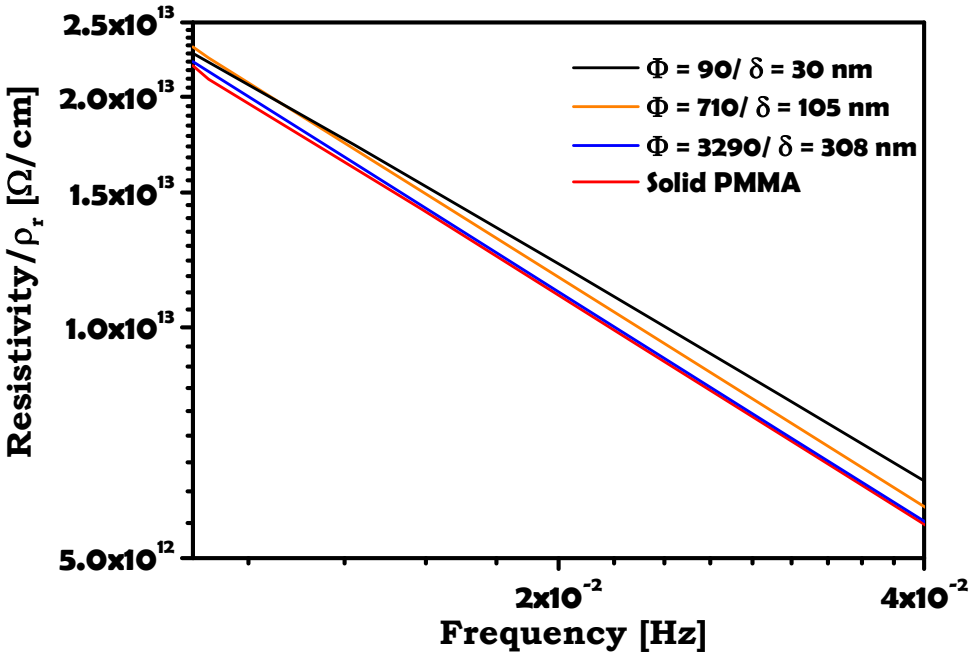

Figure S3. Resistivity of most representative neat PMMA porous and solid samples measured in the low frequency range.

Resistivity measurements at medium-high frequencies (**Figure S3**) show that microporous materials present a similar behavior as DC measurements (**Figure 2.b)**, with resistivity values near to the solid PMMA results; on the contrary, nanoporous materials do not show the same behavior as DC measurements, increasing their resistivity when the pore size decreases, as can be expected assuming a rising tortuosity related to the decrease of the pore size. However, the picture changes substantially at low frequencies (**Figure S3**). Resistivity differences between solid PMMA and porous

samples with pore size about or over the micron remain practically constant; but the resistivity of nanoporous samples is decreased proportionally to the reduction of the frequency, reaching values near the resistivity of both solid and microporous PMMA. This effect can be related to the presence of the MWS phenomenon in nanoporous samples, explaining the behavior found in DC measurements where both effects, rising tortuosity and MWS, can take place in porous samples with pore sizes below the micron.

5. Porous Structure

Pore size and polymer pore wall thickness of porous polymers were analyzed by means of a scanning electron microscope (SEM, model Quanta 200FEG, FEI). Samples were freeze-fractured in liquid nitrogen to assure that the microstructure or nanostructure remained intact. The fractured surface was sputter-coated with gold using a sputter coater (model SCD 005, Balzers Union).

Pore sizes were determined using an specific image processing software[9] based on ImageJ/FIJI[10]. This software provides the average pore size, pore density, and the pore size distribution, among other relevant structural parameters.

Polymer pore wall thickness was determined by measuring the thickness of the pore wall directly in the SEM micrograph with the help of the software ImageJ/FIJI. Several measurements were performed on each sample and the average value was calculated.

SEM micrographs of the samples under studio can be found in Figure 1 and Figure S4.

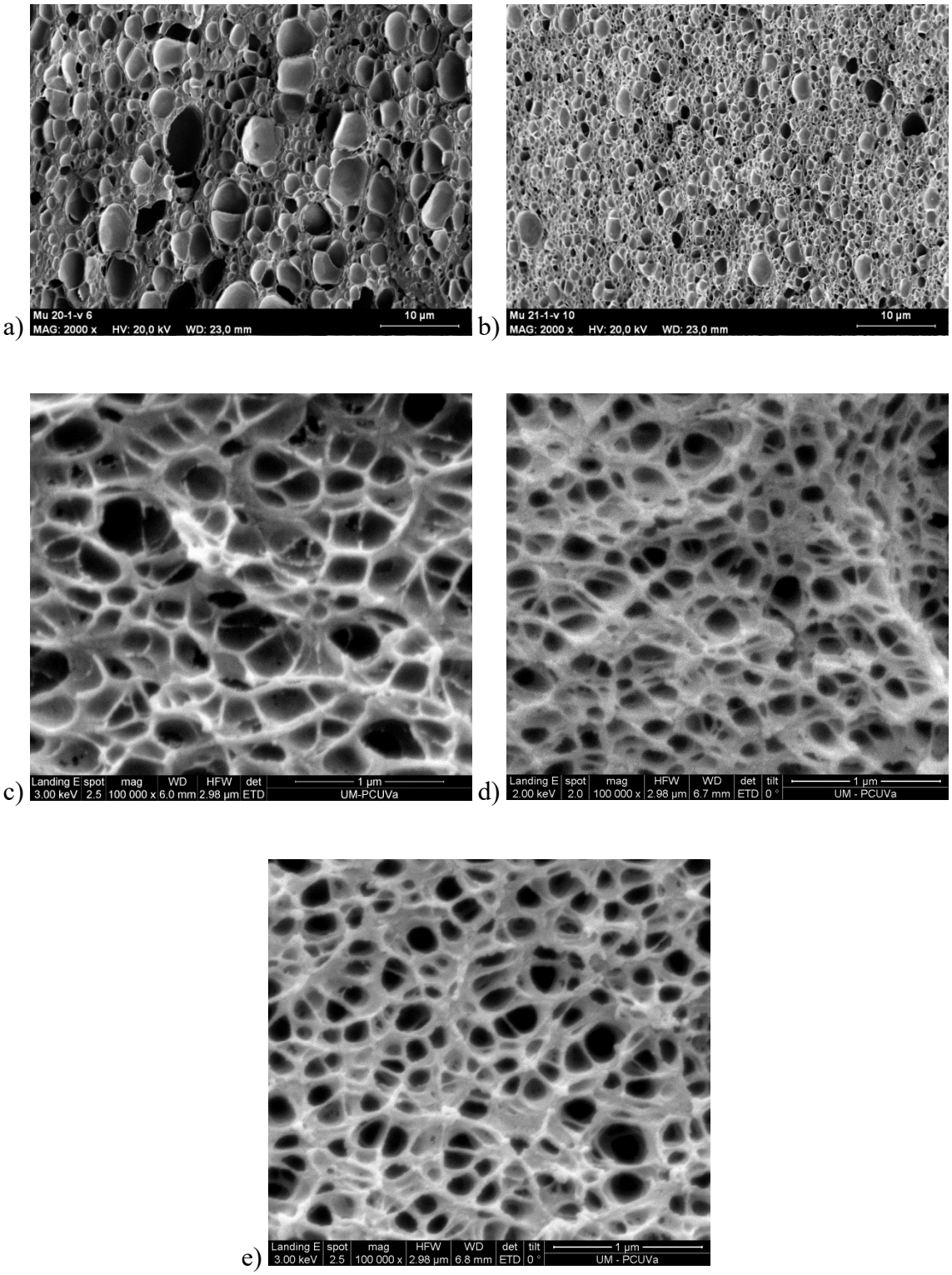

Figure S4. SEM micrographs of a) Neat PMMA produced at 15 MPa, b) Neat PMMA produced at 20 MPa, c) Neat PMMA produced at 25 MPa, d) 90/10 PMMA/MAM produced at 15 MPa, and e) 90/10 PMMA/MAM produced at 20 MPa.

Estimation of the Confinement Effect Boundary and Radius of Gyration of PMMA

Some studies about the confinement effect on the chain conformation relate the appearance of this effect with the characteristics of the polymer chains under study. In particular, Kraus et al.[11] determined, both experimentally and by modelling, that the confinement effect on thin films appears when the films thickness reaches a value below six times the radius of gyration of the polymer chains. As the pore walls can be considered two-dimensional structures similar to thin films, we have estimated the pore wall thickness values where confinement effect should be noticed, using that relationship between the radius of gyration and the confinement effect, and determining the radius of gyration with the equation proposed for PMMA by Kirste et al.[12] (Equation S3).

$$< r^2 > = 0.096 \cdot M_w^{0.98} \qquad \text{[S3]}$$

Where M_w is the average molecular weight of the PMMA chains ($M_w^{PMMA} = 83000$ g/mol). It is obtained a value of 7.97 nm for the radius of gyration of our PMMA, and therefore the expected thickness boundary for the confinement effect should be about 47 nm.

Interfacial effects on molecular confinement of polymer chains

In several works[13-16] dealing with polymers as thin films or within silica nanopores (which are the confining systems), a complex competition occurs between several conflicting phenomena that interfere with the analysis: restricted chains dynamics, disentanglement, surface chemistry and nature of confining system, adsorption at

surfaces, topology of the confinement system, or even small changes in composition brought by a miscible polymer-"pollution" (acting as a plasticizer). The resulting dominant effect is often an increase in T_g (when thickness or pore diameter decreases), but also sometimes, T_g has been observed to decrease.

References

1. J. Pinto, M. Dumon, M. Pedros, J. Reglero, M. A. Rodriguez-Perez, *Chemical Engineering Journal* **2014**, *243*, 428.

2. J.-Y. Park, G. B. McKenna, *Physical Review B* **2000**, *61*, 6667.

3. H. A. Willis, V. J. I. Zichy, P. J. Hendra, *Polymer* **1969**, *10*, 737

4. X. Xingsheng, M. Hai, Z. Qijing, Z. Yunsheng, *Journal of Optics A: Pure and Applied Optics* **2002**, *4*, 237.

5. T. Ikeda-Fukazawa, D. Kita, K. Nagashima, *Journal of Polymer Science Part B: Polymer Physics* **2008**, *46*, 831

6. K. J. Thomas, M. Sheeba, V. P. N. Nampoori, C. P. G. Vallabhan, P. Radhakrishnan, *Journal of Optics A: Pure and Applied Optics* **2008**, *10*, 055303.

7. ASTM, *Vol. D 257-99*, *ASTM International*, **2005**, 18.

8. *Broadband dielectric spectroscopy*, (Eds: F. Kremer, A. Schönhals), Springer-Verlag Berlin Heidelberg, **2003**.

9. J. Pinto, E. Solórzano, M. A. Rodriguez-Perez, J. A. de Saja, *Journal of Cellular Plastics* **2013**, *49*, 555.

10. M. D. Abràmoff, P. J. Magalhães, S. J. Ram, *Biophotonics international* **2004**, *11*, 36.

11. J. Kraus et al., *Europhysics Letters* **2000**, *49*, 210.

12. R.G. Kirste et al., *Polymer* **1975**, *16*, 120.

13. I-M. Kalogeras, *Acta Materialia* **2005**, *53*, 1621.

14. S. Kim, M-K. Mundra, C-B. Roth, J-M. Torkelson, *Macromolecules*, **2010**, *43*, 5158

15. H. Oh, P-F. Green, *Macromolecules,* **2008**, *41*, 2561

16. I-M**.** Kalogeras, E-R**.** Neagu**,** *The European Physical Journal E*, **2004**, *14*, 193

II.3. References

1. Lu X, Caps R, Fricke J, Alviso CT, and Pekala RW. Journal of non-crystalline solids 1995;188(3):226-234.
2. Schmidt D, Raman VI, Egger C, du Fresne C, and Schädler V. Materials Science and Engineering: C 2007;27(5–8):1487-1490.
3. Keddie JL, Jones RAL, and Cory RA. Europhysics Letters 1994;27:59-64.
4. Yang Z, Clough A, Lam C-H, and Tsui OKC. Macromolecules 2011;44(20):8294-8300.
5. Forrest JA, Dalnoki-Veress K, and Dutcher JR. Physical Review E 1997;56.
6. Reglero Ruiz JA, Dumon M, Pinto J, and Rodriguez-Pérez MA. Macromolecular Materials and Engineering 2011;296(8):752-759.
7. Miller D and Kumar V. Polymer 2011;52(13):2910-2919.
8. Notario B, Pinto J, and Rodriguez-Perez MA. Polymer 2015;63:116-126.
9. Forrest JA, Dalnoki-Veress K, Stevens JR, and Dutcher JR. Physical review letters 1996;77(10):2002-2005.
10. tsui OKC, Russell TP, and Hawker CJ. Macromolecules 2001;34(16):5535-5539.
11. Forrest JA, Dalnoki-Veress K, and Dutcher JR. Physical Review E 1997;56(5):5705-5716.

THERMAL CONDUCTIVITY

Belén Notario Collado

Chapter III. Thermal Conductivity

One of the most extended applications of cellular polymers is thermal insulation (buildings, pipes, fridges, transport, cryogenic applications, etc.) with a high social, environmental, and economic impact. It is estimated that about 31 % of the total energy consumption of the west countries is related to the climatization of dwelling houses, being the space heating more than 50 % of this energy (Figure III.1) [*Energy Efficiency Trends in Buildings in the EU*, *September 2012*, project co-funded by the European Union].

Thus, the development of improved thermal insulation materials can have a significant impact on both economic savings and reductions of CO_2 emissions.

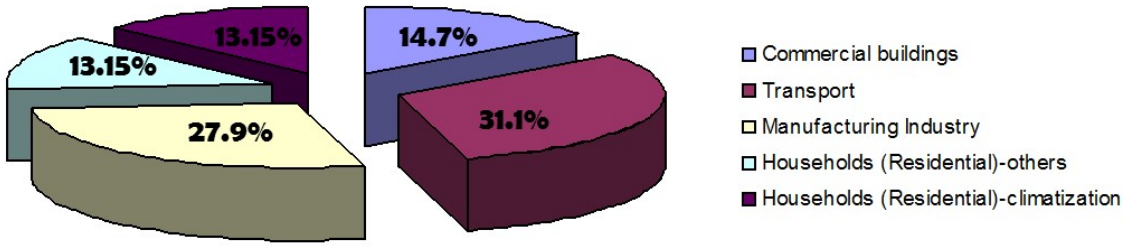

Figure III.1. Energy consumption in the European Union in 2012.

Nanocellular polymers are expected to be high performance insulation materials, due to the decrease of the heat conduction transfer through the gaseous phase (i.e. Knudsen effect [1], see section *III.2 Theoretical Background*). Confirmation of this phenomena and further development of these materials could lead to a new generation of high performance thermal insulation materials, with huge impact on the global socioeconomic framework.

III.2. Theoretical Background

The main advantage of cellular materials as thermal insulators is that the thermal conductivity of the polymer matrix, usually not so high, is reduced by the addition of the gaseous phase (with a much lower thermal conductivity).

The evaluation of the thermal conductivity of cellular materials from the conductivity data of the two component phases and the structure of the material is an interesting topic that has been approached by different authors [2-5]. It is assumed that the total thermal conductivity (λ_t) can be described by four different contributions (Eq. III-1):

$$\lambda_t = \lambda_g + \lambda_s + \lambda_c + \lambda_r \qquad \text{(III-1)}$$

Where λ_g is the conduction across the gas phase, λ_s is the conduction along the cell walls and struts of the solid material, λ_c represents the convection within the cells, and λ_r is the thermal radiation term.

It is widely accepted that convection plays a minor role in closed cell materials with cell sizes below 4 mm[6], and in open cell materials with cell sizes lower than 2 mm [7].

The effective thermal conductivity of air-filled cellular structures can be described by the Ashby model (Eq. III-2):

$$\lambda_t = \lambda_s + \lambda_g = g\lambda_s(1 - V_g) + \lambda_g V_g \quad \text{(III-2)}$$

Where *g* is an efficiency factor which allows for the tortuous shape of the cell walls and which ranges between 1/3 and 1, and V_g represents the volume fraction of voids [8].

The effective thermal conductivity of the gas phase can be described also by the Knudsen equation [7]:

$$\lambda_g = \lambda_{g0}/(1 + \beta Kn) \quad \text{(III-3)}$$

Where λ_{go} is the thermal conductivity of the gas (usually air, λ_{air} = 0.026 W/mK at room temperature and pressure), β is a parameter that takes into account the energy transfer between gas molecules and the limiting solid structure (about 2 for air), and *Kn* is the Knudsen number that is obtained by dividing the mean free path of the gas molecules (l_g ≈ 70 nm for air at room temperature) between the average pore diameter (Φ):

$$Kn = l_g/\Phi \quad \text{(III-4)}$$

Combining equations III-3 and III-4 follows that λ_g decreases significantly when the cell size decreases below the micron. Thus for cellular materials with cells sizes in the nanometer range, a reduction of the thermal conductivity of the gaseous phase should be expected.

In the case of the radiation term, it can be calculated in microcellular polymers using the Williams and Aldao model [2] whereas in nanocellular polymers the conventional models to calculate the radiation terms are not suitable. Models for the calculation of the radiation term on cellular polymers usually assume that the wavelength of the infrared radiation is lower than the cell size of the foam, but in nanocellular polymers this assumption is not right. However, some theoretical results predicted that the radiation term could present an insignificant contribution on nanocellular polymers even at low densities [9]. Then, the radiation term will be neglected in the theoretical predictions of the thermal conductivity of nanocellular polymers; but it should be taking into account that it is not possible to ensure that the radiation term is negligible at low densities on nanocellular polymers, as there is no experimental evidence.

Williams and Aldao model gives acceptable values of the thermal radiation term by considering the main characteristics of cellular structure, the thickness of the cellular material, and the optical properties of the solid material. The model is based on a radiation term predicted as follows:

$$\lambda_r = \frac{4\sigma T^3 L}{1 + \left(\frac{L}{\Phi}\right)\left(\frac{1}{T_N} - 1\right)} \quad \text{(III-5)}$$

Where σ is the Stefan-Boltzman constant, T the temperature, L the material thickness (in our case L = 5 mm), Φ the cell size, and T_N is the net fraction radiant energy sent forward by a solid membrane of thickness L_s (more details about this model are given in the article of this chapter)

Therefore, with the complete model (Ashby + Knudsen + Radiation (estimated in microcellular polymers and neglected in nanocellular polymers)), the contribution (in percentage) of each term of the total thermal conductivity is evaluated as a function of the relative density (Figure III.2) for two different cases: a PMMA-based foam in the micrometer range (Figure III.2 left – top and bottom) and a PMMA-based foam in the nanometer range (Figure III.2 right – top and bottom).

As it can be observed, the contribution of the gaseous phase becomes the main component of the cellular material thermal conductivity at the relative densities usually employed in thermal insulation (below 0.1) (Figure III.2a). For instance, for a relative density of 0.1 the gas phase contribution is about 50 %, the solid phase contributes with 40 %, and the radiation term contribution is around 10 % of the total conductivity. Then the total thermal conductivity at low relative densities is significantly higher than that of the solid matrix (Figure III.2c).

In nanocellular materials theoretical models predict that the contribution of the solid phase will remain the predominant term even at very low densities (unlike microcellular polymers), being achieved by the gas thermal conductivity (50 % solid – 50 % gas) only at relative densities around 0.05 (assuming a cell size of 100 nm) (see Figure III.2b). Meanwhile the radiation term is expected to present an insignificant contribution on nanocellular foams even at low densities [10]. Moreover, if smaller cell sizes are considered (e.g. 10 nm), then the gaseous contribution will be negligible even at very low densities.

Thus, when the cell size is reduced to the nanometer regime, the overall thermal conductivity is decreased in comparison with microcellular polymerss (Figure III.2 c and d). For instance for a relative density of 0.1 the overall thermal conductivity of nanocellular polymers is reduced by a factor of 2. This fact is mainly attributed to the reduction of the thermal conductivity of the gaseous phase.

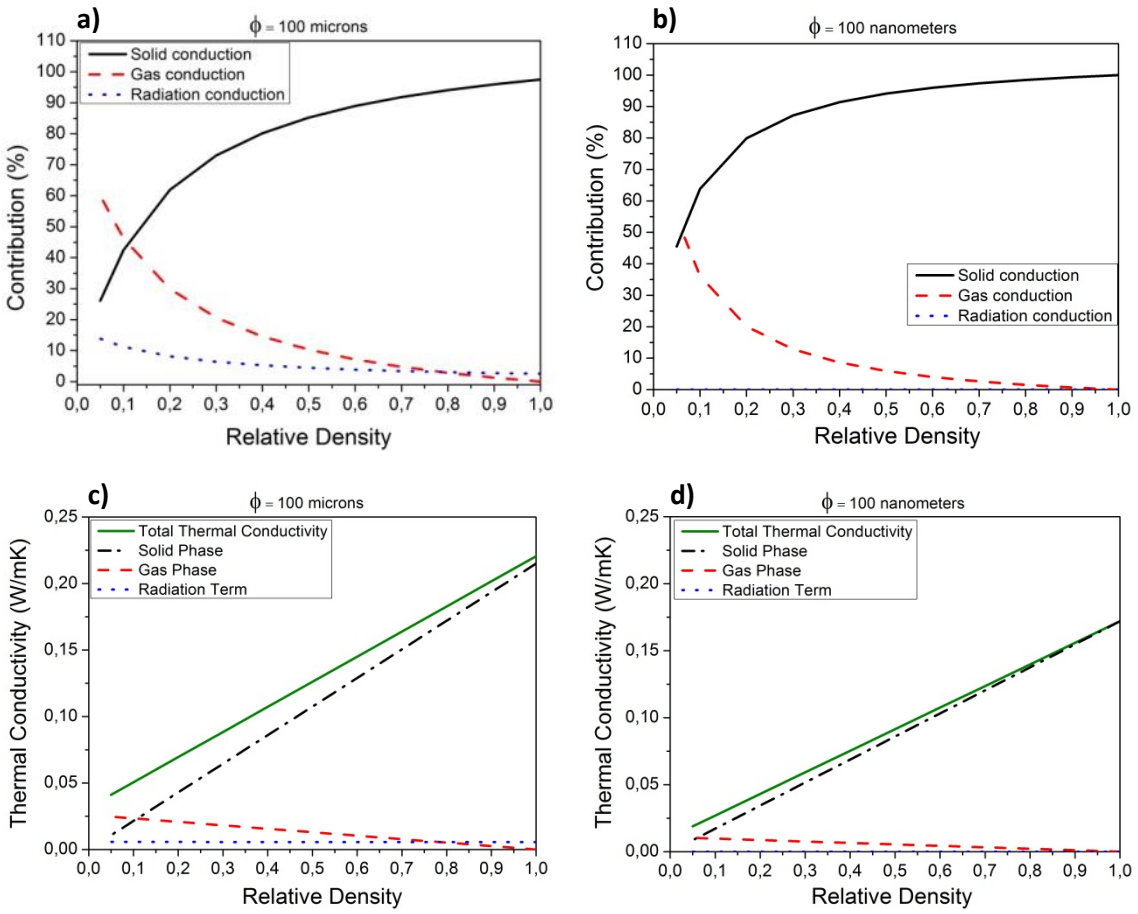

Figure III.2. Top: Contribution (in percentage) of the solid phase, gaseous phase, and radiation term to the thermal conductivity of a polymer foam: a) microcellular polymer (Φ = 100 µm), b) nanocellular polymer (Φ = 100 nm).
Bottom: Thermal conductivity of the solid phase, gaseous phase, radiation term, and total thermal conductivity of a polymer foam: c) microcellular polymer (Φ = 100 µm), d) nanocellular polymer (Φ = 100 nm).

Then, the main challenge in thermal insulation with foams is to decrease the thermal conductivity of the gaseous phase.

In this sense nanocellular polymers arise as one promising approach to reduce the thermal conductivity at room temperature because it is expected that these materials will present the so called Knudsen effect [1, 11]. This phenomenon implies that when the cell size is comparable or smaller than the mean free path of the gas phase, the molecules of the latter collide more often with the molecules forming the solid part than among them. A schematic representation of this effect can be found in Figure III.3, where the gas molecules are represented assuming a radius equal to their mean free path (l_g).

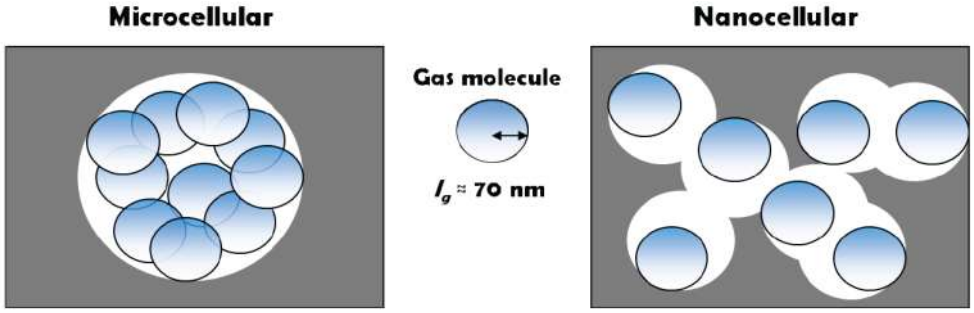

Figure III.3. Behavior of gas molecules of air in microcellular foams (left) and in a nanocellular foams with pore diameter similar to the mean free path l_g of the gas phase (right). Gas molecules interact between them in the microcellular foams, allowing the heat transmission; whereas no interaction, or a reduced one, is found between the gas molecules on the nanocellular polymer, reducing the heat transfer through the gas phase.

As it can be observed in Figure III.2b and d and also in Figure III.4 (theoretical reduction of the thermal conductivity of the gas phase (assuming air as the gas in the cells and pore size about 100 nm) due to Knudsen effect), the contribution of the gaseous phase strongly reduces when cell size is below the micron.

The shadow area of Figure III.4 represents the cell size range of selected PMMA/MAM and PE cellular polymers employed in this chapter. Also PE foams were employed as reference materials in which Knudsen effect should not appear due to a large cell size. This material allows us testing the validity and accuracy of the developed experimental methodology, since it was the first time that this approach has been successfully employed in cellular polymers.

All the selected samples present an open cellular structure, which allow extracting the gas inside the cellular materials in order to perform the measurements, explained in detail in the article included at the end of this section.

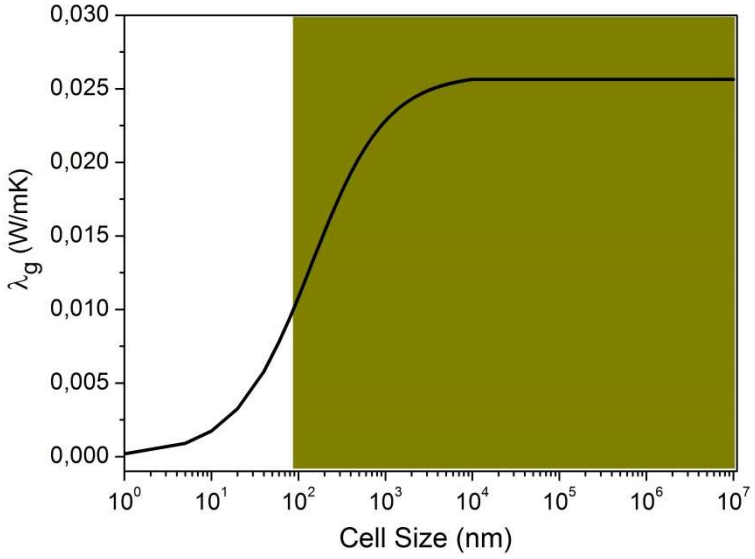

$$\lambda_g = \frac{\lambda_{g0}}{\left(1 + \beta\left(l_g/\Phi\right)\right)}$$

Figure III.4. Predicted relationship between the air thermal conductivity and the cell size due to the Knudsen effect. Shadow area in dark yellow represents the cell size range of selected PMMA/MAM and PE cellular polymers used for this study. Knudsen equation has been included on the right side of the curve, where λ_g is the thermal conductivity of the gaseous

phase, λ_{g0} is the thermal conductivity of free air (0.026 W/m·K at room temperature), β is a parameter that takes into account the energy transfer between gas molecules and the limiting solid structure (about 2 for air), l_g is the mean free path of the gas molecules ($l_g \approx 70$ nm at room temperature), and Φ is the average pore diameter.

As Figure III.4 shows, our nanocellular and microcellular polymers cover an appropriate range to be able to elucidate the Knudsen effect. A study about this phenomenon was carried out and published in **Polymer 56 (2015)**, with the title **"*Experimental Validation of the Knudsen Effect in Nanocellular Polymeric Foams*"**.

In this work it has been demonstrated for the first time that on the one hand Knudsen effect takes place in nanocellular polymers, and on the other hand that the developed methodology is appropriate to detect the presence of this effect.

The reduction of the conductivity of the gaseous phase due to the Knudsen effect was somewhat expected that had been previously demonstrated both theoretically and experimentally (aerogels), presenting the experimental results a good agreement with the theoretically expected trends [11, 12].

Polymer 56 (2015) 57–67

Contents lists available at ScienceDirect

Polymer

journal homepage: www.elsevier.com/locate/polymer

Experimental validation of the Knudsen effect in nanocellular polymeric foams

B. Notario [a], J. Pinto [a, b], E. Solorzano [a], J.A. de Saja [a], M. Dumon [c], M.A. Rodríguez-Pérez [a, *]

[a] Cellular Materials Laboratory (CellMat), Condensed Matter Physics Department, University of Valladolid, 47011 Valladolid, Spain
[b] Nanophysics – Smart Materials Group, Istituto Italiano di Tecnologia (IIT), Via Morego, 30, 16163 Genova, Italy
[c] Laboratoire de Chimie de Polymères Organiques (LCPO), Institut Polytechnique de Bordeaux (IPB), 16 Avenue Pey Berland, 33607 Pessac-Cedex, France

ARTICLE INFO

Article history:
Received 31 July 2014
Received in revised form
26 September 2014
Accepted 1 October 2014
Available online 12 October 2014

Keywords:
Nanocellular foams
Knudsen effect
Thermal conductivity

ABSTRACT

This paper is focused on demonstrating that it is possible to reduce the thermal conductivity of polymeric foams by reducing the average cell size below the micron. For this purpose, a wide set of samples with cell sizes from 90 nm to 100 μm and relative densities from 0.12 to 0.6 has been produced and analyzed. In addition, a characterization procedure that allows identifying independently some of the heat transfer mechanisms in polymeric foams has been developed. As a result, it has been demonstrated that Knudsen effect takes place in nanocellular polymeric foams, being this effect very positive to reduce the overall heat transfer.

Through the understanding of the underlying mechanisms it has possible to model the thermal conductivity behavior of these materials in the entire range of cell sizes, and overall porosities. It has been proved that the reduction of the cell size has an effect on the thermal conductivity through the solid phase, this contribution is reduced due to an increment of the tortuosity of the cellular structure and/or a confinement effect in the polymeric matrix.

1. Introduction

Households represent about a 25% of the total energy consumption of the occidental countries, being the space heating more than 50% of this energy (from 60 to 80% in European countries in 2010 [*Energy Efficiency Trends in Buildings in the EU, September 2012*, project co-funded by the European Union)]). Then, by increasing the efficiency of the households heating, and therefore decreasing this energy consumption, it would be possible to obtain both significant economic savings and reductions of the CO_2 emissions. In fact, new dwellings built in 2009 consumed 30%–60% less than dwellings built in 1990 due to the thermal regulations developed in this period.

One of the main strategies to increase the efficiency of the households heating is to improve the thermal insulation of the dwellings, being cellular polymers widely used with this purpose. Their main advantage of these materials is that the thermal conductivity of the polymer matrix, usually not so high, is reduced by the addition of a gaseous phase with a much lower conductivity. For this reason, the analysis of the thermal conductivity of cellular materials from their two component phases and their structure is an interesting topic that has been extensively studied by different authors [1–8].

In a cellular material, it is assumed that the total thermal conductivity (λ_t) can be described by four different contributions (Eq. (1)):

$$\lambda_t = \lambda_g + \lambda_s + \lambda_c + \lambda_r \quad (1)$$

where λ_g is the conduction across the gas phase, λ_s is the conduction along the cell walls and struts of the solid material, λ_c represents the convection within the cells, and λ_r is the thermal radiation term.

In order to reduce the thermal conductivity, there are different approaches. Conduction across the solid phase (λ_s) can be decreased through the development of low density foams in which the contribution of the solid matrix is reduced. The addition of micro-particles and nanoparticles (such as carbon black, carbon nanotubes, etc.) to the polymer matrix allows reducing the radiative term (λ_r) due to an increment of the mean extinction coefficient [9,10].

* Corresponding author.
E-mail address: marrod@fmc.uva.es (M.A. Rodríguez-Pérez).

http://dx.doi.org/10.1016/j.polymer.2014.10.006
0032-3861/

On the other hand, it is widely accepted that convection plays a minor role in closed cell materials with cell sizes below 4 mm [11] and also in open cell materials with cell sizes lower than 2 mm [12]. Then, the convection term (λ_c) can be suppressed by developing cellular polymers with cell sizes below 2 mm.

And finally, conduction through the gas (λ_g) phase can be reduced by using two different strategies:

The first one aims at substituting the gas inside the cells, usually air ($\lambda_{air} = 0.026$ W/m K at room temperature), by gases with lower thermal conductivity. But this approach presents two disadvantages: first of all, the gas should be retained inside the foam (which is actually very difficult in the long-term); and secondly, the typical gases with good performance are not very convenient from the environmental point of view. Thus, this method although it is still very common in commercial products is not an optimum solution.

The second approach involves reducing the cell size to the nanometer range, because it is expected that these nanocellular materials present the well-known Knudsen effect [10,13].

This effect implies that when cell size is comparable or smaller than the mean free path of the liquid or gas, the molecules of the latter collide more often with the molecules forming the surrounding solid part than among them. Therefore, the energy transfer through the gas molecules is reduced.

Then, in gas-filled cellular structures, the effective gaseous thermal conductivity (λ'_g) can be described by the Knudsen equation [10]:

$$\lambda'_g = \frac{\lambda'_{go}}{(1+\beta Kn)} \tag{2}$$

where λ'_{go} is the thermal conductivity of the gas (usually air, $\lambda_{air} = 0.026$ W/m K at room temperature and pressure), β is a parameter that takes into account the energy transfer between gas molecules and the limiting solid structure (about 2 for air), and Kn is the Knudsen number that is obtained by dividing the mean free path of the gas molecules ($l_g \approx 70$ nm for air at room temperature) between the average pore diameter (Φ):

$$Kn = \frac{l_g}{\Phi} \tag{3}$$

Combining Eqs. (2) and (3) is obtained that λ'_g decreases significantly when the cell size decreases below the micron. Thus for cellular materials with cells sizes in the nanometer range a reduction of the thermal conductivity of the gaseous phase should be expected. This strategy has the additional advantage of being time independent, so the thermal conductivity is effectively reduced in long-term.

This phenomena was studied by L.W. Hrubesh and co-workers [9] who analyzed how to reduce the thermal conductivity of air-filled aerogels through the analysis of the three major components of thermal transport (conduction through the solid and gas phases, as well as radiation). They found, among others mechanisms, that a reduction of the pore size resulted in a significant reduction of the thermal conductivity of the gaseous phase. This reduction of the thermal conductivity was justified by the Knudsen effect.

Meanwhile, X. Lu et al. [10] studied the correlation between the structure of resorcinol-formaldehyde (RF-) aerogel monoliths and their thermal conductivity. They observed that pore size clearly influenced the conductivity through the gas phase due to the Knudsen effect, obtaining extremely low thermal conductivity values.

Polyisocyanurate aerogels were synthesized by O.J. Lee et al. [14], and their thermal conductivity was determined from vacuum to ambient pressure in order to determine their average pore size. They found that thermal conductivity data can be used to estimate the average pore size using Knudsen equations.

Zirconia ceramics with pore volume fractions from 45 to 75% and pore sizes below 100 nm were prepared and their thermal conductivity was characterized by B. Nait-Ali and co-workers [15]. They concluded that for obtaining a thermally insulating material, the microstructure should exhibit a high volume fraction of pores, which should be as small as possible in order to reduce the thermal conductivity through the gas phase, as Knudsen effect predicts.

Therefore, Knudsen effect has been previously experimentally demonstrated in aerogels or porous ceramics [9,10,14–17], and also in dynamic fluids [18,19]. However, as far as we know, there are not experimental results showing this effect in polymeric foams (i.e. polymeric porous materials obtained by a foaming process); probably due to the technical difficulties associated to the production of nanocellular polymeric foams with appropriate density, cell sizes and external dimensions to characterize their properties as thermal insulating materials.

Nevertheless, there are some theoretical works [20,21] in which the thermal conductivity behavior of microcellular and nanocellular polymeric foams have been studied. C. Forest and co-workers [20] studied the different heat transfer mechanisms of a polystyrene foam with cell sizes both in the micro and nanometer range. First of all, they showed how thermal conductivity of the gaseous phase decreases as cell size decreases due to the Knudsen effect. In addition, they carried out a comparative study between the Ashby model and a model developed for aerogels [9] for the conduction through the solid phase, obtaining that the model developed for aerogels underestimates the contribution of the solid matrix.

The effect of cell size on the thermal conductivity of polymer foams was also analyzed by S.S. Sundarram et al. [21] using finite element analysis and molecular dynamics simulation methods. They observed a significant reduction of the thermal conductivity when cell is reduced from the micrometer to the nanometer range. They stated that this decrease of the thermal conductivity is mainly due to the phonon scattering effect in the solid polymer matrix, being the Knudsen effect less important. Likewise, for a constant relative density, a reduction of the gas phase contribution is predicted when cell size is reduced from 500 μm to 10 μm. However, this unexpected behavior, according to the Knudsen equations, is not found in the present work: foams with cell sizes around 10 μm and foams with cell sizes around 1000 μm present the same gaseous thermal conductivity.

Nanocellular materials and, in particular, nanocellular polymeric foams are promising materials in the cellular materials field due to the expected improvement in some of their physical properties in comparison with conventional or microcellular foams [13,22]. It is expected that these materials will have better mechanical properties than those of conventional cellular materials or microcellular materials [23]. In addition, it is expected that if amorphous transparent polymers are foamed obtaining materials with cell sizes below 50 nm, the cellular material could keep the transparent character of the former solid [24]. Therefore, using these novel materials it would be possible to generate products that cannot be manufactured nowadays.

The most promising technique used to produce nanocellular polymeric foams is the gas dissolution foaming process and in particular the high-pressure or supercritical CO_2 gas dissolution foaming, where CO_2 is used as a physical blowing agent [25–28]. Also, CO_2 presents several advantages for this process due to its excellent characteristics of diffusion in the supercritical state, and the relatively mild conditions to reach this state (31 °C and 7.3 MPa). Likewise, carbon dioxide is a *green* solvent that can be

removed without residue or production of any pollutant compound [29,30].

One of the main difficulties of foaming processes to produce nanocellular structures resides in the thermodynamics of the polymer-gas systems. Formation of nanometric cells leads to a huge increment of the interfacial (surface) area and the interfacial (surface) free energy, being necessary the use of different approaches to achieve the high cell nucleation densities needed to produce nanocellular foams (above 10^{14} nuclei/cm^3).

It is known that the addition of several types of particles that could act as nucleating agents (like talc, titanium oxide, nanosilica, and other type of nanoparticles) leads to an increase of the potential nucleation sites [31,32]. Also, the increase of the pressure drop rate and the increase of the saturation pressure involve a higher number of nuclei formed by homogeneous nucleation [27]. And finally, the use of copolymers, both block copolymers [33–35] and random copolymers [36], can enhance the nucleation up to values appropriate to produce nanocellular foams.

Recently, different approaches have been carried out to produce nanocellular foams: Costeux and Zhu obtained nanocellular foams with cell sizes between 100 and 300 nm, and relative densities between 0.15 and 0.3. They use acrylic copolymers and silica nanoparticles [32]. Homogeneous polyetherimide (PEI) foams with cell sizes between 40 and 100 nm and relative densities from 0.36 to 0.75 were produced by Aher and co-workers [37]. Also, Costeux et al. obtained nanocellular foams of styrenic and acrylic polymers with cell sizes below 100 nm and relative densities from 0.3 to 0.4 [38].

By the use of the block copolymer approach, nanocellular foams can be produced from blends of PMMA [poly(methyl methacrylate)] and MAM triblock copolymer [poly(methyl methacrylate)-block poly(butyl acrylate)-block poly(methyl methacrylate)] [34,35,39,40]. Previous studies showed that PMMA-based nanocellular foams present a nanosized cellular structure (cell sizes around or lower than 200 nm) and a high cell nucleation density up to 10^{14} cells/cm^3 [34,39]. Also, Pinto et al. demonstrated that the final cellular structure of the foam is controlled by the nanostructure of the solid precursor, being this structure almost independent of the foaming parameters [34,40].

Taking advantage of this production route based on PMMA/MAM blends, that allows controlling the porosity of the foams, and the morphology and size of the cells [40], a wide range of foams with homogeneous cellular structures, cell sizes from 90 nm to 100 μm and relative densities from 0.12 to 0.6 have been produced in this study. Furthermore, the produced samples had suitable dimensions to be thermally characterized with the main objective of providing an experimental validation of the Knudsen effect in polymeric foams. With this purpose, an appropriate experimental set-up has been developed and a special protocol to carry out the measurements has been established.

2. Experimental part

2.1. Materials and production process

Optically transparent poly(methyl methacrylate) (PMMA) and block copolymer poly(methyl methacrylate)-co-poly(butyl acrylate)-co-poly(methyl methacrylate) (MAM) were kindly supplied by Arkema Company (France) in the form of pellets. PMMA presents a glass transition temperature (T_g) about 112 °C and a density (ρ) of 1180 kg/m^3. MAM triblock copolymer, 36 wt% of poly(butyl acrylate) (PBA) has a density of 1080 kg/m^3.

Polymer blends of PMMA containing 5, 50, and 75 wt. % of MAM were produced as follows. Both materials, PMMA and MAM, were dried in vacuum (680 mm Hg) at 80 °C during 4 h before processing. Mixing and extrusion were carried out using a Scamex CE02 single-screw extruder ($L/D = 28$ $d = 45$ mm) with a temperature profile from 165 to 225 °C at a screw speed of 60 rpm in the desired proportions. Pellets were produced using a continuous cutting machine operating at the end of the line at a constant speed of 240 rpm.

In a second step, these blends and the neat PMMA and MAM were injection molded into pieces 50 × 15 mm^2 with 3 mm in thickness, using a small scale injection molding machine developed by DSM Xplore. The working temperature was fixed at 240 °C, whereas mold temperature was set at 60 °C. The injection pressure was fixed at 1 MPa. All samples were transparent and showed a good surface appearance without presence of air bubbles inside the parts.

Foaming experiments were carried out in a high-pressure vessel with a capacity of 300 cm^3 provided by TOP Industry (France), by a solid state foaming process [41,42] using CO_2 as physical foaming agent.

In this study, samples were saturated at 20 and 30 MPa, and at different temperatures between room temperature and 70 Celsius (see Table 3) during 16 h to assure a complete dissolution of CO_2 in the polymer. After the saturation process, foaming was carried out by releasing the pressure at a pressure drop rate of 30 MPa/min (details of foaming process can be found elsewhere [43]). The morphology of the cellular structure (open or closed cell) is controlled by the amount of PBA in the blends as it was demonstrated previously [40].

On the other hand, a low density polyethylene PE003 with a melt flow index of 2 g/10 min (measured at 190 °C and 2.16 kg), density of 920 kg/m^3, and a melting point of 110 °C was kindly supplied by Repsol Alcudia in the form of pellets. PE foams were manufactured following the two-stage molding procedure [44,45] using azodicarbonamide as blowing agent and dycumil peroxide as crosslinking agent. After the production of the foams blocks, the cells were opened by mechanical deformation. This procedure [46,47] allows obtaining a 100% open cell polyethylene based foam. These materials were used as a reference materials in which Knudsen effect should not appear due to a large cell size.

2.2. Samples preparation

PMMA/MAM, PMMA, and MAM foams were polished using a polishing machine (mod. LaboPOl2-LaboForce3, Struers) equipped with a silicon carbide grinding paper (P 600); with the aim of obtaining homogeneous surfaces to assure an appropriate contact with the sensor used to measure the thermal conductivity. In addition, this procedure allows removing the outer solid or densified skin (if any). After polishing, samples had an average thickness of 5 mm and dimensions of 25 mm × 25 mm.

Polyethylene foams were cut from the central part of the blocks to avoid possible effects related to the typical inhomogeneous density and cellular structure of the blocks produced with the compression molding technology [48]. The thickness of the analyzed samples was 10 mm and the diameter 25 mm.

Table 1
Results for the characterization of the solid samples.

Sample	ρ (g/cm^3)	V_f	Φ (nm)	λ_t (W/m K)	λ_s (W/m K)
Neat PMMA	1.18	0	–	0.2150	–
PMMA/MAM 95/5	1.18	0	–	0.2150	–
PMMA/MAM 90/10	1.18	0	–	0.2150	–
PMMA/MAM 50/50	1.16	0	–	0.2134	–
PMMA/MAM 25/75	1.14	0	–	0.2101	–
Neat MAM	1.08	0	–	0.213 [55]	–
PE	0.92	0	–	0.409 [56]	–

Table 2
Cellular structure results for those samples in which Knudsen effect has been validated. Again, OC denotes Open Cell foams and CC denotes Closed Cell foams.

Sample	Cell morphology	ρ (g/cm^3)	Φ	Anisotropy ratio	Asymmetry coefficient	Standard deviation (SD)/Φ
PMMA	CC	0.57	820 nm	1.57	0.63	0.33
PMMA/MAM 95/5	CC	0.51	235 nm	0.93	−0.23	0.44
PMMA/MAM 95/5	CC	0.49	300 nm	0.85	0.55	0.25
PMMA/MAM 0/50	OC	0.71	94 nm	0.90	0.74	0.35
PMMA/MAM 50/50	OC	0.65	130 nm	0.95	0.81	0.37
PMMA/MAM 50/50	OC	0.60	150 nm	1.19	0.13	0.28
PMMA/MAM 50/50	OC	0.69	200 nm	1.11	0.87	0.35
PMMA/MAM 25/75	OC	0.33	8.07 μm	1.19	−0.14	0.21
PMMA/MAM 25/75	OC	0.32	8.53 μm	1.17	−0.16	0.19
PE	OC	0.024	710 μm	1.67	0.25	0.20
PE	OC	0.021	946 μm	2.44	1.38	0.15
PE	OC	0.028	1277 μm	1.21	1.15	0.19
PE	OC	0.032	1117 μm	1.71	0.82	0.15

PMMA/MAM, PMMA, MAM and PE foams were stored at controlled temperature and humidity (23 °C and 50% humidity) at least three days before measuring their properties in order to avoid inconsistencies in the measurements due to differences in temperature or humidity between the different samples.

2.3. Characterization techniques

2.3.1. Density

Density measurements of solid and foamed PMMA/MAM, PMMA, and MAM samples were performed by the water-displacement method, based on Archimedes' principle, using the density determination kit for an AT261 Mettler-Toledo balance. Three measurements were carried out for each sample. In the case of PE foams, density was obtained as the ratio of the mass and volume of the sample. The estimated accuracy was 2%.

2.3.2. X-ray analysis

The procedure for the determination of the contribution of the gaseous phase to the total thermal conductivity (see below) requires samples with a high homogeneity and without internal defects. Then, an important step in this work was the selection of appropriate samples by means of x-ray radiography [49]. This technique allow us detecting these internal defects or inhomogeneities without introducing any damage in the samples (i.e. is a non-destructive technique).

Fig. 1 shows X-ray radiographs of some samples with internal defects or inhomogeneities (top) and some homogeneous samples (bottom).

All the samples produced (more than 50 foams in total) were characterized by means of this technique. Only thirteen PMMA-based foams and four PE foams (Table 2), without defects or inhomogeneities, were finally selected for further studies.

2.3.3. Cellular structure

Cellular structure of foamed samples was analyzed by SEM using an FEI Quanta 200FEG scanning electron microscope. Foams were frozen in liquid nitrogen and fractured to assure that the microstructure remained intact. The fractured surface was coated with gold using a sputter coater (model SCD 004, Balzers Union). Some of the key parameters of the cellular structure were with a specialized software [50] based on ImageJ/FIJI [51]. This software provides the cell size distribution, the average cell size, the standard deviation of the cell size distribution, the cell anisotropy ratio distribution, the average cell anisotropy ratio, the asymmetry coefficient, the cell density N_v (number of cells per cubic centimeter of the foam), and the cell nucleation density N_0 (number of cells per cubic centimeter of the solid precursor).

The number of cells per cubic centimeter of the foamed material (N_v) was calculated using Kumar's theoretical approximation [52]. In this method, no direct measurements of cell dimensions over the micrograph are required, only the micrograph area (A) and the total

Table 3
Results of foamed samples characterization where OC denotes Open Cell foams, and CC denotes Closed Cell foams.

Sample	Foaming P(MPa)/T (°C)	Cell morphology	ρ (g/cm^3)	V_f	Φ	λ_t (W/m K)	λ_s (W/m K)
PMMA	30/50	CC	0.57	0.52	820 nm	0.1072	0.1067
PMMA/MAM 95/5	30/50	CC	0.51	0.57	235 nm	0.0925	0.0902
PMMA/MAM 95/5	30/60	CC	0.49	0.58	300 nm	0.0884	0.0878
PMMA/MAM 90/10	30/40	CC	0.48	0.59	220 nm	0.090	–
PMMA/MAM 90/10	30/50	CC	0.47	0.60	290 nm	0.0884	–
PMMA/MAM 90/10	30/60	CC	0.44	0.63	970 nm	0.0886	–
PMMA/MAM 90/10	30/70	CC	0.42	0.64	950 nm	0.0837	–
PMMA/MAM 50/50	20/23	OC	0.71	0.39	94 nm	0.1043	0.1003
PMMA/MAM 50/50	30/23	OC	0.60	0.49	150 nm	0.0948	0.090
PMMA/MAM 50/50	30/40	OC	0.65	0.44	130 nm	0.0947	0.0901
PMMA/MAM 50/50	30/50	OC	0.69	0.40	200 nm	0.1015	0.0944
PMMA/MAM 25/75	30/60	OC	0.33	0.71	8.07 μm	0.07825	0.0604
PMMA/MAM 25/75	30/70	OC	0.32	0.72	8.53 μm	0.0729	0.0552
MAM	30/40	OC	0.21	0.80	7.53 μm	0.0619	–
MAM	30/50	OC	0.20	0.81	7.50 μm	0.0669	–
MAM	30/60	OC	0.20	0.81	7.38 μm	0.0611	–
MAM [55]	30/40	OC	0.20	0.8	9.00 μm	0.0628	–
MAM [55]	30/40	OC	0.18	0.82	44 μm	0.0627	–
MAM [55]	30/40	OC	0.16	0.84	51 μm	0.0589	–
MAM [55]	30/40	OC	0.15	0.85	61 μm	0.0599	–

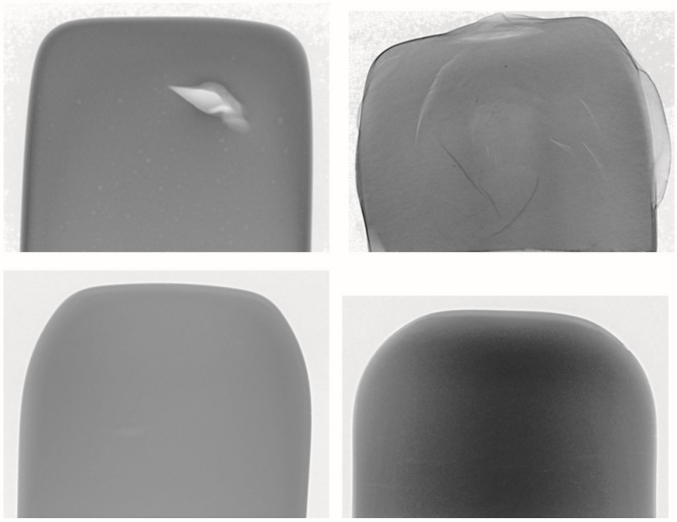

Fig. 1. X-ray radioscopy images of foams with internal defects (top) and homogeneous foams (bottom).

number of cells (n) contained are measured. From these values and the magnification factor of the micrograph (M), N_v can be calculated using Eq. (4):

$$N_v = \left[\frac{(nM^2)}{A}\right]^{3/2} \tag{4}$$

This method also provides an expression (Eq. (5)) to estimate the cell nucleation density (N_0, number of cells per cubic centimeter of the solid unfoamed material) from N_v and the relative density of the foam (ρ_{rel}). This equation assumes that coalescence did not occur during the cell growing and stabilization stages:

$$N_0 = \frac{N_v}{\rho_{rel}} \tag{5}$$

2.3.4. Thermal conductivity

Thermal conductivity of microcellular and nanocellular foams was measured by the Transient Plane Source (TPS) technique using a thermal conductivimeter mod. HDMD (Hotdisk). The TPS is a standard technique for thermal properties characterization of different materials (metals, ceramics, polymers, liquids, etc.) [53].

The basic principle of this method relies on a plane element that acts both as temperature sensor and heat source. This element consists of an electrical conducting pattern of thin nickel foil (10 μm thick) in the form of double spiral, inserted between two insulating layers made of kapton (70 μm thick). The TPS element is located between two samples with both sensor faces in contact with the two sample surfaces. Two samples of similar characteristics are required for this purpose. To perform the experiments a constant electric power is supplied to the hot-disk sensor. The increase in temperature $\Delta T(t)$ is directly related to the variation in the sensor resistance $R(t)$ by the equation:

$$R(t) = R_0[1 + \alpha\Delta T(t)] \tag{6}$$

where R_0 is the disk resistance at the beginning of the recording (initial resistance) and α is the temperature coefficient of resistance of the nickel foil.

Assuming an infinite sample and the conductive pattern being in the XY plane of a coordinate system, the temperature rise at a point (XY) at time t is obtained by solving the equation for the heat conduction, which relates change in temperature with time [54]. In the particular case of our sensor geometry, n concentric ring sources, the spatial average $\overline{\Delta T(\tau)}$ can be obtained through the equation:

$$\overline{\Delta T(\tau)} = P_0\left(\pi^{3/2}a\lambda\right)^{-1} D(\tau) \tag{7}$$

where P_0 is a Bessel function, $D(\tau)$ is a geometric function characteristic of the number n of concentric rings and $\overline{\Delta T(\tau)}$ is the temperature increase of the sensor expressed in terms of only one variable τ, defined as:

$$\tau = \left(\frac{t}{\theta}\right)^{\frac{1}{2}}; \quad \theta = \frac{a^2}{k} \tag{8}$$

where t is the measurement time from the start of transient heating, θ is the characteristic time, which depends on parameters of both the sensor and the sample, a is the sensor radius and k is the thermal diffusivity of the sample. Thermal resistance can be obtained by fitting the experimental data to the straight line given by Eq. (6), and thermal diffusivity is calculated from Eq. (8) taking into account the θ value determined experimentally.

This technique has been used previously on MAM, and PE foams with good results [12,55]. Moreover, our experimental set-up (Fig. 2) allows carrying out measurements both at atmospheric pressure and under vacuum conditions.

To obtain the contribution of the gaseous phase to the thermal conductivity, it has been followed a similar methodology to the one developed by X. Lu et al. [10]. They studied the thermal conductivity of open cell RF-aerogel as a function of gas pressure and found that with a pressure drop from 1000 to 50 mbar they were able to eliminate the conduction across the gas phase.

Therefore, in this work, two sets of measurements have been performed. One of them at atmospheric pressure that provides the value of the total thermal conductivity λ_t, and another one under

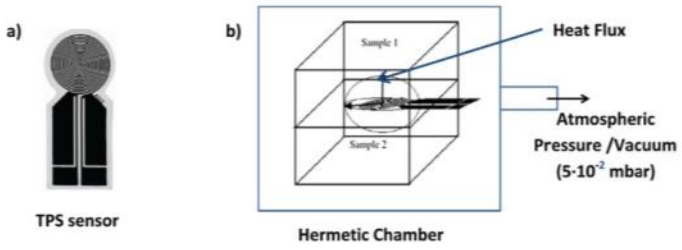

Fig. 2. Schematic view of the developed methodology: a) TPS sensor, b) experimental set-up.

vacuum conditions (at 5×10^{-2} mbar approximately, even lower than the values previously used in the literature [10], in order to ensure the gas desorption from cells and cancel the gaseous phase contribution) that provides the thermal conductivity of the sample without the contribution of the gaseous phase. Under these two conditions, the radiation term remains constant, because this term is mainly controlled by the value of the mean extinction coefficient which depends on structural parameters of the foam [56]; therefore, the gas desorption from cells does not affect it.

These measurements have been carried out with a TPS sensor of radius 3.189 mm as follows: first of all, samples were placed in the experimental set-up (Fig. 2), inside the vacuum chamber, with a constant pressure between the two pieces. Then, the vacuum chamber was closed. Samples and experimental set-up were allowed to reach an equilibrium temperature before the beginning of the measurements (normally during 30 min). At atmospheric pressure, samples were measured five times with a time span of 5 min in order to avoid temperature drift. Typical power (W) and total measurement time (t) employed were about 0.006 W and about 55 s, respectively. After the measurement under atmospheric pressure, the vacuum pump was activated. Once the desired vacuum conditions were reached, samples and experimental set-up were allowed again to reach an equilibrium temperature before the beginning of the measurements (typically during 60 min). Measurements under vacuum conditions were taken during 12 h with a time spam of 1 h due to the lower heat dissipation. Measurements parameters (power and time) were slightly adjusted due to the lower heat dissipation under vacuum conditions. In this case, a power about 0.005 W and a time about 60 s were used. It was assumed that the diffusion of the gas was completed when several consecutive measurements present a constant value.

The difference between the two sets of measurements (under atmospheric pressure and under vacuum conditions) provides the contribution of the gaseous phase λ_g to the thermal conductivity according to Eq. (1).

3. Results and discussion

3.1. Characterization of the solid samples

The main characteristics of the solid precursors have been summarized in Table 1. From the characterization of the three different PMMA/MAM solid blends, it is observed that there are not important differences between them (neither compared to the neat PMMA solid). This was an expected result because the main component in each blend is the PMMA (for instance a blend with 25% of neat PMMA and 75% of MAM triblock copolymer is composed by 85% of PMMA and only 15% of PBA (poly(butyl acrylate))). Therefore, it is possible to compare the thermal conductivity of foams produced from different blends without a significant influence of the composition. PE solid precursors were previously characterized elsewhere [56].

3.2. Characterization of foamed materials

3.2.1. Cellular structure

Representative images of the cellular structure can be observed in Fig. 3. The analysis of the structure allows distinguishing four groups of foams in our materials: nanocellular PMMA/MAM open cell foams (the top left), microcellular PMMA/MAM open cell foams (top right), nanocellular PMMA/MAM closed cell foams (bottom left), and PE foams (bottom right).

As it can be observed the nature of the cell openings is different depending on the system: in the case of nanocellular the PMMA/MAM foams (top left), the gas phase is completely interconnected, whereas in the case of both microcellular PE and PMMA/MAM foams, the open cell character is given by the presence of some holes in the cell walls (top and bottom right).

PMMA-based foams present open or closed cell morphologies depending on the PBA content [40]. Thus foams of PMMA containing 50 and 75 wt. % of MAM, as well as, neat MAM foams are open cell materials under the conditions of pressure and temperature at which they have been manufactured (see Fig. 3, top right and left). However, this does not occur with neat PMMA foams neither with foams of PMMA containing 5 and 10 wt. % of MAM which are closed cell cellular materials (see Fig. 3, bottom left) [40].

On the other hand, PE foams are also open cell materials (see Fig. 3, bottom right) due to the manufacturing process which allows obtaining 100% open cell foams.

One of main objectives of this work is the validation of the Knudsen effect, in which the cellular structure is a main issue. For this reason, a detailed analysis of the cellular structure has been carried out in those samples that were selected for the study (see *X-Ray Analysis* section). Average cell size together with average anisotropy, asymmetry coefficient, and the standard deviation divided by the average cell size are summarized in Table 2.

It is observed that PMMA-based foams, both microcellular and nanocellular, are almost isotropic (anisotropy ratio close to 1), whereas PE foams present anisotropy (anisotropy ratio higher than 1.

The ratio between the standard deviation of the cell size distribution and the average cell size has been also analyzed. This parameter provides information about the homogeneity of the cellular structure. The results obtained show that both microcellular and nanocellular foams present very homogeneous cellular structures ($SD/\Phi < 0.5$), being the foams in the micrometer range slightly more homogeneous (both for PMMA-based foams and for PE foams).

Finally, the asymmetry coefficient provides information on the shape of the distribution. For our purposes this magnitude provides

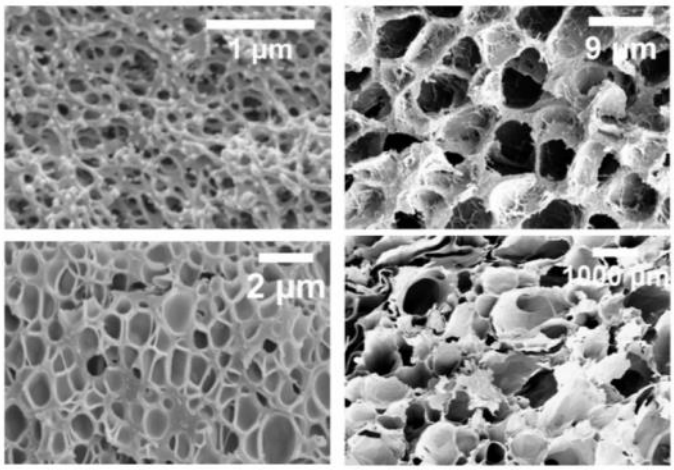

Fig. 3. SEM micrographs of the cellular structure of nanocellular PMMA/MAM open cell foam (top left), microcellular PMMA/MAM open cell foam (top right), nanocellular PMMA/MAM closed cell foam (bottom left), and microcellular PE foam (bottom right).

valuable information about the presence, or not, of a bi-modal cell size distribution. Presence of a bi-modal cell size distribution could introduce difficulties in the evaluation of the Knudsen effect, as it would be difficult to state a well-defined value of the average cell size to be related with the measured thermal conductivity of the gaseous phase. When the value of the asymmetry coefficient is close or higher than one, a bi-modal cell size distribution is taking place. In this study, this only occurs with two PE samples, whereas in the rest of the cases, the shape of the distribution is mono-modal. Thus, no difficulties due to bi-modal cell size distributions can be expected in the analysis of the results, as the only samples with bi-modal distribution present cell sizes clearly in the micrometric range.

Therefore, our production process allows obtaining nanocellular and microcellular foams with a high homogeneity in their cellular structure, being suitable for a study that requires a significant accuracy as the one that is presented in the following sections.

3.2.2. Relationship between thermal conductivity and cell size

In this section, a comparison between the thermal conductivity behavior of microcellular and nanocellular foams is carried out. The experimental results for the thermal conductivity of microcellular and nanocellular PMMA, PMMA/MAM, and MAM foams are included in Fig. 4 as a function of the relative density. Some results from MAM foams taken from a previous publication [55] have also been included (Table 3). It should be noticed that these foams were produced using different pressure drop rates; all of them lower than those used in this work.

Two different trends can be found in these results, allowing differentiating between PMMA-based foams with cell sizes over and below 700 nm. Then, it seems that the cell size could present a relevant influence on the thermal conductivity of PMMA-based foams when the average cell size is reduced below the micron.

In order to analyze the possible influence of the cell size independently of the density of the foams, the thermal conductivity of

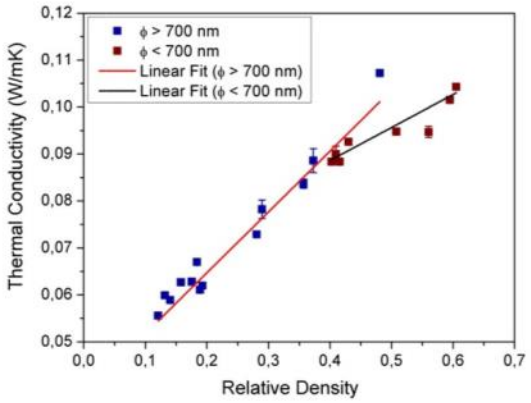

Fig. 4. Relationship between the thermal conductivity and the relative density for microcellular and nanocellular PMMA-based foams.

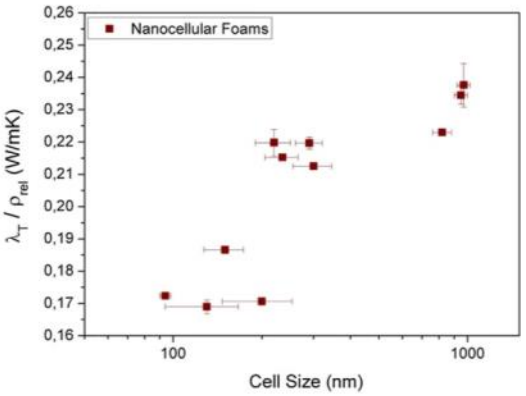

Fig. 5. Relationship between the thermal conductivity divided by the relative density and the pore size for nanocellular foamed samples.

the nanocellular foams divided by their relative density ($\rho_{rel} = \rho_{foam}/\rho_{solid}$) has been plotted as a function of the cell size (Fig. 5).

The results show a strong relationship between the thermal conductivity and the cell size. This trend could be attributed to effects associated with a reduction of the dimensions of the elements constituting the solid phase or the gaseous phase. Regarding the modifications of the solid phase, there may be modifications of the polymer properties as well as a tortuosity increase. Meanwhile, in the gas phase the Knudsen effect could take place. It is important to take into account that for the relative densities of foams with cell sizes below 700 nm, larger than 0.35 (see Fig. 4), the radiation contribution can be neglected [1] and cannot justify the observed trend between the thermal conductivity and the cell size (Fig. 5).

In the following sections we will attempt to define and quantify which mechanisms are responsible of this reduction in the thermal conductivity as a function of the cell size.

3.2.3. Validation of the Knudsen effect

In order to identify the mechanisms involved in the reduction of the thermal conductivity with cell size, the behavior of the contribution of the gas phase was studied, according to the procedure explained in the experimental part. As it was previously explained this procedure was carried out only in some selected samples.

Some of these samples with high structural and cellular homogeneity presented closed cell morphologies. For these particular materials it was expected that extracting the gas from the cells could be difficult. The results confirmed the expectations and therefore, it was not possible to determine the contribution of the gas phase on closed nanocellular foams from the measurements at atmospheric pressure and under vacuum conditions (for these samples the obtained values of the thermal conductivity were practically the same on both conditions (Table 3)).

On the contrary, the selected foams with open cell morphologies do allow us quantifying the contribution of the gas phase. These foams reached a constant value of their thermal conductivity after 60 min under vacuum conditions, being stable during the whole measurement process (during 12 h).

From the measured values of the thermal conductivity of the foamed samples at atmospheric pressure (λ_t) and under vacuum (λ_s) (Table 3), it was possible to calculate the gas thermal conductivity (λ_g') using Eq. (9).

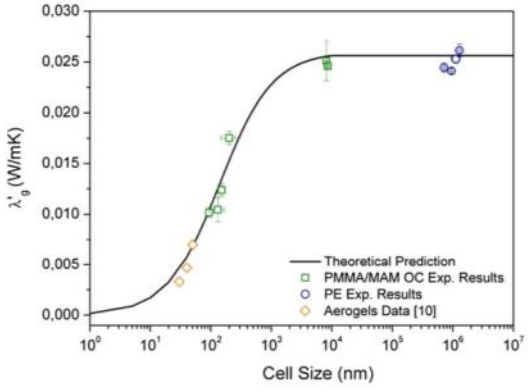

Fig. 6. Effect of the cell size on the gas thermal conductivity in open cell polymeric foams together with the theoretical predictions obtained from the Knudsen equation, and some of the previous results in aerogels [10].

The obtained results are shown in Fig. 6 as a function of the cell size, together with the values predicted by the Knudsen effect equation for the same range of cell sizes (Eqs. (2) and (3)).

The experimental results from open cell polymeric foams (PMMA/MAM OC foams and PE foams) are consistent with the theoretical prediction of the Knudsen effect, showing the same trend than previous results obtained in aerogels [10] (Fig. 6). Therefore, we found that the Knudsen effect takes place on polymeric foams, and also that this effect is independent of the surrounding solid material and depends only on the confinement of the gaseous phase.

The results obtained for the microcellular polyethylene (PE) samples allow us testing the validity and accuracy of the developed methodology. As expected, the results show that open cell PE foams with large cell sizes (larger than 700 microns) do not present Knudsen effect, being the contribution of their gaseous phase the expected value of the conductivity of the air without confinement. Then, the methodology proposed in this study seems to work properly in polymeric foams, allowing quantifying the contribution of the gas phase to the thermal conductivity in open cell foams.

3.2.4. Modeling of the thermal conductivity

Once it has been demonstrated that the Knudsen effect is one of the mechanisms that reduce the thermal conductivity of nanocellular polymeric foams, we will try to model the thermal behavior of these materials in order to determine if there are other mechanisms involved in the reduction of the thermal conductivity of nanocellular foams.

As a starting point we introduce the Ashby model, based on Glicksman's theoretical assumptions, which considers that the thermal conductivity, due to conduction mechanisms, is given by:

$$\lambda_t = \lambda_s + \lambda_g = g\lambda_s'(1 - V_g) + \lambda_g' V_g \tag{9}$$

where λ_s and λ_g are the conductivities of the solid and gas phases, respectively; g is an efficiency factor (structural factor) which takes into account the tortuous shape of the cell walls and which ranges between 1/3 and 1, and V_g represents the volume fraction of voids. For MAM microcellular foams it is known that the model fits the experimental results with $g = 1$ [55].

Then, in order to take into account the findings of this work, the Knudsen equations (Eqs. (2) and (3)) are combined with the Ashby model (Eq. (9)) to provide an equation able to predict the thermal conductivity of nanocellular foams (Eq. (10)):

$$\lambda_t = g\lambda_s'(1 - V_g) + \frac{\lambda_{g0}' V_g}{(1 + \beta l_g/\Phi)} \tag{10}$$

Fig. 7a, b shows the experimental values of the thermal conductivity or nanocellular foams as a function of the relative density. In addition, several theoretical predictions are included in these figures, assuming a constant structural factor and different cell sizes (Fig. 7a), or by modifying both the structural factor and the cell size according to the experimental results (Fig. 7b).

It is found that the Knudsen effect by itself cannot explain the reduction of the thermal conductivity of these foams (Fig. 7a); being necessary to modify progressively the structural factor as a function of the cell size to obtain an accurate fitting between experimental results and theoretical predictions (Fig. 7b). Thus, it seems that the cell size reduction also induces changes in the contribution of the solid phase, either by an increase of the tortuosity or by a modification of the polymer properties due to a possible confinement effect [39].

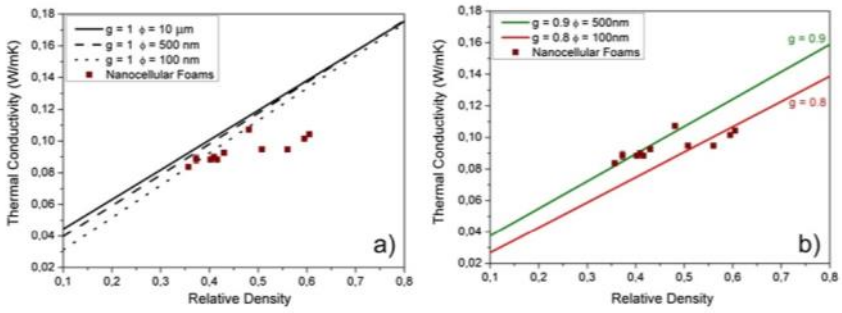

Fig. 7. Comparison between experimental results and the theoretical model for: a) structural factor $g = 1$ and different cell sizes (100 nm, 500 nm, and 10 μm), b) different structural factors and cell sizes ($g = 0.9$ and 500 nm; $g = 0.8$ and 100 nm).

The previous analysis/modeling is correct for the relative densities under study and also for large densities, because as it was previously mentioned the radiation contribution is negligible in this density range [1] and convention is always negligible for the cell sizes under study. However, it we want to extend the modeling to lower densities radiation could play an important role and has to be considered.

The radiation term can be calculated in microcellular foams using the Williams and Aldao model [1]. This model gives acceptable values of the thermal radiation term by considering the main characteristics of cellular structure, the thickness of the cellular material, and the optical properties of the solid material. The model is based on a radiation term predicted as follows:

$$\lambda_r = \frac{4\sigma T^3 L}{1 + \left(\frac{L}{\Phi}\right)\left(\frac{1}{T_N} - 1\right)} \tag{11}$$

where σ is the Stefan-Boltzman constant, T the temperature, L the material thickness (in our case $L = 5$ mm), Φ the cell size, and T_N is the net fraction radiant energy sent forward by a solid membrane of thickness L_s. This fraction energy is given by:

$$T_N = \frac{(1-r)}{(1-rt)}\left\{\frac{(1-r)t}{(1+rt)} + \frac{(1-t)}{2}\right\} \tag{12}$$

where r is the fraction of incident energy reflected by each gas–solid interface. This quantity is related to the refractive index of the solid matrix w (in our case this value was $w = 1.507$ in the IR radiation range of 600–2000 nm [57]) by:

$$r = \left[\frac{w-1}{w+1}\right]^2 \tag{13}$$

And the thickness of the solid membrane can be calculated by Ref. [1]:

$$L_s = (1 - f_s)\cdot\Phi\cdot 3.5347\cdot\rho_{rel} \tag{14}$$

where f_s is the mass fraction in the struts (we have considered a value of $f_s = 0.33$ for microcellular foams), and ρ_{rel} is the relative density of the foam.

Finally, the coefficient t is the fraction of energy transmitted through the solid membrane of thickness L_s (cell wall thickness), which is given by:

$$t = \exp(-aL_s) \tag{15}$$

where a is the absorption coefficient of the solid matrix (in this study, an average value od $a = 0.2468\ cm^{-1}$ in the IR radiation range of 600–2000 nm was considered [57]).

In the case of nanocellular foams the conventional models to calculate the radiation terms are in principle not suitable. Models for the calculation of the radiation term on polymeric foams usually assume that the wavelength of the infrared radiation is lower than the cell size of the foam, but in nanocellular foams this assumption is not correct. Some recent theoretical results predicted that the radiation term could present an insignificant contribution on nanocellular foams even at low densities [58]. Following these theoretical predictions we will assume as a first approximation that the radiation term of nanocellular foams can be neglected even at low densities, however this should be considered as an approximation because as far as we know there is no experimental evidence of this. Therefore, the predictions for nanocellular foams will provide a lower bound of the thermal conductivity.

Using the complete model (Ashby + Knudsen + Radiation (estimated in microcellular foams and neglected in nanocellular foams)), the contribution (in percentage) of each heat transfer mechanisms to the total thermal conductivity is evaluated as a function of the relative density (Fig. 8) for two different cases: a PMMA-based foam in the micrometer range (cell size 100 microns) (Fig. 8 left) and a PMMA-based foam in the nanometer range (cell size 100 nm) (Fig. 8 right).

From the obtained results, it is observed that radiation term can be neglected in microcellular PMMA-based foams with relative densities over 0.4. Also, it could be expected that the radiation term will be also negligible in medium and high densities nanocellular foams due to the strong influence of the relative density on this term. Then, as it was previously mentioned for medium and high density foams the reduction of the thermal conductivity is only due to a combination of the Knudsen effect and a modification of the contribution of the solid matrix.

Accuracy of the proposed models can be proved by comparison with the experimental results of the thermal conductivity of the samples studied in this work (Fig. 9). The structural factor g used for these calculations has been selected according to the previous results, being 1 for microcellular foams, 0.9 for the foams with a cell size between 800 and 900 nm, 0.85 for those foams with a cell size between 200 and 300 nm, and 0.8 for foams with a cell size lower than 200 nm (see Table 3).

Fig. 9 shows a good agreement between theoretical predictions and experimental results for both microcellular and nanocellular

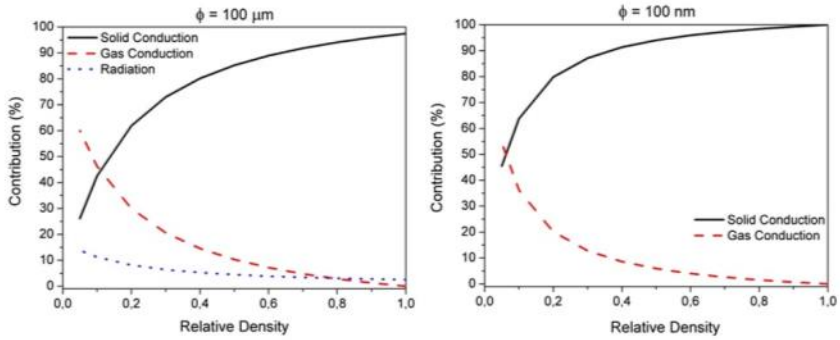

Fig. 8. Contribution (in percentage) of the solid phase, gaseous phase, and radiation term to the thermal conductivity of a microcellular PMMA foam (left) and of the solid and gaseous phase of a nanocellular PMMA foam (right).

foams. In addition, there are not important differences in the thermal behavior of open cell or closed cell foams (both represented in Fig. 9 and fitted by the model). So, the Knudsen effect and the modification of the solid matrix contribution due to the nanocellular structure seem to be independent on the morphology of the cell and only depends on the average cell size.

Finally, a comparison of the expected thermal conductivity predicted from the developed models for three different cases: microcellular foam (100 microns) and two nanocellular foams (100 and 10 nm, respectively) is shown in Fig. 10. The relative density range shown in Fig. 10 (from 0.05 to 0.6) corresponds to the range of foams used in this work as well as to the range of densities commonly used in thermal insulation applications.

A very strong reduction in the thermal conductivity at low densities ($\rho_{rel} = 0.05$, usual density of polymeric foams used thermal insulation) is found between microcellular (100 μm) and nanocellular foams (100 nm or 10 nm). The values can be reduced (for a relative density of 0.05) from around 0.042 W/m K to around 0.017 W/m K for materials with cell sizes of 100 nm, and to values as small as 0.007 W/m K for cell sizes of 10 nm. It should be noticed that this is an optimistic estimation as the radiation term has been neglected for nanocellular foams and, therefore, the thermal conductivity would be higher than the predicted values for low density nanocellular foams. However, even assuming that the radiation term of low density nanocellular foams takes values equal to those of microcellular foams it can be expected a reduction higher than 40%.

Then, it is confirmed that nanocellular foams have a great potential in insulation applications. However, it should be noticed that the production of a foam by gas dissolution foaming with those features ($\rho_{rel} = 0.05$ and $\Phi = 100$ nm) would require a much higher cell nucleation density ($N_0 = 3.6 \times 10^{16}$ nuclei/cm^3) than those obtained up to date [32,34,38–40].

4. Conclusions

In this work, it has been demonstrated for the first time the presence of the Knudsen effect in polymeric foams. A clear transition between the thermal conductivity of microcellular and nanocellular polymeric foams has been found, and the phenomena behind this behavior have been identified.

On the one hand, it has been developed and tested an experimental procedure that allows quantifying the contribution of the gaseous phase to the total thermal conductivity for nanocellular open cell foams. Then, by this methodology and using nanocellular foams with open cell structure and relative densities between 0.35

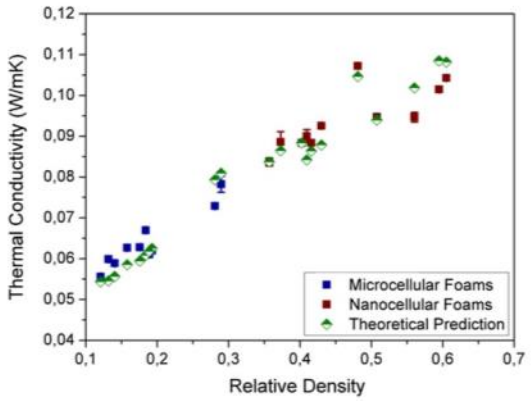

Fig. 9. Comparison between the theoretical model and experimental results.

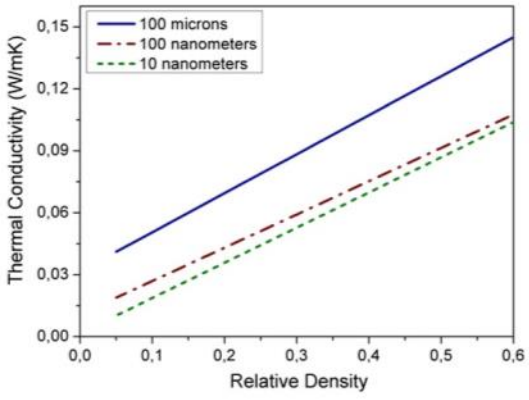

Fig. 10. Theoretical thermal conductivity as a function of the relative density for PMMA foams for different cell sizes.

and 0.6 it has been demonstrated experimentally that nanocellular open cell polymeric foams present the Knudsen effect, finding a significant reduction of their thermal conductivity.

On the other hand, an interesting additional result has been found. The reduction of the cell size below the micron also decreases the thermal conductivity of the solid phase. A possible explanation of this behavior can be found in the increment of the solid phase tortuosity due to the presence of the nanocells or the modification of the polymer properties due to a confinement effect.

Moreover, the thermal conductivity of PMMA-based foams of medium and high relative densities has been modeled according to these findings and well-established equations. An accurate fit has been obtained using the Ashby model and the appropriate considerations about the Knudsen effect, the evolution of the solid phase contribution, and the influence of the porosity. A remarkable conclusion obtained from the modeling is that closed cell nanocellular PMMA-based foams present the same behavior than open cell PMMA-based foams, being necessary to take into account the Knudsen effect and the modification of the solid phase to reproduce the experimental results with the model.

Finally, it should be noticed that these results were obtained with samples of a significant thickness and produced by an industrially scalable process. Moreover, the estimations from the model tested in this work shown a reduction factor about 2.5 at low densities between the thermal conductivity of microcellular and nanocellular foams. Therefore, the potential benefits of nanocellular foams compared to microcellular foams in thermal insulation applications have been demonstrated.

Acknowledgments

Financial support from FPU grant AP2008-03603 (J. Pinto) and FPI grant BES-2013-062852 (B. Notario) from the Spanish Ministry of Education is gratefully acknowledged. Financial assistance from MINECO (MAT 2012-34901) and the Junta of Castile and Leon (VA035U13) is gratefully acknowledged.

References

[1] Solorzano E, Rodriguez-Perez MA, Lázaro J, de Saja JA. Adv Eng Mater 2009;11(10):818–24.
[2] Russell HW. J Am Ceram Soc 1935;18(1–12):1–5.
[3] Bedeaux D, Kapral R. J Chem Phys 1983;79.
[4] Leach AG. J Phys D: Appl Phys 1993;26(5).
[5] Cunningham A. ICHMT digital library online, vol. 24; 1987. p. 32–51.
[6] Schuetz MA, Glicksman LR. J Cell Plast 1984;20(2):114–21.
[7] Collishaw PG, Evans JRG. J Mater Sci 1994;29(9):2261–73.
[8] Kuhn J, Ebert HP, Arduini-Schuster MC, Büttner D, Fricke J. Int J Heat Mass Transf 1992;35(7):1795–801.
[9] Hrubesh LW, Pekala RW. J Mater Res 1994;9(03):731–8.
[10] Lu X, Caps R, Fricke J, Alviso CT, Pekala RW. J Non-Cryst Solids 1995;188(3):226–34.
[11] Holman JP. Heat transfer. New York: McGraw-Hill; 1981.
[12] Alvarez-Lainez M, Rodriguez-Perez MA, De Saja JA. J Polym Sci Part B: Polym Phys 2008;46(2):212–21.
[13] Schmidt D, Raman VI, Egger C, du Fresne C, Schädler V. Mater Sci Eng C 2007;27(5–8):1487–90.
[14] Lee OJ, Lee KH, Yim TJ, Kim SY, Yoo KP. Non-Cryst Solids 2002;298:287–92.
[15] Nait-Ali B, Haberko K, Vesteghem H, Absi J, Smith DS. J Eur Ceram Soc 2006;26(16):3567–74.
[16] Mu D, Liu Z-S, Huang C, Djilali N. Microfluid Nanofluid 2007;4(3):257–60.
[17] Reichenauer G, Heinemann U, Ebert HP. Colloids Surf A: Physicochem Eng Aspects 2007;300(1–2):204–10.
[18] Chen X, Pfender E. Plasma Chem Plasma Process 1983;3:97–113.
[19] Zhang YH, Gu XJ, Barber RW, Emerson DR. Phys Rev E 2006;74(046704).
[20] Forest C, Chaumont P, Cassagnau P, Swoboda B, Sonntag P. Prog Polym Sci 2014. http://dx.doi.org/10.1016/j.progpolymsci.2014.07.001.
[21] Sundarram SS, Li W. Polym Eng Sci 2013;53(9):1901–9.
[22] Yokoyama BH, Li L, Nemoto T, Sugiyama K. Adv Mater 2004;16(17):1542–6.
[23] Miller D, Kumar V. Polymer 2011;52(13):2910–9.
[24] Pajonk GM. J Non-Cryst Solids 1998;225:307–14.
[25] Olson DA, Chen L, Hillmyer MA. Chem Mater 2007;20(3):869–90.
[26] Kazarian SG. Polym Sci Ser C 2000;42(1):78–101.
[27] Tsivintzelis I, Angelopoulou AG, Panayiotou C. Polymer 2007;48(20):5928–39.
[28] Reverchon E, Cardea J. J Supercrit Fluid 2007;40:144–52.
[29] Jacobs LJM, Kemmere MF, Keurentjes JTF. Green Chem 2008;10(7):731–8.
[30] Wells SL, DeSimone J. Angew Chem Int Ed 2001;40(3):518–27.
[31] Siripurapu S, DeSimone JM, Khan SA, Spontak RJ. Macromolecules 2005;38(6):2271–80.
[32] Costeux S, Zhu L. Polymer 2013;54(11):2785–95.
[33] Spitael P, Macosko CW, McClurg RB. Macromolecules 2004;37(18):6874–82.
[34] Pinto J, Dumon M, Pedros M, Reglero JA, Rodriguez-Perez MA. Chem Eng J 2014;243C:428–35.
[35] Ruiz JAR, Pedros M, Tallon J-M, Dumon M. J Supercrit Fluid 2011;58(1):168–76.
[36] Costeux S, Jeon H, Bunker S, Khan I. Nanocellular foams from acrylic polymers: experiments and modeling. In: SPE foams 2012 Conference. Barcelona, Spain; 2012.
[37] Aher B, Olson NM, Kumar V. J Mater Res 2013;28(17):2366–73.
[38] Costeux S, Bunker SP, Jeon HK. J Mater Res 2013;28(17):2351–65.
[39] Reglero Ruiz JA, Dumon M, Pinto J, Rodriguez-Pérez MA. Macromol Mater Eng 2011;296(8):752–9.
[40] Pinto J, Dumon M, Rodriguez-Perez MA, Garcia R, Dietz C. J Phys Chem C 2014;118(9):4656–63.
[41] Goel SK, Beckman EJ. Cell Polym 1993;12(4):251–74.
[42] Nawaby AV, Handa YP, Liao X, Yoshitaka Y, Tomohiro M. Polym Int 2007;56(1):67–73.
[43] Pinto J, Reglero-Ruiz JA, Dumon M, Rodriguez-Perez MA. J Supercrit Fluid 2014;94:198–205.
[44] Eaves D. Handbook of polymer foams. Rapra Technology; 2004.
[45] Puri RR, Collington KT. Cell Polym 1988;7:56–84.
[46] Park CP. Acoustical open-cell polylefins and process for making. Dow Global Technologies Inc; 2003.
[47] Hiroo I. Process for producing open-cell polyethylene foam materials and the resultant product. U.S. Patent1989;4:814.
[48] Almanza O, Rabago LOAy, Martínez-Díez JA, Rodriguez-Perez MA, JAd Saja. J Cell Plast 2001;37:21.
[49] Escudero J, Solorzano E, Rodriguez-Perez MA, Garcia-Moreno F, De Saja JA. Cell Polym 2009;28(4):289–302.
[50] Pinto J, Solórzano E, Rodriguez-Perez MA, de Saja JA. J Cell Plast 2013;49(6):555–75.
[51] Abràmoff MD, Magalhães PJ, Ram SJ. Biophot Int 2004;11(7):36–42.
[52] Kumar V, Suh NP. Polym Eng Sci 1990;30(20):1323–9.
[53] UNE-EN ISO 22007-2 AC. Determinación de la conductividad térmica y la difusividad térmica. Parte 2: Método de la fuente de calor plana transitoria (disco caliente). Plásticos, vol. UNE-EN ISO 22007-2: AENOR. 2012. p. 23.
[54] Gustavsson M, Karawacki E, Gustafsson SE. Rev Sci Instrum 1994;65:3856–9.
[55] Reglero Ruiz JA, Saiz-Arroyo C, Dumon M, Rodríguez-Perez MA, Gonzalez L. Polym Int 2011;60(1):146–52.
[56] Campo-Arnáiz RA, Rodríguez-Pérez MA, Calvo B, de Saja JA. J Polym Sci Part B: Polym Phys 2005;43(13):1608–17.
[57] Khashan MA, Nassif AY. Opt Commun 2001;188:129–39.
[58] Ferkl P, Pokorný R, Bobák M, Kosek J. Chem Eng Sci 2013;97:50–8.

III.4. Additional Clarifications

Our experimental results have been contrasted with a theoretical study based on the different contributions to the thermal conductivity, using for this purpose the Ashby model. In this way it was possible to detect that the Knudsen effect was able to explain partially the measured reduction of the thermal conductivity (37 % of the total reduction of the thermal conductivity was due to the Knudsen effect). However, it did not explain the complete reduction of the conductivity of the foamed samples. Being necessary to explain the overall thermal conductivity reduction also in terms of a modification of the thermal conductivity of the solid phase. In this paper two possible explanations were proposed to this new and unexpected phenomenon: a possible increase of the tortuosity (Figure III.5) or the existence of a confinement effect of the polymer chains (Figure III.6) [13]. However, at the time of the publication of this article, we had no clues about which one could be right or if a combination of both could be possible.

Further studies (*Chapter II, "Molecular Confinement of Solid and Gaseous Phases of Freestanding Nanoporous Polymers Inducing Enhanced and Unexpected Physical Properties"*) demonstrated the coexistence of a confinement effect and a raising tortuosity when cell size goes from the micrometer to the nanometer scale.

On the other hand, other theoretical studies (*Introduction*, "*Nanoporous Polymeric Materials: A New Class of Materials with Enhanced Properties*") have also demonstrated that a reduction of the thermal conductivity through the solid phase can take place, being possible to attribute this reduction of the conductivity to a different phonon scattering mechanism (which is related to an increment of the tortuosity of the porous structure).

If the proven confinement effect directly influences the thermal conductivity it will increase the same due to the alignment and untangled of the backbone polymer chain (which is the one who transfer the energy or electrons). But there is no evidence of this fact.

On the contrary, resistivity measurements clearly showed the influence of the tortuosity, confirming that the latter increases when it goes from the micro to the nano scale. So it makes sense to adjust the structural factor (*g*) in the model of the thermal conductivity.

As a conclusion, it has been confirmed later that the expected variation of the tortuosity exists, being the most likely explanation for the reduction of the thermal conductivity due to a different phonon scattering mechanism. This fact corresponds directly to the *g* factor modification introduced in the theoretical model. However, no evidence that the confinement of polymer chains itself produce variations in the conductivity of the solid matrix have been found till now. Then, it was demonstrated that the confinement of the solid and gaseous phases to the nanometer scale influence the thermal conductivity through the Knudsen effect and the tortuosity of the solid matrix.

For instance, in low density materials, besides the expected huge reductions in thermal conductivity due to the demonstrated Knudsen effect, additional reductions can also take place owing to the increased tortuosity of the solid matrix, leading to total reductions around 59 % for relative densities of 0.05 and cell sizes of 100 nm.

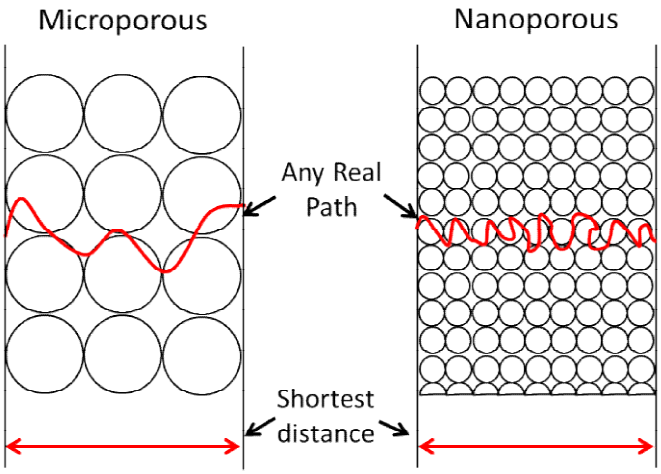

Figure III.5. Schematic representation of the solid phase tortuosity increase from microcellular to nanocellular polymers.

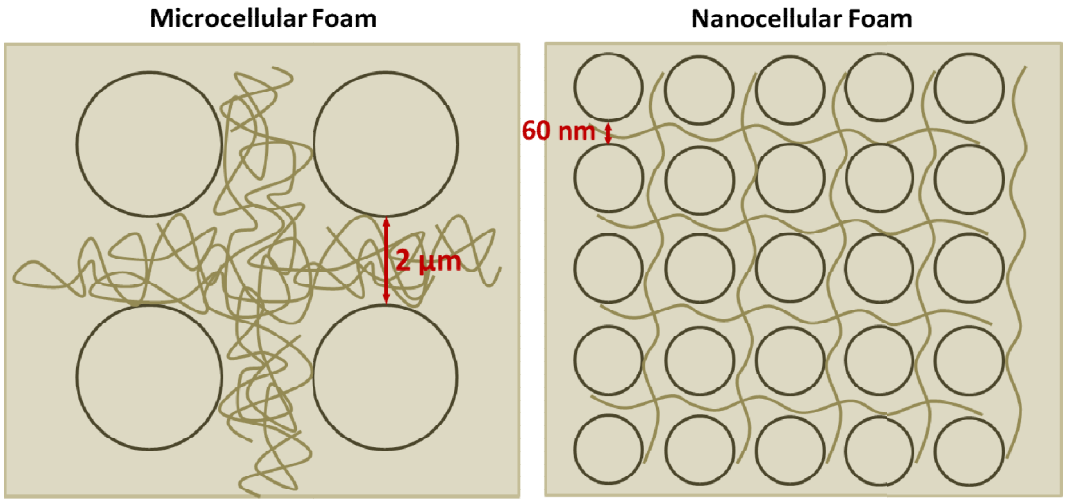

Figure III.6. Scheme of the expected molecular confinement in nanocellular polymers. In the left image, polymer chains are entangled because they have enough space, whereas in the right image polymer macromolecules are stretched due to the limitation of space.

III.5. References

1. Schmidt D, Raman VI, Egger C, du Fresne C, and Schädler V. Materials Science and Engineering: C 2007;27(5–8):1487-1490.
2. Solorzano E, Rodriguez-Perez MA, Lázaro J, and de Saja JA. Advanced Engineering Materials 2009;11(10):818-824.
3. Bedeaux D and Kapral R. The Journal of Chemical Physics 1983;79.
4. Kuhn J, Ebert HP, Arduini-Schuster MC, Büttner D, and Fricke J. International journal of heat and mass transfer 1992;35(7):1795-1801.
5. Cunningham A. ICHMT DIGITAL LIBRARY ONLINE 1987;24:32-51.
6. Holman JP. Heat Transfer. New York: McGraw-Hill, 1981.
7. Alvarez-Lainez M, Rodriguez-Perez MA, and De Saja JA. Journal of Polymer Science Part B: Polymer Physics 2008;46(2):212-221.
8. Reglero Ruiz JA, Saiz-Arroyo C, Dumon M, Rodríguez-Perez MA, and Gonzalez L. Polymer international 2011;60(1):146-152.
9. UNE-EN ISO 22007-2 AC. Determinación de la conductividad térmica y la difusividad térmica. Parte 2: Método de la fuente de calor plana transitoria (disco caliente). Plásticos, vol. UNE-EN ISO 22007-2: AENOR, 2012. pp. 23.
10. Ferkl P, Pokorný R, Bobák M, and Kosek J. Chemical Engineering Science 2013;97:50-58.
11. Lu X, Caps R, Fricke J, Alviso CT, and Pekala RW. Journal of non-crystalline solids 1995;188(3):226-234.
12. Sundarram SS and Li W. Polymer Engineering & Science 2013;53(9):1901-1909.
13. Reglero Ruiz JA, Dumon M, Pinto J, and Rodriguez-Pérez MA. Macromolecular Materials and Engineering 2011;296(8):752-759.

MECHANICAL PROPERTIES

Belén Notario Collado

Chapter IV. Mechanical Properties

Mechanical properties of cellular materials depend on both the properties of the solid matrix and the characteristics of the cellular structure. Focusing on the cellular structure, there are two main approaches to improve it (and thus the mechanical properties of the cellular material): increasing the homogeneity of the cellular structure [1], and reducing the average cell size of the foam [2].

Both strategies were proved at Massachusetts Institute of Technology (MIT) in the 80s with the development of microcellular polymers. Indeed, it was demonstrated that microcellular polymers exhibit, in general, enhanced mechanical properties over conventional foams. Particularly, significant improvements were obtained in the tensile strength [3] as well as in the impact properties [4].

Therefore, nowadays, it is expected that a further reduction of the cell size to the nanometer range (nanocellular materials) will lead to cellular materials with enhanced mechanical properties as compared to those of conventional and microcellular polymers [5, 6]. However, there is a lack of studies in this topic owing to the difficult task of manufacturing nanocellular polymers with appropriate dimensions and geometries.

In this chapter, the mechanical properties of closed cell microcellular (cell sizes about 7 µm and 11 µm) and nanocellular (cell sizes about 300 nm and 200 nm) PMMA foams with similar densities (around 0.5) and appropriate dimensions and geometries have been analyzed in detail, being possible to determine experimentally several expected advantages of nanocellular polymers. Likewise, the production route followed to obtain these samples is described and carefully explained. This work, entitle ***"Towards a new generation of polymeric foams: PMMA nanocellular foams with enhanced physical properties"***, was published in **Polymer 63 (2015)**.

In this work, the development of microcellular and nanocellular PMMA with tunable size and similar densities allowed the study of the transition from the micro to the nano scale of different mechanical properties, such as the mechanical behavior at high and low strain rates, the shore hardness, and the dynamic mechanical behavior.

The study of the cellular structure revealed that the optimized production route followed allows obtaining microcellular and nanocellular polymers with very homogeneous cellular structures. This structural homogeneity together with their tunable dimensions and shape made these samples suitable for a wide range of mechanical tests.

It was demonstrated that the glass transition temperature of foams with cells in the nanometer range is increased by 7º C with respect to both the microcellular polymers and the solid matrix. This fact is associated with the existence of a possible confinement effect of the polymer macromolecules. This statement was confirmed later by the demonstration of such confinement effect included in *Chapter II*, *"Molecular Confinement of Solid and Gaseous Phases of Freestanding Nanoporous Polymers Inducing Enhanced and Unexpected Physical Properties",* which confirms the prediction made.

Furthermore, the modulus of elasticity, the mechanical behavior at high strain rates as well as the shore hardness of nanocellular polymers is clearly increased as compared to microcellular polymers.

On the contrary, it was found that the strain to failure (in tension) and the toughness (in tension) were worst in the case of nanocellular polymers. This phenomenon was attributed on the one hand to the lower stress supported by the cell walls of nanocellular polymers that causes and early breakdown of the nanocellular material; and on the other hand, to the confinement effect which results in an increase rigidity of the polymer matrix.

Thus, it was experimentally demonstrated that these novel nanocellular polymers exhibit in general enhanced physical properties in comparison with microcellular polymers. In addition, the assumptions or hypothesis given in the article (induced in this chapter) at that time to explain some unexpected results were later confirmed in *Chapter II*.

Polymer 63 (2015) 116–126

Contents lists available at ScienceDirect

Polymer

journal homepage: www.elsevier.com/locate/polymer

Towards a new generation of polymeric foams: PMMA nanocellular foams with enhanced physical properties

B. Notario [a, *], J. Pinto [b], M.A. Rodríguez-Pérez [a]

[a] Cellular Materials Laboratory (CellMat), Condensed Matter Physics Department, University of Valladolid, 47011 Valladolid, Spain
[b] Nanophysics – Smart Materials Group, Istituto Italiano di Tecnologia (IIT), Via Morego, 30, 16163 Genova, Italy

ARTICLE INFO

Article history:
Received 26 December 2014
Received in revised form
30 January 2015
Accepted 2 March 2015
Available online 9 March 2015

Keywords:
Nanocellular foams
Mechanical properties
Cellular polymers

ABSTRACT

Could the reduction of the cell size to the nanometer range yield better mechanical properties than those of microcellular and conventional foams? This study answers this question taking advantage of the unusual ability of the solid state poly(methyl methacrylate) (PMMA)-CO_2 system to produce comparable bulk foams both in the micrometer and nanometer range.

Several microcellular and nanocellular foams with cell sizes from 11 μm to 200 nm and relative densities about 0.5 have been produced and characterized. In particular, the cellular structure has been characterized in detail as well as the dynamic mechanical behavior, the mechanical behavior at high and low strain rates, and the shore hardness. As a result, it has been demonstrated that nanocellular foams present a significant improvement in several physical properties due to the modified cellular structure. These results confirm nanocellular foams as a new generation of polymeric foams with enhanced properties.

1. Introduction

In 2013, the global market of polymer foams was about 19.1 million tons according to the report "The future of polymer foams to 2019" [1]. This market represents around $87 billion, including those foams used in packaging, construction, automotive, and comfort applications. Furthermore, it is expected that this market continues growing reaching 25.1 million tons in 2019.

Most of these polymer foams are used in construction applications, due to their good thermal and mechanical properties. For instance, rigid polyurethane (PU) foams are mainly used as thermal insulators in construction; polystyrene (PS) foams are used as insulators in construction and in packaging applications; and polyvinylchloride (PVC) foams are characterized to have good thermal insulation properties, very good mechanical strength and to be usual materials for sandwich panels.

Thus, in those applications in which weight is a key factor, cellular materials (due to their reduced density in comparison with the former solid) arise to provide us a remarkable solution.

It is well known that density of foamed samples plays a main role on the physical properties of cellular materials. This dependence between density and physical property of the cellular material is given by the Gibson and Ashby equation [2]:

$$P_f = C \cdot P_s \cdot \left(\frac{\rho_f}{\rho_s}\right)^n \quad (1)$$

According to this equation, the property of a cellular material (P_f) is equal to the property of the same material 100% solid (P_s) multiply by the relative density (ρ_f/ρ_s) to the n. C and n are two parameters that can be determined experimentally. C usually takes values around 1 for the majority of the physical properties and cellular materials, whereas n normally takes values comprised between 1 and 2. In the case of mechanical properties, n usually takes a value of 2. In this work, the analysis of the mechanical response will be carried out using this assumption (except in some cases that will be specified), i.e. by dividing the property of the foam by the square of the relative density.

On the other hand, the properties of cellular materials depend on both the properties of the solid matrix and the characteristics of the cellular structure. Focusing on the cellular structure, two of the most common strategies to improve it (and therefore the properties of the foam) can be found in the literature: increasing the

* Corresponding author.
E-mail address: belen.notario@fmc.uva.es (B. Notario).

http://dx.doi.org/10.1016/j.polymer.2015.03.003
0032-3861/

homogeneity of the cellular structure (i.e. have very narrow cell size distributions) [3], and reducing the average cell size of the foam [4].

The validity of both strategies was proved at Massachusetts Institute of Technology (MIT) in the 80s with the development of microcellular foams [5]. Since then, many research groups have investigated the mechanical properties of these materials. Results have shown that microcellular foams present improved tensile and impact properties over conventional foams in systems such as polyethersulfone (PESF) and polyphenylsulfone (PPSF) [6], polyvinyl chloride (PVC) [7], blends of polyethylene and isotactic polypropylene (PE/i-PP) [8], and polycarbonate (PC) [9]. For instance, the impact strength of microcellular PVC foams decreased linearly with relative density [7]. This behavior is better than expected because as mentioned above, the mechanical properties usually depend on the square of the relative density. It has been hypothesized that this improved behavior takes place due to the reduction of the cell size as well as due to the homogeneity of the cellular structure.

Nevertheless, because of the difficulty of manufacturing microcellular polymeric foams with different cell sizes for a constant density, the studies related to the effect of cell size on the mechanical properties are still scarce. C. Barlow and co-workers [10] obtained that when cell size is within the micrometer range, the impact strength of microcellular PC foams increases as cell size increases. On the contrary, no effects were obtained in the case of expanded polystyrene (EPS) [11], in which the impact strength was not affected by the cell size (at least in the range analyzed (1–300 μm)). Regarding to tensile fracture, it was found that in microcellular polyethylene terephthalate (PETE) and polypropylene (PP) foams this value increases when decreasing the cell size [12].

The effects of foaming conditions on the cellular structure, and thus on the mechanical behavior of microcellular foams, have been also studied [11,13,14]. Microcellular morphologies developed in poly (lactic acid) (PLA) [13], thermoplastic polyolefin (TPO) [14], and expanded polystyrene (EPS) [11] showed a strong dependence on the process parameters. This variation in the cellular structure significantly affects the final mechanical properties of the foam.

As expected, microcellular foams generally show improved mechanical properties over conventional foams. Specially, significant improvements were found in the tensile fracture [12] as well as in the impact properties [7].

Currently, the next goal in the cellular materials science and technology is reducing the cell size from values about 50 microns (typical for microcellular materials) to values about or below 100–200 nm. These materials known as sub-microcellular and nanocellular materials are very promising materials: the reduction of the cell size to the nanometer range should enhance some of their physical properties in comparison with those of conventional and microcellular foams [15,16]. Furthermore, these new materials could achieve non-expected improvements in other properties or new effects could appear due to the dimension of the cell size and cell walls in the nanometer range.

For instance, it is expected that nanocellular foams produced from amorphous polymers with a well-defined cellular structure with cell sizes under the wavelength of the visible radiation could keep, up to some extent, the transparent character of the former solid [17].

On the other hand, it has been proved that cell size reduction allows a significant reduction of the thermal conductivity due to the decrease of the heat conduction through the gas phase (Knudsen effect [15]). This behavior has been demonstrated both in aerogels [18,19] and recently in nanocellular polymeric foams [20].

Likewise, these nanocellular materials could have better mechanical properties than those of conventional cellular materials or microcellular ones. D. Miller et al. [21] studied the tensile and impact properties of microcellular and nanocellular polyetherimide (PEI) foams. They produced microcellular and nanocellular foams of three different densities, in order to clearly distinguish the effect of cell size over a density range. Tensile results reveal that cell size did not affect the modulus of elasticity and the yield strength, while the strain to failure and tensile toughness was increased by a factor of 2–3 when cell size is reduce to the nanometer range. In addition, impact resistance of nanocellular foams exhibit a higher value than that of the microcellular ones.

The mechanical response of low-density poly (methyl methacrylate) (PMMA) based nanocellular foams was studied by J. A. Reglero-Ruiz et al. [22] by means of a dynamic mechanical analyzer (DMA). Three-point bending results provides that Young's modulus of PMMA-based nanocellular foams seems to present higher values than those of microcellular PMMA foams from the literature.

Nevertheless, the lack of further or deeper studies in this area is due to the difficult task of producing nanocellular foams with appropriate dimensions.

The main problem of manufacturing nanocellular materials resides in the thermodynamics of the foaming processes (commonly the gas dissolution foaming method [23–26]). Creation of nanometric cells increases substantially the interfacial (surface) area and the interfacial (surface) free energy, being necessary to use different approaches to achieve the high cell nucleation densities required to produce nanocellular foams (above 10^{14} nuclei/cm^3).

For instance, Costeux et al. obtained nanocellular foams with relative densities between 0.15 and 0.3, and with cell sizes between 100 and 300 nm, from acrylic copolymers by adding nanosilica particles [27]. D. Miller and coworkers obtained polyetherimide (PEI) foams with relative densities of 0.4 and higher, and cell sizes from 50 nm to 1 micron by varying the saturation pressure [28]. And T. Otsuka et al. produced nanocellular foams of polystyrene (PS) and PMMA blends with cell sizes around 50 nm and cell densities of $8.5 \cdot 10^{14}$ cells/cm^3 [29].

By using block copolymers, nanocellular foams can be achieved from blends of PMMA [poly(methyl methacrylate)] and MAM triblock copolymer [poly(methyl methacrylate)-block poly(butyl acrylate)-block poly(methyl methacrylate)] [22,30–32]. Previous studies demonstrated that PMMA-based nanocellular foams present a nanosized cellular structure and a cell nucleation density up to 10^{14} cells/cm^3 [30,32].

Nevertheless, all these previous studies have difficulties either to obtain large samples or to produce comparable microcellular and nanocellular foams (since nanocellular structures are achieved by adding nanoparticles, by using copolymers, etc.). These drawbacks make the samples obtained in these studies in general unsuitable for measuring their physical properties with the aim of studying the transition between the microcellular and nanocellular range.

In this work, samples have been produced by varying the saturation pressure. A well-known method to control the number of nuclei formed by homogeneous nucleation [25]. This method was previously used as a prior approach to produce microcellular and nanocellular PMMA foams [30].

In this study, this methodology was optimized in order to obtain a better control over both the cellular structure and the density; leading into a wide set of samples not only with appropriate cell sizes and densities, but with appropriate and tunable dimensions to be tested by different standard methodologies. By this way, it has been possible to confirm experimentally several expected advantages of the nanocellular polymer foams.

2. Experimental part

2.1. Materials and foam production

Optically transparent poly(methyl methacrylate) (PMMA) was kindly supplied by Altuglas-Arkema Company (France) in the form

of pellets. The PMMA used presents a glass transition temperature (T_g) of 115 °C and a density (ρ) of 1180 kg/m^3.

PMMA pellets were first dried in vacuum (680 mm Hg) at 80 °C during 4 h before processing. Then, they were compression molded into precursors of 155 mm × 75 mm and 4 mm in thickness using a two-hot plates press. The temperature of the press was fixed at 250 °C. The material was first molten without pressure for 9 min, then it was compacted under a constant pressure of 21.8 bars for another minute and finally it was cooled down under the same pressure. Transparent samples obtained showed a good surface appearance with no presence of air bubbles inside the parts. Finally, these molded precursors were cut at the desired dimensions (depending on the test to be performed) and used later for foaming.

Foaming experiments were carried out in a high pressure vessel (model PARR 4681) provided by Parr Instrument Company, with a capacity of 1 L and capable of operating at a maximum temperature of 350 °C and a maximum pressure of 41 MPa. The reactor is equipped with an accurate pressure pump controller (model SFT-10) provided by Supercritical Fluid Technologies Inc., and it is controlled automatically to keep the pressure at the desired values. The vessel is equipped with a clamp heater of 1200 W, and its temperature is controlled via a CAL 3300 temperature controller. The CO_2 vessel temperature and pressure were monitored in the course of the process. Therefore, a collection of experiments were performed using the so-called solid state foaming process [33,34]. This process with amorphous polymers has three stages: the saturation (under fixed gas pressure and temperature), desorption (room pressure and temperature), and foaming of the sample (at a temperature over or near the effective T_g of the polymer).

Prior to this work, it was observed that cell size of PMMA presents a strong dependence with saturation pressure. In fact it was possible to obtain both micro and nanocellular foams using the same raw material [30]. However, the final density of the foams was also related to the cell size and/or to the saturation pressure (Fig. 1), and therefore microcellular and nanocellular foams with comparable densities were not obtained.

According to these previous results, in this study it was decided to work at room temperature during the saturation stage and at four different pressures to obtain two different microcellular foams (at 13 and 15 MPa) and two different nanocellular ones (at 31 and 32 MPa). All samples were saturated during 20 h to assure equilibrium dissolution of CO_2 in the polymer. After the saturation process, the pressure inside the vessel was released. During the desorption step, the samples temperature decrease to values clearly below room temperature (adiabatic depressurization), so when samples are removed from the pressure vessel they are cooled and solid [35]. Unlike previous studies, in this one a step of controlled foaming is introduced in order to control the final density of the samples. Foaming of the samples was carried out in a thermostatic water bath at temperatures between 25 and 60 °C and times between 40 s and 5 min. The temperatures used were lower than the glass transition temperature of PMMA because the effective glass transition temperature of plasticized PMMA with CO_2 can reach values near room temperature [33] or even below room temperature in some particular conditions [34].

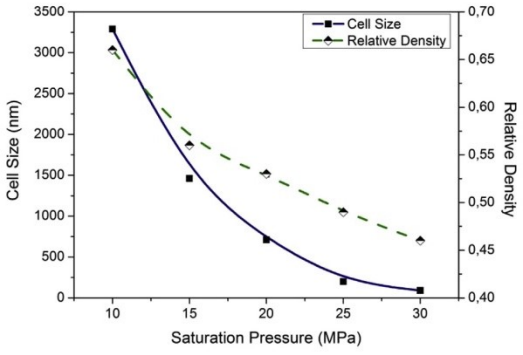

Fig. 1. Variation of the cell size and density with the saturation pressure for neat PMMA [30].

2.2. Samples preparation

PMMA foamed samples were polished using a polishing machine (model LaboPOl2-LaboForce3, Struers) equipped with a silicon carbide grinding paper (P 180) to obtain homogeneous surfaces and to remove the outer solid or dense skin of the samples [36]. After polishing, samples had an average thickness of around 5 mm.

Then, solid and polished samples were machined in different ways according to the test to be performed. Thus, DMA samples (both solid and foamed samples) were prepared using a precision cutting machine Mod. 1000 from IsoMet. The test pieces were prepared to be approximately 2 mm in thickness, 7 mm in width, and 25 mm in length.

Tensile and impact specimens (both solid and foamed samples) were prepared according to UNE-EN ISO 2818 [37] "Plastics. Preparation of test specimens by machining". In particular, tensile samples were created according to Type 1BA (UNE-EN ISO 527-2 [38]) sample specifications.

Finally, it should be noticed that solid and foamed PMMA samples were stored at controlled temperature and humidity (23 °C and 50% humidity) at least three days before being measured in order to avoid discrepancies in the measurements due to differences in temperature or humidity between the different samples.

2.3. Characterization techniques

2.3.1. Density

Foamed and solid sample densities were determined by water-displacement method, based on Archimedes' principle, using the density determination kit for an AT261 Mettler-Toledo balance. At least three measurements were carried out for each sample produced.

2.3.2. X-ray analysis

The determination of the mechanical properties of cellular materials requires very homogeneous foamed samples without internal defects that could be an important source of inaccuracy in the measurements. Then, the first step in this study was the selection of appropriate samples by using the X-ray radiography technique [39], with the aim of excluding those samples presenting defects or inhomogeneities without damage for the samples.

Fig. 2 shows X-ray radiographs of a foamed sample with internal defects or inhomogeneities (red arrows) (top) and a homogeneous sample (bottom).

All the foams produced were characterized by means of this technique, but only those samples without defects were finally chosen to be analyzed with the techniques explained later in this section.

2.3.3. Cellular structure

Cellular structure of foamed samples was analyzed by means of scanning electron microscopy (model JSM 820, Jeol). Samples were freeze-fractured in liquid nitrogen to assure that the microstructure or nanostructure remained intact. The fractured surface was

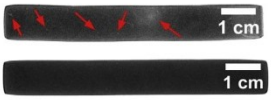

Fig. 2. X-ray radioscopy images of a foam with structural defects (red arrows) (top) and homogeneous foam (bottom) without internal defects. (For interpretation of the references to colour in this figure legend, the reader is referred to the web version of this article.)

sputter-coated with gold using a sputter coater (model SCD 005, Balzers Union). Cell sizes were determined using a specific image processing software [40] based on ImageJ/FIJI [41]. This software provides the cell size distribution, the average cell size, the standard deviation of the cell size distribution, the cell anisotropy ratio distribution, the average cell anisotropy ratio, the cell density N_v (number of cells per cubic centimeter of the foam), and the cell nucleation density N_0 (number of cell nuclei per cubic centimeter of the solid precursor) that can be calculated from N_v according to equation (2) [42]:

$$N_0 = N_v \frac{\rho_s}{\rho_f} \tag{2}$$

where ρ_s is the density of the solid material and ρ_f is the density of the foam.

2.3.4. Mechanical behavior

Viscoelastic behavior of foamed samples both at room temperature and as a function of temperature was analyzed using a dynamic mechanical analyzer model DMA 7 from Perkin Elmer. The experiments were performed in a three-point bending configuration with a frequency of 1 Hz and a dynamic stress of $3 \cdot 10^4$ kPa for foams and of $1 \cdot 10^5$ kPa for the solids. A static stress of 1.2 times the value of the dynamic stress was applied in all the conducted tests. Measurements as a function of temperature were carried out at a rate of 3 °C/min from −20 to 150 °C. The onset of temperature was maintained constant during 3 min before starting the experiment in order to assure an equilibrium temperature.

Mechanical properties in tension at low strain rates were determined using universal testing machine Instron model 5.500R6025. At least three specimens were tested for each kind of sample, all of them at room temperature. Tensile tests were carried out at a strain rate of 0.5 mm/min according to UNE-EN ISO 527/2 [38].

A 0.5 J pendulum for impact testing (Charpy, Izod, Tensile) Frank was used in order to determine the mechanical behavior at high strain rates. At least three specimens were used for each sample, all of them carried out at controlled humidity and temperature and performed according to UNE-EN ISO 179-1 [43].

Shore hardness D was measured by means of a Bareiss durometer model U/72. At least three specimens were used for each sample, all of them carried out at controlled humidity and temperature and performed according to UNE-EN ISO 868 [44].

3. Results and discussion

In order to achieve similar densities and porosities among samples with cells in the micrometer and nanometer range, and thus clearly distinguish the effect of cell size, foaming parameters were finely tuned. By modifying the saturation pressure, the cell nucleation density (N_0) is varied, and consequently the final average cell size and the final expansion degree is varied (see Fig. 1 of section *Materials and Foam Production*). On the other hand, by adjusting the foaming temperature, it is possible to vary the final expansion degree (i.e. the porosity) without much larger cell size variations (because the volume of the cell is proportional to the cube of its radius (assuming spherical cells)).

Table 1 summarizes the foaming conditions together with density results for the solid, the microcellular and the nanocellular foams. As a result of the simultaneous control of N_0 and the degree of expansion, differences between density (ρ) values of microcellular and nanocellular foams are significantly reduced, obtaining in all the cases foams in a range of porosity (V_f) between 0.5 and 0.6. This fact allows us to perform the accurate comparative study that will be explained in the next sections.

A large number of samples were manufactured for each set of processing parameters, obtaining an excellent reproducibility between them. For this reason, from now on for each set of samples the mean values together with the standard deviations obtained for each property will be displayed. As it can be observed later in the graphs, the overall reproducibility of the experiments was significantly good.

From now on, samples saturated at 13 MPa will be denoted as Micro 1, samples saturated at 15 MPa will be denoted as Micro 2, samples saturated at 31 MPa will be denoted as Nano 1, and samples saturated at 32 MPa will be denoted as Nano 2.

3.1. Cellular structure

The main goal of this work is to clearly distinguish the effect of cell size on the mechanical behavior of PMMA foams. For this reason, a detailed analysis of the cellular structure has been carried out in those samples that were selected for the study (see *X-Ray Analysis* section).

Cellular structure of foamed samples was analyzed in two different planes: *ZY* plane and *ZX* plane (see Fig. 3).

Representative SEM images of the foamed samples in the two different planes can be observed in Fig. 4 (*ZY* plane) and in Fig. 5 (*ZX* plane). The analysis of the structure allows distinguishing two groups of foams: microcellular (top part of Figs. 4 and 5) and nanocellular (bottom part of Figs. 4 and 5) PMMA foams. All of them present closed cell morphologies due to the conditions of pressure and temperature at which they have been manufactured [32]. In addition, a reduction of the cell size related to the increase of the saturation pressure (Micro 2 with respect to Micro 1, and Nano 2 with respect to Nano 1) is also observed.

Distribution of the cell size of these foams is showed on Fig. 6. Along with the decrease in the average cell size (from Fig. 6a–d) it is also observed that cell size distribution becomes more narrow in the case of nanocellular foams.

Other parameters of the cellular structure such as the average cell size, cell nucleation density (N_0), average anisotropy ratio, the asymmetry coefficient, and the standard deviation divided by the average cell size are summarized in Table 2.

Regarding to average cell size, the two different scales in which we are working can be clearly distinguished (micrometer and

Table 1
Foaming parameters and density results of foamed and solid samples.

Name	Saturation pressure (MPa)	Foaming temperature (°C)	Foaming time (s)	ρ (g/cm^3)	V_f
PMMA_solid	–	–	–	1.18	0
Micro 1 PMMA foam	13	60	40	0.61	0.48
Micro 2 PMMA foam	15	60	45	0.57	0.51
Nano 1 PMMA foam	31	25	300	0.51	0.57
Nano 2 PMMA foam	32	25	300	0.49	0.58

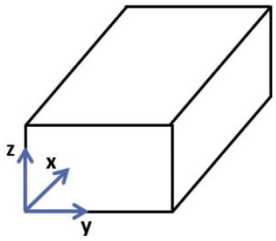

Fig. 3. Schematic view of the planes analyzed, where *Z* is the compression molding direction and the thickness direction of the foams.

nanometer range). Moreover, for each scale, two different set of samples with different cell sizes were obtained.

From cell nucleation density data (N_0) a difference of five orders of magnitude between foams in the micro and nanometer range is found. These results are in good agreement with those obtained by Pinto et al. [30], who produced polymer foams from neat PMMA both in the micrometer and nanometer scale. Their microcellular foams present a cell nucleation density around 10^{10} cells/cm^3, whereas their nanocellular foams present a cell nucleation density of 10^{15} cells/cm^3.

It is observed that PMMA foams, microcellular and nanocellular, are almost isotropic (anisotropy ratio close to 1), although nanocellular foams are slightly oriented in the *Z* direction.

The standard deviation of the cell size distribution divided by the average cell size has been also analyzed. This parameter provides information about the homogeneity of the cellular structure. The results obtained confirm that both microcellular and nanocellular foams present homogeneous cellular structures ($SD/\Phi < 0.5$), being more homogeneous for foams in the nanometer range.

Finally, the asymmetry coefficient provides information on the shape of the distribution. In our case, this magnitude provides significant information about the presence, or not, of a bi-modal cell size distribution. Presence of a bi-modal cell size distribution could introduce difficulties in the evaluation of the mechanical response, as there would not be a well-defined value of the average cell size to relate to the measured mechanical behavior [45]. When the value of the asymmetry coefficient is close or higher than one, it implies that there is a bi-modal cell size distribution. In this study,

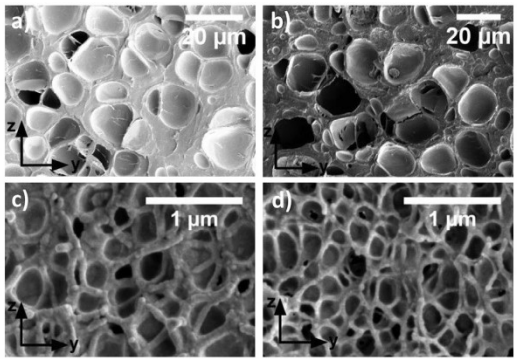

Fig. 4. SEM micrographs of the cellular structure of a) Micro 1 PMMA foam (top left), b) Micro 2 PMMA foam (top right), c) Nano 1 PMMA foam (bottom left), and d) Nano 2 PMMA foam (bottom right) in the *ZY* plane.

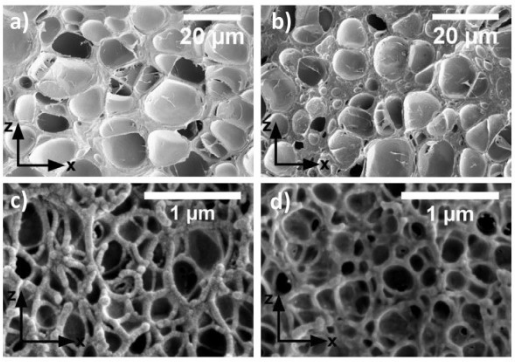

Fig. 5. SEM micrographs of the cellular structure of a) Micro 1 PMMA foam (top left), b) Micro 2 PMMA foam (top right), c) Nano 1 PMMA foam (bottom left), and d) Nano 2 PMMA foam (bottom right) in the *ZX* plane.

this does not take place in any case, thus, the shape of the distribution is mono-modal (see Fig. 6). So, no difficulties due to bi-modal cell size distributions can be expected in the analysis of the results.

Therefore, our production route allows obtaining nanocellular and microcellular foams with a high homogeneity in their cellular structure, being adequate for the study presented in the following sections.

3.2. Viscoelastic behavior

3.2.1. Tan δ

The viscoelastic behavior of solid and foamed PMMA was studied on these samples. Fig. 7 illustrates the temperature dependence of *tan δ* of both solid and microcellular and nanocellular foams. The factor *tan δ* is very sensitive to the structural changes of the materials, and can be calculated from the ratio of the loss modulus to the storage modulus (E''/E') measured by DMA.

The *tan δ* plot shows one main peak at around 120 °C that corresponds to an α-relaxation [46]. The maximum of the α-relaxation is normally associated with the glass transition temperature of the material (T_g). It is observed that by reducing the average cell size the *tan δ* peak values of the PMMA matrix shifts to higher temperatures. The nanocellular foams present T_gs 7 °C higher than that of both the microcellular foams and the solid matrix (see Table 3). These results are in good agreement with previous studies in which the glass transition temperature was measured by differential scanning calorimetry (DSC) [22]. This effect is normally attributed to a possible confining effect [22,47] due to the average cell size reduction and the increase of cell density that leads to a lower cell wall thickness. An increase of the glass transition temperature implies a higher energy needed to activate the molecular mobility. Since in this study cell wall thickness of nanocellular foams is reduced to 60 nm, it seems that the confinement of the polymer chains can be taking place, hindering the activation of long-range molecular motions.

In addition, in Fig. 7 it is also observed that the reduction of the cell size to the nanometer range increases the intensity of the *tan δ* peak from 1.4 to 1.7. It seems that once the molecular motion has been activated, these ones are more intense in the nanocellular material than in the microcellular one.

Finally, Fig. 8 shows a zoom of the temperature dependence of *tan δ* of both microcellular and nanocellular foams. The *tan δ* plot shows one peak at around 15 °C, which has been identified in the

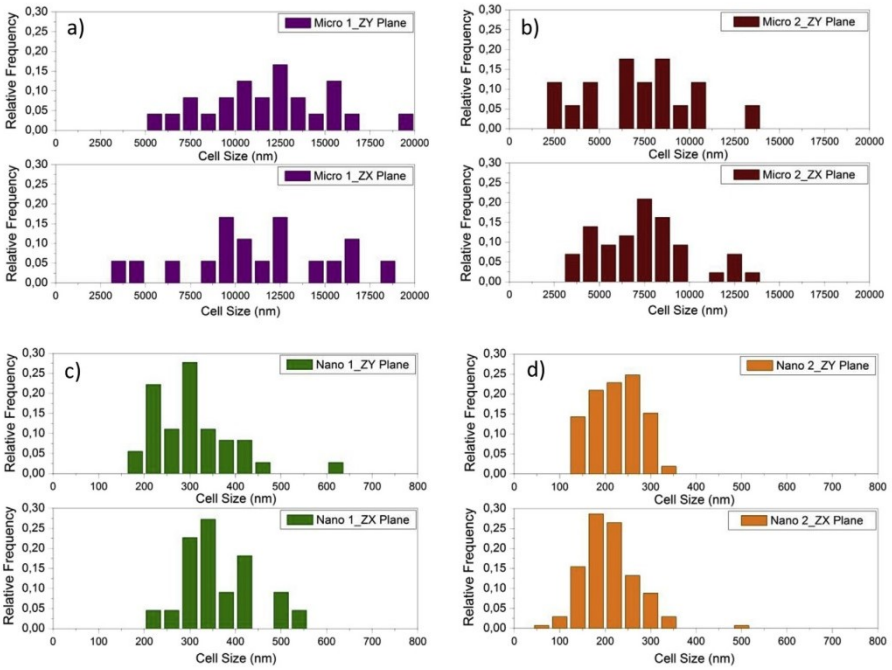

Fig. 6. Cell size distributions of a) Micro 1 PMMA foam (top left), b) Micro 2 PMMA foam (top right), c) Nano 1 PMMA foam (bottom left), and d) Nano 2 PMMA foam (bottom right), in the *ZY* and *ZX* planes.

literature as a β-relaxation associated with a rotational isomerism of the pendant ester group [46]. Table 4 shows the values of this β-relaxation measured at room temperature. The results show that the nanocellular foams exhibit a *tan δ* higher than that of both the microcellular foams and the solid material. So it might be thought that the polymer molecules, despite their confinement, are capable of activating certain energy absorption mechanisms, typically associated with short-range molecular motions. Then it is as if the confinement effect allows certain local energy dissipation mechanisms being more effective.

In general, microcellular and nanocellular foams exhibit an unexpected behavior compared to previous results obtained on samples of PMMA reinforced with nanoparticles where it was found that the *tan δ* peak intensity was reduced and was shifted to higher values [48–50].

Table 2
Cellular structure results for the microcellular (denoted as Micro 1 and Micro 2) and nanocellular (denoted as Nano 1 and Nano 2) PMMA foams.

Name	Plane	Cell size (Φ) (nm)	N_0 (cells/cm^3)	Anisotropy ratio (R) (Z/Y or Z/X respectively)	Asymmetry coefficient	Standard deviation (SD)/Φ
Micro 1	ZY	11,880	$1.1\cdot10^{9}$	1.06	0.74	0.57
Micro 1	ZX	11,330	$1.1\cdot10^{9}$	1.20	0.60	0.40
Micro 2	ZY	7190	$5.4\cdot10^{9}$	1.03	0.48	0.41
Micro 2	ZX	7540	$4.7\cdot10^{9}$	1.09	0.49	0.42
Nano 1	ZY	300	$6.8\cdot10^{13}$	1.05	0.55	0.23
Nano 1	ZX	360	$4.9\cdot10^{13}$	1.20	0.56	0.17
Nano 2	ZY	210	$3.2\cdot10^{14}$	1.15	−0.17	0.18
Nano 2	ZX	205	$2.8\cdot10^{14}$	1.18	0.23	0.20

3.2.2. Storage modulus

Fig. 9 shows the variation with temperature of the storage modulus divided by the square of the relative density for microcellular and nanocellular foams. The storage modulus connects with the elastic modulus of the materials (E).

In all the temperature range under study, the modulus of the nanocellular foams is higher than that of the microcellular ones. The behavior of the solid material has not been included in Fig. 9

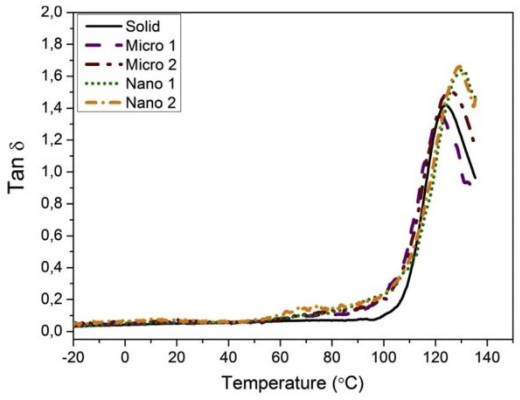

Fig. 7. *Tan δ* vs temperature obtained by DMA for both PMMA solid and for PMMA microcellular and nanocellular foams.

Table 3
Glass transition temperature obtained by DMA for both PMMA solid and for PMMA microcellular and nanocellular foams.

Name	T_g (°C)
Solid	122.6
Micro 1	121.4
Micro 2	124.8
Nano 1	129.7
Nano 2	126.1

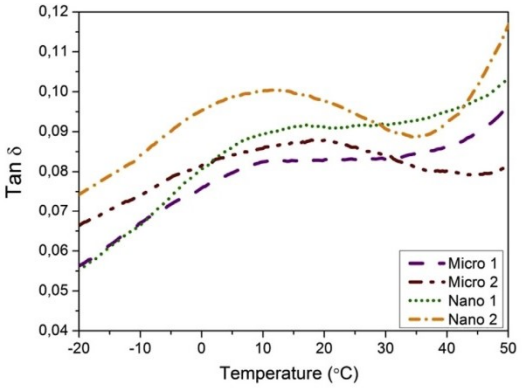

Fig. 8. : Zoom of the curve *tan δ* vs temperature that shows the *β* relaxation for PMMA microcellular and nanocellular foams.

because the DMA was not able to accurately measure it due to its high Young's modulus of about 3100 MPa (according to the value provided by the supplier).

A same trend it is found when the storage modulus is measured at room temperature (Table 4). According to these results, an improvement of around 37% of the storage modulus of the nanocellular foams with respect to the microcellular ones is found.

However, nanocellular foams present anisotropic cells elongated along the thickness direction (see *Cellular Structure* section). It is known that the anisotropy of the cells has a great influence on the Young's modulus. Foams with anisotropic cells present enhanced values of E in the direction of the long axis of the cells; on the contrary, values of E measured in a direction perpendicular to the long axis of the cells are significantly lower than expected [2].

In order to clearly distinguish the effect of cell size from the effect of the anisotropy on the results obtained, a quantitative analysis of the possible influence of the anisotropy on the Young's modulus was performed.

In this work, determination of E by DMA was carried out in a direction parallel to the long axis of the cells. In this case, the influence of the anisotropy ratio for closed cell foams is given by Ref. [2]:

$$E_a = E_i R + E_i(1 - f_s)\frac{1 + (1/R)^3}{1 + (1/R)} \quad (3)$$

where E_a represents the Young's modulus of an anisotropic foam, E_i is the modulus of the same foam if it is isotropic, R is the anisotropy ratio, and f_s is the mass fraction in the struts (it has been considered a value of $f_s = 0.33$).

The values obtained for E_i are summarized in Table 5, in which it has been considered as anisotropy ratio an average value of the anisotropy in the *ZY* and *ZX* direction. It is observed that, even if the foams were isotropic, the differences found between microcellular and nanocellular foams will be maintained.

Therefore, the significant increase found in the storage modulus of the nanocellular foams with respect to the microcellular ones can be attributed to the presence of the nanocellular structure, with more uniform cellular structure, cell sizes in the nanometer range, and perhaps the modification of the properties of the solid matrix due to the confinement into such nanometric dimensions.

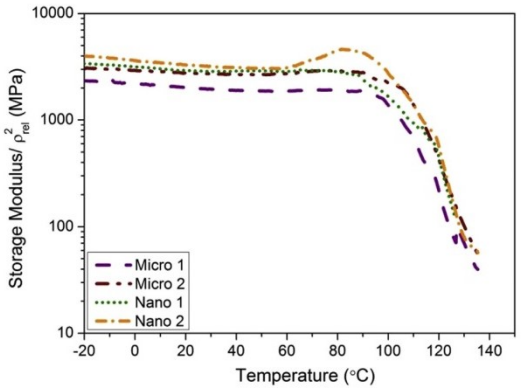

Fig. 9. Storage modulus normalized by the square of the relative density for both PMMA microcellular and nanocellular foams.

3.3. Tensile tests

An analysis of the mechanical behavior at low strain rates of both solid and foamed PMMA is carried out in this section. The stress–strain curves obtained in the tensile experiments are presented in Fig. 10. In addition, Table 6 summarizes the main tensile parameters: the average Young's modulus, stress at break, strain at break, and toughness values.

Probably, one of the most interesting results is the effect of cell size on the strain at break. Microcellular foams failed at mean strains around 3.6% (a value close to the solid), whereas

Table 4
Storage modulus together with *tan δ* obtained at room temperature for both PMMA microcellular and nanocellular foams.

Name	Relative density	Storage Modulus (MPa)	Storage Modulus/ρ^2_{rel} (MPa)	Tan δ
Micro 1	0.52	579 ± 27.2	2169	0.083 ± 0.005
Micro 2	0.49	693 ± 91.9	2884	0.087 ± 0.006
Nano 1	0.43	570 ± 5.13	3083	0.091 ± 0.003
Nano 2	0.42	611 ± 91.9	3448	0.096 ± 0.005

Table 5
Young's modulus obtained by equation (3) assuming isotropic microcellular and nanocellular foams.

Name	Relative density	Average anisotropy ratio	E_i/ρ^2_{rel} (MPa)
Micro 1	0.52	1.13	1236
Micro 2	0.49	1.06	1703
Nano 1	0.43	1.12	1783
Nano 2	0.42	1.16	1975

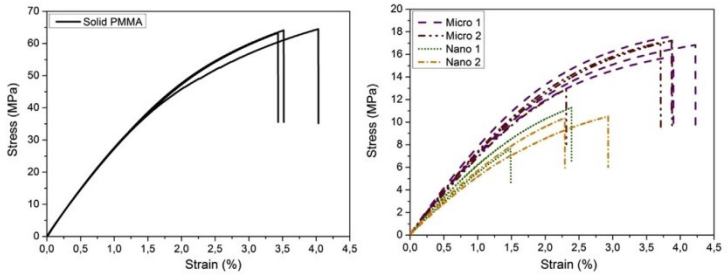

Fig. 10. Tensile stress–strain curves for solid PMMA (left) and for microcellular and nanocellular PMMA foams (right).

nanocellular foams failed long before (at mean strains around 2.3%). The glass transition temperature results (Fig. 7, *Viscoelastic Behavior* section) show an increase of 7 °C in the temperature of nanocellular foams in comparison with both the microcellular foams and the solid matrix. The confinement of the polymer chains within the cell walls, associated with the increase found in the T_g, will result in an increase of the rigidity of the polymer matrix. This fact, together with the lower stress supported by the cell walls of nanocellular foams (with a thickness value significantly lower than that of the microcellular ones; from approximately 1.5 μm in the case of the microcellular foams to around 60 nm in the case of the nanocellular ones), causes an early breakdown of the nanocellular foams.

As a direct result of the reduction strain at break, the amount of energy absorb (toughness) before fracture is significantly lower in nanocellular foams than in microcellular ones. The toughness is calculated as the area under the stress–strain curve. Similarly, the ultimate tensile strength of nanocellular foams (mean value 10) is also lower than that of microcellular ones (mean value 16).

Finally, the Young's modulus obtained by the tensile tests was divided by the square of the relative density to study the influence of the cell size (Fig. 11). This representation has been carried out in order to better compare the trend of the modulus of elasticity found by DMA between microcellular and nanocellular foams with the results obtained in the tensile tests. According to the results shown in Fig. 11, nanocellular foams exhibit a slightly higher Young's modulus value than the microcellular ones (improvement of 11%).

Nevertheless, the anisotropy presented in nanocellular foams may be influencing these results. As already mentioned in *Viscoelastic Behavior* section, depending on whether the measurement is performed in a plane perpendicular or parallel to the orientation of the long axis of the cell, the value obtained of E can be higher or lower than the expected [2]. In order to differentiate the effect of cell size from the effect of the anisotropy on the Young's modulus results, a quantitative analysis based on Gibson and Ashby models is carried out.

In tensile test, Young's modulus was determined in a direction perpendicular to the long axis of the cells (samples were stretched in the X direction (see Fig. 3)). In this situation, the influence of the anisotropy ratio for closed cell foams is given by Ref. [2]:

Table 6
Summary of tensile test measurement data.

Name	Relative density	Mean Young's Modulus (MPa)	Mean stress at break (MPa)	Mean strain at break (%)	Toughness (J cm^{-3} 10^{-2})
Solid	1	3225 ± 18	64.12 ± 0.53	3.66 ± 0.32	1.46 ± 0.17
Micro 1	0.52	791 ± 45	16.75 ± 0.92	4.00 ± 0.20	0.44 ± 0.03
Micro 2	0.49	758 ± 26	15.72 ± 2.44	3.30 ± 0.86	0.33 ± 0.14
Nano 1	0.43	643 ± 42	10.02 ± 2.11	2.09 ± 0.52	0.13 ± 0.05
Nano 2	0.42	577 ± 20	9.77 ± 0.74	2.61 ± 0.45	0.16 ± 0.03

$$E_a = \frac{E_i}{2}\frac{1}{\frac{R}{1+(1/R)^3}+(1-f_s)\frac{1}{1+(1/R)}} \quad (4)$$

where again E_a represents the Young's modulus of an anisotropic foam, E_i is the modulus of the same foam if it is isotropic, R is the anisotropy ratio, and f_s is the mass fraction in the struts (it has been considered a value of $f_s = 0.33$).

Table 7 shows the values obtained for E_i. It is observed that even if foams were isotropic, the increase in the Young's modulus of nanocellular foams with respect to microcellular ones will remain. So, the reduction of the cell size to the nanometer range enhanced the modulus of elasticity, confirming the results found by DMA.

3.4. Impact resistance

In this section, a comparison between the mechanical behavior at high strain rates of both the solid and the microcellular and nanocellular foams is carried out. The results corresponding to the impact resistance tests (Fig. 12) show that there is a clear transition in the values between microcellular and nanocellular foams, whereas the solid material presents a behavior similar to microcellular foams.

This significant increase of about 25% in the impact resistance of nanocellular foams with respect to microcellular ones could be produce either by the reduction of the cell size or by the slight anisotropy presented on nanocellular foams (see *Cellular Structure* section).

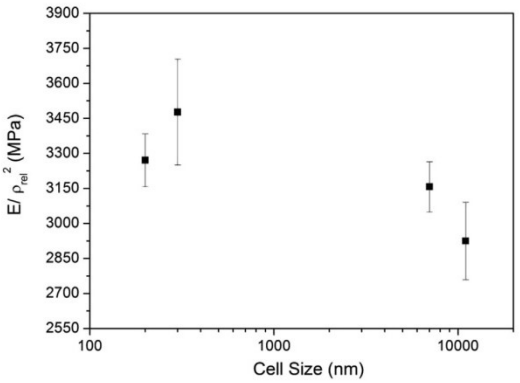

Fig. 11. Young's modulus results from tensile tests for microcellular and nanocellular PMMA foams.

Table 7
Young's modulus obtained by equation (4) assuming isotropic microcellular and nanocellular foams.

Name	Relative density	Average anisotropy ratio	E_i/ρ_{rel}^2 (MPa)
Micro 1	0.52	1.13	5984
Micro 2	0.49	1.06	5814
Nano 1	0.43	1.12	7063
Nano 2	0.42	1.16	7027

Focusing on the anisotropy, Gibson and Ashby studied the influence of this parameter on the impact resistance depending on the direction in which the crack propagates for open cell foams [2]. Either if the crack propagates in a direction perpendicular or parallel to the anisotropy of the foam, values of impact resistance measured are always lower than those of an isotropic foam with the same average cell size [2]. If the crack propagates perpendicular to the orientation of the cells, the value decreases by a factor $1/R$. If the crack propagates parallel to the long axis of the cells, this value is decreased by a factor $1/\sqrt{R^3}$.

In our case, foams are closed cell. As far as we know, there is not theoretical model describing the effect of anisotropy on the impact strength of closed cell foams. However, it is possible to find in the literature models for both open and closed cell structures for the other properties under study. And it was found that although models for open cell and closed cell foams produce different absolute values, the trends concerning the influence of R on the properties are equivalent. Then, since our goal is only to try to see qualitatively the influence of the anisotropy in the experimental results, we will use the equation for open cell foams to analyze the influence of the anisotropy on the impact strength of our foams. In this study, the 0.5 J pendulum for impact testing impacted on the sample in the ZX plane (see Fig. 3) thus the crack propagates in the Y direction (i.e. in a direction perpendicular to the anisotropy of the cells because cells are oriented along the Z axis). According to Gibson and Ashby, the impact resistance should be reduced by a factor $1/R$ as follows:

$$K_a = K_i \frac{1}{R} \tag{5}$$

where K_a is the impact strength of an anisotropic foam, and K_i is the impact strength of the same foam if it is isotropic.

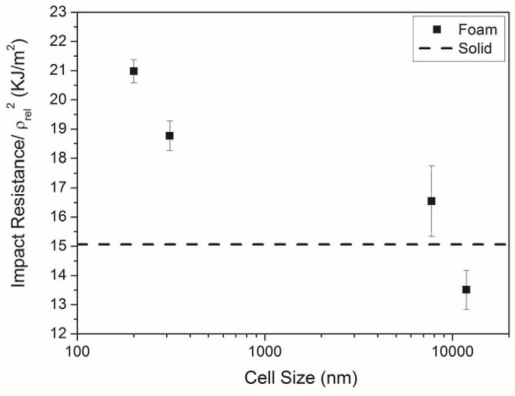

Fig. 12. Mechanical behavior at high strain rates divided by the square of the relative density for both PMMA solid and for PMMA microcellular and nanocellular foams.

Table 8 shows the values obtained for K_i together with the average anisotropy ratio for microcellular and nanocellular foams. From the results obtained it can be observed that if nanocellular foams were isotropic, the differences obtained between microcellular and nanocellular foams would be even greater (of around a 37%). Therefore the increase of a 25% found in Fig. 12 in the impact resistance of nanocellular foams with respect to the microcellular ones can be attributed to the presence of the nanocellular structure.

Traditionally it has been considered that the presence of voids in a cellular material favors the impact resistance as they act as stress concentrators. During crack propagation, holes relieve the triaxial tension in front of the crack tip [51–53]. Special attention has been taken in several studies [9,10,51–53] to a possible reduction of the stress concentration when cell size is reduced. However, no conclusive results have been obtained between stress concentration and cell size due to the small range of cell sizes analyzed. In this work, PMMA cell size has been reduced from the micro to the nanometer range, and thus it has been demonstrated that the stress concentration decrease has been greatly enhanced. Our results are in good agreement with those obtained by D. Miller et al. for PEI foams [21]. They also observed that for a constant relative density, nanocellular foams present a higher value than microcellular ones.

The results obtained by Charpy are opposite to those found by mechanical testing. Tensile tests showed that the energy absorb by nanocellular foams was lower than that of microcellular ones, whereas the opposite was found by impact tests. The geometry of the specimen as well as the direction of the applied forces is totally different in each case. Thus, the fracture mechanisms involved in each experiment are not comparable with each other. However, more studies will be needed in order to provide further explanations for these results.

3.5. Shore hardness D

Finally, the shore hardness of microcellular and nanocellular foams has been also analyzed in two different directions: Z and Y direction (see Fig. 3). M.A. Rodriguez-Perez and coworkers showed that the shore hardness exhibits a linear relationship with density [54]. Therefore, in this case, we will use this assumption.

The variation with cell size of the shore hardness divided by the relative density in the Z (Fig. 13 left) and Y direction (Fig. 13 right) is showed in Fig. 13. These results show again that there is a clear transition in the values of the shore hardness between microcellular and nanocellular foams. This significant increase in the hardness of nanocellular foams with respect to microcellular ones is higher in the Z direction (improvement of around 18%) than in the Y direction (improvement of around 12%).

This significant improvement found in the shore hardness of nanocellular foams with respect to microcellular ones could be attributed either to the reduction of the cell size or to the anisotropy present in nanocellular foams (see *Cellular Structure* section).

It is expected that anisotropic foams present higher values of hardness measured in a direction parallel to the anisotropy, and lower values measured in a direction perpendicular to the anisotropy. Thus, according to their anisotropy, nanocellular foams should

Table 8
Impact strength obtained by equation (5) assuming isotropic microcellular and nanocellular foams.

Name	Relative density	Average anisotropy ratio	K_i/ρ_{rel}^2 (KJ/m^2)
Micro 1	0.52	1.13	15.3
Micro 2	0.49	1.06	17.6
Nano 1	0.43	1.12	21.0
Nano 2	0.42	1.16	24.4

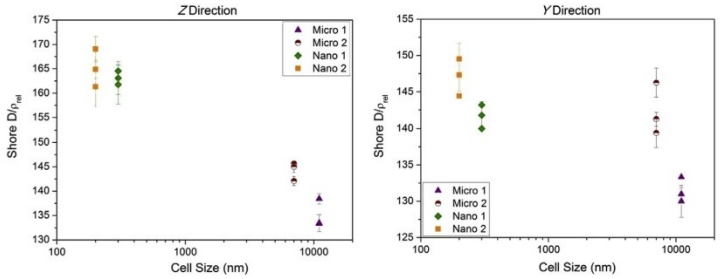

Fig. 13. Shore hardness normalized by the relative density in the *Z* direction (left) and in the *Y* direction (right) for both PMMA microcellular and nanocellular foams.

Table 9
Ratios of the mean Shore D value in the *Z* direction divided by the mean Shore D values in the *Y* direction.

Name	Relative density	Average anisotropy ratio	Shore D (*Z* direction)/Shore D (*Y* direction)
Micro 1	0.52	1.13	1.02
Micro 2	0.49	1.06	1.01
Nano 1	0.43	1.12	1.15
Nano 2	0.42	1.16	1.12

present higher values than microcellular foams in the *Z* direction and lower values in the *Y* direction. However, nanocellular foams present a higher hardness in both directions, thus the enhancement of their hardness should be related to their nanocellular structure and not to their anisotropy.

Furthermore, if the ratios of the value obtained in *Z* direction and the value obtained in the *Y* direction are calculated (Table 9), it can be observed that despite having similar anisotropies (e.g. Micro 1 and Nano 1), microcellular foams exhibit lower ratios in comparison with nanocellular ones. This fact suggests that in nanocellular foams, one additional possible oriented reinforcement mechanisms that is taking place is the confinement effect of the polymer chains. These polymer chains are oriented mainly in the plane of the anisotropy (*Z* direction), thus the reinforcement in that direction could be significantly higher than in the perpendicular one (*Y* direction), as the results shown.

Therefore, again, the improvement shown in the shore hardness of nanocellular foams with respect to microcellular ones can be attributed to the presence of the nanocellular structure, with more uniform cellular structure, cell sizes in the nanometer range, and perhaps the modification of the properties of the solid matrix due to the confinement into such nanometric dimensions.

4. Conclusions

In this paper, microcellular and nanocellular PMMA samples with comparable densities and macroscopic dimensions, adjustable to different standard measurement devices, have been produced by the solid state foaming process. The development of these samples with tunable size and similar densities has allowed the study of the transition from the micro to the nano scale of different mechanical properties in PMMA polymer foams.

First of all, a detailed characterization of the cellular structure has been carried out. The results showed that our production process is able to manufacture microcellular and nanocellular foams with very homogeneous cellular structures, and with a high reproducibility.

Secondly, it has been demonstrated that nanocellular foams present several enhanced physical properties in comparison with microcellular foams due the presence of the nanocellular structure with more uniform cellular structure, cell sizes in the nanometric range, and perhaps the modification of the properties of the solid matrix due to the confinement into such nanometric dimensions.

On one side, the glass transition temperature of foams in the nanometer range is increased by 7 °C with respect to both the microcellular foams and the solid matrix (associated with a confining effect of the polymer chains). This fact could allow expanding the temperature range of application. Also the modulus of elasticity of nanocellular foams is significantly increased, being this tendency found both by DMA and by tensile tests. Moreover, the mechanical behavior at high strain rates as well as the shore hardness of nanocellular foams are clearly increased in comparison with microcellular foams, achieving improvements of 25% and 15%, respectively.

On the contrary, it was found in the mechanical response at low strain rates that the strain to failure and the toughness were worst in the case of nanocellular foams due to the increased rigidity of the polymer matrix, and the reduction of the cell wall thickness.

Then, it has been experimentally confirmed that this new class of polymeric foams, the nanocellular foams, present in general enhanced physical properties in comparison with microcellular or conventional polymeric foams. In addition, it should be noticed that these results have been obtained with samples produced by an industrially scalable process. Therefore some of the potential benefits of nanocellular foams in comparison with microcellular ones in technological sectors such as construction, cushioning, and packaging have been demonstrated.

Acknowledgments

Financial support from FPI grant BES-2013-062852 (B. Notario) from the Spanish Ministry of Education is gratefully acknowledged. Financial assistance from MINECO (MAT 2012-34901) and the Junta of Castile and Leon (VA035U13) is gratefully acknowledged. Professor M. Dumon from the University of Bordeaux is gratefully acknowledged for supplying the PMMA.

References

[1] The future of polymer Foams to 2019. Smithers Rapra.
[2] Gibson LJ, Ashby MF. Cellular solids: structure and properties. 2nd ed. Cambridge: Cambridge University Press; 1997.
[3] Bureau MN, Kumar V. J Cell Plast 2006;42(3):229–40.
[4] Kumar V, Seeler KA, VanderWel M, Weller J. J Eng Mater Technol 1994;116(4):439–45.
[5] Weller E, Kumar V. Handbook of polymeric foams. UK: Rapra Technology; 2004.
[6] Sun H, Sur GS, Mark JE. Eur Polym J 2002;38:2373–81.
[7] Juntunen RP, Kumar V, Weller JE. J Vinyl Addit Technol 2000;6(2):93–9.
[8] Doroudiani S, Park CB, Kortschot MT. Polym Eng Sci 1998;38(7).

[9] Collias DI, Baird DG. Polymer 1994;35(18):3978–83.
[10] Barlow C, Kumar V, Flinn B, Bordia RK, Weller J. J Eng Mater Technol 2001;123:229–33.
[11] Doroudiani S, Kortschot MT. J Appl Polym Sci 2003;90(5):1421–6.
[12] Shimbo M, Higashitani I, Miyano Y. J Cell Plast 2007;43(2):157–67.
[13] Matuana LM. Bioresour Technol 2008;99(9):3643–50.
[14] Wong S, Naguib HE, Park CB. Adv Polym Technol 2007;26(4):232–46.
[15] Schmidt D, Raman VI, Egger C, du Fresne C, Schädler V. Mater Sci Eng C 2007;27(5–8):1487–90.
[16] Yokoyama BH, Li L, Nemoto T, Sugiyama K. Adv Mater 2004;16(17):1542–6.
[17] Pajonk GM. J Non-cryst Solids 1998;225:307–14.
[18] Lu X, Caps R, Fricke J, Alviso CT, Pekala RW. J Non-cryst Solids 1995;188(3):226–34.
[19] Hrubesh LW, Pekala RW. J Mater Res 1994;9(03):731–8.
[20] Notario B, Pinto J, Solorzano E, Saja JAd, Dumon M, Rodriguez-Perez MA. Polymer 2015;56:57–67.
[21] Miller D, Kumar V. Polymer 2011;52(13):2910–9.
[22] Reglero Ruiz JA, Dumon M, Pinto J, Rodriguez-Pérez MA. Macromol Mater Eng 2011;296(8):752–9.
[23] Olson DA, Chen L, Hillmyer MA. Chem Mater 2007;20(3):869–90.
[24] Kazarian SG. Polym Sci Ser C 2000;42(1):78–101.
[25] Tsivintzelis I, Angelopoulou AG, Panayiotou C. Polymer 2007;48(20):5928–39.
[26] Reverchon E, Cardea J. J Supercrit Fluids 2007;40:144–52.
[27] Costeux S, Zhu L. Polymer 2013;54(11):2785–95.
[28] Miller D, Chatchaisucha P, Kumar V. Polymer 2009;50(23):5576–84.
[29] Otsuka T, Taki K, Ohshima M. Macromol Mater Eng 2008;293(1):78–82.
[30] Pinto J, Dumon M, Pedros M, Reglero JA, Rodriguez-Perez MA. Chem Eng J 2014;243C:428–35.
[31] Ruiz JAR, Pedros M, Tallon J-M, Dumon M. J Supercrit Fluids 2011;58(1):168–76.
[32] Pinto J, Dumon M, Rodriguez-Perez MA, Garcia R, Dietz C. J Phys Chem C 2014;118(9):4656–63.
[33] Goel SK, Beckman EJ. Cell Polym 1993;12(4):251–74.
[34] Nawaby AV, Handa YP, Liao X, Yoshitaka Y, Tomohiro M. Polym Int 2007;56(1):67–73.
[35] Pinto J, Reglero-Ruiz JA, Dumon M, Rodriguez-Perez MA. J Supercrit Fluids 2014;94:198–205.
[36] Pinto J, Pardo S, Solórzano E, Rodríguez-Pérez MA, Dumon M, de Saja JA. Defect Diffus Forum 2012;326–328:434–9.
[37] 2818 U-EI. Preparación de probetas por mecanizado. Plásticos, vol. UNE-EN ISO 2818. AENOR; 1997. p. 17.
[38] 527-2 U-EI. Determinación de las propiedades en tracción. Parte 2: Condiciones de ensayo de plásticos para moldeo y extrusión. Plásticos, vol. UNE-EN ISO 527-2. AENOR; 2012. p. 17.
[39] Escudero J, Solorzano E, Rodriguez-Perez MA, Garcia-Moreno F, De Saja JA. Cell Polym 2009;28(4):289–302.
[40] Pinto J, Solórzano E, Rodriguez-Perez MA, de Saja JA. J Cell Plast 2013;49(6):555–75.
[41] Abràmoff MD, Magalhães PJ, Ram SJ. Biophot Int 2004;11(7):36–42.
[42] Kumar V, Suh NP. Polym Eng Sci 1990;30(20):1323–9.
[43] 179-1 U-EI. Determinación de las propiedades al impacto Charpy. Parte 1: Ensayo de impacto no instrumentado. Plásticos, vol. UNE-EN ISO 179-1. AENOR; 2011. p. 29.
[44] 868 U-EI. Determinación de la dureza de indentación por medio de un durómetro (dureza Shore). Plásticos y ebonita. AENOR; 2003. p. 11.
[45] Lee ST, Park CB, Ramesh NS. Polymeric foams. Science and technology. Boca Raton - Florida: CRC Press; 2007.
[46] Davis WJ, Pethrick RA. Polymer 1998;39(2):225–66.
[47] Rindfleisch F, DiNoia TP, McHugh MA. J Phys Chem 1996;100(38):15581–7.
[48] Sugimoto H, Daimatsu K, Nakanishi E, Ogasawara Y, Yasumura T, Inomata K. Polymer 2006;47(11):3754–9.
[49] Hu Y-H, Chen C-Y, Wang C-C. Polym Degrad Stab 2004;84(3):545–53.
[50] Saladino ML, Motaung TE, Luyt AS, Spinella A, Nasillo G, Caponetti E. Polym Degrad Stab 2012;97(3):452–9.
[51] Sue HJ, Yee AF. Polym Eng Sci 1996;36(18):2320–6.
[52] Sue HJ, Huang J, Yee AF. Polymer 1992;33(22):4868–71.
[53] Borggreve RJM, Gaymans RJ, Eichenwald HM. Polymer 1989;30:78–83.
[54] Rodriguez-Perez Ma, Simoes Rd, Roman-Lorza S, Alvarez-Lainez M, Montoya-Mesa C, Constantino Cjl, et al. Polym Eng Sci 2012;52(1):62–70.

IV.3. References

1. Bureau MN and Kumar V. Journal of Cellular Plastics 2006;42(3):229-240.
2. Kumar V, Seeler KA, VanderWel M, and Weller J. Journal of Engineering Materials and Technology 1994;116(4):439-445.
3. Shimbo M, Higashitani I, and Miyano Y. Journal of Cellular Plastics 2007;43(2):157-167.
4. Juntunen RP, Kumar V, and Weller JE. Journal of Vinyl & Additive Technology 2000;6(2):93-99.
5. Schmidt D, Raman VI, Egger C, du Fresne C, and Schädler V. Materials Science and Engineering: C 2007;27(5–8):1487-1490.
6. Yokoyama BH, Li L, Nemoto T, and Sugiyama K. Advanced Materials 2004;16(17):1542-1546.

DIELECTRIC PROPERTIES

Chapter V. Dielectric Properties

Continuing improvement of very large scale integration of microelectronic circuits has reached the point where multilayer metallization and the interlayer dielectric have become the limiting factors in process integration and device performance. The major improvements in performance of microelectronics come from device size miniaturization, which leads to faster device speeds. As the devices scale to smaller feature sizes, the transistor capacitance and resistance are reduced. As a result, the resistance-capacitance delay caused by interconnect tends to limit the chip performance. For this reason a new generation of low dielectric constant (*k*) materials is required to mitigate the interconnect resistance-capacitance (RC) delays, cross-talk noise, and power dissipation.

This demand of low *k* materials has stimulated great efforts to explore the applicability of cellular materials, especially cellular polymeric systems, to replace silicon dioxide (SiO_2, $k > 3.5$) as the inter-level dielectric. The low dielectric constant of the polymer ($k < 3$) [1] together with that of the air ($k = 1$) make these porous polymeric systems promising candidates as low *k* systems.

In this chapter the dielectric behavior of microcellular and nanocellular PMMA are studied. The results obtained have been summarized in the paper entitle ***"Dielectric behavior of porous PMMA: from the micrometer to the nanometer scale"***, submitted to **Polymer (2016)**.

In this work, several PMMA foams with cell sizes between 90 nm and 3 μm were produced by the gas dissolution foaming method, modifying the saturation pressure between 10 and 30 MPa. The dielectric behavior was studied by means of a DC electrical resistivity adapter and a broadband dielectric spectrometer, varying both the frequency and the temperature.

A clear change in the samples' dielectric behavior was found, passing from a capacitive behavior in the case of microcellular polymers to a combination of a capacitive and a resistive response in the nanocellular ones. Likewise, it was demonstrated that the confinement effect of the polymeric macromolecules is stable in the temperature range studied (from -20 to 110 ºC). Furthermore a sharp reduction of the dielectric constant of nanocellular polymers was obtained as compared to the solid, showing that the development of nanocellular polymeric materials is the way to achieve the next-generation low dielectric constant materials.

The dielectric constant of cellular PMMA was estimated by using the most typical models found in literature.

One of the equations that describes the dielectric constant k_f of a two phase system is the so-called Lichterecker mixing rule [2]:

$$k_f^{\alpha} = k_s^{\alpha}(1 - V_g) + k_g^{\alpha} V_g \qquad \text{(V-1)}$$

Where k_s and k_g are the dielectric constants of the solid and gaseous phase respectively, V_g is the volume fraction of voids (i.e. the porosity), and α is a parameter that determines the type of rule of mixtures. If $\alpha = -1$, this equation is the serial mixing rule (which represents a lower limit of the dielectric constant):

$$\frac{1}{k_f} = \frac{(1 - V_g)}{k_s} + \frac{V_g}{k_g} \quad \text{(V-2)}$$

When α = 1, the equation is the parallel mixing rule (an upper limit of the dielectric constant):

$$k_f = k_s(1 - V_g) + k_g V_g \quad \text{(V-3)}$$

However, perhaps the most common equation in this field is the Maxwell Garnett formula that takes into account that one of the phases are dispersed spheres [3]:

$$k_f = k_s + 3(1 - \rho_{rel})k_s \frac{k_g - k_s}{k_g + 2k_s - (1 - \rho_{rel})(k_g - k_s)} \quad \text{(V-4)}$$

This formula is in wide use in very diverse fields of application. The beauty of the Maxwell Garnett formula is its simple appearance combined with its broad applicability.

Figure V.1 illustrates the variation of the dielectric constant for the cellular PMMA used in this work as a function of porosity and the predictions of the previous models. As stated by these expressions, an increase porosity leads to a reduction of the dielectric constant. Furthermore, according to the article in this chapter, these models are not able to adjust with good accuracy the experimental results. Therefore, it is necessary to develop new theoretical models that include the variations suffered by the solid and gaseous phases when the pore size is reduced to the nanometer scale.

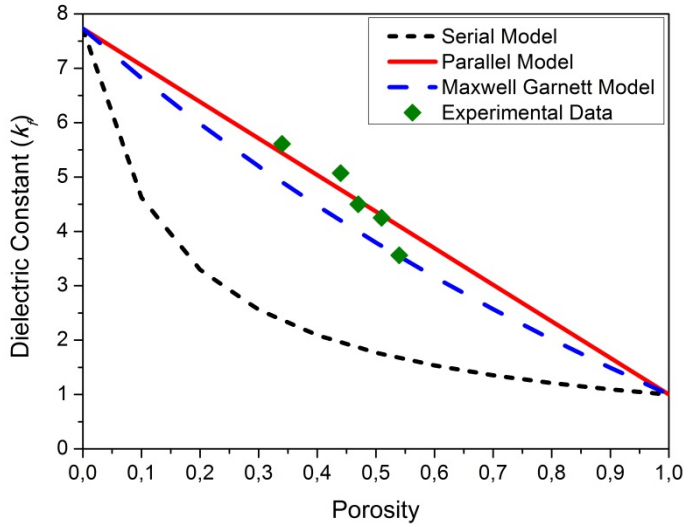

Figure V.1. Evolution of the dielectric constant as a function of porosity according to equations V-2-4 for the particular case of the cellular PMMA used in this thesis work (k_s = 7.73), together with the experimental results

Finally, experimental results also corroborated the electrical behavior of nanocellular PMMA explained previously in *Chapter II* as well as the increase of the *Tan δ* with the reduction of the cell size previously measured by mechanical characterization (*Chapter IV*).

DIELECTRIC BEHAVIOR OF POROUS PMMA: FROM THE MICROMETER TO THE NANOMETER SCALE

B. Notario[a], J. Pinto[b], R. Verdejo[c], M.A. Rodríguez-Pérez[a]

a. Cellular Materials Laboratory (CellMat), Condensed Matter Physics Department, University of Valladolid. Paseo de Belén 7, 47011 Valladolid, Spain. belen.notario@fmc.uva.es

b. Nanophysics – Smart Materials Group, Istituto Italiano di Tecnologia (IIT). Via Morego 30, 16163 Genova, Italy.

c. Institute of Polymer Science and Technology (ICTP-CSIC). Juan de la Cierva 3, 28006 Madrid, Spain.

ABSTRACT

In recent years, great attention has been paid to nanocellular polymeric foams in microelectronic as the next generation of low dielectric constant materials. In this work the dielectric behavior of microcellular and nanocellular poly(methyl methacrylate) (PMMA) foams has been characterized, both in the frequency and in the temperature domain, in order to study potential effects of the change of scale of the cellular structure. Experimental results have shown clear differences in the dielectric behavior of the samples when reducing the cell size from the micro to the nanoscale, a sharp reduction of the dielectric constant with porosity, and the experimental verification that the confinement effect do not depend on the temperature.

Keywords: nanocellular foams, dielectric properties, cellular polymers

1. INTRODUCTION

Polymer nanofoams have recently attracted significant attention in the microelectronics industry as a means of fabricating low dielectric constant materials (k) [1-6]. As the devices scale to smaller feature sizes, a new generation of low dielectric constant materials is needed to minimize cross talk and maximize signal propagation speed. The low dielectric constant of the polymer along with that of the air (k = 1) make polymeric foams potential candidates as low k systems [7].

In microelectronics, nanocellular foams are required due to the feature size of the developing devices, having to be the cells smaller than the thickness of the films (ideally an order of magnitude lower [8]). Therefore, in principle, it is not expected that these materials can bring new effects or improvements in other properties due to the dimension of the cell size in the nanoscale; however, previous works have shown the appearance of striking results in the

dielectric behavior of nanocellular polymeric foams such as the emergence of the Maxwell Wagner Sillars (MWS) phenomenon in PMMA- based nanocellular foams [9].

In this study, the dielectric properties of microcellular and nanocellular PMMA foams have been analyzed varying both the frequency and the temperature. A clear change in the sample's behavior was found, passing from a capacitive behavior in the case of microcellular foams to a combination of a capacitive and a resistive response in the nanocellular ones. Likewise a strong reduction (of around 50 % for a relative density of 0.46) of the dielectric constant was obtained between solid and nanocellular foams. Furthermore, it was demonstrated that the confinement effect of polymeric macromolecules is not dependent on the temperature. Finally, this work has also helped to: (a) corroborate the dielectric behavior of PMMA nanofoams; (b) demonstrate other scale-related effects previously measured by mechanical characterization.

2. EXPERIMENTAL SECTION

PMMA was supplied by Arkema Company (France) in the form of pellets. This polymer presents a density (ρ) of 1180 Kg/m^3 and a glass transition temperature (T_g) around 112 ºC.

PMMA pellets were injected into pieces of 50 x 15 mm^2 with 3 mm thickness (model DSM Xplore), and used later for foaming.

Foaming experiments were performed at room temperature following the solid state foaming process (details elsewhere [9]), modifying the saturation pressure between 10 and 30 MPa (Table 1).

Dense skin of foamed samples was removed using a polishing machine (model LaboPOl2-LaboForce3, Struers). Then solid and polished samples were machined using a precision cutting machine (Mod. 1000, IsoMet) to be approximately 10 x 10 mm^2 with 1 mm in thickness. The cellular structure of foams was characterized elsewhere [9] (Table 1).

The dielectric behavior of cellular polymers was evaluated by means of a DC electrical resistivity adapter (Keithley 6105, model) and a broadband dielectric spectrometer (ALPHA Novocontrol Technologies GmbH, model).

DC resistivity data were determined according to ASTM D257-99 [10]. Solid and foamed samples were measured four times at + 500 V, -500 V, + 500 V, -500 V. Time of electrification was 60 seconds, and the time of discharge before making a measurement with reversed voltage was 4 minutes. Resistivity (R) was calculated as follows:

$$R = \frac{A \cdot V}{t \cdot I} \quad (1)$$

Where A and t are the area and thickness of the sample respectively, V the voltage applied, and I the current intensity measured.

In the case of broadband dielectric measurements, foamed and solid samples were held in a dielectric cell between two parallel gold-plated electrodes. The thickness of the samples was taken as the distance between the electrodes and was determine using a micrometer gauge. The complex dielectric permittivity ($\varepsilon^*=\varepsilon'- i\varepsilon''$) of the solid and foamed materials was measured over a frequency window of 10^{-2} < F/Hz < 10^6 (F is the frequency of the applied electric field) in the temperature range from −20 to 110 °C. The amplitude of the alternating current (ac) electric signal applied to the samples was 1 V. Furthermore, the real part of the complex dielectric permittivity, ε', (or dielectric constant, k) was modeled using the series model [11], the parallel model [11], and the Maxwell Garnett model [12].

Table 1. Main characteristic of the analyzed foams

Sample - Cell Size (Φ) (nm)	Saturation Pressure (MPa)	Relative Density (ρ_{rel})	K at 1 KHz	K_f Series Model [11]	K_f Parallel Model [11]	K_f Maxwell Garnett Model [12]
- (Solid)	0 (Solid)	1	7.73	-	-	-
90	30	0.46	3.56	1.66	4.01	3.53
200	25	0.49	4.25	1.74	4.28	3.73
710	20	0.53	4.50	1.85	4.63	3.99
1460	15	0.56	5.07	1.95	4.89	4.19
3290	10	0.66	5.61	2.35	5.76	4.90

3. RESULTS AND DISCUSSION

J. Pinto and coworkers [9] demonstrated the appearance of an electrical conductivity component and an interfacial polarization phenomena (or MWS) in nanocellular PMMA based foams at low frequencies. MWS occurs in heterogeneous materials, such as blends or composites, at the interfaces, leading to a separation of charges. They assumed then, that the conductivity component could be attributed to a nanopores conductive mechanism of opposing cells walls showing the aforementioned accumulation of charges (Figure 1, right). Nevertheless, further studies are needed to clarify the conductive mechanism through the nanopores. Furthermore they found an increase electrical resistivity of PMMA based foams when cell size shift from the micro to the nanoscale due to an increase tortuosity (ratio between the distance of any real path and the shortest distance between two points (Figure 1, right)). The combination of these two phenomena (tortuosity and MWS) led to a clearly different dielectric behavior between microcellular and nanocellular foams.

The appearance of both phenomena can be clearly observed in Figure 1 left where the evolution of the resistivity (at room temperature and direct current (DC)) of PMMA foams as a function of the relative density is illustrated. Again an increase of the resistivity is observed due to an increase tortuosity when cell size changes from the micro to the nanometer range. Likewise, a reduction of the resistivity proportional to the reduction of the cell size in the nanoscale is detected owing to a conductive mechanism, resulting in a possible nanopores conductive mechanism (due to the accumulation of charges in opposing cell walls) at low frequencies.

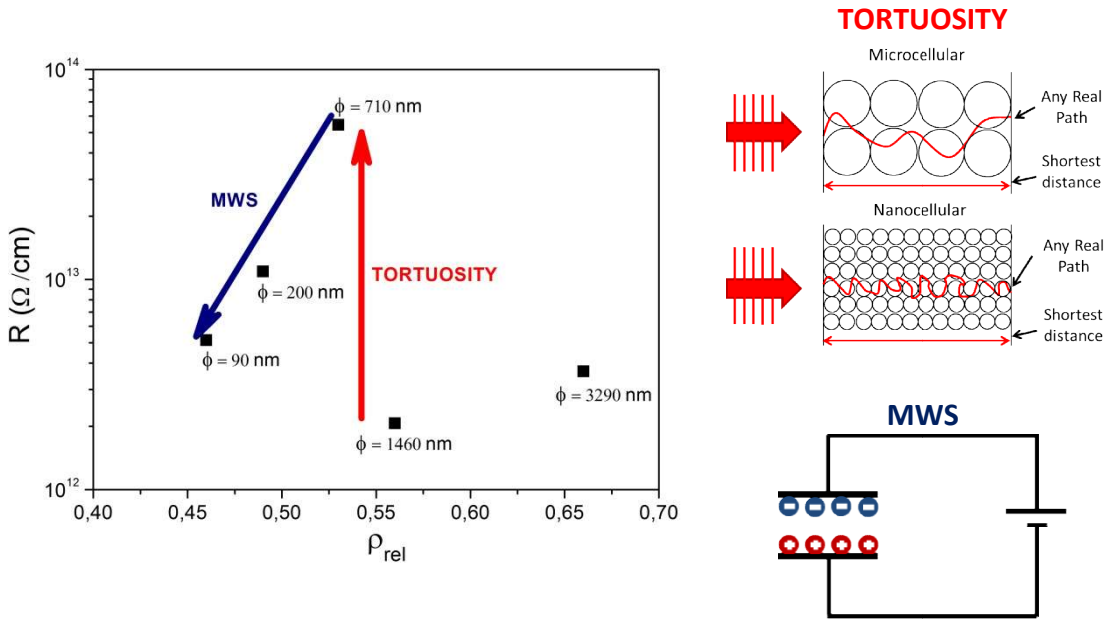

Figure 1. Left) Evolution of the DC electrical resistivity as a function of the relative density. Right) Scheme of the tortuosity (top) and MWS (bottom) phenomenon

Moving to the frequency domain, dielectric measurements at room temperature confirmed previously published experimental results related to the mechanical properties (*Tan δ*) of microcellular and nanocellular PMMA [13]. Figure 2 illustrates the evolution of the *Tan δ* at room temperature as a function of the frequency for the solid, microcellular, and nanocellular PMMA foams. Once again, it can be observed how at low and medium frequencies *Tan δ* increases considerably when cell size is reduced to the nanometer range, remaining unaltered for solid and microcellular foams in the whole frequency range. This increase in *Tan δ* is related to the so called confinement effect [9].

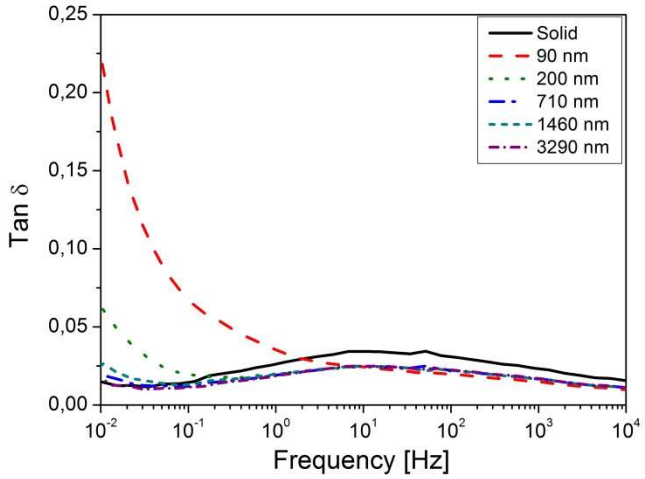

Figure 2.Evolution of *Tan δ* at room temperature vs frequency for the solid, microcellular, and nanocellular PMMA

As mentioned before, nanocellular polymeric foams are required in the microelectronics due to the reduced dimensions of the devices. Table 1 shows the dielectric constant values of solid and microcellular and nanocellular PMMA at a frequency of 1 KHz. A reduction of *k* of around 50 % is obtained between the solid and the nanofoam with a relative density of 0.46. The value

obtained is far from the one currently required by the industry of microelectronics ($k < 2$ [14]); however, it shows that the way to achieve low dielectric constant materials passes through the development of nanocellular polymeric systems (although perhaps using starting materials with a lower dielectric constant than PMMA).

The most common models used to determine the value of the dielectric constant do not fit well the experimental results (see Table 1). This is because the models only take into account the fraction of voids ($1-\rho_{rel}$) of the foams, assuming that the properties of the constituent phases (both the solid and gas) do not change with cell size. In this work and in other previous ones [9, 13, 15, 16] it has been demonstrated that both the gas within the pores and the polymeric chains in the solid matrix undergo significant changes in their properties when the cell size is decreased to the nanometer range. Once these changes are fully understood they should be covered by the theoretical models.

On the other hand, the complex plot of the impedance (Z) or Nyquist plot has been represented for the solid, microcellular and nanocellular PMMA (Figure 3). Nyquist curves include the entire range of frequencies measured and are used to obtain information about the equivalent electric circuit. In this study a clear change in the samples behaviour is observed. The solid sample presents a dominating capacitor configuration over the entire frequency range. Nevertheless, since an ideal capacitor appears as a vertical straight line (infinite resistance), the slope indicates a slight resistive contribution most likely arising from the capacitor losses present in any dielectric material. This slope then starts to decrease with the presence of the cellular architecture reaching its minimum angle in the nanocellular material. Hence, the nanocellular PMMA develops a resistive behaviour and can be modelled as a capacitor in parallel with a resistor. Reduction of the capacitive behaviour found on nanoporous PMMA foams could be related to the progressive immobilization of the polymer chains leading to a progressive decrease of free dipoles able to rotate with the reduction of the pore size.

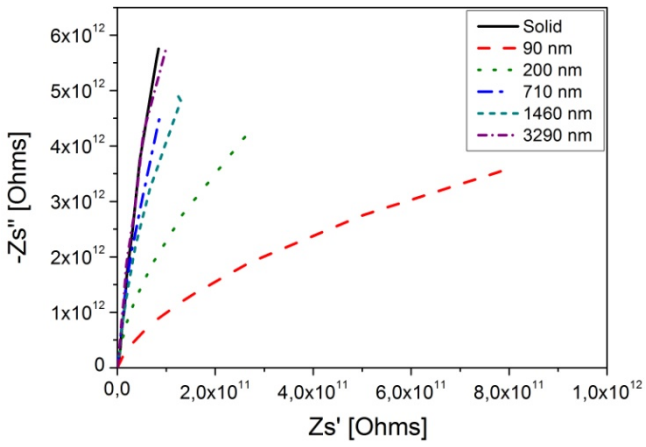

Figure 3. Nyquist plot for solid, microcellular, and nanocellular PMMA

Finally, measurements in the temperature domain were also conducted by varying the frequency. In the case of the shape parameters alpha and beta, no clear trends were detected as a function of temperature between microcellular and nanocellular foams. This behaviour must be further studied due to the previous evidences found in the *Tan δ*. On the other side,

the behaviour previously observed in which $\Delta\varepsilon/\Delta\varepsilon^{solid}$ decreased as a function of cell size [9], has been demonstrated to remain stable in the range of temperatures measured (from −20 to 110 °C) (Figure 4). This reduction of $\Delta\varepsilon/\Delta\varepsilon^{solid}$ is related to a progressive decrease of the number of free dipoles able to rotate, i.e., it is related to the confinement effect of the nanocellular system.

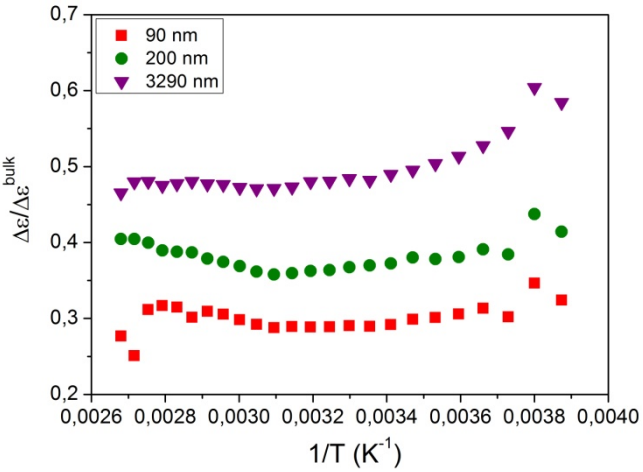

Figure 4. Evolution of the normalized dielectric strength as a function of the inverse of temperature

4. CONCLUSIONS

In this paper the dielectric properties of microcellular and nanocellular PMMA were studied, finding a clear evolution from a capacitive behavior to a combination of a resistive and a capacitive response when cell size goes from the micro to the nanometer range. It was found that the dielectric constant of nanocellular PMMA is strongly reduced as compared to solid PMMA, showing that the development of nanocellular polymeric materials is the way to achieve the next-generation low dielectric constant materials (as long as unexpected phenomena like the MWS do not appear at high frequencies). Furthermore, experimental results have confirmed the confinement of the polymer chains along the temperature domain (from -20 to 110 °C), showing a great stability up to temperatures close to the glass transition temperature (T_g) of the solid. Finally, some mechanical properties previously published of nanocellular materials as well as the dielectric spectrum of PMMA foams have been verified and confirmed [9, 13]. Nowadays, the unexpected conductive mechanism found at low frequencies in nanocellular foams is not a problem for the implementation of nanocellular polymeric systems as low dielectric constant materials (since they have to work at high frequencies), but it can be a warning to study these systems in more detail.

Acknowledgments

Financial support from FPI grant BES-2013-062852 (B. Notario) from the Spanish Ministry of Education, MINECO (MAT 2012-34901), and the Junta of Castile and Leon (VA035U13) is gratefully acknowledged.

References

1. Muruganand S, Varayandass SK, Mangalaraj D, and Vijayan TM. Polymer international 2001;50(10):1089-1094.
2. Kuntman A and Kuntman H. Microelectronics Journal 2000;31(8):629-634.
3. Simpson JO and Clair AKS. Thin Solid Films 1997;308-309:480-485.
4. Zhang YH, Dang ZM, Xin JH, Daoud WA, Ji J-H, Liu YY, B.Fei, Li Y-Q, Wu JT, Yang SY, and Li LF. Macromolecular rapid communications 2005;26(18):1473-1477.
5. Fu GD, Yuan Z, Kang ET, Neoh KG, Lai DM, and Huan ACH. Advanced Functional Materials 2005;15(2):315-322.
6. Xu Y, Tsai YP, Tu KN, Zhao B, Liu QZ, Brogo M, Sheng GTT, and Tung CH. Applied Physics Letters 1999;75(6):853.
7. Miller RD. Science 1999;286(5439):421-423.
8. Ro HW, Kim KJ, Theato P, Gidley DW, and Yoon DY. Macromolecules 2005;38(3):1031-1034.
9. Pinto J, Notario B, Verdejo R, Dumon M, Costeux S, and Rodriguez-Perez MA. Advanced Materials 2015;Submitted.
10. ASTM. Standard Test Methods for DC Resistance or Conductance of Insulating Materials. vol. D 257-99: ASTM International, 2005. pp. 18.
11. Wu Y, Zhao X, Li F, and Fan Z. Journal of Electroceramics 2003;11:227-239.
12. Sihvola A. Electromagnetic mixing formulas and applications. London, United Kingdom: The Institution of Electrical Engineers, 1999.
13. Notario B, Pinto J, and Rodriguez-Perez MA. Polymer 2015;63:116-126.
14. Association SI. National Technology Roadmap for Semiconductors. San Jose, California, 1997.
15. Notario B, Pinto J, Solorzano E, Saja JAd, Dumon M, and Rodriguez-Perez MA. Polymer 2015;56:57-67.
16. Miller D and Kumar V. Polymer 2011;52(13):2910-2919.

V.3 References

1. Miller RD. Science 1999;286(5439):421-423.
2. Wu Y, Zhao X, Li F, and Fan Z. Journal of Electroceramics 2003;11:227-239.
3. Sihvola A. Electromagnetic mixing formulas and applications. London, United Kingdom: The Institution of Electrical Engineers, 1999.

ACOUSTIC PROPERTIES

Chapter VI. Acoustic Properties

Foamed polymeric materials are used as acoustic absorbers and acoustic insulators in several applications such as building, construction, transportation, and industrial, among others. According to the report *Acoustic Insulation Market by Type (Mineral Wool, Glass Wool, Foamed Plastics), by Application (Building & Construction, Industrial, Transportation) - Global Trends and Forecasts to 2019* [1], the acoustic insulation market is estimated to witness a CAGR (Compound Annual Growth Rate) of 5.80 % between 2014 and 2019, and is expected to generate a global market value of $4.159,04 million by 2019. In particular the cellular polymer market is dominated by the Asia-Pacific region securing more than one third of global market share.

In this way, the development of improved soundproofing cellular polymers can have an important effect on both economic savings and reductions of energy consumptions.

Nanocellular polymers are expected to exhibit a different wave propagation behavior as compared to microcellular polymers due to a different sound wave transmission through the gaseous (i.e. Knudsen effect) and solid phase [2]. Confirmation of these phenomena together with a further development of these materials could lead to a new class of acoustic insulation materials, with different properties.

VI.2. Theoretical Background

Cellular polymeric materials, due to their porosity, are considered acoustically absorbent [3]. In particular, materials presenting open cells are ideal for this aim because when the acoustic wave enter into these materials air particles vibrate and crash into the walls. This shock and friction against the cellular structure causes that the acoustic energy transmitted is transformed, and partially absorbed, into heat energy [4]. Then, the sound absorption capacity of the cellular material will depend on the percentage of open cell that it possesses.

On the other hand, if the structure of the material is flexible, deformations produced by the energy of the incident wave will take place in the surface separating the material from the receiving air. Thus, this deformation will be transmitted along the material structure, being gradually attenuated and absorbed [4].

Mechanisms of sound absorption are well known for conventional cellular polymeric materials with cell sizes in the micro scale. However, nowadays there is just one theoretical and none experimental studies specifically focused on cellular polymers whose cell size is in the nanometer range.

M. Ayub and coworkers [2] stated that the acoustic mechanisms of nanocellular materials will exhibit a different behavior as the gas and solid phases present a different acoustic behavior due to the change in the scale. According to them wave propagation in nanoscale is characterized by the Knudsen regime since the mean free path of the gas is comparable or smaller than the cell size of the system. In the same way, they stated that acoustic waves propagate in air, a polyatomic and compressible gas. This compression of the gas will be a

source for acoustic losses (relaxation losses) associated with the redistribution of the internal energy of the gas molecules (translational motions into rotation and vibration motions). In addition, they also affirmed that acoustic pressure waves will create structural vibrations of the cell walls modifying the flow of the acoustic wave.

However, although they provided insight into the acoustic absorption mechanisms at the nanoscale, up to date no one has been able to prove these predictions.

On the other side, our previous studies [5-7] have shown significant differences in critical parameters that could influence the acoustic behavior: the existence of the confinement effect on the solid polymer matrix, the different mechanical properties between microcellular and nanocellular PMMA, the increased tortuosity of nanocellular materials, or the presence of the Knudsen regime in nanopores. Then, it is logical to expect a different acoustic behavior between materials whose pore size is in a different scale.

For all the aforementioned reasons, it was decided to study the acoustic properties of nanocellular and microcellular PMMA in order to see if there were indeed differences between each other due to the change of scale in the cellular structure.

For this purpose, closed cell nanocellular and microcellular PMMA were obtained following the solid state foaming process previously optimized (for more details see *Chapter I*), modifying the saturation pressure between 13 and 32 MPa (cell size from 11600 to 200 nm, respectively) (Figure VI.1). Although this type of cellular structure is completely different from the typical structure of open cell materials used in soundproofing, it allowed us to carry out a preliminary study about the effects of scale in the acoustic properties of foamed PMMA. This study was carried out and published in **Materials Letters 168 (2016)**, with the title ***"Nanoporous PMMA: a Novel System with Promising Acoustic Properties"***.

Figure VI.1. Nanocellular PMMA acoustically characterized both in transmission and absorption

The acoustic behavior of cellular materials was characterized by measuring the absorption and the transmission coefficient in the frequency range from 500 – 6000 Hz by means of an impedance tube (model Brüel & Kjaer, 4206).

This equipment is based on the use of the Fourier transform to convert pressure sound, that comes through the microphones (0.6 cm of diameter), in both absorbance and transmittance values.

The impedance tube has a generator that is responsible for producing the vibrations in a wide frequency range (known as random or white noise), whereas incident and reflected

components are determined by the sound pressure that arrives to the microphones coupled to the impedance tube.

The whole system is monitored by a computer and controlled by its own software.

Absorption experiments were carried out using the two-microphone method [8] (Figure VI.2). In this case, sound waves reach the sample, being some of them absorbed and some reflected. The reflected waves interfere with the incident ones, creating a standing wave, i.e. a wave that has fixed points called nodes and that is not propagating. Microphones attached to the tube and connected to the computer record the acoustic pressure at two specific points of the tube and using this data the equipment is able to determine the absorption coefficient [4, 8, 9].

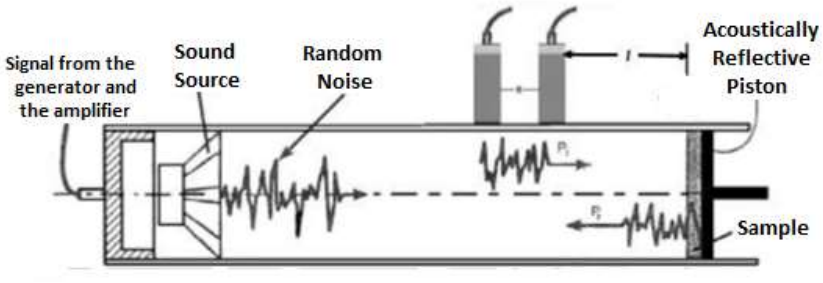

Figure VI.2. Scheme illustrating the interior of an impedance tube in the absorption configuration

To measure the transmission loss, the impedance tube is used according to the four-microphone method [10] (Figure VI.3). In this method the sample separates two cavities. One, in which the source is located, and the other one in which the sound is received. The equipment measures the sound pressure in the two cavities and from this data the transmission loss of the analyzed sample is obtained [8].

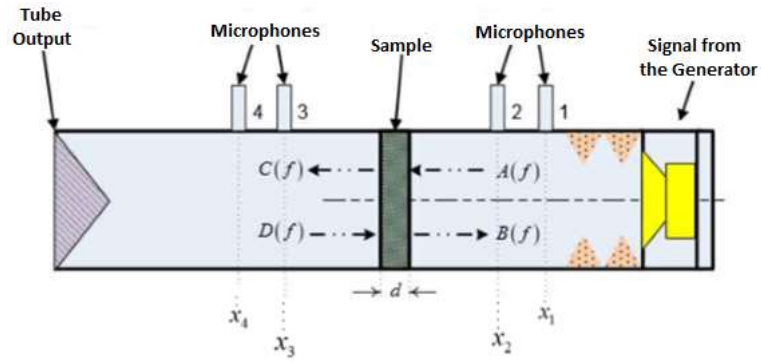

Figure VI.3. Diagram showing the interior of the impedance tube in the transmission configuration

In this work it was measured for the first time the acoustic behavior of microcellular and nanocellular PMMA, showing a different response between them both in absorption and transmission loss. The results showed, once again, the strong difference in physical properties between micro and nanocellular polymers.

Materials Letters 168 (2016) 76–79

Contents lists available at ScienceDirect

Materials Letters

journal homepage: www.elsevier.com/locate/matlet

Nanoporous PMMA: A novel system with different acoustic properties

B. Notario [a,*], A. Ballesteros [a], J. Pinto [b], M.A. Rodríguez-Pérez [a]

[a] Cellular Materials Laboratory (CellMat), Condensed Matter Physics Department, University of Valladolid, 47011 Valladolid, Spain
[b] Nanophysics—Smart Materials Group, Istituto Italiano di Tecnologia (IIT), Via Morego 30, 16163 Genova, Italy

ARTICLE INFO

Article history:
Received 22 October 2015
Received in revised form
6 January 2016
Accepted 9 January 2016
Available online 11 January 2016

Keywords:
Nanoporous polymeric materials
Acoustic properties
Absorption
Transmission loss

ABSTRACT

The acoustic properties of closed cell nanoporous and microporous poly(methyl methacrylate) (PMMA) foams have been well characterized, showing that nanoporous PMMA exhibit a different absorption coefficient and transmission loss behavior in comparison with microporous PMMA. Experimental differences may be explained by the different wave propagation mechanism in the micro and nanoscale, which is determined by the confinement of both the gas (Knudsen regime) and the solid phases. These results place nanoporous materials as a new class of polymeric porous material with potential properties in the field of acoustics, especially in multifunctional systems requiring a certain degree of soundproofing.

1. Introduction

Currently one of the most exciting topics in porous material science is focused on the reduction of the pore size of porous material from the micrometer to the nanometer scale using technologies with the potential to be up-scaled. These new materials known as nanoporous foams (two-phase structures composed of a continuous solid phase and either continuous or discontinuous gaseous phase whose pore size is about or below 100–200 nm [1]) are very promising due to several improvements in their physical properties. For instance, B. Notario and coworkers [2] showed in poly(methyl methacrylate) (PMMA) based nanoporous materials that a pore size reduction allowed a significant reduction of the thermal conductivity due to the decrease of the heat conduction transfer through the gas phase (Knudsen effect) and due to an increment of the tortuosity of the solid matrix. Later the same authors [3] reported that the modulus of elasticity, the mechanical behavior at high strain rates as well as the shore hardness of nanoporous PMMA foams was clearly increased in comparison to microporous materials. A similar study of the mechanical behavior of nanoporous polyetherimide (PEI) was carried out by d. Miller et al. [4], finding that the tensile toughness and the strain to failure were increased by a factor of 2–3 when pore size is in the nanoscale. Moreover, impact resistance of nanoporous PEI foams presented a higher value than that of the microporous PEI. Furthermore, Zhou and coworkers [5] found a higher flexural modulus and strength in nanoporous PEI as compare to the solid.

This combination of properties makes these materials promising and appropriate for a significant no. of applications in different market sectors: construction, insulation, automotive, etc.

Due to all the aforementioned differences found in the physical properties between micro and nanoporous systems, this paper aims at. studying the acoustic behavior of closed pore microporous and nanoporous PMMA foams to find potential differences due to the significant modification of the morphology of the nanoporous system. Once again a significant effect owing to scaling was found both in absorption coefficient and transmission loss, opening the door to the development of new polymeric nanoporous materials with promising acoustic properties.

2. Experimental section

PMMA was kindly supplied by Arkema Company (France) in. the form of pellets. This polymer presents a glass transition temperature (T_g) about 112 °C and a density (ρ) of 1180 kg/m^3.

PMMA pellets were compression molded into precursors of 155 mm × 75 mm × 4 mm^3 using a two-hot plates press, cut at the desired dimensions (radius=29 mm; thickness=4 mm), and used later for foaming [3].

Foaming experiments were performed following the solid state foaming process previously optimized (details elsewhere [3]), modifying the saturation pressure between 13 and 32 MPa (Table 1). After depressurization samples were introduce in a thermostatic water bath in a controlled foaming step, intended to obtain samples with similar relative densities to better compare the differences in the acoustic properties between them.

Dense skin of foamed samples was removed using a polishing

* Corresponding autor. Tel.: +34 983423194.
E-mail address: belen.notario@fmc.uva.es (B. Notario).

http://dx.doi.org/10.1016/j.matlet.2016.01.037
0167-577X/

Table 1
Main characteristics of the porous materials studied.

Sample	Pore size (Φ) (nm)	Relative density	*Absorption* main frequency peak (Hz)	*Absorption* peak height	*Absorption* normalized coefficient	*TL* Main frequency peak (Hz)
M-1	11605	0.54	3873	0.21	0.12	3453
M-2	7365	0.46	4085	0.25	0.15	x
N-1	330	0.42	3926	0.21	0.09	5477
N-2	205	0.41	4171	0.25	0.11	x

machine (model LaboPOl2-LaboForce3, Struers). The presence of inhomogeneities or defects inside the porous materials was analyzed by X-Ray radiography. The cellular structure of porous samples was characterized by scanning electron microscopy (SEM) (FEI, Quanta 200 g). The average pore size was determined with a specialized software based on ImageJ/ FIJI [6].

The acoustic behavior of porous systems was evaluated by measuring the absorption and the transmission coefficient (ratio between the absorbed and the incident energy, and ratio between the transmitted and the incident energy, respectively) in. the frequency range of 500–6000 Hz. For this purpose the two-microphone (absorption [7]) or the four-microphone method (transmission [8]) (model Brüel & Kjaer, 4206) was used, according to ASTM E1050 and ISO 10534-2:2002 [9]. The accuracy of the results was assured by performing six measurements for each material. The normalized absorption coefficient ($\bar{\alpha}$) was evaluated according to [10]:

$$\bar{\alpha}=\frac{\int_{f_1}^{f_2}\alpha(f)df}{f_2-f_1} \quad (1)$$

Where f_1 and f_2 correspond to the extremal frequencies among which the study was conducted (i.e. $f_1=500$ Hz and $f_2=6000$ Hz).

3. Results and discussion

The procedure to determine the acoustic behavior requires samples without internal structural defects. Thus an important step in this work was the choice of suitable samples by using X-ray radiography [11]. This approach allows us detecting these internal inhomogeneities without damaging the sample (Fig. 1).

All the samples manufactured in this work were analyzed using this approach, selecting only those ones with a homogenous structure for their acoustic characterization.

Representative SEM images of the porous structure are shown in Fig. 2. The study of the structure allows distinguishing two groups of foams: microporous (top part of Fig. 2) and nanoporous (bottom part of Fig. 2) PMMA. The entire systems exhibit closed pore morphologies due to the manufacturing conditions. This kind of porous structure is completely different from the typical porous structure of open pore materials used in acoustic insulation; nevertheless, these porous materials will allow us to analyze the effects of change in the scale.

Fig. 3 shows the average absorption acoustic response of microporous (left) and nanoporous (right) PMMA foams, illustrating well-defined sound absorption spectrums. Both systems present main absorption values of 0.21–0.25 around 4000 Hz (Table 1), and exhibit an absorption coefficient normalized (Eq. 1) between 0.10–0.15. While microporous materials exhibit only one wide peak, nanoporous materials show two narrower peaks at different frequencies (2100 Hz and 5700 Hz). Furthermore, at high frequencies (6000 Hz) nanoporous PMMA do not absorb, unlike micro. Owing to the complexity of analyzing the acoustic properties of porous materials (due to their multiple forms of wave attenuation), nowadays there is a lack of theoretical and experimental studies able to elucidate the underlying mechanisms of these systems (and especially of the nanoporous ones). Nevertheless, because of the statements given by M. Ayud et al. [12] (acoustic waves propagates in. the air according to Knudsen regime in the nanoscale, gas exhibits different molecular motions in nanopores, gas and solid present different acoustic absorption mechanisms within the nanometer regime) and the different behavior found previously by B. Notario and coworkers [2,3] between microporous and nanoporous foams (confinement effect of polymeric macromolecules in. the nanoscale, increased tortuosity of nanoporous materials, Knudsen regime in nanopores), it was expected to obtain a different experimental acoustic behavior between materials whose pore size is in a different scale (as demonstrated in Fig. 3). However, further studies are needed to understand the real underlying phenomena.

Due to the low absorption coefficient value, these materials will be classified as low absorbers materials. However, although they present α values lower than the polyurethane (PU) ($\alpha=0.97$ at 4000 Hz), they exhibit α values well above than that of other materials commonly used in. construction like concrete ($\alpha=0.04$ at 4000 Hz) or wood ($\alpha=0.07$ at 4000 Hz). Thus they could be used in multifunctional systems requiring a certain degree of soundproofing as well as in improved thermal isolation or mechanical properties.

Transmission loss (TL) behavior of microporous (M-1) and

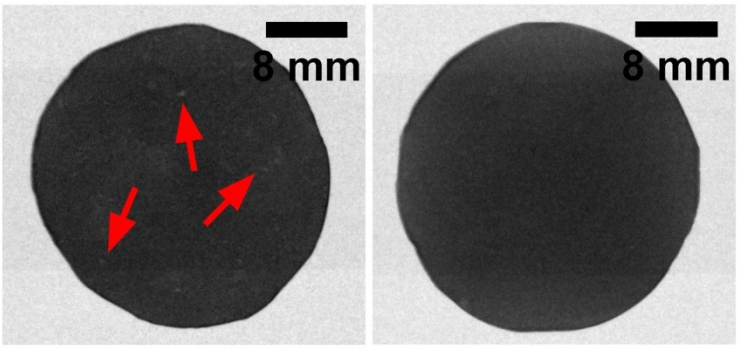

Fig. 1. X-ray radioscopy images of a homogeneous porous material (left) and a porous material with structural internal defects (right, red arrows). (For interpretation of the references to color in this figure legend, the reader is referred to the web version of this article.)

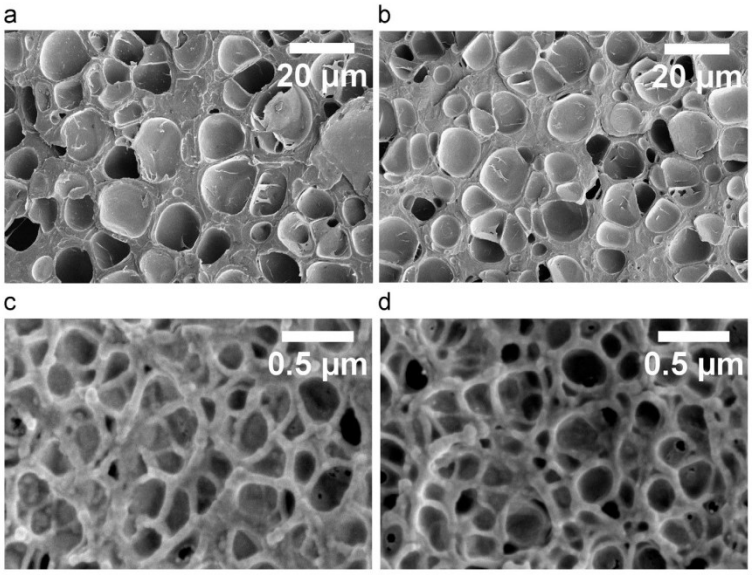

Fig. 2. SEM micrographs of the porous structure of (a) M-1 PMMA foam, (b) M-2 PMMA foam, (c) N-1 PMMA foam, (d) N-2 PMMA foam.

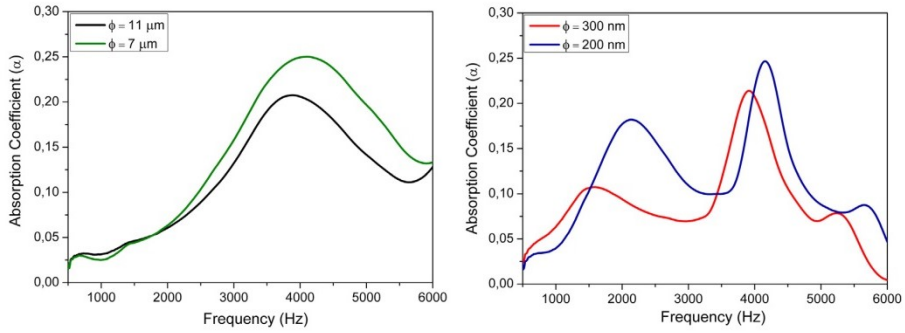

Fig. 3. Average absorption coefficient as a function of frequency. Left) Microporous PMMA Right) Nanoporous PMMA.

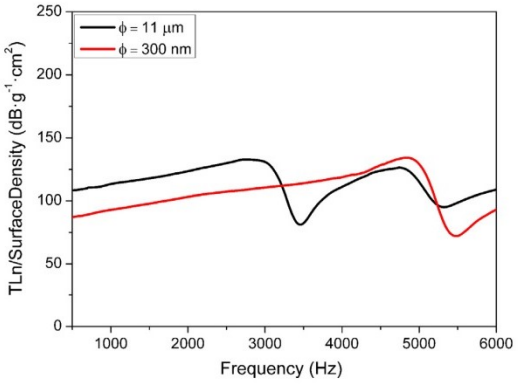

Fig. 4. Average TL coefficient divided by the surface density for a microporous and a nanoporous PMMA foams.

nanoporous samples (N-1) was also analyzed. The average of the transmission loss spectrums are shown in Fig. 4. Again important differences can be observed in the acoustic behavior: nanoporous foams present one peak around 5500 Hz, whereas microporous materials present two: around 3450 and 4500 Hz (Table 1). Again a scale change results in a different acoustic behavior, although further studies are needed to explain these differences.

4. Conclusions

in. this paper the acoustic properties of microporous and nanoporous PMMA foams were studied, finding a different acoustic behavior both in. the absorption coefficient and transmission loss. It is the first time that such systems are studied, and thus further studies are needed to understand the underlying mechanisms. These results are very promising, making nanoporous materials potential candidates in the sound field, especially in multifunction systems that require a certain degree of soundproofing.

Acknowledgments

Financial support from FPI Grant BES-2013-062852 (B. Notario) from the Spanish Ministry of Education, MINECO (MAT 2012-34901), and the Junta of Castile and Leon (VA035U13) is gratefully acknowledged.

References

[1] L.J. Gibson, M.F. Ashby, Cellular Solids: Structure and Properties, 2nd ed., Cambridge University Press, Cambridge, 1997.
[2] B. Notario, J. Pinto, E. Solorzano, J.Ad Saja, M. Dumon, M.A. Rodriguez-Perez, Experimental validation of the Knudsen effect in nanocellular polymeric foams, Polymer 56 (2015) 57–67.
[3] B. Notario, J. Pinto, M.A. Rodriguez-Perez, Towards a new generation of polymeric foams: PMMA nanocellular foams with enhanced physical properties, Polymer 63 (2015) 116–126.
[4] D. Miller, V. Kumar, Microcellular and nanocellular solid-state polyetherimide (PEI) foams using sub-critical carbon dioxide II. Tensile and impact properties, Polymer 52 (2011) 2910–2919.
[5] C. Zhou, N. Vaccaro, S.S. Sundarram, W. Li, Fabrication and characterization of polyetherimide nanofoams using supercritical CO_2, J. Cell. Plast. 48 (2012) 239–255.
[6] M.D. Abràmoff, P.J. Magalhães, S.J. Ram, Image processing with ImageJ, Biophotonics Int. 11 (2004) 36–42.
[7] H. Koruk, An assessment of the performance of impedance tube method, Noise Control. Eng. J. 62 (2014) 264–274.
[8] J.G. Proakis, D.G. Manolakis Introduction to Digital Signal Processing. UK1988.
[9] ASTM. Standard Test Method for Impedance and Absorption of Acoustical Materials Using a Tube, Two Microphones and a Digital Frequency Analysis System.
[10] M.A. Rodriguez-Perez, M. Álvarez-Láinez, J.A. de Saja, Microstructure and physical properties of open-cell polyolefin foams, J. Appl. Polym. Sci. 114 (2009) 1176–1186.
[11] J. Escudero, E. Solorzano, M.A. Rodriguez-Perez, F. Garcia-Moreno, J.A. De Saja, Structural characterization and mechanical behaviour of ldpe structural foams. A comparison with conventional foams, Cell. Polym. 28 (2009) 289–302.
[12] M. Ayub, A.C. Zander, C.Q. Howard, B.S. Cazzolato, D.M. Huang A review of MD Simulations of Acoustic Absorption Mechanisms at the Nanoscale. Proceedings of Acoustics 2013. Australia2013.

VI.4. Additional Clarifications

Although, as mentioned above, nowadays there are no theoretical models developed specifically for systems with cells in the nanoscale, in this section we have tried to fit the results to some of the best known theoretical models used in acoustic for microcellular materials, in order to analyze if these models are able to explain the differences found and presented in the previous paper.

In the next sections, the most important results both in absorption and transmission are summarized.

VI.4.1 Absorption

In addition to the difficult of the no existence of specific theoretical models developed for nanoscale systems, we have to take into account that most of the acoustic theoretical models for microcellular polymers are focused on open cell foams (Biot-Allard [11, 12], Chandler and Johnson [13, 14], Tarnow [15, 16]). This fact further increases the difficulty to fit the experimental data obtained since these models cannot be used in our study.

In the case of closed cell systems, the main absorption mechanism is based on the vibration of the material at the resonance frequency (f_r) when the sound wave impinges on its surface. Thus, a first relationship of interest that has been applied to the materials under study is that the resonance frequency at $\lambda/4$ in the absorption spectrum can be estimated using the following expression [12]:

$$f_r = \frac{1}{4d}\sqrt{\frac{Re(K_c)}{\rho_f}} \qquad \text{(VI-1)}$$

Where d and ρ_f are the diameter and the density of the cellular polymer respectively, and the term $Re(K_c)$ is the real part of K_c (bulk modulus), which can be calculated as follows:

$$K_c = \frac{E(1-\upsilon)}{(1+\upsilon)(1-2\upsilon)} \qquad \text{(VI-2)}$$

Where υ is the Poisson´s ratio (a value of 0.35 has been considered [4]) and E is the real part of the storage modulus, which has been determined by means of DMA (see *Chapter IV*). Such modulus was obtained at a frequency of 1 Hz.

To estimate the value of E at around 1000 Hz (values measured for the resonance frequency) the principle of time-temperature superposition was used. According to it, a decade of increase in frequency corresponds to a reduction of 7 ºC in temperature [17]. Therefore, the value of the modulus at 1000 Hz and room temperature is estimated from the DMA data at 1 Hz and -3 ºC.

Table VI-1 compares the experimental results (f_{exp}) with the values predicted by equation VI-1. As it can be observed there is a deviation up to 2000 % between these two values, being this difference even greater in the case of nanocellular polymers (up to 2100 %). Therefore, it seems that the peaks detected in the acoustic absorption curves are not due to this mechanism.

Table VI-1. Experimental and theoretical resonance frequencies for microcellular and nanocellular polymers

Samples	*d* (m)	ρ_f (Kg/m^3)	*E'* (MPa) at 3 ºC [6]	f_r (Hz)	f_{exp} (Hz)
M-1	0.004	637.2	640.4	79378.1	3873.3
M-2	0.004	564	667.8	86161.9	4084.7
N-1	0.004	495	592.9	86655.0	3926.1
N-2	0.004	483.8	611.5	89017.3	4170.8

On the other hand, due to the viscoelastic nature of polymers, when a wave in general, and in particular an acoustic wave, travels in the material, this will be attenuated due to the viscous component (Figure VI.4).

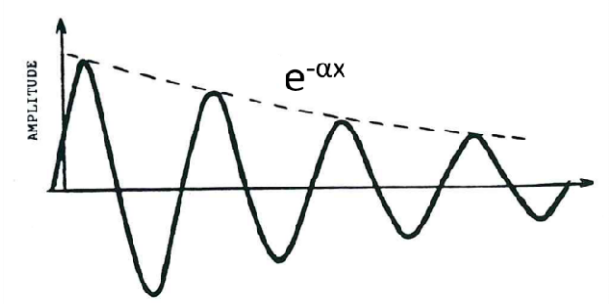

Figure VI.4. Damped sinusoid wave propagating in the *x* axis

For a longitudinal wave, the absorption coefficient (α)* can be calculated according to the following equation [18]:

$$\alpha = \left(\frac{\rho}{M'}\right)\frac{w \cdot tan(\delta)}{2} \qquad \text{(VI-3)}$$

Where α is the absorption coefficient, ρ is the cellular polymer density, w is the frequency, $tan\ \delta$ is the ratio between the loss modulus and the storage modulus (E''/E'), and M' is the real part of the compressive modulus of the material that can be calculated according to Eq. VI-4:

$$M' = K' + \frac{4}{3}G' \qquad \text{(VI-4)}$$

K' and G' represent the real part of the modules of compressibility and shear, respectively, and can be estimated as follows:

* This is not the same parameter that the impedance tube measures.

$$K' = \frac{E'}{3(1-2\upsilon)} \quad \text{(VI-5)}$$

$$G' = \frac{E'}{2(1+\upsilon)} \quad \text{(VI-6)}$$

Table VI-2. Theoretical absorption coefficient values obtained according to Eq. VI-3 for both microcellular and nanocellular PMMA

Samples	ρ_f (Kg/m^3)	E' (MPa) at 25 ºC [6]	$Tan\delta$ at 25 ºC [6]	w (Hz)	Absorption Coefficient (α)
M-1	637.2	624.4	0.083	1	0.048
M-2	564	626.6	0.087	1	0.047
N-1	495	545.1	0.091	1	0.049
N-2	483.8	585.9	0.096	1	0.050

The values of the absorption coefficient calculated using equation VI-3 are summarized in Table VI-2. Nanocellular polymers exhibit a higher absorption value than microcellular ones. This is due to the higher *Tan δ* of nanocellular PMMA. Likewise, in the absorption spectrum (see experimental data in the previous section), it can also be observed that the base line of nanocellular polymers is greater than in the case of microcellular ones. This could be due to the higher *Tan δ* of nanocellular polymers.

The absorption coefficient value was calculated at low frequencies (1 Hz). Then, to obtain results that are of practical interest in the range of absorption measured, we should resort to methods of extrapolation of viscoelastic data by the principle of time-temperature superposition. This is an interesting topic that could be considered in the future.

Finally, the Arrhenius equation (Eq. VI-7) was used to determine if the transition temperatures α and β, characteristic of PMMA, could have an effect within the frequency range studied.

$$f = f_0 exp\left(\frac{-\Delta H}{RT}\right) \quad \text{(VI-7)}$$

In Eq. VI-7 f represents the measuring frequency, f_0 is the frequency when T approaches infinity, ΔH is the activation energy, R is the universal gas constant, and T is the absolute temperature in Kelvin at the maximum of the *Tan δ* curve.

The values of the activation energies of both the alpha and the beta transition as well as the value of f_0 were obtained from literature data [19].

Table VI-3 shows the theoretical frequencies results predicted by equation VI-7. As it can be observed the values obtained are outside the range of frequencies studied. This is because as the frequency increases, the thermal transition (both alpha and beta) is shifted to higher temperature values. Therefore, to observe these transitions at room temperature it would be necessary to go to very low frequencies.

Table VI-3. Theoretical frequencies calculated using the Arrhenius equation for both microcellular and nanocellular polymers

Samples	ΔH_α (KJ/mol) [19]	$f_{0\alpha}$ (Hz) [19]	f_α (Hz) at 298 K	ΔH_β (KJ/mol) [19]	$f_{0\beta}$ (Hz) [19]	f_β (Hz) at 298 K
M-1	367.84	$1.66 \cdot 10^{48}$	$5.12 \cdot 10^{-17}$	96.09	$4.94 \cdot 10^{16}$	$6.95 \cdot 10^{-1}$
M-2	367.84	$1.66 \cdot 10^{48}$	$5.12 \cdot 10^{-17}$	96.09	$4.94 \cdot 10^{16}$	$6.95 \cdot 10^{-1}$
N-1	367.84	$1.66 \cdot 10^{48}$	$5.12 \cdot 10^{-17}$	96.09	$4.94 \cdot 10^{16}$	$6.95 \cdot 10^{-1}$
N-2	367.84	$1.66 \cdot 10^{48}$	$5.12 \cdot 10^{-17}$	96.09	$4.94 \cdot 10^{16}$	$6.95 \cdot 10^{-1}$

Therefore, with the analyzed models we cannot predict the shape of the absorption curves measured. However, the higher *Tan δ* value of nanocellular polymers is an interesting parameter indicating a higher damping in the solid phase for these materials.

VI.4.2 Transmission Loss

In the case of transmission loss one of the most used models to fit the experimental data is the one that considers the transmission of a sound wave at normal incidence through a homogeneous and solid wall.

It consists of a uniform and unlimited wall which mass, stiffness and damping per unit area are *m*, *s*, and *r*, respectively. We might assume such wall to a non-flexible plate, with a mass per unit area *m*, mounted on a suspension with viscous damping, whose coefficients of stiffness and damping per unit area are *s* and *r*. This wall separates two identical half-spaces, in which the density and sound propagation speed are *ρ* and *c*, respectively.

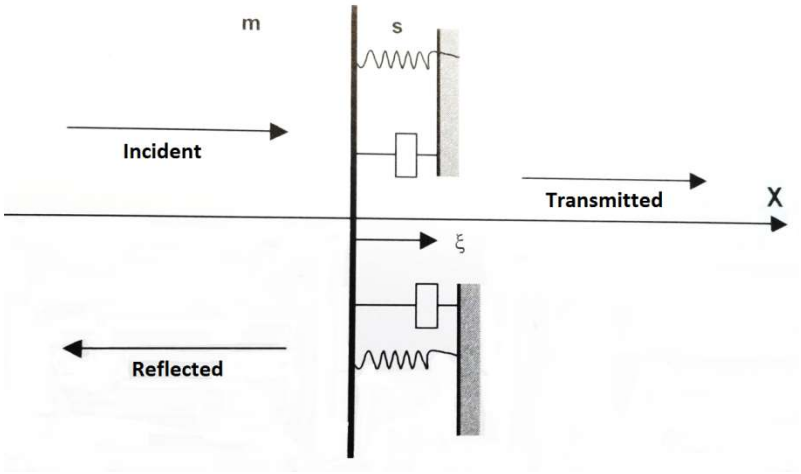

Figure VI.5. Idealized model for the study of the transmission loss in normal incidence in a homogeneous wall

Suppose that from region x < 0, a sound wave incident on this wall. Carrying out all the calculations [20], the following expression for the transmission coefficient (*τ*) is obtained:

$$\tau = \frac{4}{\left[\frac{1}{\rho c}\left(wm - \frac{s}{w}\right)\right]^2 + \left[\frac{w_0 m\eta}{\rho c} + 2\right]^2} \quad \text{(VI-8)}$$

Where the damping coefficient (r) has been replaced by $w_0 m\eta$, being η the loss factor in vacuum, w_0 the undamped natural frequency of the wall, and w the frequency.

Usually in the acoustic field the variable used is the logarithm of the inverse of the transmission coefficient [21]. This parameter is called transmission loss and is defined as:

$$TLn = 10\log\left(\frac{1}{\tau}\right) \quad \text{(VI-9)}$$

The transmission loss coefficient has a maximum value for w_0, $w_0 = (s/m)^{1/2}$. Based on the value of this frequency, three different areas in which the behavior of the *TLn* differs can be identified:

- $w << w_0$: Stiffness Controlled Area. The transmission loss coefficient is defined as:

$$TLn = 20\log s - 20\log f - 20\log(4\pi^2\rho) \quad \text{(VI-10)}$$

  Here, the *TLn* is mainly determined by the stiffness, being insensitive to the mass and damping.

  Equation VI-10 is not valid for systems in which the mass per unit area is very low, since the approximations won´t be fulfilled.

- $w >> w_0$: Mass Controlled Area. The equation in this case is:

$$TLn \approx 20\log(mf) - 42 \quad \text{(VI-11)}$$

  The *TLn* is mainly determined by the mass per unit area and is quite independent of the damping and stiffness.

- $w = w_0$. The equation for the transmission loss is determined by:

$$TLn = 20\log f_0 + 20\log m + 20\log\eta - 20\log\left(\frac{\rho c}{\pi}\right) \quad \text{(VI-12)}$$

According to this, the transmission loss is full when the radiation damping is greater than the mechanical damping. Otherwise, i.e. when the mechanical damping is higher, the mass, stiffness, and damping influence the transmission.

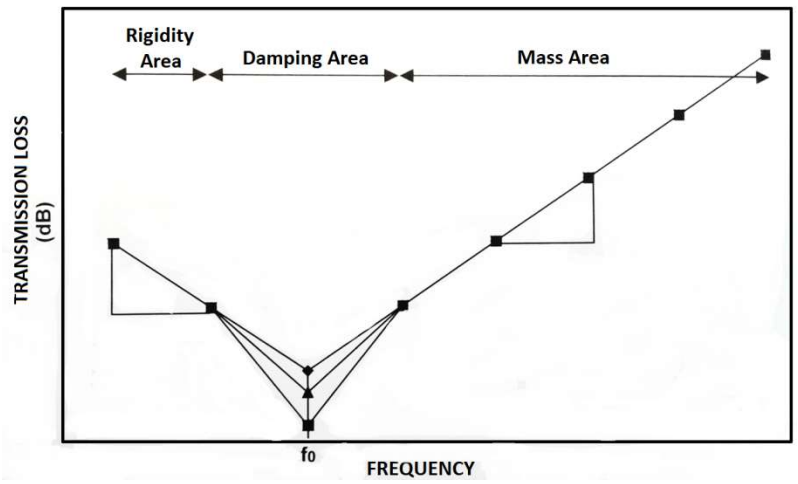

Figure VI.6. Theoretical transmission loss of a simple wall, with mass, stiffness, and damping. Normal incidence

Figure VI.6 illustrates equations VI-10-12. At very low frequencies the sound transmission is controlled by the stiffness of the wall. When the frequency is increased, the resonance frequency is reached, f_0, becoming the wall virtually transparent to the sound. If the frequency continues increasing, *TLn* is controlled by the mass of the wall.

Experimental curves of transmission loss obtained in this study for microcellular and nanocellular PMMA exhibit the same shape as that shown in Figure VI.6. The undamped natural frequency (f_0) was calculated.

As shown in Table VI-4 the values obtained for f_0 are large as compared to the experimental values (standard deviation around 32 % for microcellular polymers and around 127 % for nanocellular ones). The value of f_0 for the microcellular PMMA is relatively good; however, the differences between experimental and theoretical data are higher when we shift to the nanoscale (as the value of f_0 was underestimated, it was decided not to represent the rest of the curve). Moreover, the trend obtained is opposite to the experimental results since nanocellular polymers exhibited a higher f_0 than microcellular ones.

The main reason for this poor fit could be that this model is developed for solid walls and not for cellular materials. Then, further modifications or new theoretical models are needed.

Table VI-4. Experimental and theoretical undamped natural frequencies for microcellular (M-1) and nanocellular (N-1) polymers

Samples	ρ_f (Kg/m^3)	f_0 (Hz)	f_{exp} (Hz)	Standard Deviation (%)
M-1	637.2	2620.02	3452.87	31.8
N-1	495	2412.91	5477.01	127

Therefore, nowadays, and due to the complexity of analyzing the acoustic properties of cellular materials, there is a lack of theoretical and experimental studies capable of understanding the underlying mechanisms of closed cell microcellular and nanocellular polymers. The

experimental results have shown that there are differences in the acoustic spectrum between them because of the change of scale (both in absorption and transmission). M. Ayub and coworkers [2] are the only ones who have tried to model the acoustic properties at the nanoscale. They proposed molecular dynamics (MD) simulations as a solution to model the acoustic mechanisms of nanoporous materials. For this purpose they described the fundamental concepts that must be taken into account when carrying out the simulation: acoustic waves propagate in the air according to Knudsen regime in the nanoscale, gas exhibits different molecular motions in nanopores, gas and solid present different acoustic absorption mechanisms within the nanometer regime. However, after reviewing the state of the art related to MD simulations, M. Ayub et al. stated that nowadays none of them have taken into account all these aspects.

Logically their methodology is not immediately applicable to our materials (since their methodology is developed for carbon nanotubes), but it may be a way forward in the future to understand the main phenomena taking place in these acoustic experiments.

VI.5. References

1. MarketsandMarkets. Acoustic Insulation Market by Type (Mineral Wool, Glass Wool, Foamed Plastics), by Application (Building & Construction, Industrial, Transportation) - Global Trends and Forecasts to 2019. 2015.
2. Ayub M, Zander AC, Howard CQ, Cazzolato BS, and Huang DM. A review of MD Simulations of Acoustic Absorption Mechanisms at the Nanoscale. Proceedings of Acoustics 2013. Australia, 2013.
3. Eaves D. Handbook of Polymer Foams: Rapra Technology, 2004.
4. Álvarez-Laínez M. Propiedades Térmicas, Mecánicas y Acústicas de Espumas de Poliolefina de Celda Abierta. Universidad de Valladolid, 2007.
5. Notario B, Pinto J, Solorzano E, Saja JAd, Dumon M, and Rodriguez-Perez MA. Polymer 2015;56:57-67.
6. Notario B, Pinto J, and Rodriguez-Perez MA. Polymer 2015;63:116-126.
7. Pinto J, Notario B, Verdejo R, Dumon M, Costeux S, and Rodriguez-Perez MA. Advanced Materials 2015;Submitted.
8. Bernardo J, Repetto CE, Stia CR, and Welti RJ. Mecánica Computacional 2011;XXX(41):3145-3155.
9. Allard JF and Atalla N. Propagation of Sound in Porous Media. New Jersey: John Wiley & Sons, 2009.
10. Proakis JG and Manolakis DG. Tratamiento digital de señales: Principios, algoritmos y aplicaciones. UK, 1998.
11. Biot MA. The Journal of the Acoustical Society of America 1962;34:1254-1264.
12. Allard JF. Propagation of Sound in Porous Media. London and New-york, 1993.
13. Chandler RN and Johnson DL. Journal of Applied Physics 1981;52:3391-3395.
14. Johnson DL, Kplik J, and Dashen R. Journal Fluid Mech. 1987;176:379-402.
15. Tarnow V. Journal Acoustic Soc. Am. 1996;99(5):3010-3017.
16. Tarnow V. J. Acoust. Soc. Am. 1996;100(6):3706-3713.
17. Corsaro R and Sperling L. American Chemical Society 1990.
18. Rodriguez-Perez MA. Estudios viscoelásticos en espumas de poliolefinas. Departamento de Física de la Materia Condensada, Cristalografía y Mineralogía. Valladolid: Valladolid, 1995.
19. Clarke RL. Biomaterials 1989;10:494-498.
20. Recuero M and Gil C. Aislamiento acústico. In: Paraninfo, editor. Acústica arquitectónica. Madrid, 1993. pp. 295-300.
21. 74-040 U. Medida del aislamiento acústico de los edificios y de los elementos constructivos. Medida en laboratorio del aislamiento al ruido aéreo de los elementos constructivos. Parte 3. AENOR, 1984. pp. 11.

CONCLUSIONS AND PERSPECTIVES

Conclusions and Perspectives

This final section summarizes all the main conclusions and remarkable achievements of this research work. This section is written according to the scope and objectives of this thesis. The conclusions cover the optimization of experimental techniques and production routes, the influence of cell size reduction on the properties of nanocellular polymers, and the study of the main properties of these materials.

As a general achievement microcellular and nanocellular PMMA with cell sizes in the range of 12 μm to 100 nm, with similar relative densities in the range of 0.4 to 0.5, and tunable size and geometry, adjustable to different standard measurement devices, have been produced by the solid state foaming process. This fact has allowed: a) to provide a better understanding of the mechanisms involved in several physical properties of nanocellular polymers; b) to study the transition from the micro to the nano scale of different physical properties (thermal, mechanical, dielectric, and acoustic properties), and to determine the validity of the assumptions made in that respect in recent years.

The most important conclusions according to the three main objectives of this research are presented (i.e. production of micro and nanocellular polymers with appropriate dimensions, geometries, and similar densities; correlation between the structure and the physical properties of nanocellular polymers; evaluation of the transition in the properties of these materials when cell size goes from the micrometer to the nanometer range.

Production of Micro and Nanocellular Foams with Control over Density:

A route to produce microcellular and nanocellular polymers with similar relative densities and appropriate dimensions and geometries for their macroscopic characterization has been established using PMMA precursors. The main achievements have been:

- Microcellular and nanocellular polymers are obtained by means of the gas dissolution foaming method using specific processing parameters: saturation pressures from 13 to 31 MPa and saturation temperatures around room temperature. A controlled foaming step in a thermostatic water bath was introduced, obtaining samples with the following features: similar relative densities (between 0.4 and 0.5), cell sizes in two different scales (micro (between 12 and 7 μm) and nano scale (between 300 and 200 nm), and appropriate dimensions to be analyze with standard protocols (sample thickness ≈ 0.5 mm).

- Nanocellular polymers were obtained from bulk samples of several millimeters of thickness, and did not required very high pressure release rates (GPa/second), or quenching of the sample after or prior the pressure release.

- Nanocellular polymers with a significant density reduction (over 50 %) were obtained. Furthermore, these cellular polymers exhibited homogeneous cellular structures with closed cell morphologies.

Therefore we have been able to solve the existing limitation of producing nanocellular and microcellular polymers with appropriate dimensions, geometries, and similar densities, overcoming the main difficulties of the production of this kind of materials for scientific studio on the physical properties characterization. We just used commercial polymers and a simple approach to produce these nanocellular polymers.

Influence of the Cell Size Reduction on Nanocellular Foams and their Properties:

The emerging side effects due to the reduction of the cell size to the nanometer scale, as well as the evolution of pore wall thickness and the tortuosity are summarized in this section in order to provide a better understanding of the influence of the nanoporous PMMA morphologies in the physical properties.

First of all, the reduction of the cell size to the nanometer range involves the confinement of the gaseous phase into such nanometric voids. As a consequence, a reduction of the thermal conductivity of the gaseous phase takes place due to the well-known Knudsen effect, as it was illustrated in *Chapter III*.

Furthermore, other phenomenon appears due to the confinement of the gaseous phase to the nano-scale. As shown in *Chapter II*, it has been demonstrated that polymeric foams with nanopores present an interfacial polarization phenomena, or Maxwell Wagner Sillars (MWS), leading into a capacitor-like behavior that can contribute significantly to electrical conduction by dielectric breakdown or by other process related to the Knudsen diffusion regime yet unidentified.

On the other hand, the reduction of the cell size from the micrometer to the nanometer range, maintaining constant the density also leads to a reduction of the thickness of the cell walls (from approximately 1.5 μm in the case of microcellular polymers to around 60 nm in the case of the nanocellular ones). This reduction of the cell wall thickness confines the polymer chains within the cell walls leading to a reduction of the mobility of the polymeric macromolecules (confinement effect). This chain confinement was demonstrated in *Chapter II* in PMMA based foams by means of Raman and Dielectric spectroscopy. It was observed that the differences found between Raman relative intensities were associated with the hindering of the vibrational modes, proving the existence of a confinement effect of the polymeric macromolecules. Likewise, the decrease of the dielectric strength with wall thickness was ascribed to a progressive reduction of the number of free dipoles able to rotate, due to the confined configuration of the nanocellular system.

As a consequence of the confinement of the polymeric macromolecules in very thin pore wall, non-expected modifications in different properties (thermal (*Chapter IV*), mechanical (*Chapter IV*), and dielectric properties (*Chapter II and V*)) have appeared along this thesis: an increment of the glass transition temperature, an increase of the stiffness of the polymer matrix, or a reduction of the number of free dipoles able to rotate.

Finally, the reduction of the size of the constituent phases (both solid and gas phases) to the nanometer scale also modify the architecture of the porous system leading to an increase in

the tortuosity of the cellular material. An increase tortuosity in PMMA based nanocellular polymers was demonstrated in *Chapter II* by measuring the DC electrical resistivity. The results revealed clear evidences of the increased tortuosity in the transition from the micro to the nanometer range. As a consequence of this increased tortuosity, a reduction of the thermal and electrical conductivity of the solid phase was detected, as shown in *Chapter III* and *II*.

Therefore, the reduction of the cell size to the nanometer range leads to the confinement of both the solid and the gaseous phase, as well as to a modification of the porous architecture. As a consequence, non-expected modifications in different properties or new phenomena appear explaining some of the results found in the different physical properties along this thesis.

Properties of PMMA based Foams:

The unique characteristics of PMMA based cellular polymers, their easy production, the variety of possible cellular structures, and their tunable sizes and geometries make them ideal materials for the study of the properties evolution when the cell size is reduced from the the microcellular to the nanocellular range. Efforts performed on this topic provided several results of significant interest:

- A clear reduction of the thermal conductivity of the gaseous phase has been found in PMMA based foams for cell sizes below the micron, validating experimentally for the first time the Knudsen effect on cellular polymeric materials.

- A clear improvement in some mechanical properties at high strain rates (Charpy impact) and at low strain rates (shore hardness and Young´s modulus) has been found between microcellular and nanocellular polymers. On the contrary, for several specific characteristics also measured at low strain rates (the strain at break and the collapse strength), the nanocellular polymers present lower properties.

- An evident transition from a capacitive to a combination of a resistive and a capacitive behavior has been detected when cell size shift from the micro to the nanoscale. A strong reduction of the dielectric constant of nanocellular PMMA as compared to the solid was found. Furthermore, it was demonstrated that the confinement effect of the polymeric macromolecules is stable in the temperature range between -10 and 110 ºC.

- A different acoustic behavior, both in absorption and transmission, has been detected between microcellular and nanocellular cellular polymers. The different wave propagation mechanism in the micro and nanoscale (which is determined by the confinement of both the gas and solid phases) could justify the experimental differences.

- New effects or non-expected phenomena have been found owing to the confinement of the constituent elements of the cellular polymer (solid and gaseous phase) in the nanometer regime such as: an increment of the glass transition temperature, a reduction of the thermal conductivity of the solid phase, and an increase of the rigidity of the polymer matrix, etc.

Then, we have been able to determine the validity of the theoretical assumptions made about the physical properties of nanocellular materials in recent years. The Knudsen effect has been demonstrated for the first time in nanocellular polymers, according to theoretical predictions. Regarding to mechanical properties some of the results are in favor (improved impact resistance, Young´s modulus, and shore hardness in nanocellular PMMA) and other are against (worst strain at break and collapse strength of nanocellular polymers) the theoretical predictions. Further studies with other polymers are needed in order to establish some additional trends. In the case of dielectric properties clear differences have been found between microcellular and nanocellular polymers, although more studies are needed in order to figure out whether there is any real influence of cell size on the dielectric behavior of these nanocellular polymeric systems. With respect to the acoustic properties further works are needed in order to understand the underlying phenomena that justify the differences found.

Furthermore the study of the physical properties of nanocellular polymers has led to the emergence of non-expected effects due to the confinement of the constituent phases of the foam, never demonstrated before.

Future Perspectives

This is the second Ph.D. thesis in CellMat about nanocellular polymers. As nanocellular polymers are one of the current frontiers on cellular materials science, raising great expectations due to their potential properties and applications, we hope that the knowledge acquired during this research could be a starting point for new research works, some of which could be focused on the following topics.

- Transition between microcellular and nanocellular polymers:

    - To extend the study of the mechanical properties to other properties such as impact strength (falling dart), fatigue, etc., and to a wider range of relative densities, cell sizes, and polymers.

    - To study the evolution of other properties such as optics, filtration phenomena, thermal expansion, etc., between microcellular and nanocellular polymers.

    - To use other polymers of interest (such as polycarbonate (PC), polyethylenimine (PEI)) and analyze the thermal, mechanical, dielectric, and acoustic properties of the same, comparing the results with those obtained with PMMA and blends of PMMA/MAM.

- Research on PMMA and PMMA/MAM blends:

    - To study the post-foaming process on PMMA based foams, trying to reach significant density reductions. Two approaches have been proposed: post-foaming at low temperatures than those used, and post-foaming under pressure.

    - To reduce the saturation temperature in order to obtain nanocellular polymers whose cell size is in the order of tens of nanometers.

    - To develop filtration devices based on PMMA/MAM nanocellular polymers and characterize them.

    - To add nanoparticles (e.g. nanoclays) to neat PMMA to develop an additional approach to produce nanocellular polymers.

    - To develop sensor devices on PMMA and PMMA/MAM nanocellular oams by adding nanoparticles, and characterize them.

    - To look for other applications of PMMA based foams.

- Looking for other polymers:

    - Analyze if it is possible to develop other block copolymers with CO_2-philic soft blocks that can lead to the production of nanocellular polymers with higher nucleation densities. From the accumulated knowledge on this research and the previous one [1] new block copolymers with optimal properties to enhance the nucleation can be looked for.

    - To analyze high performance polymers (such us polyimide (PI), polyether ether ketone (PEEK), polysulfone (PSU), etc.) that can produce nanocellular polymers with better physical properties.

- Continuous production route: current production route requires long processing times (i.e. saturation times about 16-24 h) in a non-continuous production route. Then, the development of a continuous and fast production route of nanocellular polymers is the main issue required for the industrial production of these materials.

References

1. Pinto J. Fabrication and Characterization of Nanocellular Polymeric Materials from Nanostructured Polymers. University of Valladolid & University of Bordeaux, 2014.